Cyclic stretch of brain microvascular endothelial cells and regulation of amyloid processing and expression: evidence for contribution of vascular pulsatility in Alzheimer's disease

Sumudu V. S. Gangoda
(MRes, B Biotechnology Hons)

A thesis submitted in fulfilment of the requirements for the degree of

Doctor of Philosophy

Supervisor: Prof. Alberto Avolio

Associate-supervisor: Dr. Mark Butlin

Co-supervisor: Dr. Vivek Gupta

Department of Biomedical Sciences

Faculty of Medicine and Health Sciences

Macquarie University

Submitted for examination: 16 February 2018

Final submission: 27 June 2018

MACQUARIE University
SYDNEY·AUSTRALIA

Declaration of originality

I hereby declare that the work presented in this thesis has not been submitted for a higher degree to any other university or institution. To the best of my knowledge this submission contains no material previously published or written by another person, except where due reference is stated otherwise. Any contribution made to the research by others is explicitly acknowledged.

Sumudu V. S. Gangoda

Department of Biomedical Sciences

Faculty of Medicine and Health Sciences

Macquarie University

16 February 2018

Declaration of contributions

All the work presented in this thesis was solely performed by Gangoda SVS. except for the contributions that are specified below for Chapters 4 and 9. Some written content in sections 2.1 and 2.2 of the literature review has been extracted from the Masters of Research thesis of Gangoda SVS and expanded on in the context of this PhD thesis.

Chapter 4

This chapter presents the effect of cyclic stretch on APP expression and processing, and associated inflammatory signalling, with contents based on the publication:

> **Gangoda SVS**, Avadhanam B, Jufri NF, Sohn EH, Butlin M, Gupta V, Chung R & Avolio AP (2018) Pulsatile stretch as a novel modulator of amyloid precursor protein processing and associated inflammatory markers in human cerebral endothelial cells. *Sci. Rep.* **8**, 1689.

The study designed by Ms. Gangoda SVS, Mrs. Avadhanam B, Ms. Jufri NF and Prof. Sohn EH. Experiments were conducted by Ms. Gangoda SVS, as was the data analysis, and writing of the manuscript. Prof. Avolio AP, Prof. Chung R, Dr. Gupta V and Dr. Butlin M supervised the study, checked analysis, assisted in interpreting the results, and made manuscript revisions.

Chapter 9

All animal treatments and tissue collection were performed by Dr. Butlin M Post-mortem tissue processing to obtain the data presented in this chapter were performed, analysed and prepared by Ms. Gangoda SVS Tissue sectioning and staining procedures were performed with the assistance of Miss Georgevsky D, Mrs. Avadhanam B and Miss Van der Wall R.

Ethics approval

Work presented in Chapter 9 was using *ex vivo* tissue donated from studies conducted under animal research authority 2015/021 (Macquarie University Animal Ethics Committee), 'Effect of dietary salt on blood vessel stiffness and glycosaminoglycans'.

Acknowledgements

The three years of my PhD journey has gone past so fast though it was like a roller coaster ride. The people who were in the ride with me however made it smoother, more comfortable and less scary for me. I take this opportunity to convey my gratitude and acknowledge those who have been in it with me in making the completion of this journey a lot more enjoyable and exciting.

Firstly, to my Principal Supervisor, Prof. Alberto Avolio, who has enlightened me about the true essence of philosophy, 'the love of knowledge', that has immensely allowed me to enhance my appreciation in academic research, and to think outside the box. I feel very privileged to be mentored by such a brilliant supervisor like him and, to be given the opportunity in pursuing a PhD as part of his team. I would like to express my deepest gratitude for the encouragement, support, and guidance that he has provided me at all times, and for the inspiration that he has been whilst sharing his wisdom and philosophical perspective, which has shed a new light on both my professional and also on personal life.

To my Associate Supervisor, Dr. Mark Butlin, whom I looked up to in designing and carrying out experiments, and critical evaluation and analysis of research. His professional approach has always been a role model for me, and has truly influenced me to sharpen my quality of work in keeping up to his standards. I thank Mark for his kind support and guidance, and for helping me develop as an independent researcher. The long and short discussions that we had along the journey, have helped me to be more insightful and thorough when fine-tuning my thesis.

To my Co-Supervisor, Dr. Vivek Gupta, for the much-needed guidance and support in experimental troubleshooting and emphasising the elements required in building up an

emerging research profile. The open and friendly platform that he has created for discussion and asking questions in interpretation of results has always improved my depth of the subject and experimental techniques. I thank Vivek for his insights that have assisted me to succeed in experiments. I also acknowledge Vivek for showing me how to reach out for opportunities outside of research, and for sharing his expertise in western blotting, cell culture and tissue processing techniques. His guidance has also greatly helped me develop as an independent researcher and build up my troubleshooting skills in research.

To Prof. Roger Chung, for his kind guidance and direction in my experimental design, approach and interpretation. I thank Roger for giving his valuable time to discuss my findings and showing me further avenues for my research and for proof-reading my manuscript.

To Prof. Eun-Hwa Sohn, I thank her for her direction and guidance in my experiments and proof-reading my manuscript. She also gave me valuable feedback continuously throughout my PhD. Her assistance in organising the visit of the two students, Jenny (Miss. Park Jae Eun) and Chaery (Miss. Gwak Chae Ryeong) and, efforts in designing the red ginseng experiments are highly appreciated. It has been such a pleasure to recruit my first ever research students, whilst making valuable contributions to my work and improving my teaching skills.

I thank Jenny and Chaery, for being such wonderful students, allowing me to gain valuable teaching experience, and apply my knowledge on a different scale. They have shown so much initiative and enthusiasm. I acknowledge their efforts in helping me complete the red ginseng study.

To Bhargava, my fellow colleague, for being a dear friend and my partner in crime who has been patient in all my crisis situations, and has listened to, and supported me at all times. It

has been a pleasure working with her, especially when troubleshooting the issues with the stretching machine and fine tuning our experiments.

To Dr. Lucinda McRobb for her generous assistance in my PCR troubleshooting and providing the ADAM10 antibody for my westerns. I thank Lucinda for being patient with me and her kindness in explaining things to help my analyses.

To Dana, Rowan, Roshana and Britt for their valuable assistance in tissue processing work in the salt study with a friendly attitude. I thank them for sharing their expertise in tissue processing, staining procedures and microscopy.

To Isabella, for always helping me with a friendly smile in getting through times of stress and offering advice through her PhD experience. I thank Isabella for her time spent on providing me with valuable feedback on my presentations and written work.

To all my colleagues from the vascular group, Parisa, Fatemeh, Mi-Ok and Dr. Martin Turner and Dr. Karen Peebles; I thank them all for making it an enjoyable journey with such memorable and thought-provoking group meetings.

I would like to acknowledge the Skipper award that has allowed me to travel overseas and present my work at the symposium titled 'Alzheimer's disease as a neurovascular inflammatory disorder', which was held at The New York Academy of Sciences. It has also allowed me to visit two prestigious research institutes, Weill Cornell Medical College, New York, and Johns Hopkins Hospital, Baltimore.

Also, I thank Dr. Constantino Iadecola at the Weill Cornell Medical College, New York, and Professor Subroto Chatterjee at the Johns Hopkins Hospital, Baltimore for giving me the

opportunity to discuss my work with them, and for exposing me to their research that was undertaken at their institutes. To Prof. Joesef Anrather, Assit. Prof. Giuseppe Faraco and Assit. Prof. Laibak Park, whom I met in New York, and to Dr. Djahida Bedja, whom I met in Baltimore, for their generous and warm hospitality, and for welcoming me to their laboratories and explaining their work. The knowledge and inspiration I gathered from their work has immensely helped me improve my research.

To everyone at FMHs who have helped me in some way or another, of whom I cannot list all their names here. My special thanks go to Marina, Phil, Anna and Vivienne; for the conversations that I had with them have helped me improve my experimental outcomes. To the fellow PhD students and colleagues from other groups, Bhooma, Summan, Sindu, Samridhi, Chitra, Yogita, Nitin, Cyril and Maxinne for their friendship, and support. I also thank Louise, Lucy and Tamara for all the technical assistance they have provided me, and for being such a friendly and cooperative team to support the ongoing research and management of laboratory facilities.

To my friends outside of research, my besties Sadi, Hani, Ash, Katherine, Annisha, Shashi, Hansi and Thushari; I thank them all for the moral support and sincerity they have extended to me from the beginning to end of this journey. Their encouragement and positive outlook have helped me overcome times of turbulence during this journey.

To my friends and family, I thank them for their well wishes and blessings in support of my journey. Special thanks to my uncle, Mr. Jayantha Gangoda, my greatest inspiration who has been very influential on my academic and personal development, and to whom I always look up to. I thank him for his immense efforts and trust placed in me to pursue and complete my higher studies in Australia. His unconditional love and affection towards my family is what I

am truly and deeply grateful him the most for. I am sure he is very happy for what I have accomplished today.

To my mother in law, Mrs. Lalith Mallika Wickramasinghe, I thank her for her love, understanding, and all her endeavours in support of my studies. I also thank my sisters in laws, Thilini and Sandamali, my brother in law, Dasun; for their kind support and love towards my studies and life. I am so blessed to have them all in my life.

To my siblings, Sanuja, Ayesha and Dinuja, I thank them all for being so supportive, caring and loving. Their blessings and support has meant so much to me and I thank them all for being there for me no matter what, and for being wonderful siblings that they are.

To my parents, Chandra and Shanthi, and to my grandma, Mrs. Sirimangala Basnayake, for their unconditional love, compassion, blessings and guidance that I am fortunate to have in all endeavours throughout my life. I have no words to express how influential that they all have been to me in becoming who I am today, for which I am grateful ever for. For all the struggles that they have been through for me, I hope I have made them all proud on this day that I complete my Doctorate.

And to my loving husband, Sameera, for being the so supportive and caring husband that he is. His love, care and understanding have made me strong and resilient through the thick and thin in this journey. I thank Sameera for his love despite of me being so engrossed on work at times. His encouragement and positive vibe have always been instrumental for my continuous progress throughout this journey, even at times of stress. I thank him for all the colours he adds to my life that makes it more beautiful and joyful, and I am so blessed to have him in my life.

Publications

Theses

1. **Gangoda, SVS** Effects of HYPER on oxidative stress and inflammation in human coronary artery endothelial cells. Honours thesis, University of Technology Sydney, November 2012.

2. **Gangoda, SVS** High blood pressure and cyclic stretch alter cerebral amyloid deposition and endothelial function. Master of Research thesis, Macquarie University, October 2014.

Articles

3. Gupta V, Gupta VB, Chitranshi N, **Gangoda S**, Vander Wall R, Abbasi M, Golzan M, Dheer Y, Shah T, Avolio A, Chung R, Martins R & Graham S (2016) One protein, multiple pathologies: multifaceted involvement of amyloid β in neurodegenerative disorders of the brain and retina. *Cell. Mol. Life Sci.*, 1–19.

4. **Gangoda SVS**, Avadhanam B, Jufri NF, Sohn EH, Butlin M, Gupta V, Chung R & Avolio AP (2018) Pulsatile stretch as a novel modulator of amyloid precursor protein processing and associated inflammatory markers in human cerebral endothelial cells. *Sci. Rep.* **8**, 1689.

5. Avolio A, Kim MO, **Gangoda S**, Avadhanam B, Tan I, Butlin M, Adji A & O'Rourke M (2018) Cerebral hemodynamics: effects of systemic arterial pulsatile function and hypertension. *Curr. Hypertens. Rep.* **In press**.

Conference abstracts published in journals

6. **Gangoda SVS**, Jang SA, Jufri NF, Koo HJ, Butlin M, Avolio AP & Sohn EH (2014) Ethanol impairs expression of estrogen receptors and increases ICAM-1 and galectin-3 in human umbilical vein and cerebral microvascular endothelial cells. *Hypertension* **63**, e140–e173. (The Annual Scientific Meeting of The High Blood Pressure Research Council of Australia, Melbourne, Australia, November 2013)

7. **Gangoda SVS**, Butlin M, Gupta V & Avolio AP (2015) High Blood Pressure and Cyclic Stretch Alter Cerebral Amyloid Deposition and Endothelial Function. *J. Hypertens.* **65**, E35–E35. (The Annual Scientific Meeting of The High Blood Pressure Research Council of Australia, Adelaide, Australia, November 2014)

8. Avadhanam BRL, **Gangoda SVS**, Gupta V, Butlin M & Avolio AP (2015) Effect of Cyclic Stretch on Endothelial Nitric Oxide Synthase and Associated Cell Survival Pathways in Vascular Endothelial Cells. *J. Hypertens.* **65**, e25–e44. (The Annual Scientific

Meeting of The High Blood Pressure Research Council of Australia, Adelaide, Australia, November 2014)

9. **Gangoda SVS**, Butlin M, Gupta V, Chung R & Avolio A (2016) Pulsatile Stretch Alaters Expression and Processing of Amyloid Precursor Protein in Human Cerebral Endothelial Cells. *J. Hypertens.* **34**, e24. (The Annual Scientific Meeting of The High Blood Pressure Research Council of Australia, Victoria, Australia, December 2015)

10. Avadhanam B, **Gangoda S**, Butlin M, Vivek G & Avolio A (2017) Cyclic Stretch Frequency-modulated Response of Protein Expression Related to Nitric Oxide Release in Human Umbilical Vein Endothelial Cells. *Pulse* **5**, 7–81. (Pulse of Asia, Taipei, Taiwan, May 2017)

11. **Gangoda SVS**, Veppala B, Butlin M, Gupta V, Chung R & Avolio A (2017) Cyclic Stretch Mediates Changes in Amyloid Precursor Protein Expression and Nitric Oxide Signalling in Human Cerebral Endothelial Cells Pre-Exposed to a Glycosphingolipid Inhibitor. *Alzheimer's Dement.* **13**, P1304. (Alzheimer's Association International Conference, London, United Kingdom, July 2017)

12. **Gangoda S**, Veppala B, Butlin M, Gupta V, Chung R & Avolio A (2017) Pulsatile Stretch Alters Amyloid Precursor Protein Expression and Nitric Oxide Signalling in Human Cerebral Endothelial Cells Pre-Exposed to Glycosphingolipid Inhibition. *J. Hypertens.* **35**, e85. (The Annual Scientific Meeting of The High Blood Pressure Research Council of Australia, Victoria, Australia, December 2017)

Conference abstracts published in conference proceedings

13. **Gangoda SVS**, Jang SA, Jufri NF, Koo HJ, Butlin M, Avolio AP & Sohn EH Ethanol impairs expression of estrogen receptors and increases ICAM-1 and Galectin-3 in human umbilical vein and cerebral microvascular endothelial cells. The MQ BioFocus Research Centre Annual Interdisciplinary Research Conference, Sydney, Australia, December 2013.

14. **Gangoda SVS**, Butlin M, Gupta V, Chung R & Avolio AP Pulsatile stretch alters expression and processing of amyloid precursor protein in human cerebral endothelial cells. The European Meeting of Hypertension, Porte Maillot, Paris, June 2016.

15. **Gangoda SVS**, Avadhanam BRL, Butlin M, Sohn EH, Gupta V, Chung R & Avolio AP Amyloid precursor protein processing and inflammatory markers modulated by pulsatile stretch of human cerebral endothelial cells. Pulse of Asia, Seoul, Korea, September 2016.

16. **Gangoda SVS**, Avadhanam BRL, Butlin M, Sohn EH, Gupta V, Chung R & Avolio AP Pulsatile stretch modulates amyloid precursor protein processing and inflammatory markers in human cerebral endothelial cells. Alzheimer's Disease as a Neurovascular

Inflammatory Disorder Symposium, New York, The United States of America, December 2016.

17. **Gangoda SVS**, Avadhanam BRL, Butlin M, Gupta V, Chung R & Avolio AP Pulsatile stretch alters amyloid precursor protein expression and nitric oxide signalling in human cerebral endothelial cells pre- exposed to a glycosphingolipid inhibitor. European Society of Hypertension, Milan, Italy, June 2017.

18. **Gangoda SVS**, Butlin M, Gupta V & Avolio AP Pulsatile Stretch Leads to Elevated Amyloid Burden and Impaired Nitric Oxide Signalling in Human Cerebral Microvascular Endothelial Cells. Annual Encourage Research Symposium, Sydney, Australia, October 2017.

19. **Gangoda SVS**, Butlin M, Gupta V & Avolio AP Pulsatile stretch and proteins associated with Alzheimer's disease in human brain endothelial cells. Brisbane Life Science Early Career Research Symposium, Brisbane, Australia, November 2017.

20. **Gangoda SVS**, Avadhanam BRL, Butlin M, Gupta V, Chung R & Avolio AP Pulsatile stretch and pre-exposure to glycosphingolipid inhibition modulates amyloid precursor protein expression and nitric oxide signalling in cerebral endothelial cells. Cerebral Vascular Biology, Melbourne, Australia, November 2017.

Abstract

Alzheimer's disease (AD) is characterised by amyloid-β (Aβ) plaques arising from amyloid precursor protein (APP) processed by β secretase-1 (BACE-1). Increasing evidence suggests a role of vascular factors in AD, namely hypertension, elevated pulse pressure and arterial stiffness, all associated with increased vascular pulsatility imposing mechanical stretch on the endothelium. This thesis addresses the role of cyclic stretch on human cerebral microvascular endothelial cells (HCMECs) in expression and processing of APP. It also investigates effect of high salt diet on APP processing in rat brains, given associations of high salt diet and cognitive impairment. *In vitro* studies involved cultured HCMECs subjected to 0%, 5%, 10% or 15% stretch (18 hours, 1 Hz) and analysis of protein and RNA expression, nitric oxide and Aβ levels. *In vivo* study included treatment of rats with high (8% NaCl, HS) or a low (0.26% NaCl, control) for 10-13 weeks and examination of brain tissue. Established for the first time was that APP expression and Aβ secretion are altered in response to HCMECs stretch, and that this response is differentially mediated in early and late passage HCMECs. In late passage HCMECs, APP and BACE-1 expression increased 2-3-fold with 10 and 15% stretch compared to 0%, with proportional increases in Aβ42/Aβ40 with % stretch (R^2=0.21). In early passage HCMECs stretched at 15%, APP expression, BACE-1, Aβ42 levels were decreased 2-3-fold compared to late passage HCMECs. Glycosphingolipid inhibition prior to cyclic stretching at 15% increased APP expression and Aβ42 secretion 1-fold. I*n vivo* findings provide preliminary evidence of altered APP processing in HS rats compared to controls parallel with increases in markers of arterial stiffness. Overall results suggest a role of arterial stiffness and vascular pulsatility strengthening the evidence of vascular contributions to AD. Future studies identifying associated molecular mechanisms will provide novel therapeutic targets for AD.

Table of Contents

List of Abbreviations

Aβ	Amyloid-beta
ABC	Adenosine triphosphate-binding cassette
AD	Alzheimer's disease
ADAM	A-disintegrin-and-metalloproteinase
ADMA	Asymmetric dimethylarginine
AICD	Amyloid precursor protein intracellular domain
Akt	Serine/threonine-specific protein kinase
APOB	Apolipoprotein B-100
APP	Amyloid precursor protein
BACE-1	Beta-secretase 1
BAEC	Bovine aortic endothelial cells
BBB	Blood Brain Barrier
BCA	Bicinchoninic acid assay
BCEC	Bovine capillary ECs
BMEC	Brain microvascular endothelial cells
BMI	Body mass index
BP	Blood pressure
C-terminus	Carboxy terminus
CAA	Cerebral amyloid angiopathy
cAMP	cyclic adenosine monophosphate
cDNA	Complementary deoxyribonucleic acid
cGMP	Cyclic guanosine monophosphate
CSF	Cerebrospinal fluid
D-PDMP	Dl-threo-1-phenyl-2-decanoylamino-3-morpholino-1-propanol
DC	Dendritic cells
DMAPP	1S,2R-d-erythro-2-N-myristoylamino)-1-phenyl-1-propanol
DRMs	Detergent-resistant membrane fractions
ECM	Extracellular matrix protein
ECs	Endothelial cells
EDTA	Ethylene diamine tetraacetic acid
eNOS	Endothelial nitric oxide synthase
ERK	Extracellular signal-regulated kinase-1
FC	Frontal cortex
GAPDH	Glyceraldehyde 3-phosphate dehydrogenase
GSK	Glycogen synthase kinase
H and E	Hematoxylin and eosin
HASMC	Human airway smooth muscle cells
HC	Hippocampal
HCEC	Human capillary and microvascular endothelial cells
HCMEC-SV40	Human Cerebral Microvascular Endothelial Cells - SV40

HRP	Horse radish peroxidase
HS	High salt
HST	High salt treated with antihypertensive
HUVEC	Human umbilical vein ECs
ICAM-1	Intercellular cell adhesion molecule-1
IL-17	interlukin-17
ITGB3	Integrin β-3
L-NAME	N (G)-Nitro-L-Arginine Methyl Ester
LDH	lactose dehydrogenase
LMA	Late middle aged
LRP-1	Lipoprotein receptor-related protein 1
MAP	Mean arterial pressure
MDDC	Monocyte-derived-dendritic cells
mRNA	Messenger ribonucleic acid
NFT	Neurofibrillary tangles
NFκB	Nuclear factor kappa B
NMR	Nuclear magnetic resonance
NO	Nitric oxide
NOS	Nitric oxide synthase
N-terminus	Amino terminus
pAkt	Phosphorylated Akt
PASCs	Pulmonary arterial smooth muscle cells
PBS	Phosphate buffer solution
PDMS	Polydimethylsiloxane
PEN-2	Presenilin enhancer-2
peNOS	Phosphorylated eNOS
PET	Positron emission tomography
pGSK	Phosphorylated GSK
PI3K	Phosphoinositide 3-kinase
PKA	Protein kinase A
PrI	Propidium iodide
PSEN	Presenilin
PVDF	Polyvinylidene difluoride
RAGE	Receptor for advanced glycation end products
RIPA	Radioimmunoprecipitation assay
RNA	Ribonucleic acid
ROS	Reactive oxygen species
ROUT	robust regression and outlier removal
RT-qPCR	Real-time quantitative reverse transcription polymerase chain reaction
sAPPα	Soluble APP-alpha
sAPPβ	Soluble APP-beta
SBP	Systolic blood pressure

SD	Sprague-Dawley
SDS	Sodium dodecyl sulfate
SDS-PAGE	Sodium dodecyl sulfate polyacrylamide gel electrophoresis
SHR	Spontaneously hypertensive rat
SHR-SP	Spontaneously hypertensive stroke-prone rats
SHR-SR	Spontaneously hypertensive rat-stroke resistant
Smase	Sphingomyelinase
SNP	Sodium nitroprusside
SOD	Superoxide dismutase
TBS-T	Tris buffered saline-Tween
Tg	Transgenic
tMCAO	Transient middle cerebral artery occlusion
TNF-α	Tumour necrosis factor-alpha
TRP	Transient receptor potential
TRPV4	TRP-Vanilloid-4
WKY	Wistar Kyoto rat
β-turn-β	β-strand-turn-β-strand
Aβ	Amyloid-beta
ABC	Adenosine triphosphate-binding cassette
AD	Alzheimer's disease
ADAM	A-disintegrin-and-metalloproteinase
ADMA	Asymmetric dimethylarginine
AICD	Amyloid precursor protein intracellular domain
Akt	Serine/threonine-specific protein kinase
APOB	Apolipoprotein B-100
APP	Amyloid precursor protein
BACE-1	Beta-secretase 1
BAEC	Bovine aortic endothelial cells
BBB	Blood Brain Barrier
BCA	Bicinchoninic acid assay
BCEC	Bovine capillary ECs
BMEC	Brain microvascular endothelial cells
BMI	Body mass index
BP	Blood pressure
C-terminus	Carboxy terminus
CAA	Cerebral amyloid angiopathy
cAMP	cyclic adenosine monophosphate
cDNA	Complementary deoxyribonucleic acid
cGMP	Cyclic guanosine monophosphate
CSF	Cerebrospinal fluid
D-PDMP	Dl-threo-1-phenyl-2-decanoylamino-3-morpholino-1-propanol
DC	Dendritic cells

DMAPP	1S,2R-d-erythro-2-N-myristoylamino)-1-phenyl-1-propanol
DRMs	Detergent-resistant membrane fractions
ECM	Extracellular matrix protein
ECs	Endothelial cells
EDTA	Ethylene diamine tetraacetic acid
eNOS	Endothelial nitric oxide synthase
ERK	Extracellular signal-regulated kinase-1
FC	Frontal cortex
GAPDH	Glyceraldehyde 3-phosphate dehydrogenase
GSK	Glycogen synthase kinase
H and E	Hematoxylin and eosin
HASMC	Human airway smooth muscle cells
HC	Hippocampal
HCEC	Human capillary and microvascular endothelial cells
HCMEC-SV40	Human Cerebral Microvascular Endothelial Cells - SV40
HRP	Horse radish peroxidase
HS	High salt
HST	High salt treated with antihypertensive
HUVEC	Human umbilical vein ECs
ICAM-1	Intercellular cell adhesion molecule-1
IL-17	interlukin-17
ITGB3	Integrin β-3
L-NAME	N (G)-Nitro-L-Arginine Methyl Ester
LDH	lactose dehydrogenase
LMA	Late middle aged
LRP-1	Lipoprotein receptor-related protein 1
MAP	Mean arterial pressure
MDDC	Monocyte-derived-dendritic cells
mRNA	Messenger ribonucleic acid
NFT	Neurofibrillary tangles
NFκB	Nuclear factor kappa B
NMR	Nuclear magnetic resonance
NO	Nitric oxide
NOS	Nitric oxide synthase
N-terminus	Amino terminus
PASCs	Pulmonary arterial smooth muscle cells
PBS	Phosphate buffer solution
PDMS	Polydimethylsiloxane
PEN-2	Presenilin enhancer-2
PET	Positron emission tomography
PI3K	Phosphoinositide 3-kinase
PKA	Protein kinase A

PrI	Propidium iodide
PSEN	Presenilin
PVDF	Polyvinylidene difluoride
RAGE	Receptor for advanced glycation end products
RIPA	Radioimmunoprecipitation assay
RNA	Ribonucleic acid
ROS	Reactive oxygen species
ROUT	robust regression and outlier removal
RT-qPCR	Real-time quantitative reverse transcription polymerase chain reaction
sAPPα	Soluble APP-alpha
SBP	Systolic blood pressure
SD	Sprague-Dawley
SDS	Sodium dodecyl sulfate
SDS-PAGE	Sodium dodecyl sulfate polyacrylamide gel electrophoresis
SHR	Spontaneously hypertensive rat
SHR-SP	Spontaneously hypertensive stroke-prone rats
SHR-SR	Spontaneously hypertensive rat-stroke resistant
Smase	Sphingomyelinase
SNP	Sodium nitroprusside
SOD	Superoxide dismutase
TBS-T	Tris buffered saline-Tween
Tg	Transgenic
tMCAO	Transient middle cerebral artery occlusion
TNF-α	Tumour necrosis factor-alpha
TRP	Transient receptor potential
TRPV4	TRP-Vanilloid-4
WKY	Wistar Kyoto rat
β-turn-β	β-strand-turn-β-strand

Chapter 1

Introduction

Vascular factors are involved in many chronic diseases including Alzheimer's disease (AD), the foremost cause of dementia. Although vascular factors such as hypertension, elevated pulse pressure and arterial stiffness are associated risk factors for AD, and are cumulative with age, the principal non-modifiable risk factor for AD, their contributions towards AD are often underestimated [1–8]. Whilst it is starting to become accepted that AD is a multifaceted chronic disease, to date, reliable mechanisms underlying these vascular associations have not been established. Of note, hypertension and arterial stiffness could induce elevated pulse pressure within blood vessels that in turn could cause increased vascular pulsatility, inducing mechanical stretch of endothelial cells (ECs) that line the inner vascular walls [9,10]. Thus, vascular pulsatility is implicated in endothelial mechanotransduction that modulates gene and protein expression to maintain vascular homeostasis (Figure 1.1).

One of the major proteins implicated in AD is amyloid precursor protein (APP), which is expressed in a number of cell types including ECs [11]. APP gives rise to the neurotoxic peptide amyloid-β (Aβ), which becomes aggregated to form Aβ plaques, a clinical characteristic of AD [11]. APP is processed by secretases including β-secretase 1 (BACE-1), and a disintegrin and

metalloproteinase 10 (ADAM10), to release processed APP fragments including Aβ and soluble APPα, via the amyloidogenic and non-amyloidogenic pathways respectively [12,13].

Previous studies linking AD, stiffness and hypertension, highlighted a potential role of mechanical stretch that may affect APP processing pathways [2–8]. These associations indicate the multi-factorial nature of AD pathophysiology, and indicate the involvement of changes in structural properties of membranes in response to increased mechanical stretch of the vascular wall consequent of elevated pulse pressure that could in turn modulate the vascular architecture and function. This involves alterations in structural and functional proteins and lipids that compose cell membranes and signaling molecules that receive and transduce mechanical signals in response to vessel stretch, in particular those that are present in the vascular endothelium.

In line with this, it was hypothesised that cyclic mechanical stretch of cerebral ECs regulates proteins and lipids that are modified in AD (Figure 1.1). Within the scope of this thesis, the changes in membrane-associated proteins and signalling molecules such as APP, BACE-1, ADAM10, endothelial nitric oxide synthase (eNOS), intercellular cell adhesion molecule-1 (ICAM-1), glycogen synthase kinases (GSK-3), the serine threonine kinase, Akt, and caveolin-1, all of which are known to be involved in AD pathophysiology [11–18], are investigated in response to cyclic mechanical stretch in cerebral ECs (Figure 1.1).

Chapter 2 details the existing literature on this topic area. Chapter 3 describes the methodological approaches that have been optimised in this thesis, since cyclic stretching of human cerebral microvascular endothelial cell-SV40 (HCMEC) cell line to investigate protein and gene expression utilising the techniques used in this thesis has not been investigated to date in the ShellPa stretch device (Menicon Life Science, Japan), which is a relatively novel stretch system.

Mechanical stretch as a stimulus for APP processing in ECs has not been studied to date. Due to the possible role of mechanical stretch placed upon ECs subsequent of elevated vascular pulsatility, Chapter 4 (presenting the recent publication [19]) and Chapter 5 encompass the *in vitro* studies investigating whether cyclic stretch, magnitude dependently modulates APP, BACE-1, ADAM10, eNOS, GSK-3, Akt, and caveolin-1, and NO and Aβ levels in HCMECs of passage 17-19. Stretch magnitudes of 0%, 5%, 10% and 15% are compared at a frequency of 1 Hz within an 18-hour time duration, which provided an optimal protein yield for post-stretch analysis. A stretch magnitude of 5% is considered physiological and 15-20% stretch is considered pathological [20]. The frequency of 1 Hz represents a heart rate of 60 beats/minute, which is in the range of resting human heart rate. The degree of stretch (%) is defined the as relative elongation of the chamber.

A recent study demonstrated that APP processing is altered between early and late passage primary human brain microvascular endothelial cells [21]. Additionally, ageing is a predisposing factor for AD, whilst age related cerebrovascular disease is considered to contribute for AD, endothelial cell senescence is associated with age-related vascular diseases [1,22,23]. Chapter 6 includes a study that investigates whether the responses to cyclic stretching at a magnitude of 15% differ between early (Passage 7-9) and late (Passage 17-19) passage HCMECs in terms of APP and other associated proteins and signalling molecules including NO and Aβ.

Chapter 7 and Chapter 8 examine the effect of cyclic stretch in HCMECs pre-exposed to a biochemical stimulus. Since Aβ plays a central role in AD pathophysiology, Chapter 7 includes a study that explores changes in APP, BACE-1, ADAM10, eNOS, GSK-3, Akt, and caveolin-1, and NO and Aβ levels in HCMECs stretched at 15%, 1 Hz for 18 hours that were pre-exposed to an Aβ treatment. Sphingolipids such as ceramide are implicated in AD and the recent Baltimore Longitudinal Study of Ageing demonstrated that plasma ceramide and sphingomyelin levels were associated with risk of AD [14,15]. Accordingly, Chapter 8 investigates

changes in APP, eNOS, GSK-3, Akt, and NO and Aβ levels in HCMECs in response to cyclic stretch pre-treated with a glycosphingolipid inhibitor.

Hypertension, elevated pulse pressure and arterial stiffness are vascular risk factors for AD whilst, a diet rich in salt has been shown to induce hypertension, arterial stiffness and to lead to cognitive deficits [2–8,24,25]. Final chapter of the thesis (Chapter 9) presents a preliminary animal study that evaluates whether high salt diet consumption changes APP processing in the brain tissue of rats.

Taken together, this thesis investigates the relevance of cyclic stretch and arterial stiffness as modulators of APP expression and processing. Accordingly, the overall aims of this thesis are summarised below (Figure 1.1):

I. Establish cell culture, and protein and RNA extraction protocols in the ShellPa cell stretch device (Chapter 3)
II. Determine effect of cyclic stretch on APP and NO signalling (Chapter 4).
III. Investigate potential signalling pathways that mediate endothelial responses to cyclic stretch (Chapter 5)
IV. Study the effect of endothelial cell senescence and cyclic stretch on APP expression, amyloid secretion and NO signalling (Chapter 6)
V. Investigate stretch mediated endothelial changes in cerebral endothelial cells pre-exposed to Aβ (Chapter 7)
VI. Investigate stretch mediated endothelial changes and glycosphingolipid inhibition (Chapter 8)
VII. Study the effect of a high salt diet in rat brain tissue (as an animal model of arterial stiffness) on APP and eNOS (Chapter 9).

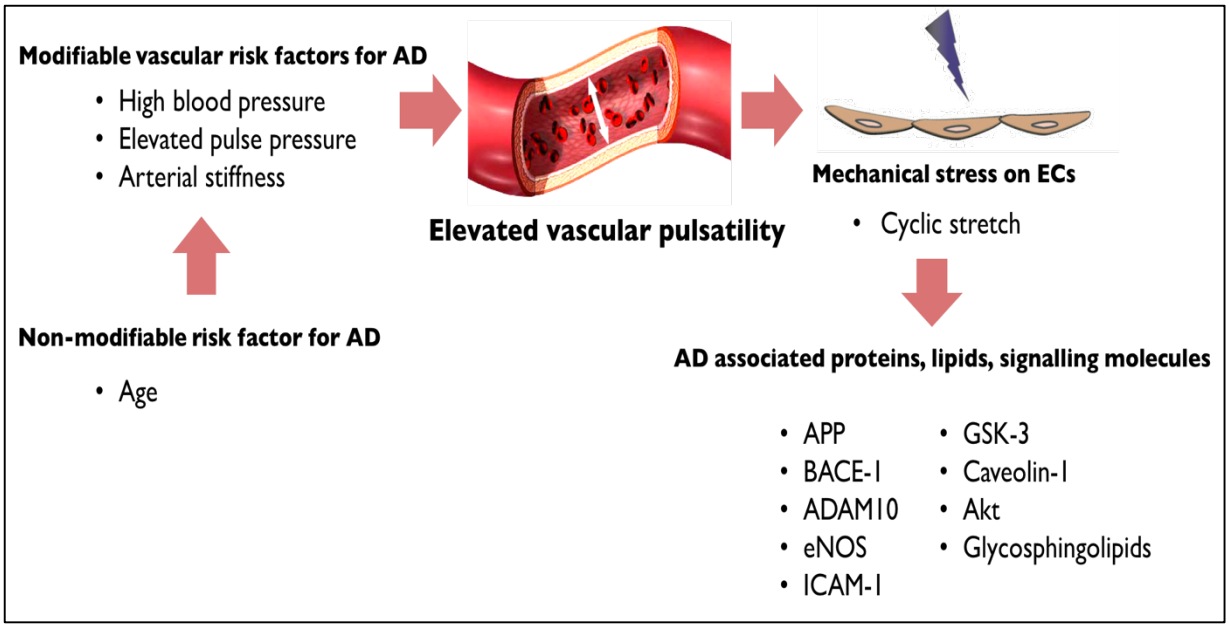

Figure 1.1 Summary of hypothesis of cell culture studies investigated in the thesis. High blood pressure, elevated pulse pressure and arterial stiffness are amongst the modifiable vascular risk factors for AD, all of which are accumulative with age, the greatest non-modifiable risk factor for AD. These vascular factors could elevate vascular pulsatility that eventuate mechanical stress on endothelial cells. Resultant mechanical stretch on ECs could be implicated in investigating cyclic stretch as a mechanistic stimulus that regulates proteins, lipids and signalling molecules that are associated with AD including APP, BACE-1, ADAM10, eNOS, ICAM-1, GSK-3, caveolin-1, Akt and glycosphingolipids. Abbreviations: AD, Alzheimer's disease, APP, amyloid precursor protein, ADAM10, a disintegrin and metalloproteinase 10, BACE-1, β-secretase 1, ECs, endothelial cells, eNOS, endothelial nitric oxide synthase, ICAM-1, intercellular cell adhesion molecule-1, glycogen synthase kinase-3, GSK-3.

Chapter 2

Literature Review

2.1 Alzheimer's disease (AD)

Alzheimer's disease (AD) is the most prevalent cause of dementia accounting for 60-80% of all dementias [1]. Dementia is a syndrome that results in cognitive impairment which, according to the World Health Organisation, is estimated to increase by 10 million cases every year globally [26]. The numbers are considerably increasing as a consequence of the ageing population, lack of effective treatments and adequate diagnostic techniques. Due to the significant disease burden and the impact on disability, AD, the foremost cause of dementia, has attracted considerable attention in research and is yet to be addressed adequately [1,11,27].

Amyloid plaques and neurofibrillary tangles (NFT) in the brain are well known characteristics of AD (Figure 2.1) [11]. These were first described by Dr. Alois Alzheimer "as miliary foci scattered throughout the cerebral cortex due to the deposition of a peculiar substance" after examining the post-mortem brain tissue of his patient Auguste D, who suffered from AD and died in 1908 [11,28]. Later on, during the mid to late 1980s, it was discovered that these deposits are mainly composed of the small peptide called amyloid-β (Aβ), which is 39-42 amino acid-long, while the intraneuronal NFTs comprise aggregates of abnormally hyperphosphorylated

tau protein [29,30]. According to the 'Amyloid hypothesis', Aβ accumulation is thought to be central to AD pathophysiology [31,32]. Herein, Aβ will be discussed as it forms the platform for the current thesis.

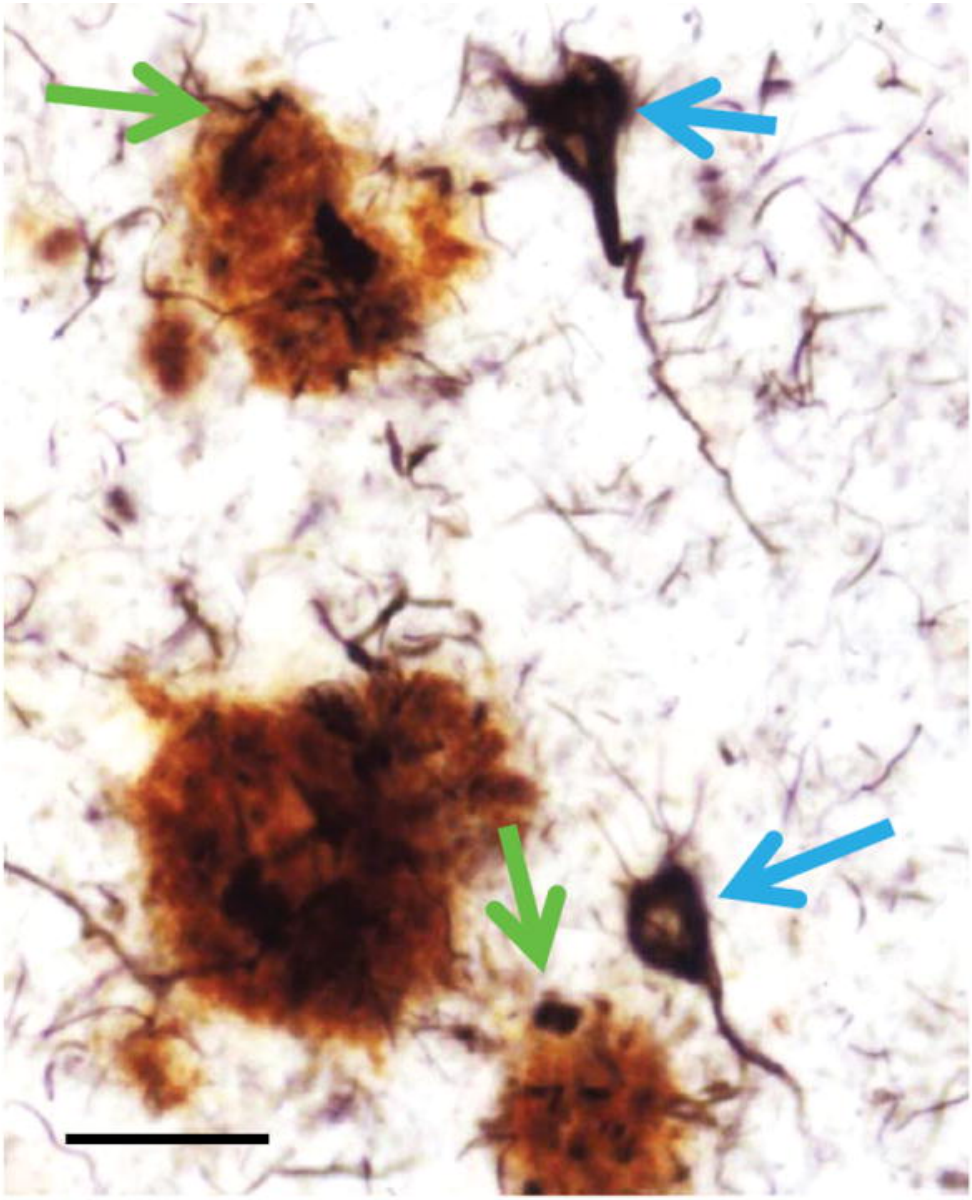

Figure 2.1 Immunohistochemically double-stained photomicrograph of a cerebral neocortical section from an AD brain for Aβ and microtubule-associated protein tau. Reddish brown deposits (blue arrows) represent Aβ plaques, which are extracellular while the black deposits that are developed within neurons represent NFTs (green arrows). The dystrophic neurites present in the Aβ plaques termed 'neuritic plaques' indicate aberrant tau pathology seen in AD. Scale bar = 50 μm. (From Nelson *et al.* [33] with permission). Abbreviations: Aβ, amyloid beta; AD, Alzheimer's disease; NFT, neurofibrillary tangles

2.2 Amyloid deposits

Amyloid deposits, or Aβ plaques, have been observed in a number of post-mortem tissue specimens including the brain, kidneys, spleen and liver as "lardaceous" or "waxy" substances as early as the 1700's [34]. Due to the starch-like appearance of these deposits, they were misidentified as starchy material and incorrectly named as 'amyloid' (literally meaning "starch-like") [34]. However, it is now known that amyloid deposits are self-propagating protein aggregates that are rich in β-sheet structure, which will be discussed in detail in section 2.2.2.

2.2.1 Aβ production

Aβ peptides are proteolytic cleavage products of the amyloid precursor protein (APP), which is a transmembrane protein expressed in a number of cell types including endothelial cells (ECs) [35]. APP is cleaved and processed by a number of enzymes. These include α-secretases, such as a disintegrin and metalloproteinase (ADAM)-family enzymes (e.g. ADAM9, ADAM10 and ADAM17), β-secretases (e.g. β-secretase 1 (BACE-1)), and γ-secretases (e.g. presenilin (PSEN) 1 or 2; Figure 2.2) [12,13]. Importantly, mutations of both *APP* and *PSEN* genes have been shown to be associated with familial AD, which typically present before the age of 65, suggesting APP cleavage plays a critical role in the pathogenesis of AD and thus supporting the amyloid hypothesis [36,37]. The cleavage and processing of APP occur in two distinct pathways, namely, non-amyloidogenic and amyloidogenic pathways [30]. As implied by the names, the former does not result in Aβ secretion while the latter does.

Briefly, the non-amyloidogenic pathway is the common pathway of APP cleavage, in which α-secretases produce a large amino (N)-terminal ectodomain, soluble APPα (sAPPα), 83 amino acids away from the carboxyl (C) terminus, which is then secreted into the extracellular medium. This 83-amino-acid-long C terminal fragment known as C83 is retained in the

membrane to be cleaved off by γ-secretases to produce the short fragment p3 at a subsequent stage. Notably, the initial cleavage of APP by α-secretases occurs within the Aβ domain, thus formation of Aβ is prevented (Figure 2.2) [30].

In contrast, the amyloidogenic pathway is an alternative APP cleavage pathway that leads to Aβ generation. In this pathway, the proteolysis is initiated by β-secretases rather than α-secretases, 99 amino acids away from the C terminus [30]. This cleavage releases soluble APPβ (sAPPβ) into the extracellular space, subsequently leaving the 99-amino-acid C-terminal stub, known as C99, anchored to the membrane [30,38]. The C99 fragments, which have N termini corresponding to the first amino acid of Aβ, are then cleaved off by γ-secretases between 38 and 43 residues liberating intact Aβ peptides (Figure 2.2), which could be in soluble or fibrillar forms (discussed in 2.2.2) [30].

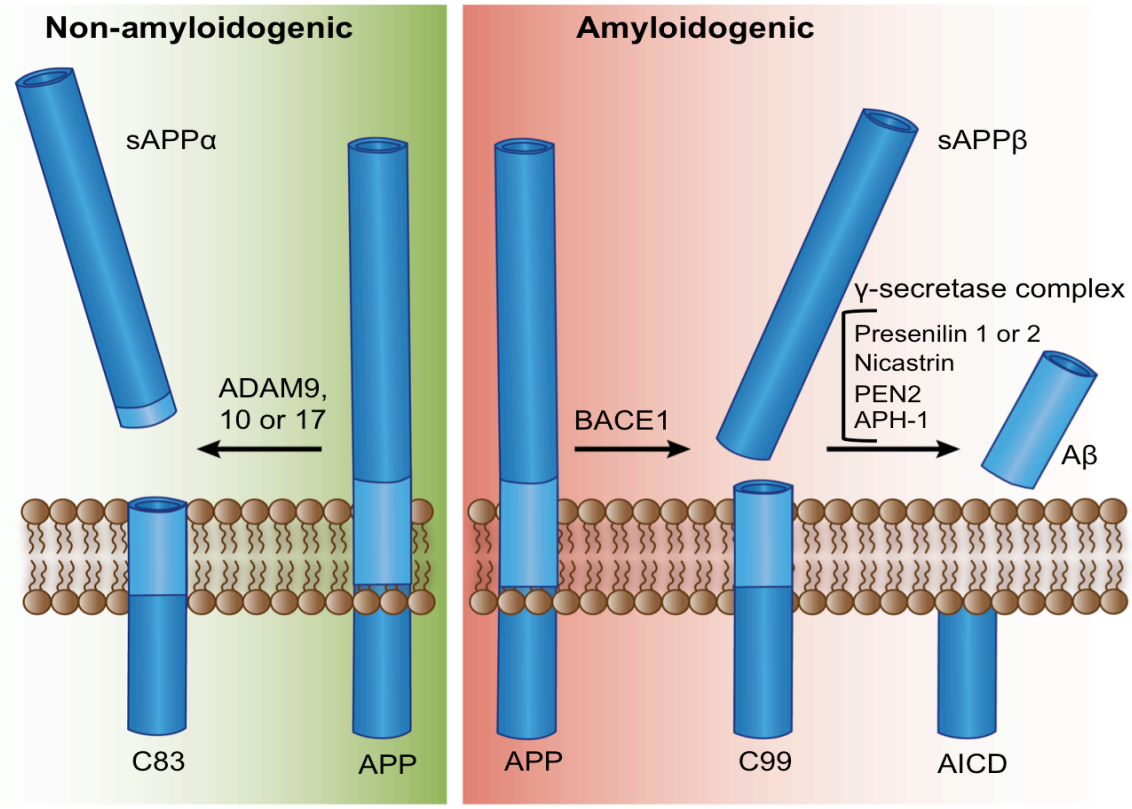

Figure 2.2 Non-amyloidogenic and amyloidogenic processing of APP. APP is cleaved into sAPPα and C83 residue by ADAM9, 10 or 17 in the non-amyloidogenic pathway (left). In contrast, in the amyloidogenic pathway (right), APP is first cleaved into sAPPβ and C99 residue by BACE-1. The C99 fragment is then further cleaved off by the γ-secretase complex including PSEN 1 or 2, nicastrin, PEN2 and APH-1 into AICD and intact Aβ peptides (Modified from LaFerla *et al.* [30]). Abbreviations: Aβ, Amyloid beta; ADAM, a-disintegrin-and-metalloproteinase; AICD, amyloid precursor protein intracellular domain; APH-1, anterior pharynx-defective 1; APP, amyloid precursor protein; BACE-1, β secretase 1; PEN-2, presenilin enhancer-2

2.2.2 Structures of Aβ

The majority of the resulting Aβ peptides through amyloidogenic processing of APP are 40 amino acids long (Aβ40), but approximately 10% are the 42-amino-acids-long variant (Aβ42). Notably, both Aβ42 and Aβ40 peptides can lead to the formation of many toxic aggregated structures including oligomers, protofibrils and fibrils that are found within AD-lesions (Figure 2.3 & Figure 2.4) [39–42]. However, Aβ42, which is more hydrophobic, is more prone to the formation of fibrils, which predominate in senile plaques [39–43]. Aβ42 has also demonstrated a higher propensity to form amyloid fibrillar aggregates *in vitro* [39–43]. Given the significant contribution of Aβ42 and Aβ40 to plaque formation in AD, their structures have been extensively studied to elucidate aggregation pathways involved and in developing novel therapeutics [39–43].

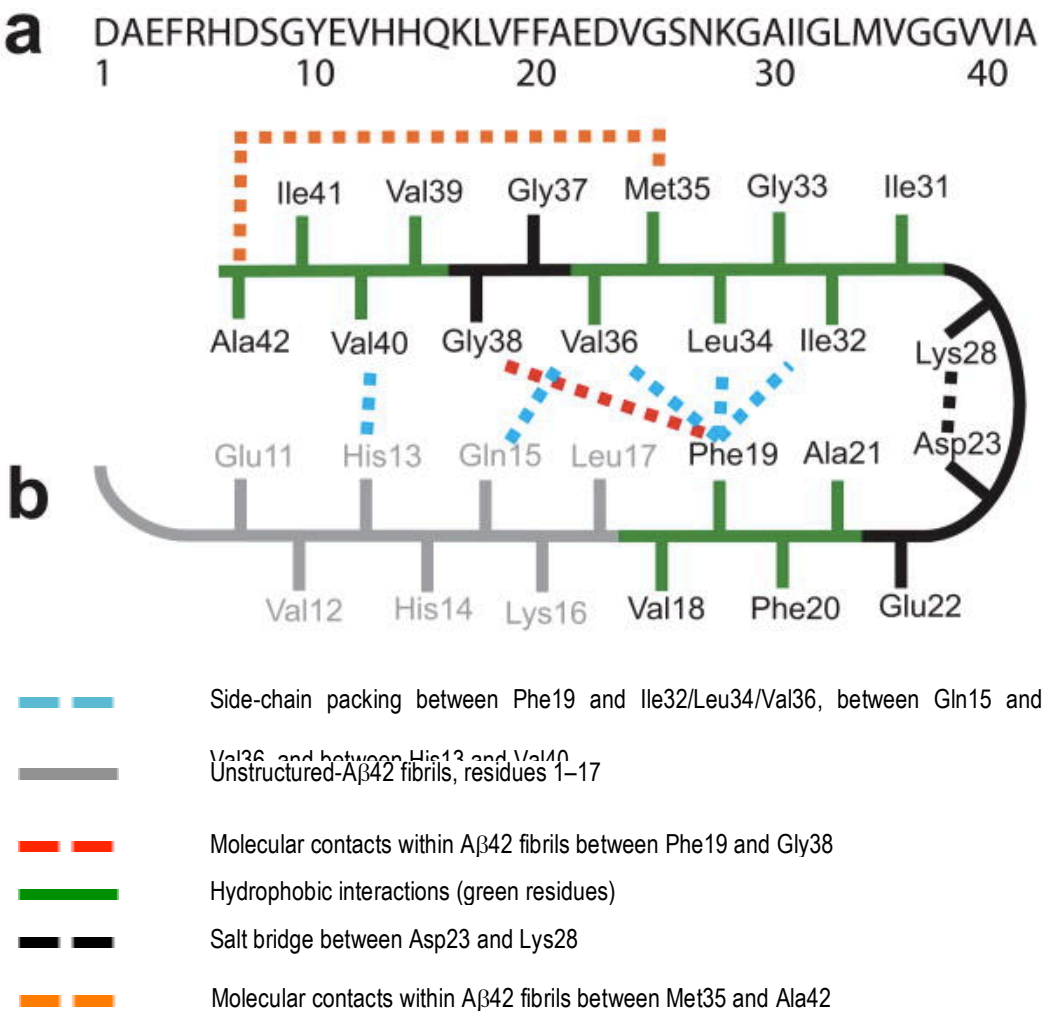

Figure 2.3 Sequence and structure of the Aβ40 and Aβ42 peptide fibrils. (a) Human APP-derived-Aβ42 sequence. (b) Structures of Aβ40 and Aβ42 fibrils indicated by NMR results. Aβ40 fibrils comprise unstructured residues 1–10 and β-turn-β fold adopted-residues 11–40. In contrast, Aβ42 fibrils may comprise unstructured residues 1-17 with a β-turn-β fold structure with residues 18-42. β-sheets are defined as a typical secondary structure of proteins that are made of β strands, a polypeptide chain of commonly of 3-10 amino acids with the backbone in an extended confirmation, connected laterally via hydrogen bonds on the backbone of a polypeptide. (From Ahmed *et al.* [40] with permission). Abbreviations: Aβ, amyloid beta; NMR, nuclear magnetic resonance

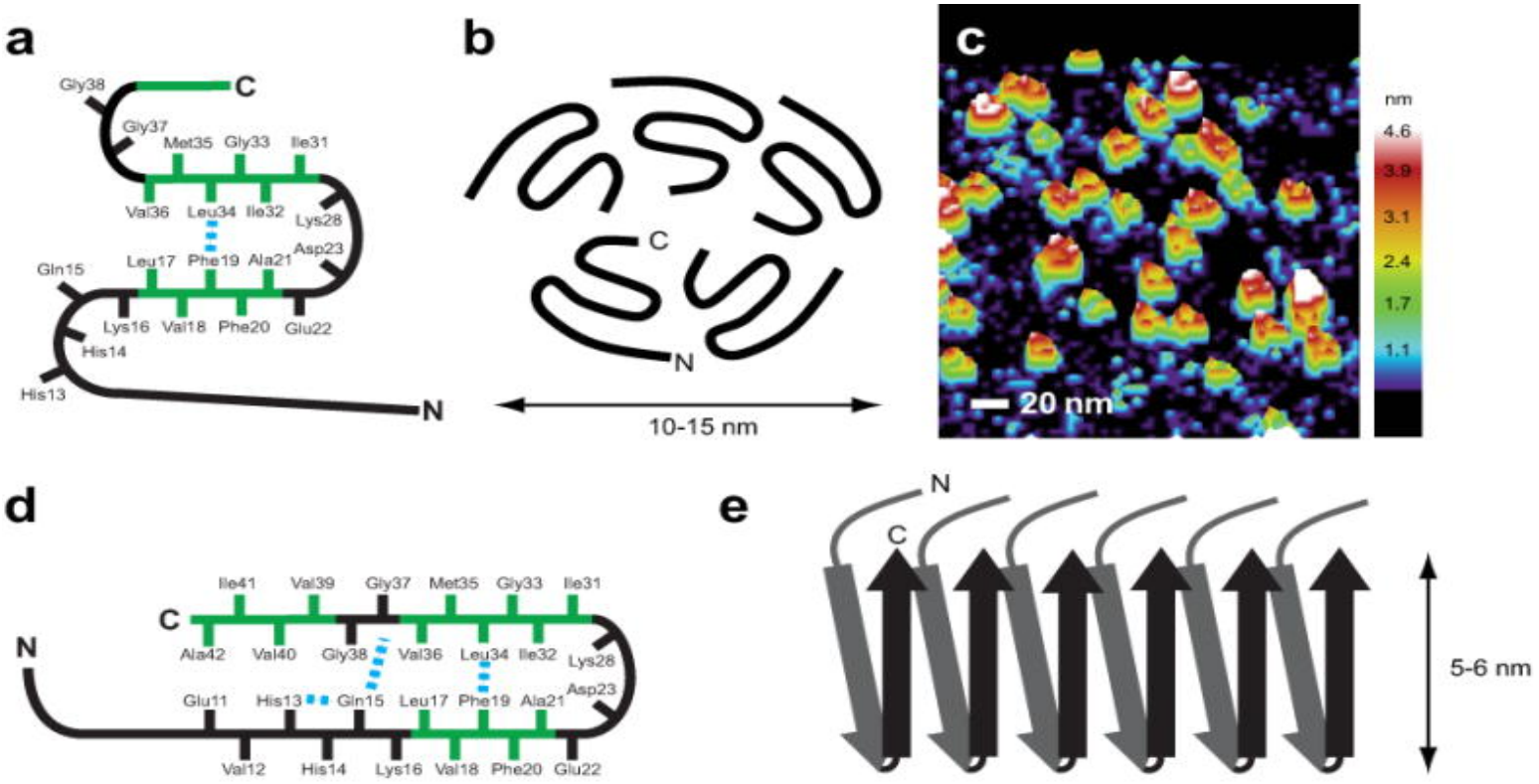

Figure 2.4 Molecular representations of Aβ42 oligomers and fibrils. (a) Schematic representation of the monomer unit in the oligomer structure of Aβ42, in which solid-state NMR measurements have demonstrated that Phe19 interacts with Leu34. (b) Schematic of the Aβ42 pentamer based on size exclusion chromatography and atomic force microscopy and solvent accessibility. (c) 3D image of the Aβ42 oligomers obtained through AFM. (d) Schematic representation of the monomer that makes up Aβ42 fibrils. (e) The parallel and in-register packing orientation and staggering of the individual β-strands in a single protofibril, which combine to form mature fibrils. (From Ahmed *et al.* [40] with permission). Abbreviations: Aβ, amyloid beta; AFM, atomic force microscopy; NMR, nuclear magnetic resonance

Despite Aβ42 being considered the predominant contributor to AD plaques, presence of neurotoxic intermediates of Aβ40 prior to fibril formation have also been demonstrated by solid-state nuclear magnetic resonance (NMR) and electron microscopy [39]. Native Aβ peptides undergo conformational changes into spherical amyloid intermediates of 15-35 nm diameters [39]. These intermediates predominate parallel β-sheet structures that define misfolded amyloid conformations as indicated by structural comparison with Aβ fibrils [39]. Moreover, they have shown higher toxicity than fibrils in *in vitro* neurotoxicity assays in PC12 cells, a clonal cell line originating from the rat adrenal medulla [39,44].

Similar to other amyloid fibrils, Aβ fibrils consist of a cross-β structure, in which the β-strands are aligned perpendicular to the fibril axis [40]. Aβ42 fibrils comprise an N-terminus that is considered to be unstructured and two hydrophobic β-strand fragments with a parallel and in-register orientation. Figure 2.3 shows how the two β-strand regions could fold into a β-strand-turn-β-strand (β-turn-β) conformation. As suggested by mutational studies, β-turn-β conformation is possible as Phe19 on the N-terminal β-strand being able to pack against Gly38 on the C-terminal β-strand [40]. Based on NMR studies, the possibility of the C-terminal β-strand bending at Gly37/38 to allow Ala42 to contact the side-chain of Met35 has also been proposed [40].

Aβ42 models are considered to be comparable to those of Aβ40 based on solid-state NMR and scanning-tunnelling EM measurements [40]. Aβ40 fibrils also comprise an unstructured region at residues 1-10 while the rest of the residues form a staggered β-turn-β unit stabilized by a salt-bridge between Asp23 and Lys28 [40]. However, its intra-strand contacts are different to those of Aβ42, such that Phe19 interacts with Leu34, Gln15 interacts with Val36, and His13 interacts with Val40 (Figure 2.4) [40]. It has also been demonstrated that Aβ40 could have two or three β-turn-β units depending on whether the fibril is of a striated-ribbon or a twisted morphology [45]. The former showed two-fold symmetry with intermolecular contacts

between Met35 and Gly33 and between Ile31 and Gly37, whereas the latter exhibits three-fold symmetry with inter-molecular contacts between Ile31 and Val39 [45]. In both these structures, the β-turn-β units stack in a parallel and in-register orientation with relatively similar conformations [45]. Aβ aggregates can be cleared from the brain through different mechanisms as outlined in section 2.2.3.

2.2.3 Aβ clearance mechanisms

The APP-derived Aβ peptides via the amyloidogenic pathway are removed from the brain through two major mechanisms: efflux and proteolytic degradation. Intact soluble Aβ are cleared through either of these mechanisms while fibrillar Aβ are cleared predominantly through proteolytic degradation. The efflux of soluble Aβ involves crossing the blood brain barrier (BBB) either to enter the circulation, or from interstitial fluid of the brain parenchyma into the cerebrospinal fluid (CSF) [46–54]. The former is mediated by receptors such as low-density lipoprotein receptor-related protein 1 and p-glycoprotein efflux pump, while the latter is through bulk flow of interstitial fluid/ CSF, facilitated by the water channel aquaporin-4 [51–54]. These efflux mechanisms are considered to be either facilitated or inhibited through binding of chaperone proteins, such as ApoE, ApoJ, α2-macroglobulin, transthyretin and albumin [55]. The cleared-Aβ entered into the bloodstream could also be transported back into the brain via receptor for advanced glycation end products (RAGE)-mediated Aβ influx [56–58]. Fluctuations in plasma and CSF Aβ42 levels have been attributed as predictors of disease progression of AD from a cognitively healthy stage to early mild cognitive impairment stage (Figure 2.5) [47,59]. As summarised in Table 2.1, Aβ pools from different sources are also altered between cognitively normal and AD patients [59].

Table 2.1 Sources of Aβ and comparison of Aβ species between cognitively normal individuals and AD patients

Source of Aβ	Aβ species	Elderly people with normal cognition	AD patients
Brain grey matter	$A\beta_{40}$ $A\beta_{42}$	0.2 μg/g 0.8 μg/g	0.6 μg/g 6.1 μg/g
Brain white matter	$A\beta_{40}$ $A\beta_{42}$	0.1 μg/g 0.4 μg/g	1.1 μg/g 1.1 μg/g
Plasma	$A\beta_{40}$ $A\beta_{42}$	344.41 pg/ml 124.71 pg/ml	424.06 pg/ml 139.91 pg/ml
Liver	$A\beta_{40}$ $A\beta_{42}$	8.6 ng/g 67.5 ng/g	1.7 ng/g 15.5 ng/g
Packed quiescent platelets	$A\beta_{40}$ $A\beta_{42}$	84.0 ng/ml 1.7 ng/ml	NA NA
Packed activated platelets	$A\beta_{40}$ $A\beta_{42}$	56.8 ng/ml 1.6 ng/ml	NA NA
Skeletal muscle	$A\beta_{40}$ $A\beta_{42}$	29.8 ng/g 10.2 ng/g	37.8 ng/g 15.7 ng/g

In addition, ^{11}C-labelled Pittsburgh compound-B (PIB) labelled positron emission tomography (PET) imaging in human cohorts with *PSEN* mutations have shown elevated ratio of Aβ42/Aβ40 in the CSF, whilst in cognitively normal human cohorts with Aβ pathology, Aβ42/Aβ40 was reduced in the plasma, which was suggested to be a surrogate marker for Aβ deposition (Figure 2.5) [46,47]. A recent study has reported evidence of the potential of plasma based biomarkers including $APP_{669–711}/A\beta_{42}$ and $A\beta_{40}/A\beta_{42}$ ratios measured by immunoprecipitation coupled with mass spectrometry, in predicting Aβ burden comparable to the standard PIB-PET technique [60].

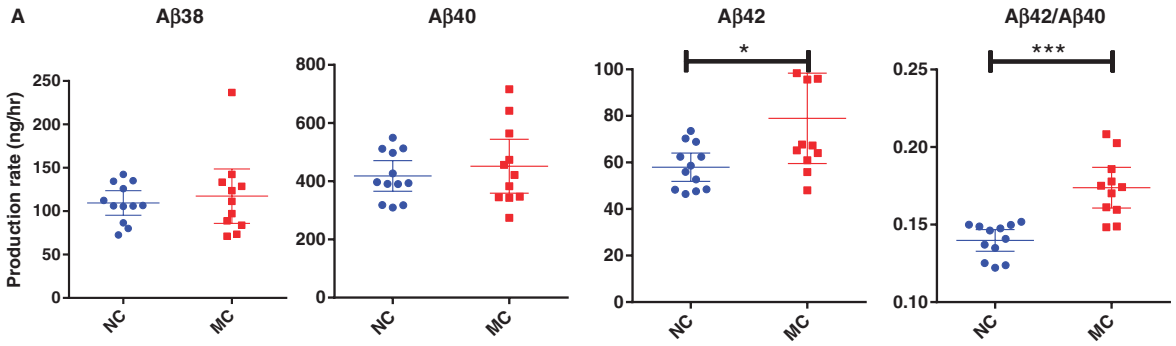

Figure 2.5 Rate of CSF Aβ production in carriers and non-carriers of *PSEN* mutation. Both Aβ42 levels and Aβ42/Aβ40 ratio were shown to be elevated in *PSEN* mutation carriers compared to non-carriers. (From Potter *et al.* [47] with permission). Abbreviations: Aβ, amyloid beta; CSF, cerebrospinal fluid; MC, mutation carriers; NC, non-mutation carriers; PSEN, presenilin

In the normal brain, the accumulation of Aβ is prevented through adequate regulation of APP processing and clearance. However, in the AD brain, these processes are thought to be disrupted, leading to consequent plaque formation (Figure 2.6) [57]. This is considered to occur via several mechanisms: cleavage of APP to Aβ over-expression of APP, and reduced clearance of Aβ from the central nervous system, as evidenced by mutational studies of familial AD [12]. However, this may not be the same in the case of sporadic AD, as numerous clinical trials that have been conducted to test the efficacy of drugs targeting these mechanisms to compensate the accumulation of Aβ have been unsuccessful [61]. Thus far, the exact relationship between Aβ accumulation and AD has not been established in terms of whether this accumulation is a causative factor or whether it is a result of the disease process itself. Although the 'Amyloid hypothesis' remains unproven, and regardless of the failure of numerous clinical trials, it is still of great importance for investigating the role of Aβ in the pathogenesis of AD.

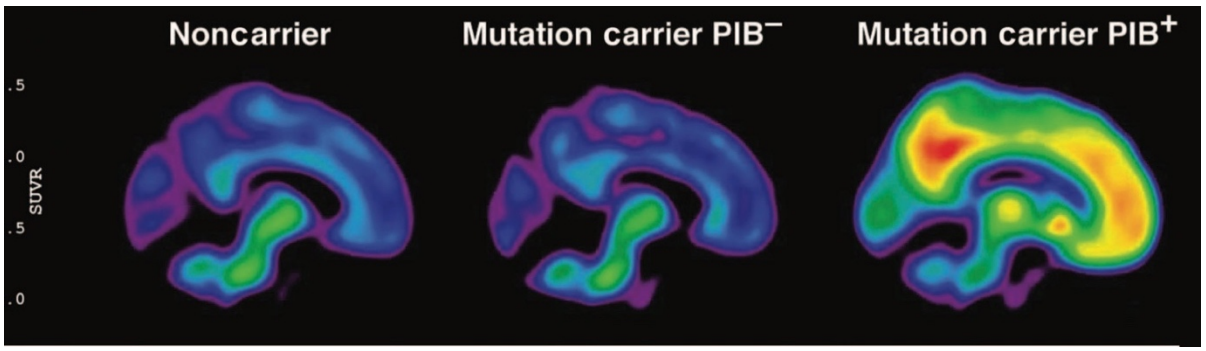

Figure 2.6 PET images in the presence or absence of, an amyloid tracer PIB, in brains of *PSEN* mutation carriers versus non-carriers. PIB^+ regions (right) in the brain image of the mutation carrier are indicative of amyloid deposits compared to the non-carrier brain (left) and the negative control image of the mutation carrier (PIB^-, middle). (From Potter *et al.* [47] with permission). Abbreviations: PET, positron emission tomography; PIB, Pittsburgh compound B

Notably, two types of Aβ plaques associated with AD have been defined in the literature [62,63]. These are perivascular and neuritic/senile plaques, which are respectively associated with blood vessels and the parenchyma [62,63]. Despite the presence of both types, the majority of the studies have been performed to investigate mainly neuritic/senile plaques rather than perivascular plaques [63]. However, the perivascular plaque has recently gained much contemplation as blood flow, which is impaired in AD, is involved in the clearance of Aβ, thus highlighting a possible role in the pathogenesis of AD [64]. Perivascular Aβ plaque formation, which is also termed 'cerebral amyloid angiopathy' (CAA), is the accumulation of Aβ surrounding cerebral blood vessels including arteries, arterioles, and capillaries [63,65]. Of the milieu of vascular effects associated with CAA, endothelial dysfunction is of major attention, which refers to impaired endothelium-dependent vasodilation due to depleted bioavailable nitric oxide (NO) reservoirs [66].

In 1997, Thomas *et al.* demonstrated that treating intact bovine cerebral arteries with Aβ40 resulted in endothelial dysfunction [67]. This was characterised by enhanced vasoconstriction and diminished vasodilation shown by measuring the % contraction and relaxation of the vessels with and without the Aβ40 treatment. Aβ40-mediated vasoactive effects were reversed

by antioxidants such as superoxide dismutase, indicating the possible involvement of oxidative stress. Endothelial damage was further demonstrated by electron micrographs. These vasoactive effects were suggested to be due to an imbalance between NO and superoxide radicals, which in turn resulted in endothelial dysfunction [67]. Another study also demonstrated similar vasoconstrictive effects *in vivo* utilising intra-arterial infusion of solubilised Aβ40 in rats, in which Aβ40 was shown to be associated with decreased cerebral blood flow and cerebrovascular resistance measured using fluorescent microspheres. This was also suggested to be mediated via the same mechanism described in the previous study [67].

These two studies along with many other studies have elucidated that Aβ is associated with cerebrovascular dysfunction [67–70]. Cerebrovascular dysfunction has been suggested to be an early event in AD, which could be initiated by oxidative stress [69,70]. This in turn is considered to lead to a vicious cycle of oxidative stress and further Aβ deposition [70]. Vascular parameters contributing to AD are discussed in Section 2.3.

2.3 Vascular risk factors in AD

Vascular parameters that orchestrate the milieu of AD and, that form the backbone of this thesis, are emphasised in this section. Amongst the many AD-related risk factors, hypertension is known to be a vascular contributor to AD pathophysiology [3,71]. It is also known that in hypertension, endothelial dysfunction plays a major role in its pathophysiology [72]. Large artery stiffening is another risk factor implicated in AD, where endothelial dysfunction is evident and that is also present in the milieu of hypertension [7,72,73]. Large artery stiffness refers to the loss of elasticity of the vascular wall of conduit arteries such as the aorta, due to changes in collagen and elastin composition that make up the vessel walls. Elevated pulse pressure, a marker of large artery stiffness and is evident in hypertension, is also associated with AD [74].

2.3.1 Hypertension, vascular stiffness and pulsatility

Hypertension is a major factor amongst the many risk factors that are concomitant with AD [2,8,75,76]. In line with this, studies have demonstrated a higher brain Aβ burden in hypertensive animal models [3,77–80]. In the mouse model of AD, Tg2576 mice, in which Aβ is elevated both in the brain and blood, angiotensin II administration via slow pressor osmotic mini pumps for two weeks at the age of 6-8 months, induced hypertension and led to increased Aβ deposition in the brain [3]. Increases in β-C terminal fragment, indicative of enhanced cleavage of APP by BACE-1, in the neocortex of wild type mice was also reported in response to angiotensin II administration [3]. The representative rat model of chronic hypertension, stroke, and progressive dementia, the spontaneously hypertensive rat-stroke resistant (SHR-SR), showed age-dependent positive intracellular and extracellular Aβ staining in ipsilateral and contralateral cerebral cortex and hippocampus at 6, 12, and 18 months of age after transient middle cerebral artery occlusion (tMCAO) [77]. SHR-SR-tMCAO rats were treated with a low and high dose of telmisartan [77], a pleiotrophic metabo-sartan with anti-neuroinflammatory, anti-neurotoxic and blood pressure lowering effects, which decreased the elevated intracellular and extracellular Aβ in SHR-SR-tMCAO in a dose dependent manner [77]. Additionally, the high-dose telmisartan induced the expected significant blood pressure lowering effect [77]. Further supporting these data, age dependent increases in cortical extracellular deposition of Aβ and APP expression were observed in non-transgenic spontaneously hypertensive stroke-prone rats (SHR-SP) compared to Wistar Kyoto (WKY) rats [79]. The deposition of Aβ was represented by lectin staining and plasma protein immunocytochemistry while the protein expression was evaluated using western blotting [79]. In ocular hypertensive models of rat glaucoma, up-regulation of caspase-3-mediated APP cleavage in hypertensive retina relative to control retina has been reported [81]. Consistently, another study showed significant increases in hippocampal Aβ42 coincident with elevated mRNA expression levels of receptor for advanced glycation end products, and BACE-1 in SHR compared to WKY rats [80]. The

mRNA and protein expression of LRP-1 were down-regulated in contrast to APP, which were up-regulated [80]. The mRNA was analysed using agarose gel electrophoresis while protein was analysed using western blotting [80]. However, these differences did not reach a statistical significance [80]. Nonetheless, these results, together with the other studies described, provided additional confirmatory evidence that altered APP processing and/or expression was associated with hypertension [77,79,81].

The involvement of hypertension in AD could be attributed to haemodynamic factors such as blood flow, which according to "peripheral sink theory" is eventually involved in the clearance of APP-derived Aβ peptides [55,56]. Additionally, haemodynamic factors such as pulsatility index and pulse pressure were positively correlated with AD [74,82]. These two factors are independent markers of vascular stiffness [8,74,83,84]. Vascular stiffness has also been shown to be associated with hypertension and reported to play a role in initiating the cognitive deficits in AD [2,8,85–90]. Together, these findings suggest a possible role of mechanical effects of hypertension, such as elevated microvascular stretch in AD, supported by the assumption that positive correlation of increased pulsatility index, pulse pressure and/or stiffness with AD would presumably coincide with increased mechanical stretch in the microvessels. Thus, one implication that large artery stiffness, hypertension and/or elevated pulse pressures collectively or independently, is that transmission of vascular pulsations into microvessels that are physiologically not designed to undergo elevated pulsations. This means that microvessels that supply end organs such as the brain become pulsatile and could be damaged, resulting in impaired blood supply due to elevated mechanical stretch resultant of vascular pulsatility.

Importantly, mechanical stretch was shown to proportionally induce vascular stiffness *in vivo* and *in vitro* [88,91]. This was indicated by augmented collagen deposition or expression in hypertension-induced rats by angiotensin II infusion and in cultured aortic fibroblasts after being subjected to mechanical stretch respectively [88,91]. Therefore, mechanical stretch may

proportionally induce changes in vascular stiffness [88]. Similar effects imposed by elevated mechanical stress were shown by fractal analysis of pressure-fixed aortic sections stained for elastin [91]. Increased loss of medial elastin function, which is a characteristic of wall stiffness, was concomitant with cumulative effect of pulsations [91].

Concordantly, the relationship between intra-arterial blood pressure, mechanical stretch and wall stiffness was reported as early as in the 1970s [92]. It was stated that increases in intra-arterial pressure imposed greater wall stiffness by establishing a length-tension relationship in helically cut strips of canine cerebral, coronary, mesenteric, renal, and femoral arteries after being stretched [92]. Apart from the role of elevated mechanical stretch in systemic high blood pressure, it was also demonstrated to be involved in intracranial or intraocular blood pressure-related pathologies such as normal pressure hydrocephalus, traumatic brain injury and glaucoma. These pathologies are also related to AD-characteristics [81,93,94]. Notably, normal pressure hydrocephalus itself is a subtype of dementia, whilst traumatic brain injury is a risk-factor for AD [95,96]. These studies further stressed that mechanical stretch could be involved in the pathogenesis of AD.

Taken together, previous studies linking AD, stiffness and hypertension consistently highlighted a possible role of mechanical stretch that may affect APP processing pathways. These associations indicate the multi-factorial nature of AD pathophysiology, suggesting an involvement of changes in structural properties of membranes in response to increased mechanical stretch of the vascular wall due to elevated pulse pressure that could in turn modulate the vascular architecture. This includes changes in structural and functional proteins and lipids that compose cell membranes and signalling molecules that receive and transduce mechanical signals in response to vessel stretch. In particular, proteins and lipids that are present in the 'vascular endothelium', which defines the outermost layer of cells on the vascular wall that is directly exposed to blood flow, are of much importance in this

context. Some of the structural and functional proteins and lipids within the scope of this thesis that could be modified due to vascular complications, such as endothelial dysfunction, hypertension and large artery stiffness, are discussed next in the context of AD pathophysiology in Section 2.4. These include membrane associated proteins such as endothelial nitric oxide synthase (eNOS), glycogen synthase kinases (GSK), caveolin-1 and membrane associated lipids such as ceramide and glycosphingolipids, which are known to associate or interact with these proteins in AD pathophysiology.

2.4 Membrane proteins and lipids in AD

2.4.1 Endothelial nitric oxide synthase (eNOS)

In terms of endothelial dysfunction, the enzyme, endothelial nitric oxide synthase (eNOS), expressed in ECs, is of much importance as it is one of the main sources of NO in the vascular endothelium. eNOS is known to be associated with plasma membrane and intracellular domains such as Golgi and nucleus [97–99]. In the plasma membrane, inactive eNOS is bound to caveolae, which are microdomains within lipid rafts and eNOS activity is considered to be inhibited or regulated by the caveolae coating transmembrane protein, caveolin-1 [97–99], which will be discussed in Section 2.4.3. Active eNOS converts L-arginine to L-citrulline to generate NO in a calcium-calmodulin dependent manner [100]. The fact that hypertension is a risk factor for AD along with the involvement of endothelial dysfunction in both pathologies points to the hypothesis that Aβ and eNOS could be interrelated [101,102]. This has driven a number of studies to evaluate possible relationships between Aβ accumulation/production and the eNOS-mediated NO production [18,66,67,103–105].

Importantly, NO production via eNOS regulates vasorelaxation and blood flow in the vasculature. In AD-patients and/or those who are at high risk of AD, the cerebral blood flow

was shown to be impaired in the brain regions assigned for memory and learning [106,107]. Moreover, elevated levels of homocysteine and asymmetric dimethylarginine (ADMA) were present in the circulation of AD-patients, which are markers of AD and/or vascular disease [106]. Notably, increased ADMA, which is an endogenous inhibitor of eNOS, correlated with a subsequent decrease in NO in the form of nitrite and nitrate [106]. Collectively, these clinical data suggest that eNOS is involved in AD. Growing evidence elucidate an association between Aβ accumulation and endothelial NO production [18,103,104].

In human brain microvascular ECs treated with the NOS inhibitor, N (G)-Nitro-L-Arginine Methyl Ester (L-NAME) and in eNOS-deficient ($eNOS^{-/-}$) mice, it was revealed that APP, BACE-1 and Aβ levels were increased [103,104]. These effects were reversed by NO supplementation while increasing cyclic guanosine monophosphate (cGMP) [104]. Another study using late middle aged (LMA) $eNOS^{-/-}$ mice (14–15 months old) also showed elevated APP, BACE-1, and Aβ in the brains compared with LMA wild-type controls. LMA $eNOS^{-/-}$ mice also demonstrated cognitive decline as indicated by their relatively worse performance in a radial arm maze test of spatial learning and memory as compared to wild-type control LMA mice. These studies illustrate the importance of the NO/cGMP signalling in regulating APP expression and processing emphasising the involvement of eNOS in AD pathology [104]. However, a recent study showed that in the immortalised human hepatic EC line, Hep-3, fibrillar $A\beta_{1-42}$ treatments of 5 and 10 μM for 12 hours caused an up-regulation of eNOS activity [12]. This is consistent with a compensatory mechanism dependent on NO bioavailability [12].

Further elucidating molecular mechanisms mediating the endothelial NO driven changes in Aβ, Suhara *et al.* [108] demonstrated that in the presence of Aβ, the serine–threonine kinase Akt was downregulated in human umbilical vein ECs with a subsequent decrease in phosphorylation of two of its downstream targets, eNOS and glycogen synthase kinase-3β

(GSK-3β). Consistently, decreased phosphorylated eNOS and GSK-3β coincided with a reduction in NO levels and increased endothelial cytotoxicity, respectively, which was reversed by constitutive activation of Akt [108]. The results indicated that Aβ could modulate eNOS and GSK-3β phosphorylation by inhibiting Akt, and that inhibition of Akt could have opposite functional effects on eNOS and GSK-3β [108]. The contribution of GSKs towards Aβ accumulation is further detailed in section 2.4.2.

2.4.2 Glycogen synthase kinase (GSK)

GSK3s, which are proline-directed serine/threonine kinases derived from two genes that give rise to GSK-3α and GSK-3β, are associated with the nuclear and cytoplasmic compartments and are involved in different physiological processes including glycogen synthesis, apoptosis and gene transcription [109,110]. GSK-3 is considered to play a pathogenic role in AD. In a mini review published in 2008, Hooper *et al.* [111] propose 'The GSK-3 hypothesis of AD', emphasising the contribution of GSK-3 towards the pathophysiology of AD. According to the GSK-3 hypothesis described by Hooper *et al.* [111], GSK-3 becomes over-active accounting for hallmark characteristics of AD such as elevated Aβ production, memory impairment, hyper-phosphorylation of tau and microglial-mediated inflammatory responses localised in plaque. In support of this hypothesis, over-activation of GSK-3 or inhibition of GSK has been demonstrated to worsen or alleviate AD characteristics, including Aβ and tau pathologies and memory impairment [110–116].

Western blot analysis of the frontal cortex of AD patients has demonstrated a significant increase in GSK-3 phosphorylated at Tyrosine 216 (pTyr216), indicative of increased GSK activity [112]. Additionally, in neuronal cultures, somatodendritic accumulation of GSK-3 (pTyr216) was evident compared to its inactive form GSK-3β phosphorylated at Serine 9 (pSer9) [112]. Active GSK-3β was also shown to be present in the cytoplasm of pre-tangle

neurons in brains at different stages of NFT formation, while the expression of GSK-3β was also found to be upregulated as revealed by microarray analysis of AD brains [110].

A recent study demonstrated that aberrant signalling by APP facilitated Ras-extracellular signal-regulated kinase-1 (ERK) signalling, GSK-3 activation, upregulation of cyclin D1, and phosphorylation of APP and tau in primary rat neurons treated with Aβ, all of which contribute to neurodegeneration [114]. The results were recapitulated by correlated increases in Aβ levels in AD brains such that the expression of Ras, activation of GSK-3, and phosphorylation of APP and tau were shown to be increased [114]. In primary cortical neurons, semliki forest virus encoding, wild-type APP (APP695) or the pathogenic APP-Swedish mutation (KM670/671NL), Aβ40 and Aβ42 levels were reduced by 60% and 78%, respectively, in wild-type APP, and in APP-Swedish mutation after 24 h of treatment with the GSK inhibitor, lithium [115]. Similarly, in the same study, a 60% reduction of endogenous Aβ levels was also demonstrated in NT2N neuronal cell line after 3 days of treatment with a clinically relevant dose of lithium (1 mM) [115]. These results were recapitulated in animal models of AD [115]. Mice expressing pathogenic, familial-AD associated forms of APP (APP-Swedish/ Tg2576) and PSEN1 ($PSEN1^{P264L/wt}$) were gavaged daily with 300 $mgkg^{-1}$ for 3 weeks, and both Aβ40 and Aβ42 levels have reduced by 40% in the RIPA-soluble fraction, while in the formic acid-extracted fraction, Aβ40 and Aβ42 dropped by 62% and 51% respectively of the brain [115].

Studies in AD transgenic mouse models of senile plaques, both senile plaques and NFTs, or wild-type controls that have been injected with recombinant adeno-associated virus 2/1 short hairpin RNA constructs, which specifically reduced expression and activity of GSK-3α or GSK-3β, demonstrated that GSK-3α mediated both senile plaques and NFT pathogenesis, while GSK-3β only modulated NFT formation [116].

GSK-3 is a known regulator involved in neuronal apoptosis and has been demonstrated to be translocated into lipid rafts in neurons in response to apoptotic stimuli and to modulate phosphorylation of tau that contributes to NFT formation and resides in lipid rafts [117]. Attenuation of both cell apoptosis and abnormal hyperphosphorylation of tau protein in the AD cell model, N2a/APP695swe, was associated with increased activation of phosphoinositide 3-kinase (PI3K)/Akt pathway that negatively regulated GSK-3β in a caveolin-1 dependent manner, which is a lipid raft-associated protein [17]. Bai *et al.* [118] reported a regulatory role of caveolin-1 in modulating GSK-3 activity via PI3K/Akt pathway in astrocytes that influences glycogen content, which is known to be crucial for learning of new motor and cognitive skills [119]. The role of caveolin-1 in AD is discussed in section 2.4.3

2.4.3 Caveolin-1

Caveolin-1 is a lipid-raft associated protein that coats the caveolae structures within the lipid rafts that are associated with eNOS activity [97–99]. A physical association or interaction of caveolin-1 and APP has also been proposed by several studies [120]. *In vitro* studies in COS-7, HEK293, and MDCK cell lines showed that APP co-fractionated with caveolin-1, while recombinant COS-7 cells that overexpressed APP co-immunoprecipitated with caveolin-1 [120]. A direct interaction was also demonstrated between a fusion protein encoding the cytoplasmic domain of APP and purified recombinant caveolin-1 protein [120]. Furthermore, overexpression of caveolin-1 was shown to increase non-amyloidogenic processing of APP by increasing α-secretase activity, which was abrogated by blocking caveolin-1 expression [120]. A more recent study demonstrated that in addition to α-secretase activity, both γ - and β - secretase activity could also be modulated by caveolin-1 [121]. Suppression of caveolin-1 expression by RNA interference resulted in significant increases in amyloidogenic proteolysis of APP by γ-secretases, production of Aβ, and in C99/C83 ratio indicative of increased β-secretase activity

[121]. These effects were reversed when caveolin-1 was overexpressed, corroborating that caveolin-1 could regulate secretase activity [121].

Differences in caveolin-1 expression levels in human AD brains have been reported [122,123]. Caveolin-1 protein levels in the hippocampus and mRNA in the frontal cortex were demonstrated to be up-regulated in AD by approximately two-fold compared to control brains [122]. Similarly, in frontal white matter of AD brains with absent/mild CAA, stronger caveolin-1 labelling was observed than in non-AD controls [123]. Analysis of regional differences in caveolin-1 labelling revealed that caveolin-1 was also significantly higher in the frontal lobe than in temporal and parietal lobes within the AD brains with absent/mild CAA when AD cases were subdivided according to the severity of CAA [123].

While caveolin-1 expression levels increased in some regions of AD brains, loss of caveolin-1 was shown to exacerbate AD pathology [122–124]. In 3-6 months old young caveolin-1 knock out mice compared to wild type mice, neuronal aging and degeneration were shown to be accelerated with reduced tolerance to cerebral ischemia-reperfusion injury and concomitant increases in Aβ, phosphorylated-tau, and astrogliosis [124]. In the same study, middle (12 months old) and aged (>18 months old) caveolin-1 knock out mice showed age dependent reductions in synaptic signalling components including caveolin-1 [124]. Based on these results, this study suggested that caveolin-1 knockout mice could serve as a non-mutational model of AD [124].

Transgenic mice with human APP comprising the V717I London mutation that overexpress APP_{695}, and their wild type mice showed age dependent differences in caveolin-1 protein expression levels [125]. In both wild type mice and transgenic mice^{V717I}, caveolin-1 levels increased significantly at 9 and 18 months of age compared to 3 months old mice of corresponding genotype [125]. However, at the age of 18 months, the caveolin-1 expression level

was markedly reduced in transgenic mice^{V717I} compared to wild type mice, with no differences at either 3 or 9 months, elaborating a role of caveolin-1 in modulating endocytosis age-dependently and in AD pathology [125].

Caveolin-1 is also implicated in cholesterol transport, which is involved in AD [126,127]. In the APP23 mouse model of AD, inhibition of Cyp46a1, which encodes for cholesterol 24-hydroxylase that controls brain cholesterol efflux, accumulation of Aβ peptides and neuronal death were evident compared to control wild type mice [127]. Transfection of rat astrocytes with siRNA directed at caveolin-1 mRNA inhibited the Aβ42-induced transport of both cholesterol and caveolin-1 from the plasma membrane to the Golgi complex, while in astrocytes that were not treated with Aβ42, cholesterol abundance in the Golgi complex was reduced [128]. This study exemplifies a role of caveolin-1 in retrograde transport of cholesterol from the plasma membrane to the Golgi complex that could potentially be important in AD [128]. The cholesterol content in caveolin-enriched-membranes is known to be regulated by ceramide, such that a 25% reduction in caveolin-1 was measured subsequent of cholesterol displacement induced by ceramide generation [129]. Contribution of ceramide, another lipid-raft associated molecule, towards AD is next discussed in Section 2.4.4.

2.4.4 Ceramide and glycosphingolipids

Ceramide, one the of simplest sphingolipids, is the core constituent of the more complex sphingolipids such as sphingomyelin and glycosphingolipids, which are abundantly present in the brain and modulate structural support and function of membrane-associated proteins, and cell signaling [130,131]. Sphingomyelin synthases synthesise sphingomyelin from ceramide while sphingomyelinases catabolise sphingomyelin back into ceramide.

Network analysis of the Alzpathway database [14], last updated in 2016, indicated a key role of ceramide and related pathways in the pathophysiology of AD. Mizuno *et al.* [132] further reported that ceramide has a dual role such that it has both inflammatory and anti-inflammatory effects that are central to AD pathology, emphasising the importance of sphingolipid homeostasis in AD. Plasma ceramide and sphingomyelin levels have been associated with risk of AD, as demonstrated by the recent Baltimore Longitudinal Study of Aging [15], while regional changes in membrane lipids such as sphingomyelin in AD brains has been reported as early as in the 1980's [133,134]. Elevated acid sphingomyelinase and acid ceramidase expression in AD brain samples correlated with reduced sphingomyelin and elevated of ceramide levels [135]. Changes in gangliosides, GM1 and GM2 were found in AD brains compared to control brains in detergent-resistant membrane fractions (DRMs), which is considered to contain lipids and proteins associated with lipid-raft domains, such as gangliosides [136]. In DRMs of AD brains from both the frontal cortex and the temporal cortex, representative of early and late stages of AD, respectively, GM1 and GM2 levels were significantly upregulated relative to control brains, while in the temporal cortex, the DRM proportions were relatively lower with depleted cholesterol levels [136]. Deregulation of ceramide species was also demonstrated in neuroglioma (H4) cells expressing the Swedish mutation of human APP (H4APPsw), an AD cell model, where the simplest ganglioside, GM3, lactosylceramide, the precursor of GM3, and ganglioside GD1a have increased significantly relative to those of the wild type H4 cells [137], further elaborating a role of sphingolipid homeostasis in AD pathology.

Ceramide-mediated changes in APP processing has also been reported [138–141]. HEK293 cells stably expressing the Swedish mutant of APP (HEK/NL) treated with the synthetic ceramide analogues dl-threo-1-phenyl-2-decanoylamino-3-morpholino-1-propanol (D-PDMP) and (1*S*,2*R*-d-erythro-2-N-myristoylamino)-1-phenyl-1-propanol (DMAPP) showed elevated Aβ42

production by modulating γ-secretase-mediated cleavage of APP [138]. D-PDMP and DMAPP, both of which are ceramide analogues, respectively inhibit glucosylceramide synthase and alkaline ceramidase, were used at a concentration of 10 μM for 24 hours [138]. Although it has been shown in CHO cells stably transfected with APP_{751} that exogenous C6-ceramide, a cell-permeable analog of ceramide, could increase Aβ levels by increasing the half-life of BACE-1 to upregulate Aβ biogenesis, the effect of PDMP and DMAPP on Aβ levels was confirmed to be due to a structural association of these synthetic compounds that directly modulated γ-secretase, rather than due to a change in ceramide metabolism [138,142]. In contrast, Tamboli *et al.* [141] reported that levels of endogenously generated Aβ immunoprecipitated from the supernatants of human SH-SY5Y neuroblastoma cells treated with 25 μM D-PDMP for 48 hours, were reduced. Similar results were obtained from Chinese hamster ovary cells expressing 695-amino acid APP or a human neuroglioma H4 cell line stably transfected with the human APP695 comprising the double Swedish mutation K595N/M596L, that were respectively treated with 15 μM D-PDMP for 48 hours and 20 μM for 2-4 days [139,140]. The discrepancies were explained by the differences in time course and concentration of the D-PDMP treatment, cell type and the source of APP [141]. Taken together, these results indicate the relevance of glycosphingolipids in modulating Aβ levels and modulating APP processing enzymes in AD.

Conversely, Aβ is also known to mediate changes in ceramide levels [135,143]. Aβ25-35 treatment of 10 μM for 10 hours resulted in a 5-fold increase in ceramide levels, and induced apoptosis ceramide-dependently in neonatal rat primary oligodendrocytes by activating the neutral sphingomyelinase–ceramide cascade [143]. Similarly, in differentiated neuronal cultures isolated from adult rat hippocampi, 1 μM of Aβ treatment for 30 minutes elevated ceramide levels markedly, resulting in significant neuronal apoptosis, which was attenuated in the presence of a recombinant acid ceramidase that completely hydrolyses ceramide into sphingosine [135].

These results indicated that Aβ-mediated increases in ceramide levels could drive apoptosis, which could contribute towards AD pathophysiology [135,143]. While ceramide is known to drive neuronal apoptosis, ceramide associated enzymes such as acid sphingomyelinases and lactosyl ceramide synthases are known to regulate intracellular adhesion molecule-1 (ICAM-1), a marker of microvascular injury implicated in AD [135,143–145], as discussed in section 2.4.5.

2.4.5 Intercellular cell adhesion molecule-1 (ICAM-1)

ICAM-1 is a glycoprotein belonging to immunoglobulin super family that is constitutively expressed at low levels in the normal endothelium and in other cells types of haemopoietic and non-haemopoietic origins, such as leucocytes and fibroblasts [146]. ICAM-1 is a membrane-bound cell adhesion molecule that gets released from activated ECs, lymphocytes, monocytes, or microglia in the soluble form [147].

ICAM-1 is proposed to be an emerging blood-based biomarker for microvascular pathology associated with AD, according to the meeting in 2012 held by the Alzheimer's Association and the Alzheimer's Drug Discovery Foundation discussing blood based biomarker development for AD [148]. Soluble ICAM-1 in the plasma was shown to be increased in AD patients compared to non-demented control subjects, with no significant changes in soluble ICAM-1 in the CSF [149]. AD patients showed significantly elevated soluble ICAM-1 levels in serum compared to both patients with non-inflammatory neurological disease and control subjects, showing an inverse relationship between soluble ICAM-1 levels and Mini-Mental State Examination scores, a marker of disease severity [150]. Additionally, elevated soluble ICAM-1 levels in the CSF of cognitively intact elderly correlated with reduced regional blood flow to the parietal cortex that was comparable to AD patients, indicating the applicability of soluble ICAM-1 as a prospective biomarker of AD [151].

Increased ICAM-1 expression was associated with AD-plaques [16,152–156]. This was shown by immunofluorescence of cortical regions of Tg2576 mice [16]. Immunostained cortical sections showed dispersedly ICAM-1-positive regions in activated microglial and brain capillary cells that were localised in close proximity to senile plaques [16]. Cluster-like accumulation of ICAM-1-immunoreactivity was also consistently shown by immunohistochemistry technique [16]. Similar findings were reported from AD brain tissue sections in which ICAM-1 immunoreactivity localised to cerebral endothelium and/or senile plaques, was significantly higher compared to that of normal brains [152,153]. This study, similar to other studies, has revealed the involvement of inflammatory responses indicated by elevated ICAM-1 in amyloid deposition [16,152–156].

ICAM-1 levels in the CSF have been shown to indicate inflammatory state of the blood-CSF barrier [157]. In monocyte-derived-dendritic cells (MDDC) that play a central role in antigen presentation in driving an immune response and which were derived from AD patients, a consistent increase in ICAM-1 expression was evident after stimulation with lipopolysaccharide compared to MDDCs derived from healthy controls [158]. Concordantly, Aβ42 treatment induced a pro-inflammatory state in DCs derived from healthy controls [158]. In postmortem brain tissue in AD patients compared to healthy controls, reactive astrocytes at the immunostained periphery of senile plaques were positive for ICAM-1, further emphasising a role of ICAM-1-mediated immune response associated with astrocytes and microglia [159].

Additionally, in rat mesenteric venules ICAM-1 phosphorylation was modulated by exogenous application of caveolin-1 scaffolding domain, which interacts with eNOS and inhibits its activity (detailed in section 2.4.3) [160]. Mesenteric venules treated with caveolin-1 scaffolding domain showed increased leukocyte adhesion and reduced basal NO levels both of which were dependent upon increased ICAM-1 phosphorylation [160], elaborating a role of ICAM-1 in regulating barrier permeability.

These studies, together with the studies that have been detailed in sections 2.4.1, 2.4.2, 2.4.3 2.4.4 and 2.4.5 emphasise the relevance of eNOS, GSKs, Caveolin-1, ceramide and ICAM-1 in the milieu of AD, outlining the multifaceted nature of the disease (Figure 2.7). Two of the common factors that are applicable to all these molecules are their association with the cell membrane and expression in the endothelium, as described in relevant sections. Hypertension, elevated pulse pressure and large artery stiffness are associated risk factors of AD, and one of the implications that these factors could independently or cumulatively propagate is increased mechanical cyclic stretch placed upon ECs. Thus, these membrane-associated proteins could be possibly altered in response to mechanical stretch of the vessel wall consequent of elevated pulse pressure involved in hypertension.

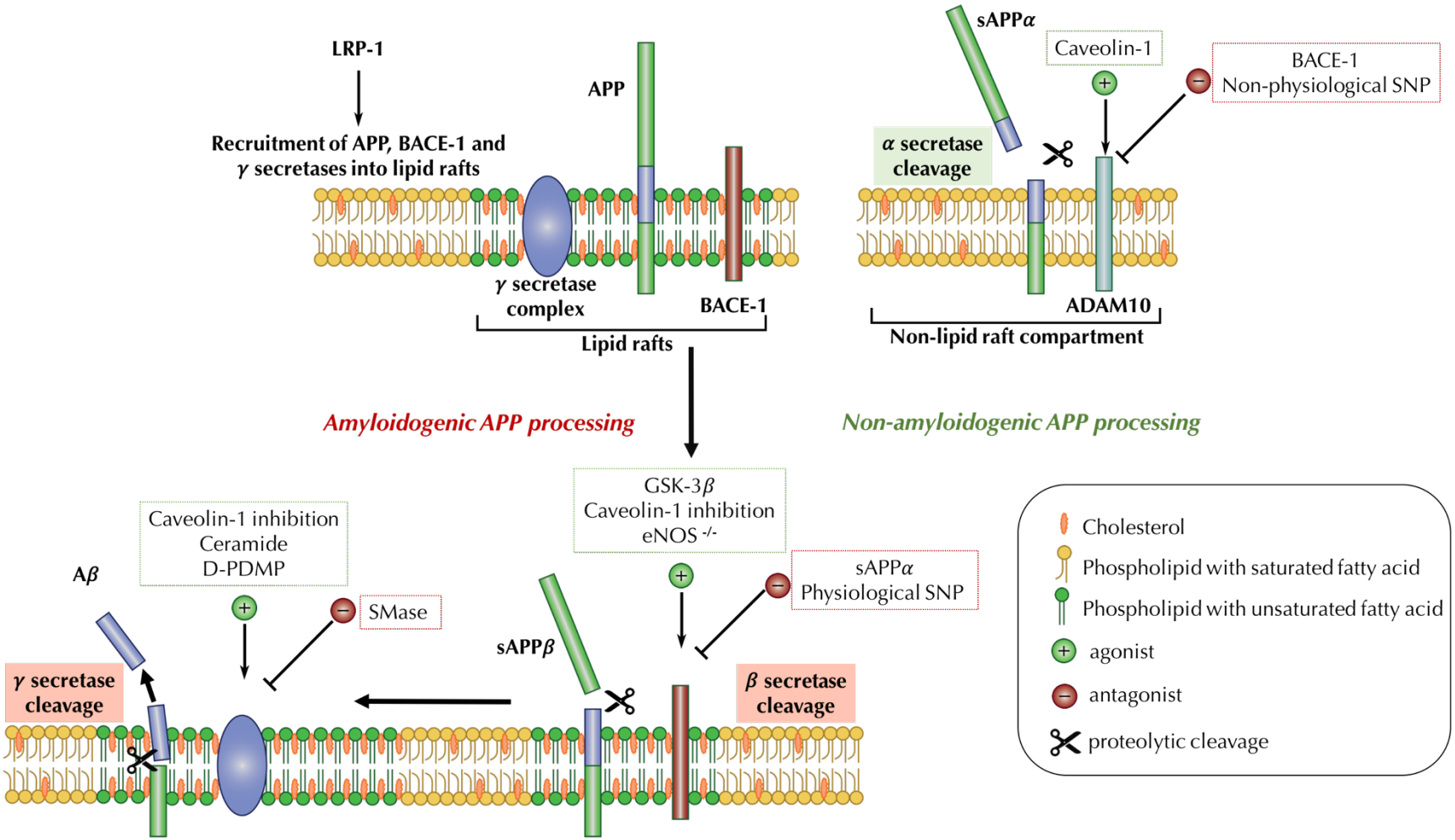

Figure 2.7 An overview of proteins and lipids discussed in section 1.4 showing their involvement in APP processing. APP is cleaved by secretases including ADAM10 and BACE-1 to be processed in non-amyloidogenic (largely occurs in non-lipid raft compartments) and amyloidogenic (largely occurs in lipid rafts) pathways respectively. Molecules shown in green boxes are agonists for the proteins pointed by the arrows, whilst the molecules in red boxes are antagonists pointed by the inhibitory sign. (Modified from Di Paolo *et al.* [161]). Abbreviations: Aβ, Amyloid beta; ADAM, a-disintegrin-and-metalloproteinase; BACE-1, β secretase 1; D-PDMP, dl-threo-1-phenyl-2-decanoylamino-3-morpholino-1-propanol; GSK, glycogen synthase kinase; sAPPα, soluble amyloid precursor protein alpha; sAPPβ, soluble amyloid precursor protein beta; SNP, sodium nitroprusside, SMase, sphingomyelinase.

2.5 Effects of mechanical cyclic stretch

To reiterate, hypertension, large artery stiffness and increased pulse pressures are independent vascular risk factors that are associated with AD [3,7,71–74]. These factors could modulate membrane associated proteins and lipids present in the endothelium that are implicated in AD, including eNOS, GSK, caveolin-1, ceramide and glycosphingolipids and ICAM-1, which are discussed in Section 2.4. This section will focus on the mechanical effects on these molecules due to altered haemodynamic forces implicated in the above vascular pathologies, such as mechanical cyclic stretch and shear stress, with a particular focus on mechanical stretch studies, since a key element of this thesis is the investigation of effects of mechanical cyclic stretch.

2.5.1 Mechanical stress and eNOS

Although the direct effects of cyclic mechanical stretch on cerebral eNOS expression have not been extensively investigated, mechanical stretch effects on eNOS activation have been well studied [162–167]. One of the prominent associations is the relationship between eNOS and blood pressure (BP) regulation, which is well established, such that eNOS activation is central to alleviating BP insults to preserve the endothelium [102,168–171]. This suggests that eNOS activation provides a negative feedback loop, counteracting elevated mechanical stretch in hypertension by producing NO to mediate vasorelaxation [102,168–171]. In line with this, the majority of the studies elucidating effects of cyclic stretch on the expression and/or the activation of eNOS have shown that eNOS activation, eNOS mediated NO production and/or expression were up-regulated as a result of mechanical stretch [162–166,172].

Several studies have demonstrated the involvement of calcium signaling and eNOS-mediated NO production in ECs in response to mechanical stretch [165,173]. In bEnd3 cells, grown on collagen-coated-BioFlex plates with silastic membranes, Berrout *et al.* showed a calcium influx

mediated by transient receptor potential (TRP) channels 1 and 2 induced by 20-55% of biaxial stretch [173]. Delivering 50 ms bursts of nitrogen gas that produced a downward deformation of the silastic membrane and adherent cells propagated the stretch pulses in this system [173]. Consequently, calcium influx mediated increased NO production by eNOS and cytoskeletal actin-stress-fiber formation [173]. This study also demonstrated a greater than 10% of stretch-induced threshold for bEnd3 cells to induce a change in calcium influx [173]. Furthermore, cyclic stretch of 18% at 25 cycles/min for 20 minutes applied on human pulmonary artery ECs in FX-4000T Flexcell Tention Plus system, showed stress fiber remodelling in terms of focal adhesion kinase phosphorylation [174]. TRP-mediated-cytoskeletal remodelling and cell stress fiber reorientation was also demonstrated in primary bovine capillary ECs (BCEC) cultured on fibronectin-coated flexible extracellular matrix substrates under 10-15% stretch at 1 Hz frequency for 1-2 hours [175]. TRP-Vanilloid-4 (TRPV4) activation has led to the activation and binding of actin receptors in a phosphatidyl inositol-3-kinase (PI3K)- dependent manner [175]. Another study also reported calcium influx through TRPV4 channels in BCEC and human dermal microvascular ECs that was mediated by force-dependent integrin signaling [176]. However, this study used a different approach called 'magnetic pulling cytometry' [176]. This involved the cultured cells being exposed to brief (500 ms) pulses of increasing tensional force (100, 450, 850 and 2000 pN) through bound magnetic microbeads (4.5 μm diameter) using an electromagnetic needle [176].

Concordant with Berrout *et al.* [173], short-term NO production in response to stretch-mediated-calcium influx was also demonstrated in bovine arterial ECs [165]. This study used the STREX stretch system, a similar apparatus to that is used in the investigations reported in this thesis, where elastic silicon chambers coated with fibronectin were subjected to uni-axial stretch (1 Hz, 20% in length for 5 or 20 minutes) [165]. Moreover, a biphasic NO production, short and long term, was demonstrated via two different mechanisms, stretch-activated channel-

mediated increase in calcium influx and phosphatidylinositol 3 OH-kinase/ serine/threonine-specific protein kinase Akt (PI3K/Akt) pathway, respectively [165]. Similarly, the former was also demonstrated in human umbilical vein ECs (HUVEC) in a c-src dependent manner, which mediated EC morphological changes downstream of calcium signaling [177,178]. A similar bi-phasic pattern of eNOS activation and NO production due to acute mechanical stretch was reported in another study [162]. This study ultilised a single-well device, which was uniformly stretched by vertical indentation [162]. However, this study reported the activation of protein kinase A (PKA) pathway along with the PI3K/Akt pathway at 15 and 30 minutes respectively, whereas HUVECs were subjected to 20–50% continuous bi-axial stretch [162]. The involvement of PI3K/Akt pathway in stretch-mediated-NO production has also been demonstrated in pulmonary vascular ECs *in situ* [179]. This study employed models of the intact lung and isolated-perfused rat lungs where the vascular pressure was elevated to induce stretch [179]. Taken together, cyclic mechanical stretch has been demonstrated to induce calcium influx mediated PKA and/or PI3K/Akt dependent NO production [162,165,166,173,178].

The importance of maintaining a physiological level of vessel stretch in regulating eNOS activity and oxidative stress was reported by Thacher *et al.* [164]. In *ex vivo* and *in vitro* vessel preparations of porcine carotid arteries and isolated porcine carotid ECs grown silicon tubes that were perfused for 24 hours, a physiological stretch level of 4-5% consequent of pulse shear stress (6±3 dynes/cm2) combined with a pulse pressure of 80±10 mmHg was compared to a reduced level of 1% stretch achieved by wrapping the arterial segment with a silicon band or by seeding the ECs inside less compliant tubes [164]. Reduction of stretch from 5% to 1 % resulted in a marked reduction in bradikynin-induced vasorelaxation (Figure 2.8) and eNOS phosphorylation at serine 1117, an activation site of eNOS, with a concomitant increase in oxidative stress markers [164], emphasising a role of cyclic mechanical stretch in maintaining NO homeostasis to regulate vasorelaxation and oxidative stress.

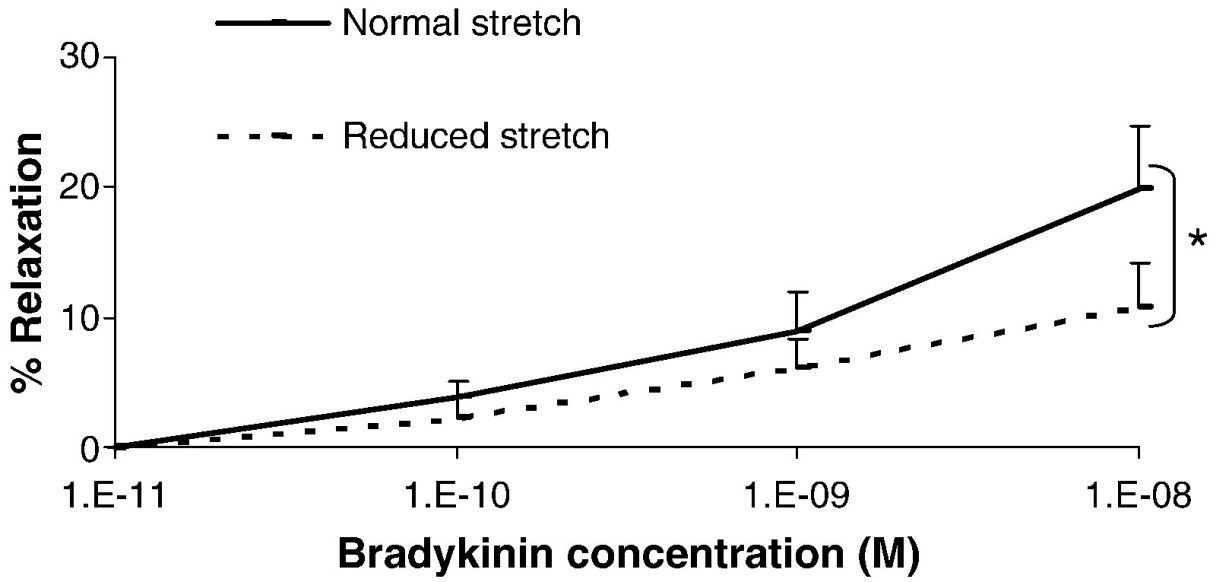

Figure 2.8 Effect of stretch on bradykinin-mediated vasorelaxation in porcine carotid arteries. Bradykinin-dependent relaxation capacity of porcine carotid artery segments after 24 hours of perfusion with a normal cyclic stretch (4–5%) compared to a reduced cyclic stretch (<1%) *ex vivo* (From Thacher *et al.* [164] with permission).

Apart from studies showing modulations in NO production and/or eNOS activity as a consequence of mechanical stretch, alterations of eNOS expression has also been reported [167,180,181]. In cultured bovine aortic endothelial cells (BAEC), 24 hours of 6% and 10 % strain have resulted in an up-regulation of eNOS transcripts and protein levels as shown by northern blot analysis, nuclear run-off transcription assays and western blotting [166]. The BAEC were grown on flexible membranes, which were subjected to deformation at 60 cycles/min with -5 or -20 kPa of vacuum in a vacuum manifold with recessed ports [166].

Several studies have elucidated that eNOS mRNA expression is differentially regulated based on the nature of mechanical stress that was involved [172,174,182]. One study used combinations of pressure, unidirectional shear stress, oscillatory shear stress and cyclic stretch for 24 hours on BAEC and EA hy926 grown in perfused silicon tubes [182]. The stretching conditions

included pulsatile shear stress with unidirectional flow comprising a component of 6 dyne/ cm^2 (amplitude = 6 dyne/ cm^2) and shear stress with an oscillatory flow with a mean of 0.3 dyne/ cm^2 (amplitude = 6 dyne/ cm^2) combined with or without 4% cyclic stretch (mean pulsatile pressure = 100 mm Hg) [182]. Northern blot analysis showed that unidirectional shear stress led to a dose-dependent increase in eNOS mRNA expression in both BAEC and EA hy926 cell line compared to the no shear static control [182]. In contrast, with oscillatory shear stress, it was shown that the mRNA expression of eNOS was significantly down-regulated at 0.3 dyne/ cm^2 of shear stress [182]. This effect was not significantly increased with the added component of 4% cyclic stretch in either of the conditions [182]. Additionally, eNOS promoter activity was measured by luciferase activity preceded by transient transfection of the cells with a sequence coding for the functional human eNOS promoter coupled to a luciferase reporter [182]. The luciferase activity revealed that the eNOS promoter activation was incremented in a magnitude-dependent manner with unidirectional shear stress [182]. Although the EA hy926 cell line appeared more sensitive to shear stress changes, both cell lines demonstrated similar trends [182]. Remarkably, regardless of the eNOS de-regulation at the mRNA level, the eNOS promoter activation was increased by 7 to 10-fold with oscillatory shear stress, which, in contrast, was significantly suppressed by cyclic stretch at all shear stress variations used [182].

In another study by Ziegler *et al.* [172] using the same apparatus as described, mRNA expression of eNOS was shown to be completely abolished as shear stress was reduced from 0.3 to 0.08 dyne/cm^2. Furthermore, it was reported that cyclic stretch did not have additional effects on eNOS mRNA expression in the presence of low, high or oscillatory shear stress [172]. The differential expression of eNOS due to unidirectional shear stress was attributed to occur via nuclear factor kappa B (NFκB) activation, while oscillatory shear stress-mediated changes were suggested to occur subsequent to activation of an unidentified negative *cis*-acting element present in the *NOS III* gene [183]. Similarly, differential regulation of eNOS by shear and cyclic

stretch in porcine carotid arteries that were perfused using an *ex vivo* arterial support system for 72 hours was reported [184]. This study combined physiological stretch of 5%, and reduced stretch of 1% with high shear (6 ± 3 dynes/cm2) or oscillatory shear (0.3 ± 3 dynes/cm^2) stress with a pulse pressure range of 80 ± 10 mmHg [184].

2.5.2 Mechanical stress and GSK

Although the effect of cyclic mechanical stretch on GSK-3 expression in ECs is not known, GSK-3β expressed in other cell types is known to be modulated by mechanical stretch [185]. Primary human airway smooth muscle cells (HASMCs) were grown on Bioflex plates that were stimulated with a 1-hour cyclic stretch at 1 Hz using the computer-controlled vacuum strain apparatus, Flexercell Strain Unit, with a vacuum pressure that generated 12% stretch [185]. The HASMCs that were stretched showed increased hypertrophy and hyperplasia dependent upon upregulation of the hypertrophic microRNA, *miR-26a*, that led to a suppression of GSK-3β mRNA translation compared to the non-stretched static control [185]. In the same stretch system described above, intestinal epithelial cells were stretched at 10 cycles/min at an average of 10% cyclic stretch for 1 hour by a computer-controlled vacuum manifold [186]. Phosphorylation of GSK-3β at serine 9 was upregulated in response to stretch with concomitant increases in phosphorylation of Akt and PI3K that resulted in a proliferative effect in stretched cells compared to static cells [186]. In a different mechanical stress apparatus where bone marrow cells mesenchymal stem cells were grown on glass surfaces and covered with thin cover glass plates on which drops of phosphate buffer solution (PBS) were placed to induce cyclic compression stress, magnitude dependent changes in GSK and Akt phosphorylation were demonstrated [187]. The stress parameters used were 0.15 Hz × 8 cm and 0.6 Hz × 8 cm (frequency and height denote drops of PBS and perpendicular distance from the drip nozzle of PBS bottle to the glass slide respectively), which respectively represent small and large-magnitudes of stress, for 30 minutes [187]. Small mechanical stress magnitude

induced phosphorylation of Akt and downregulated GSK-3β expression, while large magnitude of mechanical stress resulted in opposite effects [187]. These studies collectively indicated a regulatory role of mechanical stress on GSK activity or expression in an Akt-dependent or independent manner [185–187].

2.5.3 Mechanical stress and caveolin-1

Caveolin-1 resides in caveolae structures that are known to sense mechanical signals exerted by haemodynamic forces on the vascular endothelium and in turn converting them into biochemical signals [188]. A number of studies have established its role in shear-induced-vasorelaxation [188,189]. Caveolin-1 overexpression increased NO generation in response to shear stress but only in the presence of H_2O_2 [98]. In isolated carotid arteries from caveolin-1 knockout mice, flow dependent vasodilatory response and eNOS activation were impaired compared to wild type and caveolin-1 knockout mice with reconstructed endothelial caveolin-1[188]. This response was recently shown to be mediated by Ca^{2+}-permeable cationic channel, TRPV4, which gets translocated into endothelial caveolae in response to shear stress that in turn regulates Ca^{2+} influx to facilitate NO production [189]. This study was performed in freshly isolated bovine coronary artery ECs that were grown in thin capillary tubes and were subjected to 16 hours of shear stress at 15 dynes/cm^2 [189]. Similarly, Ca^{2+} influx that was associated with caveolae was also shown to be occurring via another TRP channel, TRPC6, in mouse embryonic fibroblasts cultured under different mechanical stressors [190]. Albinsson *et al.* showed differential effects of shear stress and mechanical stretch in portal veins isolated from caveolin-1 knockout mice such as changes in phosphorylation of Akt and ERK1/2 [191]. Akt activation was further detailed in primary rat mesangial cells exposed to 10 minutes of cyclic stretch at 1 Hz generated by a cyclic vacuum operated by a computer-based system, which was caveolin-1 dependent and mediated by epidermal growth factor-1 [192]. Caveolae structures were markedly decreased in transfected cells grown on flexible substrates that were

stretched at 20% at 1.5 Hz for 60 minutes in the absence of Eps15 Homology Domain proteins, which are recruited into the caveolae and play a functional role in complex caveolae assembly [193]. Similar results were shown in cell studies where acute mechanical stretch or osmotic tension mediated rapid disassembly of caveolae as a regulatory mechanism that preserves membrane integrity under mechanical stretch (Figure 2.9) [194]. This buffering effect was demonstrated *ex vivo* in pulmonary arterial smooth muscle cells (PASCs) from control male WKY rats, which were altered PASCs isolated from a model of pulmonary hypertension [195]. Taken together, these studies illustrated that caveolin-1 acts as a mechanosensor that regulates cellular responses to different haemodynamic mechanical stimuli present within blood vessels.

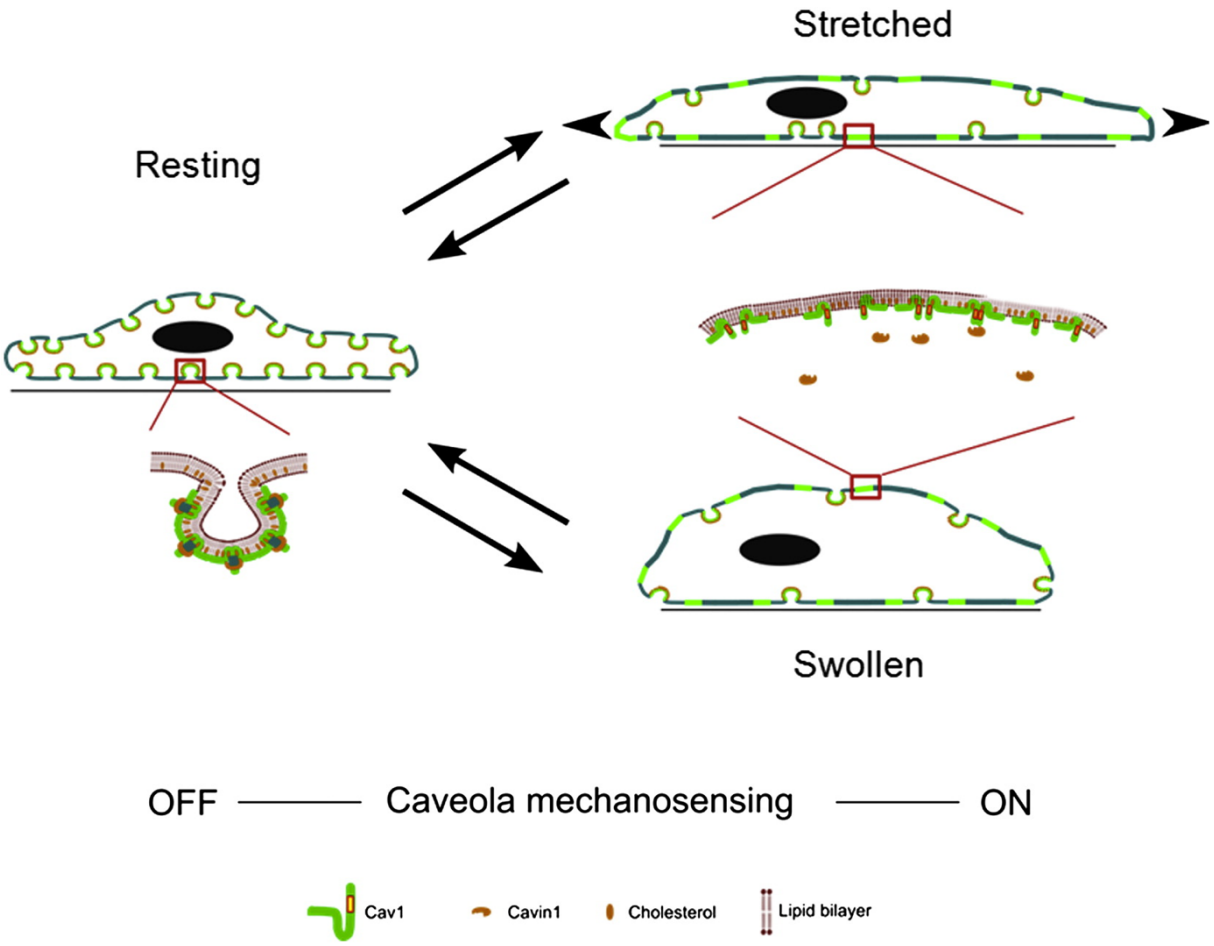

Figure 2.9 Representative diagram of changes in caveolin-1assemblies within caveolae in response to mechanical stretch**.** Caveolin-1 is associated with cavin-1 in the resting state within flask-shaped caveolae structures which dissociates and flatten out the caveolae in response to acute mechanical stress to maintain homeostasis of membrane tension. (From Sinha *et al.* [194] with permission).

2.5.4 Mechanical stress effects on ceramide and glycosphingolipids

Although not much is known about mechanical stretch-mediated effects on glycosphingolipids, such as ceramide, concomitant with changes in caveolin rearrangement in response to mechanical stretch, the turnover of glycosphingolipids that are associated with caveolae structures were altered [196]. The study utilised a study design where myoblasts grown on silicon chambers that were subjected to 15-60 minutes of stretch at 1 Hz [196]. Thus far, this study demonstrated that glycosphingolipids are affected by mechanical stretch [196]. In line with this, in spontaneously hypertensive rats, the sphingosine-1-phosphate/ceramide ratio was shown to be shifted towards ceramide accumulation compared to normotensive WKY rats [197]. This was also shown in the plasma of patients with hypertension relative to normotensive subjects, as shown on Figure 2.10 [197].

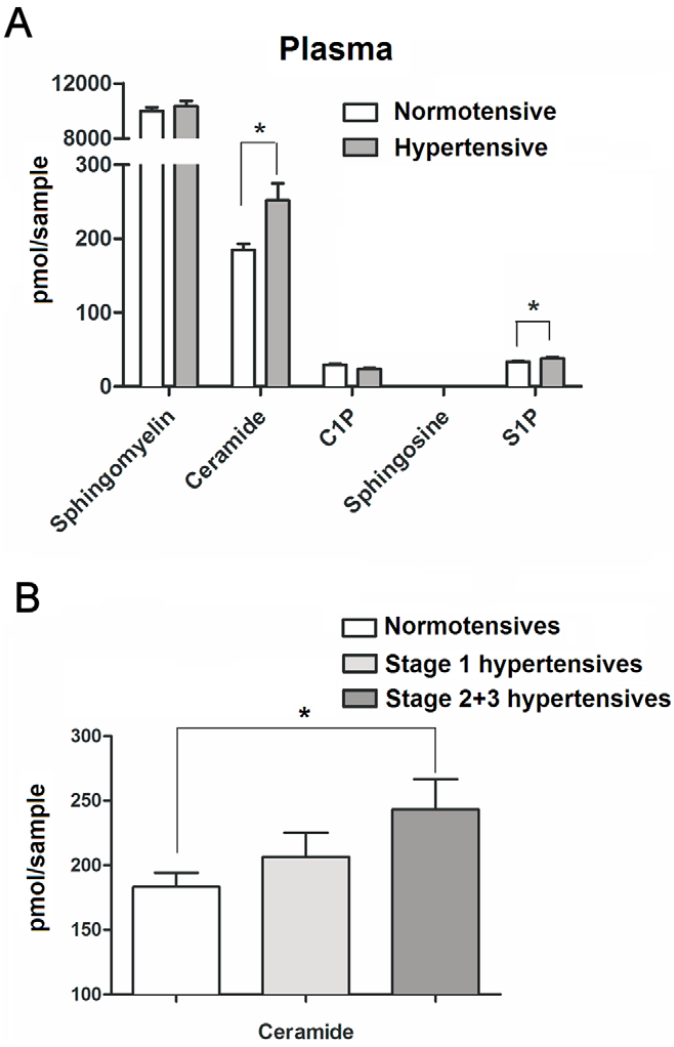

Figure 2.10 Plasma glycosphingolipid levels in patients with hypertension relative to normotensive control subjects. Relative glycosphingolipid species in normotensive (140/ 90 mmHg) and hypertensive (BP≥160/100) cohorts showing altered glycosphingolipid biology in hypertension (A). Ceramide levels in the plasma of normotensive, stage 1 and stage 2+3 of respective blood pressure limits corresponding to 140/ 90 mmHg, 140–159/90–99 mmHg and BP≥160/100 (B). (From Spijkers *et al.* [197] with permission).

Similarly, as shown by ceramide staining and mass spectrometric analysis of left ventricular tissue of pulmonary artery hypertensive patients, ceramide levels were upregulated compared to normotensive controls (Figure 2.10) [198]. Similar results were obtained from an experimental pulmonary hypertension in rats [199]. Inhibition of *de novo* synthesis of ceramide pharmacologically using myriocin, which inhibits Ser palmitoyl transferase 1, the rate-limiting enzyme in *de novo* ceramide synthesis, in C57Bl/6, high fat diet-induced hypertension and

endothelial dysfunction were attenuated [200]. Reduced levels of phosphorylation at serine 1177 was evident in those mice that were fed a high fat diet compared to those high fat-fed mice treated with the ceramide inhibitor [200]. This was attributed to a mechanism where ceramide lead to disruption of Akt-Heat shock protein 90-eNOS complex, which is crucial for eNOS phosphorylation and activation [200,201]. Collectively, these studies elaborated a potential role of mechanical stretch, which is representative for increased pulse pressures involved in hypertension in regulating ceramide reservoirs and subsequent cellular responses [196–201].

2.5.5 Mechanical stress and ICAM-1

Previous studies have shown that ICAM-1 expression was up-regulated in response to mechanical stretch [202–205]. In human pulmonary artery ECs, both mRNA and protein expression of ICAM-1 were upregulated after 24 hours of 20% cyclic stretch at a frequency of 0.5 Hz [202]. Cheng *et al.* [203] showed similar effects in a different system. In a vacuum controlled strain unit, HUVECs were deformed by a sinusoidal negative pressure with a peak level of -10, -15 or -20 kPa to produce respective average strain % of ~9%, ~11% or ~12% at a frequency of 1 Hz, which were calculated by averaging radial strain over the total plate surface area [203]. The stretching over the membrane was stated to be heterogeneous [203]. Released levels of soluble ICAM-1 increased dose-dependently at 9%, 11% or 12% strain over 24, 36 and 48 hours of strain as shown by enzyme linked immunoassay [203]. The expression of ICAM-1 mRNA and protein levels were also shown to follow a similar pattern over 1, 3, 12 or 24 hours as shown by northern blot analysis and flow cytometry respectively [203]. Additionally, in HUVECs that had undergone combinations of shear stress, oscillatory or pulsatile stretch ICAM-1 levels were upregulated [204].

Consistently with the studies elaborating how mechanical stretch could modulate ICAM-1 levels, studies have shown that ICAM-1 levels are increased in hypertensive animal studies

[206,207]. Whole cell and membrane expression of ICAM-1 was upregulated in pulmonary artery ECs exposed to circulating microparticles derived from pulmonary arterial hypertensive rats at late stage (8 week) compared to early stage (3 week) of the disease [206]. Spontaneously hypertensive rats of age 15-20 weeks had higher ICAM-1 expression in liver and kidney relative to age-matched normotensive WKY rats [207]. Furthermore, hypertension was shown to mediate upregulation of ICAM-1 independent of circulating angiotensin-II, an important humoral factor involved in regulating blood pressure and had been previously shown to modulate ICAM-1 in the vasculature [208,209]. This study was conducted in WKY rats with or without artificial constriction of the abdominal aorta to induce localised hypertension where the former resulted in localised hypertension, which prolonged till the final time point of 4 weeks in the study design [208].

Up-regulation of ICAM-1 protein expression associated with mechanical stress could lead to a number of cellular and physiological consequences [203,205,210]. Increases in ICAM-1 expression, subsequent to 20 hours of cyclic stretch at 11% and 12% have been demonstrated in HUVECs [203]. This coincided with increased monocyte adhesion to endothelial cells implicating a pathophysiological phenomenon involved in vascular diseases [203]. Similar effects were shown in an *in vitro* model of intraglomerular hypertension, where mesangial cells, a type of smooth muscle cells from the kidneys that were subjected to mechanical stretch [205].

Taken together, altered haemodynamic forces and/or hypertension could modulate eNOS, GSK, caveolin-1, ceramide and glycosphingolipids, and ICAM-1, all of which are implicated in AD. In summary, hypertension, large artery stiffness and increased pulse pressures are independent risk factors for AD, whilst increased pulse pressures are resultant of hypertension and increased vascular stiffness. Increased pulse pressures could in turn lead to increased vessel stretch that could modulate proteins and lipids present within the endothelium, which is relevant though not well studied in the context of AD.

Chapter 3

Optimisation of mechanical stretch of endothelial cells for protein and RNA quantification

Summary—The cell stretching device that is utilised in this thesis is a relatively new system and subjecting the human cerebral endothelial cells is a novel concept in the context of Alzheimer's disease. Thus, the cell stretching conditions and extraction protocols for gene and protein expression analysis required to be optimised. This study aims to detail the cell culture conditions that have been optimised in the cell culture model established in this thesis with the aim of elucidating stretch-mediated changes in protein and mRNA expression related to amyloidogenic pathway, in immortalized Human Cerebral Microvascular Endothelial Cells - SV40 (HCMEC-SV40). Fibronectin coated stretch chambers with a cell density of 4 x 10^5 cells/ml yielded the optimal conditions for stretching experiments. For western blotting, three stretching chambers had to be pooled as opposed to single stretching chamber was sufficient for RT-qPCR, for protein and RNA quantification extracted by scraping and TRIZOL method respectively. This study explicitly detailed the optimised conditions for future studies utlising the same system in endothelial cells.

3.1 Introduction

One of the main aims of this thesis is to investigate microvascular endothelial pulsatility as a potential trigger for the activation of the amyloidogenic pathway in an *in vitro* culture model. To achieve this aim, the ShellPa mechanical stretch system has been utilised to simulate the pulsatile effect on human cerebral microvascular cerebral endothelial cells (HCMECs), originating from circumferential vessel stretch consequent of hemodynamic changes, which to date has not been investigated. Thus far, the ShellPa stretch system is a relatively novel stretch system and not many long-term stretching studies have been carried out using this particular stretch system, although there are other similar systems that are relatively more established such as the STREX and Flexcell system as detailed in a recent review by Kamble *et al.* [211]. Due to novelty of this type of work on HCMECs and the stretch system being relatively new, the culture conditions had to be optimised considerably prior to further experimenting the stretch effects. This chapter aims to detail the cell culture conditions that have been optimised in the cell culture model established in this thesis with the aim of elucidating stretch-mediated changes in protein and mRNA expression related to amyloidogenic pathway, in immortalized Human Cerebral Microvascular Endothelial Cells - SV40 (HCMEC).

3.2 Methods

3.2.1 Cell attachment

Coating stretch chambers

Several types of coating materials have been utilised to determine the optimal cell attachment. The conditions used were non-coated, 5% gelatin coating, fibronectin and gelofusine coating [212,213]. The 5% gelatin (Sigma-Aldrich) solution was prepared in MilliQ water and filtered using the Stericup vacuum filtration system (Millipore). The coating was done using a sterile 1 ml automated pipette in a tissue culture hood. All coatings were done a day prior to seeding according to previously established protocols for general cell culture. Briefly, the 5% gelatin and gelofusine coatings were spread evenly on the bottom of the stretch chambers and removed once the bottom was completely covered by rotating the chambers. In contrast, the chambers with fibronectin coating were incubated at 37^0C with 5% CO_2 for 1-2 hours as per the ShellPa stretch system manufacturers' recommended protocol. The gelatin and fibronectin coated stretch chambers were dried in a sterile tissue culture hood while the gelofusine-coated chambers were kept at room temperature in a sterile container overnight for drying. The volumes of coating materials used were 250-300 or 500 μl.

Once the coating material and the volume were determined, different patterns of placing the coating material on the surface of the chambers were tested as the chamber surface tended to be hydrophobic. Adding all of the solution in the middle of the chamber, adding the coating solutions drop-wise in the corners and then in the middle, or randomly adding drop-wise throughout the surface have been tested as shown in Figure 3.1 and the chambers were gently rotated to spread the coating throughout. The optimal coating material was also tested for recyclability.

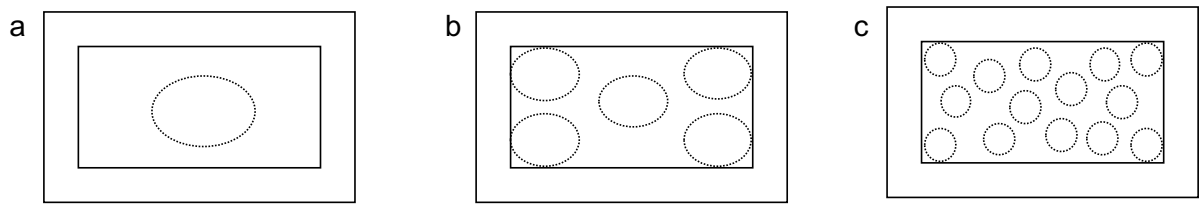

Figure 3.1 Different patterns of coating material placed on the surface of the stretch chambers. (a), (b) and (c) represent different patterns of coating material placed on the surface of the stretch chambers that have been tested.

Sterilisation of stretch chambers

Autoclaving

The stretch chambers (Menicon Life Science) were placed in autoclave bags and autoclaved using dry sterilisation setting. Sterile forceps were used to then place the chambers in 150 mm^2 plates for cell seeding in a tissue culture hood ensuring that the sterility of the inside of the chambers is retained.

Chemical sterilisation

The stretch chambers were immersed in 12.5% bleach for 1-2 hours and 80% v/v ethanol for 15-20 minutes sequentially. Then the chambers were carefully taken out of the ethanol solution inside a sterile tissue culture hood and tapped onto absorbent paper to remove any ethanol residues while maintaining sterility by taking care not to touch the inside of the chambers. The chambers were then further sterilised by exposing to ultra violet radiation (UV) for 1 hour in a tissue culture hood. This procedure was later optimised to be 30 minutes in 12.5% bleach followed by 20 minutes in 80% v/v ethanol and 30 minutes of UV exposure.

3.2.2 Protein and RNA yield

Cell seeding

Once the coating conditions were confirmed, the cell seeding density was next optimised to yield sufficient protein/RNA yield for downstream processing. Human cerebral microvascular

endothelial cells-SV40 (HCMECs) were plated at 2.5, 3, 5, 6, 8 or 8 x10^5 cells/ml seeding densities in sterile pre-coated stretch chambers. The cells were counted using a Countess automated cell counter (Thermo-Fisher Scientific). A final volume of either 500 µl or 1 ml of cells suspension was tested.

To test for the best method to achieve evenly distributed-cell attachment, different methods and patterns of cell seeding were tested. Using a standard automated 1 ml pipette fitted with sterile filtered tips (Eppendorf) or a sterile 5 ml or 10 ml serological pipettes were compared to obtain maximal even distribution of cell attachment across the bottom of the stretch chambers and between cell chambers. The tested seeding patterns are shown on Figure 3.2.

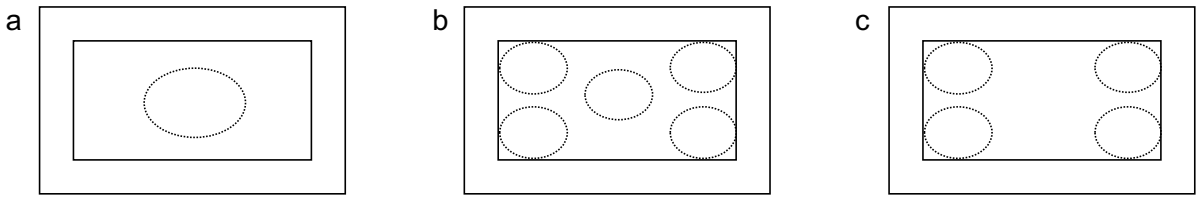

Figure 3.2 Different patterns of cell seeding on stretch chambers. (a), (b) and (c) represent different patterns of cell seeding on the surface of the stretch chambers that have been tested.

Protein extraction: Lysis protocols

A number of lysis protocols were tested to obtain the maximum protein yield possible for western blotting. HCMECs seeded on stretch chambers were harvested using the following methods for lysis and protein extraction.

Trypsinisation method

HCMECs were trypsinised by adding 50-100 µl of pre-warmed 0.05% trypsin-ethylene diamine tetraacetic acid (EDTA; Invitrogen) for 5 minutes followed by addition of M199 (Sigma) or 1 x phosphate buffered saline (PBS; Gibco) to inactivate or dilute trypsin respectively. The dislodged cells were then collected into non-sterile 1.5 ml Eppendorf tubes

and centrifuged at 1500 RPM for 10 minutes. The supernatants were then discarded and the cell pellets were re-suspended in cold 1 x phosphate buffered saline (Gibco) and centrifuged at 1500 RPM for 6 minutes to wash any residual trypsin. The supernatants were discarded after centrifugation to harvest the cells. The cell pellets were then re-suspended in 80 µl of lysis buffer (Sigma-Aldrich) into which the protease inhibitor cocktail (Sigma-Aldrich) has been added immediately prior to lysis at a concentration of 10 µl/ml of lysis buffer. Cell suspensions were incubated on ice for 1-1.5 hour/s, and were briefly vortexed every 10-15 minutes to lyse the cells. After vortexing 3 times, protein pellet was harvested by centrifugation at 13 200 RPM for 12 minutes at 4 ^{0}C and the supernatants were collected to be stored at -80 ^{0}C till bicinchoninic acid assay (BCA) protein quantification [214].

Scraping method

In comparison with the trypsinisation method, scraping using commercially available cell-scrapers was experimented to harvest cells for protein extraction. In this method, the cells were briefly washed with warm or cold 1 x PBS once or twice, to remove any residual media after the media has been discarded using vacuum suction. Radioimmunoprecipitation assay (RIPA) buffer was prepared with a formulation of 50 mM Tris-hydrochloride, pH 7.4, 150 mM sodium chloride, 5 mM EDTA, 10 mM sodium fluoride, 10 mM sodium pyrophosphate, 1% IGEPAL CA-630, 0.5% sodium deoxycholate, 0.1% sodium dodecyl sulfate (SDS) and phosphatase inhibitor (Roche; 1 tablet/ 10 ml of RIPA). Protease inhibitor cocktail (Sigma-Aldrich; 10 µl of protease inhibitor cocktail/ ml of RIPA), was added immediately prior to lysis. 20 µl of RIPA buffer per stretch chamber was used. The stretch chambers were then immediately incubated on ice or at 4 ^{0}C for at least 15 minutes. Followed by the incubation, an additional 20 µl of RIPA was added/ treatment group. Cells were then harvested by scraping. Cells harvested from 3 or 6 stretch chambers were pooled to optimise a sufficient protein yield for western blotting. Sonication (twice for 10-15 seconds) or incubation of

samples in a rotating shaker for 2 hours at 4 ^{0}C were compared to optimise the lysis protocol. The lysates were then centrifuged at 14 000 x g for 15 minutes at 4 ^{0}C [215].

RNA extraction:

Total RNA was extracted using TRIZOL (Invitrogen) according to the manufacturer's instructions after stretching. Briefly, media was discarded and the cells were washed with PBS (Gibco). 1 ml of TRIZOL reagent/ stretch chamber was then added after removing PBS and incubated for 5 minutes at room temperature. The lysates were pipetted up and down and collected into autoclaved 1.5 ml Eppendorf tubes. 0.2 ml of chloroform was added and incubated for 5 minutes at room temperature. The samples were then centrifuged at 12 000 x g for 15 minutes at 4 ^{0}C. The aqueous phase containing RNA was collected into autoclaved Eppendorf tubes. RNA was precipitated in isopropanol (1.5 ml/sample) at -20 ^{0}C overnight. Followed by centrifugation at 12 000 x g for 10 minutes at 4 ^{0}C isopropanol was discarded to isolate the RNA pellets. RNA pellets were resuspended in ice-cold 75% ethanol to be centrifuged at 7500 x g for 5 minutes at 4 ^{0}C. Ethanol was then discarded and the pellets were left to air dry. The pellets were dissolved in 15-20 µl of RNAase free water and the RNA concentrations were determined using Nano-Drop spectrophotometer. A 260/280 ratio of approximately 1.8-2.0 was used to ensure the RNA quality. Each chamber yielded a sample to be analysed using real-time quantitative reverse transcription polymerase chain reaction (RT-qPCR).

3.3 Results

3.3.1 Optimum conditions for cell attachment

Different coating materials

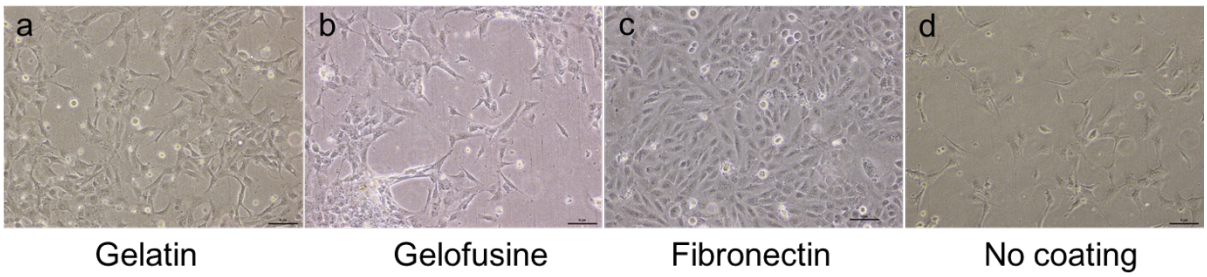

Figure 3.3 Effect of different types of coating materials on the attachment of HCMECs on stretch chambers. (a), (b) and (c) respectively show the cell attachment on stretch chambers coated with 5% gelatin, gelofusine and fibronectin compared to non-coated stretch chamber (d). The micrographs were obtained using phase contrast microscopy and the scale bar represents 10 μm.

Different types of coating materials were tested to identify the best coating material, which will facilitate highest cell attachment on stretch chambers, including gelatin, gelofusine and fibronectin coating relative to non-coated chambers (Figure 3.3). Coated chambers had better cell attachment compared to non-coated chambers and fibronectin coating was the best coating material out of the tested coating materials since it allowed for the highest cell attachment (Figure 3.3). As described in methods section, different patterns of fibronectin and cell suspension displacement onto the stretch chambers were tested. Putting fibronectin dropwise on the chamber surface allowed better spreadability of the coating material across the surface (Figure 3.1). Cells when seeded at the center initially, and then rotated for spreading still appeared to attach predominantly in the middle only (Figure 3.2) whereas when seeded in the middle and on the edges (Figure 3.2), cell spread was more consistent. The patterns depicted on Figure 3.1, and Figure 3.2 respectively, resulted in optimal spreadability of fibronectin and cells. Using a standard automated 1 ml pipette fitted with sterile filtered tips (Eppendorf) for dispensing fibronectin and a 10m l serological pipette for cell seeding gave the optimal consistency in cell distribution.

Autoclaved versus non-autoclaved stretch chambers with fresh or recycled fibronectin coating at different cell seeding densities and volumes

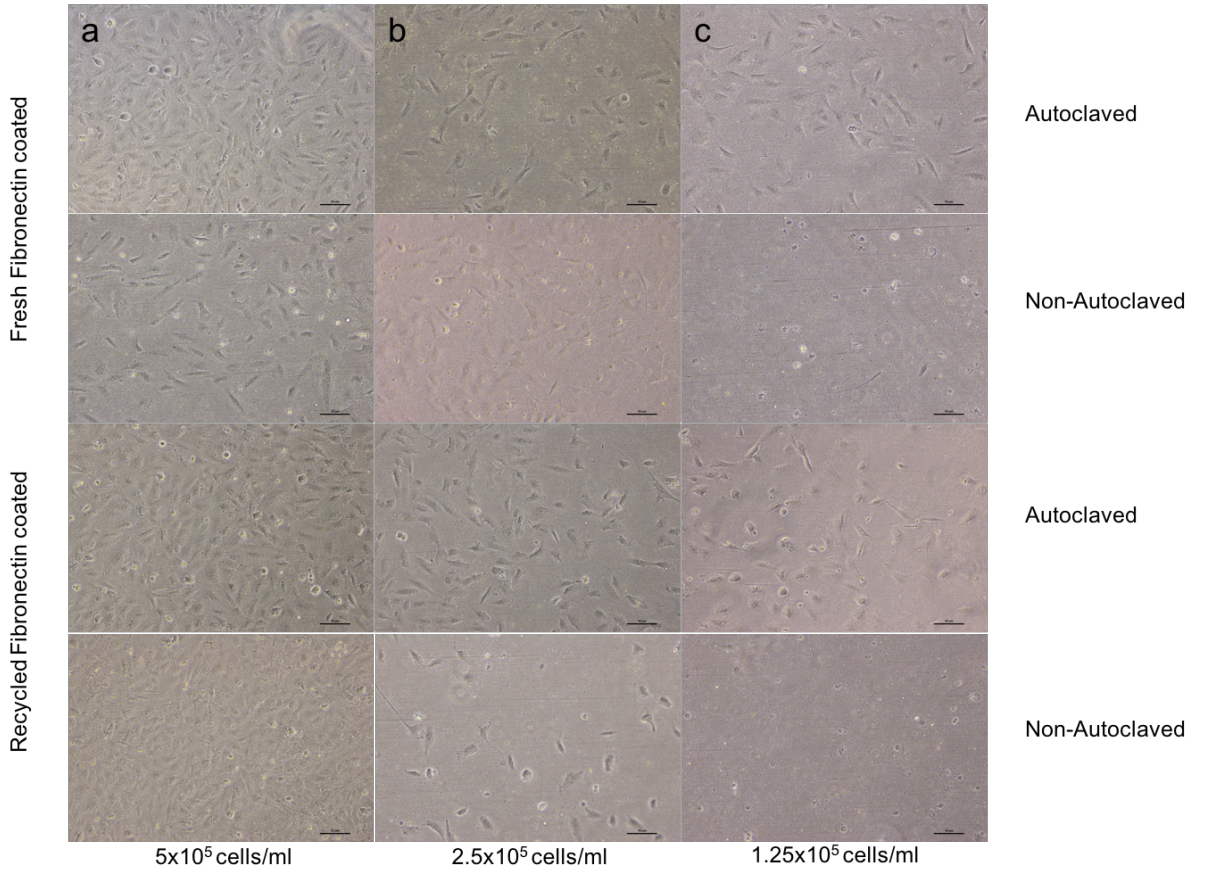

Figure 3.4 Fibronectin coating under different culture conditions. (a), (b) and (c) represent 500 µl of HCMEC suspensions prepared at 5, 2.5 or 1.25 x10^5 cells/ml cell densities respectively. The first two rows (from top to bottom) show cells that were cultured on fresh fibronectin coated stretch chambers while the other two rows showing that on recycled fibronectin coated stretch chambers. As shown on the right-hand side, each alternative row from top to bottom show whether the chambers were autoclaved or not. The micrographs were obtained using phase contrast microscopy and scale bar represents 10 µm.

Autoclaved chambers versus non-autoclaved chambers were tested for recyclability of stretch chambers with optimal cell attachment, whilst the recyclability of fibronectin at different cell densities and volumes were also investigated (Figure 3.4, Figure 3.5, Figure 3.6 & Figure 3.7) to optimise cell attachment further. Autoclaved chambers had better attachment than the non-autoclaved chambers while both fresh and recycled fibronectin coating showed similar numbers of attached cells (Figure 3.4). The initial volume of cell suspension tested was 500 µl/ stretch chamber and the densities tested were 5, 2.5 or 1.25 x10^5 cells/ml. 5x10^5 cells/ml was

found to be the optimal out of the densities tested (Figure 3.4). Next, a seeding volume of 1 ml/stretch chamber was tested as 1 ml covers the bottom of the stretch chamber better, compared to 500 µl, thus an even spread of cells can be achieved (Figure 3.5).

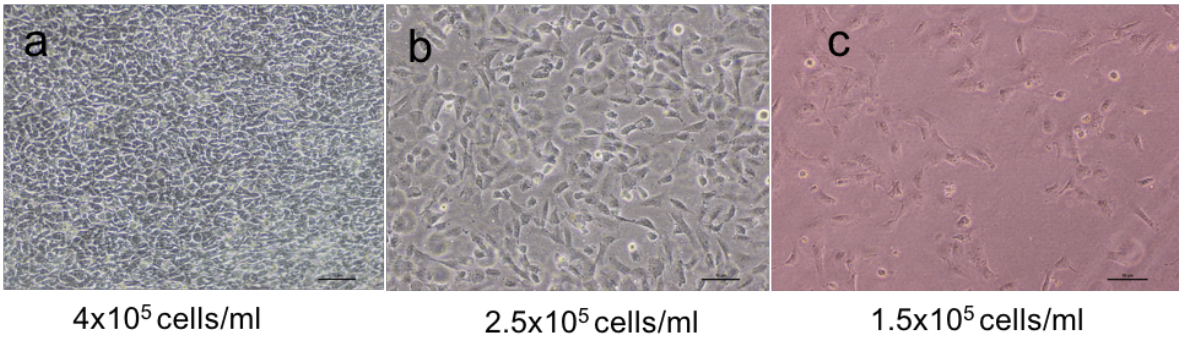

Figure 3.5 Cell density optimisation on fibronectin-coated stretch chambers. HCMECs were grown at 4, 2.5 or 1.5 x 10^5 (a-c respectively) cells/ml densities with a volume of 1 ml/chamber of corresponding cell suspensions. Micrographs were obtained upon overnight cell attachment using phase contrast microscopy. The scale bar represents 10 µm.

Cell densities of 1.5 x 10^5, 2.5 x 10^5 and 4 x 10^5 were tested with a seeding volume of 1 ml/chamber (Figure 3.5). A cell density of 2.5 x 10^5 and 4 x 10^5 cells/ml was found to be optimal, and 1 ml of seeding volume appeared better than 500 µl of seeding volume in terms of achieving an even cell spread (Figure 3.4 & Figure 3.5). Recyclability of fibronectin was then tested for cell attachment before and after stretch (Figure 3.6).

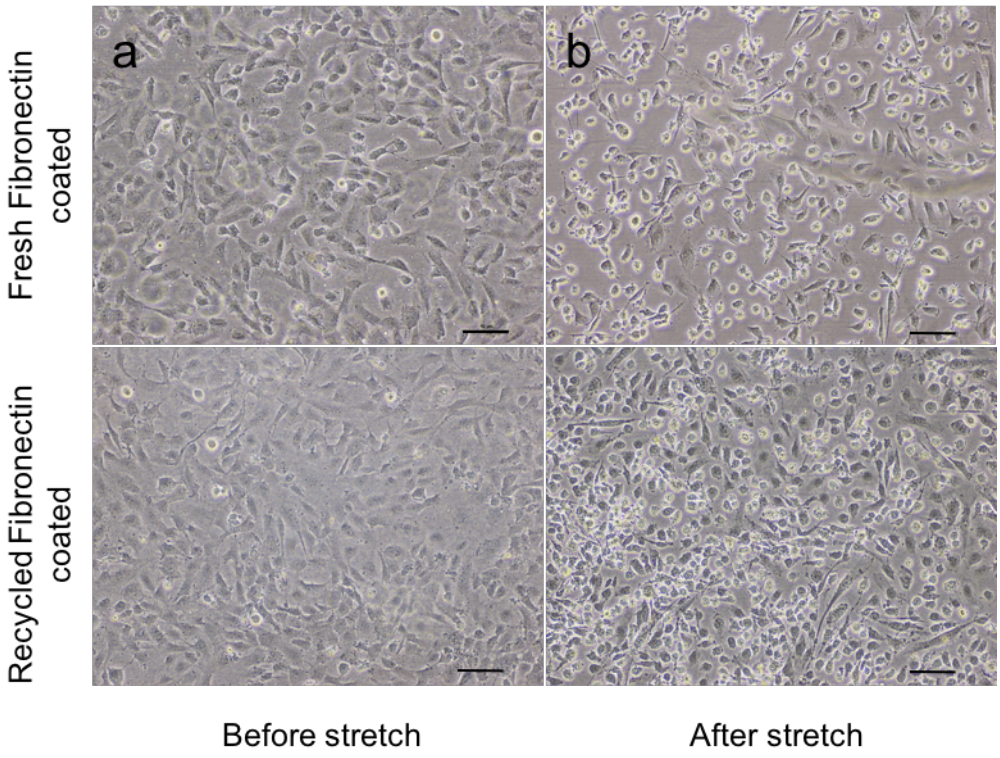

Figure 3.6 Fresh fibronectin coating versus recycled fibronectin coating before and after stretch. 1 ml of HCMEC suspensions prepared at 2.5 x 10^5 cells/ml was seeded in stretch chambers that have been coated with either fresh or recycled fibronectin. The seeded chambers were then subjected to 18 hours of 15% stretching at 1 Hz and micrographs were obtained using phase contrast microscopy. The scale bar represents 10 μm.

Fresh and recycled fibronectin were found to be comparable in terms of cell attachment (Figure 3.6) before and after stretch. Then the optimised cell attachment conditions were tested for the optimal protein and RNA yield for western blotting and RT-qPCR respectively (Figure 3.7).

3.3.2 Optimum conditions for protein/RNA yield

Cell density and protein/RNA extraction protocol optimisation

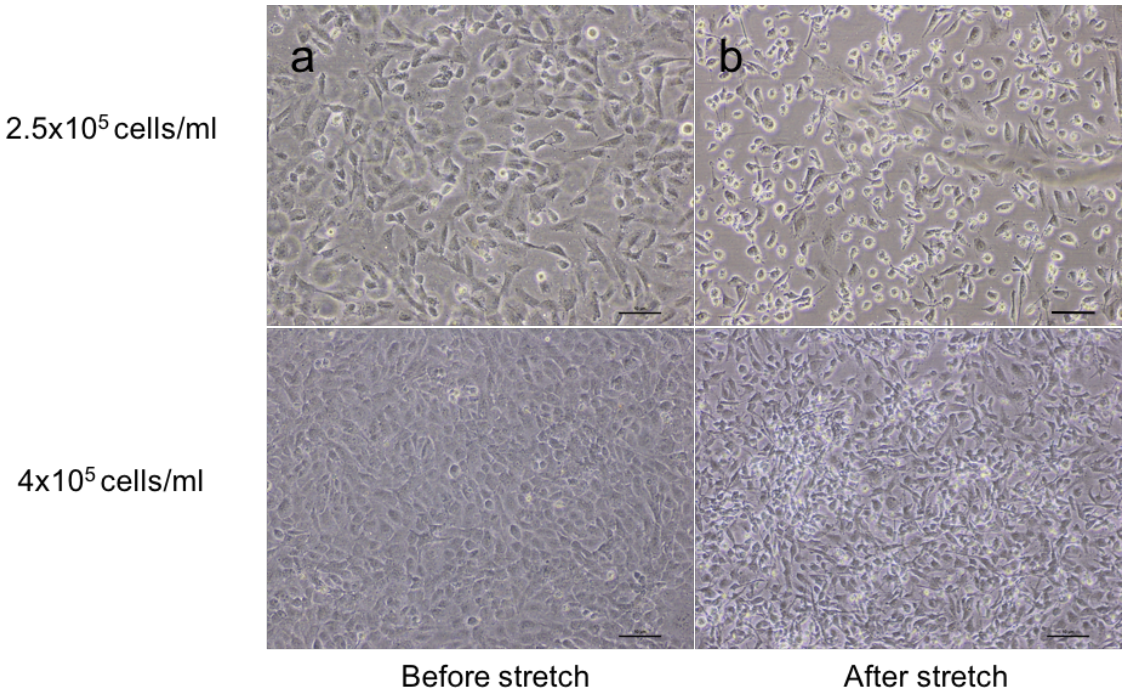

Figure 3.7 Effect of cell density under optimised culture conditions in stretch chambers. 1 ml per chamber, of HCMEC suspensions prepared at 2.5 or 4 x 10^5 cells/ml, seeded and subjected to 18 hours of 15% stretching at 1 Hz. Micrographs were obtained before (a) and after (b) stretch using phase contrast microscopy. The scale bar represents 10 μm.

Since both 2.5 x 10^5 and 4 x 10^5 cells/ml seeded chambers qualitatively showed good cell attachment, both these cell densities were tested for protein yield using BCA assay after 18 hours of 15% stretching at 1 Hz. Two different methods of protein extraction were performed. Trypsinisation and scraping method were compared. Trypsinisation yielded a protein yield of 280±77 μg/ml [mean ± standard error of the mean (SEM)] and the scraping method yielded a protein yield of 3262±428 μg/ml (mean±SEM). Thus, scraping method yielded the optimum protein yield for western blotting.

The same culture conditions (Section 3.3.1 & Section 3.3.2) that have been optimised for western blotting have been used for RNA extraction for RT-qPCR. Although for western

blotting three chambers had to be pooled to yield a sufficient protein yield, one stretch chamber sufficiently yielded RNA for one RT-qPCR sample.

3.4 Discussion

Whilst stretching of HCMECs to investigate proteins and signalling molecules associated with AD is a novel concept, the ShellPa stretch system that the HCMECs are to be stretched in, is a relatively new system compared to other stretch systems utilised in previous studies [211]. Thus, a series of experiments was designed with the aim of optimising the culture conditions for cell stretching experiments. Firstly, an economical way of reusing the stretch chambers was optimised, so that the expense of purchasing new chambers could be minimised. For this purpose, two methods of sterilisation were used as detailed in Section 3.2. Initial autoclaving along with continuous chemical sterilisation after each use of the stretch chambers enabled successful achievement of a viable method of reusing the stretch chambers without affecting the cell culture condition of the cells. However, over time, the stretch chambers appeared to become rigid and the cell detachment was inevitable, at which point the chambers could no longer used and had to be replaced with new stretching chambers of the same brand.

The stretch chambers used in these experiments are made of silicone or polydimethylsiloxane (PDMS), which is an elastic substrate on which the cells are required to be grown before being placed in the stretch unit [165]. Due to the hydrophobicity and the elastic nature of this material, cell culture conditions had to be optimised, as such properties of PDMS could affect endothelial cell functions such as adhesion, elongation and proliferation [216]. Thus, the optimum conditions for maximum cell attachment was next investigated.

Several different types of coating materials including 5% gelatin, fibronectin and gelofusine (Figure 3.3) were used as attachment factors to test for cell adherence. Although HCMECs

that are used in these experiments are cultured in flasks without any coating material, their growth on the PDMS chambers was limited without any coating as shown on Figure 3.3 due to cell detachment. The optimal attachment was obtained with fibronectin coating compared with gelatin and gelofusine coatings, which was determined through micrographs qualitatively (Figure 3.3).

Fibronectin is a known extracellular matrix ligand that enhances endothelial cell adhesion [217]. The amount of fibronectin and endothelial cell contact area with the substrate, onto which the cells attach, have been shown to influence the strength of cell adhesion and spreadability [218,219]. The spreadability of the cells in stretch experiments is an important factor as even cell attachment could affect the endothelial response to stretch. Furthermore, since it is assumed that the stretch effect across the chamber is even throughout the bottom of the chamber where the cells grow, it would be ideal to achieve an evenly spread cell layer across the chamber, such that all the cells undergo a similar degree of stretch. Therefore, the volume of fibronectin used and how the fibronectin was displaced onto the PDMS surface were optimised (Figure 3.1). Placing the fibronectin dropwise throughout the cell growing surface tended to be the best as more contact of the coating material with the growth surface would allow the cross linking to occur more readily (Figure 3.1). Consistent with this observation, different patterns of fibronectin were found to affect the spreading of fibroblasts seeded onto silicon elastomer films made from PDMS, the same material that the cell stretching chambers are made of, containing micro-contact printed with fibronectin stripes of various dimensions [220].

Two seeding volumes of 500 µl and 1 ml were also compared as volume of suspension appeared to influence the spreadability of cells as more volume would easily cover the cell growing surface and thus distribute cells evenly (Figure 3.4 & 3.5). Different patterns of cell

seeding on the PDMS surfaces (Figure 3.2) was also trialed to further improve spreadability of the cells as cell contact area could also affect the spreadability of cells on the substrate [219]. This was apparent as not all patterns of cell seeding resulted in the same outcome and the pattern that resulted in more cell contact to the substrate gave the optimal cell spreadability (Figure 3.2).

Recyclability of fibronectin was also tested to explore the possibility of reusing the material for cost effectiveness. Since fresh and recycled fibronectin resulted in similar outcomes both before and after stretch (Figure 3.7), fibronectin was used only once more after its initial use. Although the recycled fibronectin would have relatively less fibronectin content, the spread and the cell attachment was still comparable to that of fresh fibronectin. This could be explained by the fact that affinity of cell attachment could also be affected by factors other than the concentration of fibronectin such as the properties of the substrate that could in turn influence the conformation of the fibronectin and thereby cell adhesion [218].

Different cell densities were tested to achieve the best protein and RNA yield for western blotting and RT-qPCR analysis. 1 ml of cell suspension at 4 x 10^5 cells/ml yielded the best protein yield compared to all other densities tested (Figure 3.6 & Figure 3.8). Additionally, scraping versus trypsinisation methods were also investigated for optimal protein yield for western blotting. The scraping method yielded a greater quantity of protein (Section 3.3.2) compared to the trypsinisation method, thus, the scraping method outweighed the trypsin method as it was more convenient to carry out with relatively fewer steps and higher protein yield. Additionally, the scraping method was more feasible due to the possibility that trypsin could digest some of the proteins in the cell lysate, which is not ideal, and as loss of sample in sample collection could be relatively less in the scraping method. This is possible since the washing step in the trypsinisation method could wash away some of the sample as well. Although scraping could also disrupt some of the proteins in the lysate, and some of the

sample could also be lost on the surface of the scraper blade, the end yield of protein was sufficient for western blotting. Although three chambers had to be pooled to obtain a sufficient protein yield for western blotting, for RT-qPCR under the same culture conditions (Section 3.2.1 & 3.2.2), one chamber was sufficient to yield sufficient RNA for one sample. This is because the amount of sample required for RT-qPCR is much less (at ng scale as opposed to μg scale in western blotting) compared to western blotting, due to its high sensitivity throughput.

3.5 Conclusions

In conclusion, fibronectin coated stretch chambers with a cell density of 4 x 10^5 cells/ml and a seeding volume of 1 ml/stretch chamber yielded the optimal conditions for stretching experiments. The spreadability was affected by the pattern that the coating material and the cell seeding suspension was introduced onto the cell growth surface and the volume of cell suspension added since different patterns of fibronectin coating and cell seeding, and cell seeding volumes yielded variable cell spreadability. For western blotting, three stretching chambers had to be pooled as opposed to single stretching chamber was sufficient for RT-qPCR, for protein and RNA quantification extracted by scraping and TRIZOL method respectively.

Chapter 4

Cyclic stretch as a novel modulator of APP and associated inflammatory markers in human cerebral endothelial cells

This following chapter presents the effect of cyclic stretch on APP expression and processing, and associated inflammatory signalling, with contents based on the publication:

> **Gangoda SVS**, Avadhanam B, Jufri NF, Sohn EH, Butlin M, Gupta V, Chung R & Avolio AP (2018) Pulsatile stretch as a novel modulator of amyloid precursor protein processing and associated inflammatory markers in human cerebral endothelial cells. *Sci. Rep.* **8**, 1689.

Summary—Amyloid β (Aβ) deposition is a hallmark of Alzheimer's disease (AD). Vascular modifications, including altered brain endothelial cell function and structural viability of the blood-brain barrier due to vascular pulsatility, are implicated in AD pathology. Pulsatility of phenomena in the cerebral vasculature are often not considered in *in vitro* models of the blood-brain barrier. We demonstrate, for the first time, that cyclic stretch of brain vascular endothelial cells modulates amyloid precursor protein (APP) expression and the APP processing enzyme, β-secretase 1, eventuating increased-Aβ generation and secretion. Concurrent modulation of intercellular adhesion molecule 1 and endothelial nitric oxide synthase (eNOS) signaling (expression and phosphorylation of eNOS) in response to cyclic stretch indicates parallel activation of endothelial inflammatory pathways. These findings mechanistically support vascular pulsatility contributing towards cerebral Aβ levels.

4.1 Introduction

Alzheimer's disease (AD) is the most common form of dementia. Post-mortem brain tissue examination reveals amyloid plaques, which are considered to play an important role in the pathophysiology of AD [221]. The main constituent of amyloid plaques, amyloid β (Aβ) peptides, are derived from amyloid precursor protein (APP), a transmembrane protein expressed in various cell types including endothelial cells (ECs) [221].

Although AD is conventionally classified as a neurodegenerative disease, emerging evidence indicates that dysregulation of vascular factors is a common feature of disease progression [64,74,222]. Of the multitude of vascular factors implicated in AD, involvement of vascular pulsatility, endothelial dysfunction and inflammatory changes in ECs are far from clear [16,64,222]. However, there is evidence in the literature indicating that these factors are concomitant with AD [64,74,222].

Higher pulsatility index and pulse pressure, indicative of increased large artery stiffness and reduced vessel compliance, are associated with AD, lower memory scores, increased amyloid burden and cerebral microvascular damage [64,74]. Vascular stiffness is also related to endothelial dysfunction where nitric oxide (NO)-mediated-endothelium-dependent

vasodilation, which is facilitated by the enzyme, endothelial NO synthase (eNOS), is diminished. Inhibition or deficiency of eNOS was found to be associated with higher APP protein expression and secretion of Aβ, while Aβ was found to mediate vascular dysfunction by hampering eNOS-mediated NO release [103,104,223].

Additionally, vascular stiffness could lead to increased vascular inflammation, which is also known to be associated with AD [16,87]. Elevated expression and localisation of inflammatory markers such as intercellular cell adhesion molecule-1 (ICAM-1) surrounding AD-plaques have been demonstrated [16]. Together, these data corroborate the findings that high pulsatility, endothelial dysfunction and vascular inflammation are independently associated with AD [16,103,104].

These factors are also present in the milieu of hypertension, which is a major risk factor for AD [74]. Although direct correlations of antihypertensive therapy and dementia remains to be clarified, there is compelling evidence indicating that hypertension poses additive effects on cognitive impairment and that anti-hypertensive therapy could alleviate the deleterious cognitive effects [2,224]. Increased systolic pressure and decreased diastolic pressure have been shown to be positively correlated with increased amyloid burden, risk of AD incidence, reduced cognitive function and increased gray matter atrophy [2,3,74]. Notably, increased pulse pressure, vascular stiffness and hypertension could impose increased mechanical stretch on ECs. The consequence of this chronic stress placed upon cerebral microvascular ECs is currently unknown.

The present study investigated whether increasing cyclic stretch magnitude as a mechanistic stimulus in a cerebral microvascular EC culture model, could modulate processes such as expression and processing of APP, Aβ secretion, endothelial dysfunction and inflammation, all of which are contributors to AD-pathology.

4.2 Methods

4.2.1 Cell culture and maintenance

Immortalized human cerebral microvascular endothelial cells-SV40 (HCMEC-SV40) were purchased from Applied Biological Materials Inc. and maintained in M199 media (Sigma-Aldrich) supplemented with 10% fetal bovine serum and 1% penicillin/streptomycin at 37 ^{0}C with an atmospheric humidity of 5% CO_2.

Cells were seeded on fibronectin-coated (375 µg/ml) silicon chambers 24-hours prior to stretching at a seeding density of 8×10^5 cells/ml. Cells were stained with trypan blue and counted using the Countess automated cell counter (Life Technologies) according to the manufacturers' protocol. Passages 17-19 were used for all experiments.

4.2.2 Cyclic stretching of ECs

Cells were subjected to uni-axial cyclic stretch as previously described [225], using the ShellPa stretch system (B-Bridge International) under culture conditions mentioned in Section 4.2.1. The silicon chambers have 200 µm thick transparent bottoms with side-wall thickness of 400 µm to support uniform stretching across the cell substrate. The chambers were mounted in the stretching apparatus where one end of the chamber is fixed and the other connected to an actuator operated by compressed air. The actuated arm stretched the chambers at a rate of 1 Hz for 18 hours in all experiments at a maximum extension of either 5, 10 or 15%. Control condition consisted of the same placement of the chambers, but with no cyclic extension applied for the 18-hour period.1 Hz was chosen based on previous stretch studies [177,178,225] and is in the range of resting human heart rate. The degree of stretch (%) is defined the as relative elongation of the chamber.

4.2.3 Real-time quantitative reverse transcription polymerase chain reaction (RT-qPCR)

Total RNA was extracted using TRIZOL (Invitrogen) according to the manufacturers' instructions after the 18-hour period and was normalized to 100 ng/μL using the Nano-Drop spectrophotometer. A 260/280 ratio of approximately 1.8-2.0 was used to ensure the RNA quality. Total RNA of 0.4 μg was then reverse transcribed using the SuperScript VILO complementary deoxyribonucleic acid (cDNA) synthesis kit (Life Technologies) according to the manufacturers' protocol. Negative control samples (RT-) were prepared by substituting the reverse transcriptase with dH_2O as a control for genomic contamination. This was followed by real-time qPCR using TaqMan® gene expression assays and TaqMan® gene expression master mix (Applied Biosystems) according to the manufacturers' protocol. The qPCR program comprised 120 s at 50 ^{0}C (incubation for optimal activity of uracil-DNA glycosylase), 600 s at 95 ^{0}C (optimal AmpliTaq Gold, Ultra-Pure enzyme activity), 15 s at 95 ^{0}C (denaturation) followed by 60 s at 60 ^{0}C (annealing and extension) repeated for 40 cycles.

The following pre-designed primer-probe TaqMan® assays by Life Technologies: APP (Hs00169098_m1); eNOS (Hs01574659_m1); and β2 microglobulin (Hs00984230_m1). Relative changes in mRNA levels were determined by the comparative ΔΔCT method normalised with human β2 microglobulin [226].

4.2.4 Western blotting

Protein extraction After 18 hours of stretching, the media was aspirated and the cells were briefly washed twice with cold phosphate-buffered-saline followed by addition of radioimmunoprecipitation assay buffer (50 mM Tris-HCl, pH 7.4, 150 mM NaCl, 5 mM EDTA, 10mM NaF, 10 mM sodium pyrophosphate, 1% IGEPAL CA-630, 0.5% sodium deoxycholate, 0.1% sodium dodecyl sulfate (SDS)) with protease inhibitor (Sigma-Aldrich)

added immediately prior to lysis. Cells were then harvested by scraping and the lysates were centrifuged at 14,000 × g for 15 minutes at 4 ^{0}C after sonication. The protein content was quantified using BCA assay (Pierce) according to the manufacturers' protocol.

40 µg of cell lysates were mixed with 4× NuPAGE sample buffer (Life Technologies) and were heated at 44 ^{0}C for 10 minutes before loading on 10% or 4-12% NuPAGE® Novex® Bis-Tris gels. The PVDF or nitrocellulose membranes were blocked in 5% skim milk buffer in TBS-T (Tris buffered saline-Tween; 20 mM Tris-HCl, pH 7.4, 0.5 M NaCl, 0.1% Tween 20) to be probed with anti-APP (1:1000; Covance), anti-eNOS (1: 250; Cell Signaling Technologies), anti-peNOS at S1177 (1:1000; Cell Signaling Technologies), anti-BACE-1 (1:500; Cell Signaling Technologies), anti-ICAM-1 (1:1000; R&D) or anti-glyceraldehyde 3-phosphate dehydrogenase (GAPDH) (1:1000) antibodies followed by secondary antibody incubations (1:2000; R&D) as previously described [227]. The blots were developed using Clarity™ Western ECL Substrate Kit (Bio-Rad) according to the manufacturers' protocol. The protein bands were quantified using the Image Lab 5.1 software within the linear range of detection as relative % control normalized to GAPDH (Bio-Rad Labs. Inc).

4.2.5 Measuring Aβ42 secretion using ELISA

The supernatants were collected after 18 hours of stretch and were analysed for secreted Aβ42 according to the manufacturers protocol using a commercial ELISA kit (KHB3544, Life Technologies). The absorbance was read at 450 nm and the Aβ42 levels were calculated using a standard curve in pg/ml.

4.2.6 Measurement of lactose dehydrogenase (LDH) activity

HCMECs were seeded on a 96-well plate at seeding densities of 2, 1, 0.5, 0.25 and 0.125 ×10^5 cells/ml. Cells were then treated with 2 mM H_2O_2 (tested toxic to HCMECs) for 24 hours and

the supernatants were collected for LDH assay (MAK066, Sigma). According to the manufacturers' protocol, a standard curve of [NADH] versus absorbance read at 450 nm was generated to calculate the LDH activity in units/ml. A standard curve of number of H_2O_2-treated cells (taken as dead cell count) versus the corresponding LDH activity was generated to determine the correlation of dying cells with measured LDH activity at different cyclic stretch magnitudes.

4.2.7 Statistical analysis

Data was collected in 5-10 replicates from individual experiments for each condition and data are represented as mean±SEM. Results were analyzed using One-way ANOVA with post-hoc Tukey-corrected multiple comparison tests, or linear regression analysis, using GraphPad PRISM version 6.05. Outliers were identified using the robust regression and outlier removal (ROUT) method (detailed in Motulsky *et al.* [228]) in GraphPad PRISM with a Q value set at 10% that defines the threshold for outliers. % control mRNA or protein expression were treated as independent variables and % stretch was treated as the independent variable.

4.3 Results

4.3.1 Cyclic stretch modulates cerebral endothelial expression of APP

After HCMECs were stretched for 18 hours at 0%, 5%, 10% or 15% stretch magnitudes, the qPCR analysis of APP mRNA expression was significantly higher than the static control (105±17%) at 10% (184±19%, $P<0.05$) and 15% (243±17%, $P<0.001$; Figure 4.1) stretch. Linear regression analysis showed a significant linear relationship between stretch and APP mRNA expression ($R^2=0.67$, $P<0.0001$, Table 4.1). Consistent with the overall increase in mRNA expression in response to stretch, the western blot results of protein expression of APP also showed the same trend ($R^2=0.21$, $P<0.01$, Figure 4.1, Table 4.1) under the same stretch conditions. APP expression was also significantly higher at 10% (240±52%, $P<0.05$) and 15%

(265±34%, $P<0.05$) of cyclic stretch magnitudes compared to the static control (100%; Figure 4.1).

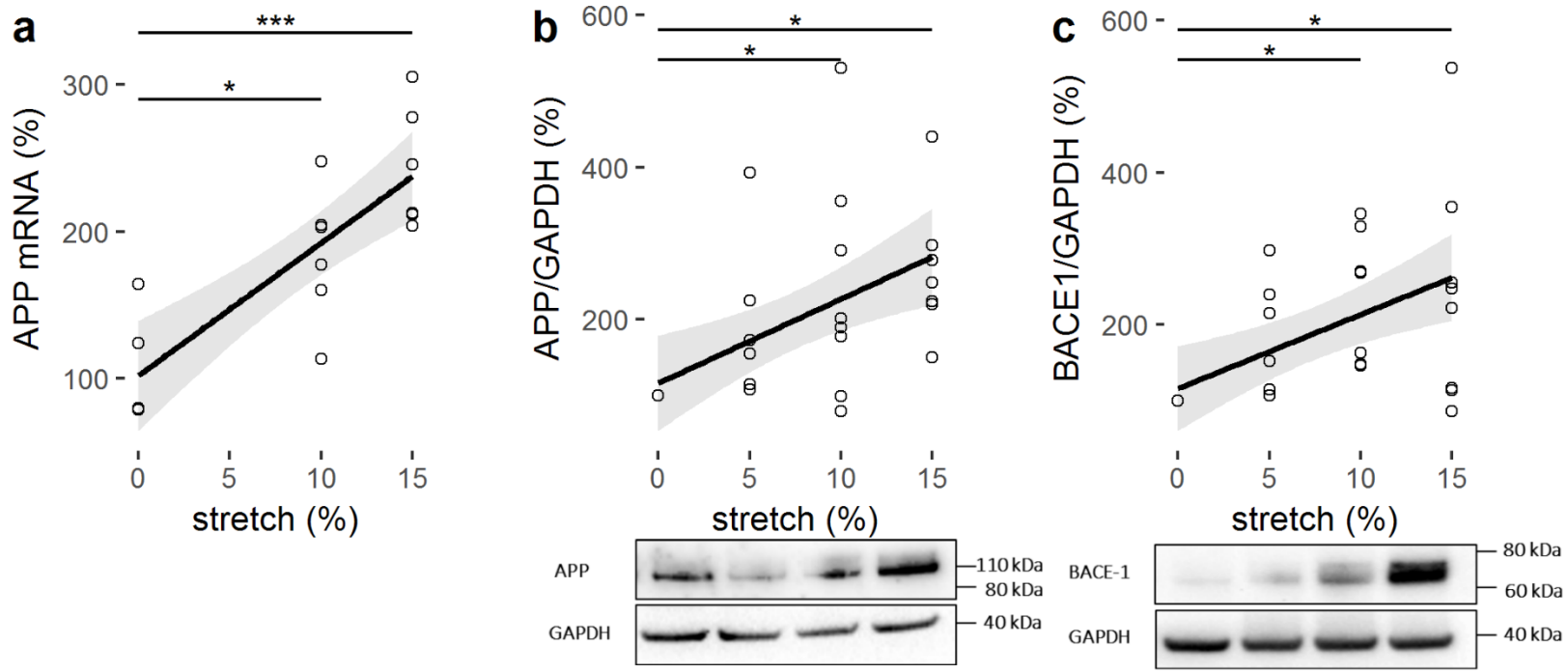

Figure 4.1 The effect of cyclic stretch on APP and BACE-1 in HCMECs. % control mRNA expression (a) and densitometric analysis of % control band intensity relative to GAPDH and the representative western blots of protein expression of (b) APP and (c) BACE-1 expression indicating amyloidogenic processing of APP at different magnitudes of cyclic (1 Hz) stretch of HCMECs over 18 hours. ***P<0.001, *P<0.05. n=5-10, analyzed using One-way ANOVA with post-hoc Tukey-corrected multiple comparison tests. Solid line shows the linear regression for the data and the shaded region the 95% confidence interval of the regression (regression statistics in Table 1). Abbreviations: APP, amyloid precursor protein; BACE-1, β-secretase 1; GAPDH, glyceraldehyde 3-phosphate dehydrogenase

4.3.2 Cyclic stretch results in amyloidogenic processing of APP and Aβ42 secretion in ECs

As for the APP expression, the protein expression of APP processing enzyme, β-secretase 1 (BACE-1), was measured in response to 18 hours of stretch at 0%, 5%, 10% or 15% stretch magnitudes using western blotting. BACE-1 was also increased at 10% (239±32%, $P<0.05$) and 15% (242±52%, $P<0.05$) stretch magnitudes (Figure 4.1), consistently with the expression of APP, with linear regression showing significant increase with stretch magnitude ($R^2=0.29$, $P<0.01$, Figure 4.1, Table 4.1).

The secreted Aβ42 levels in the supernatants from ECs that were stretched at 0, 5, 10 or 15 % stretch, showed a significant positive linear relationship with increasing magnitude of cyclic stretch ($R^2=0.21$, $P<0.01$, Figure 4.2, Table 4.1). Aβ40 levels did not change with stretch (Figure 4.2, Table 4.1) resulting in an increase in the Aβ42/ Aβ40 ratio with stretch magnitude ($R^2=0.21$, $P<0.01$, Figure 4.2, Table 4.1).

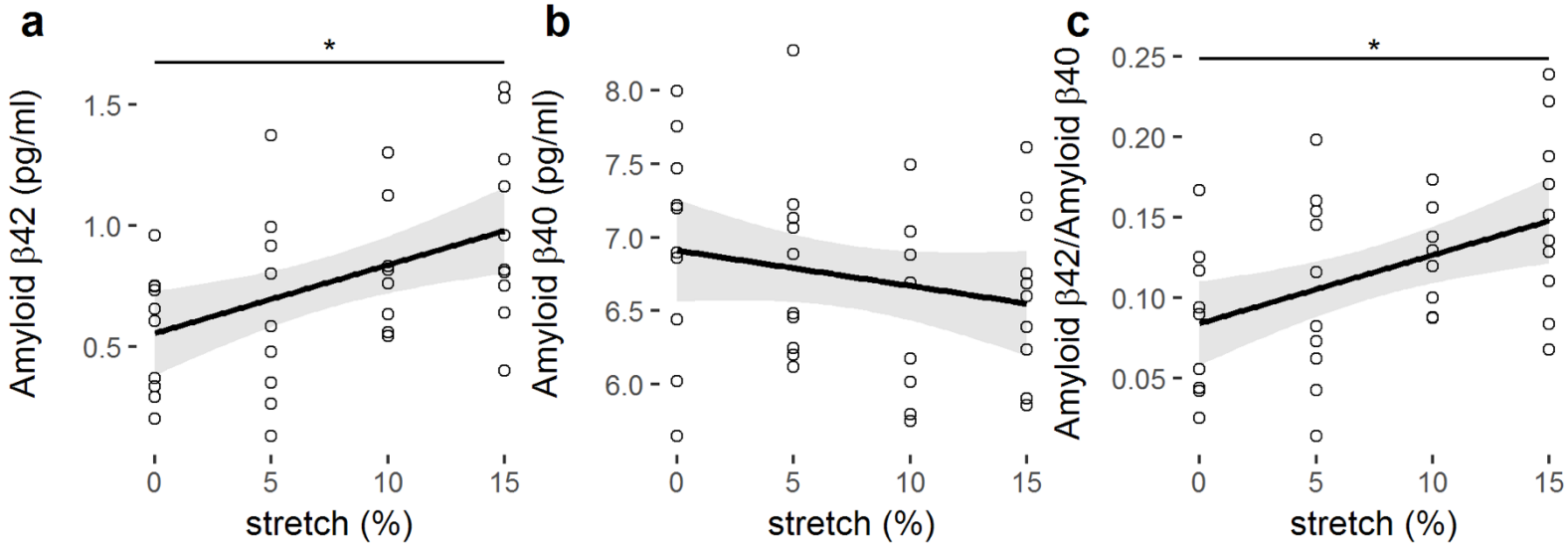

Figure 4.2 Amyloid β (a) 40 and (b) 42 secretion and (c) the ratio of the two for increasing magnitude of cyclic (1 Hz) stretch of HCMECs over 18 hours. *P<0.05. n=5-10, analyzed using One-way ANOVA with post-hoc Tukey-corrected multiple comparison tests. Solid line shows the linear regression for the data and the shaded region the 95% confidence interval of the regression (regression statistics in Table 1).

4.3.3 Cyclic stretch modifies the expression and phosphorylation of eNOS in cerebral ECs

The mRNA and protein expression of eNOS was also quantified after HCMECs had been subjected to 0%, 5%, 10% or 15% stretch for 18 hours using qPCR and western blotting respectively. There were no differences in eNOS mRNA expression at individual levels of stretch magnitude (Figure 4.3). Although the mRNA expression of eNOS was unchanged, the protein expression of eNOS showed an increasing trend with increasing stretch magnitude (R^2=0.21, P<0.01, Figure 4.3, Table 4.1). Protein expression of eNOS was significantly higher at 15% stretch magnitude (248±66%) relative to the 0% (100%; P<0.05) static control (Figure 4.3).

Phosphorylation of eNOS at serine-1177, a common activation site of eNOS, was quantified using western blotting under the same stretch conditions as for eNOS. In contrast to the upregulated eNOS protein expression levels in response to stretch, the phospho-eNOS at serine-1177 was downregulated at 5% (70 ±11%; P<0.05), 10% (46 ±8%; P<0.0001) and 15% (23 ±3%; P<0.0001) stretch magnitudes relative to the 0% static control (100%; Figure 4.3). The phospho-eNOS (peNOS) level at the 5% stretch magnitude (70 ±11%; P<0.001) was significantly higher than that at the 15% stretch magnitude (23 ±3%; Figure 4.3). Linear regression analysis revealed an inversely proportional relationship between peNOS and stretch magnitude (R^2=0.72, P<0.0001, Figure 4.3, Table 4.1).

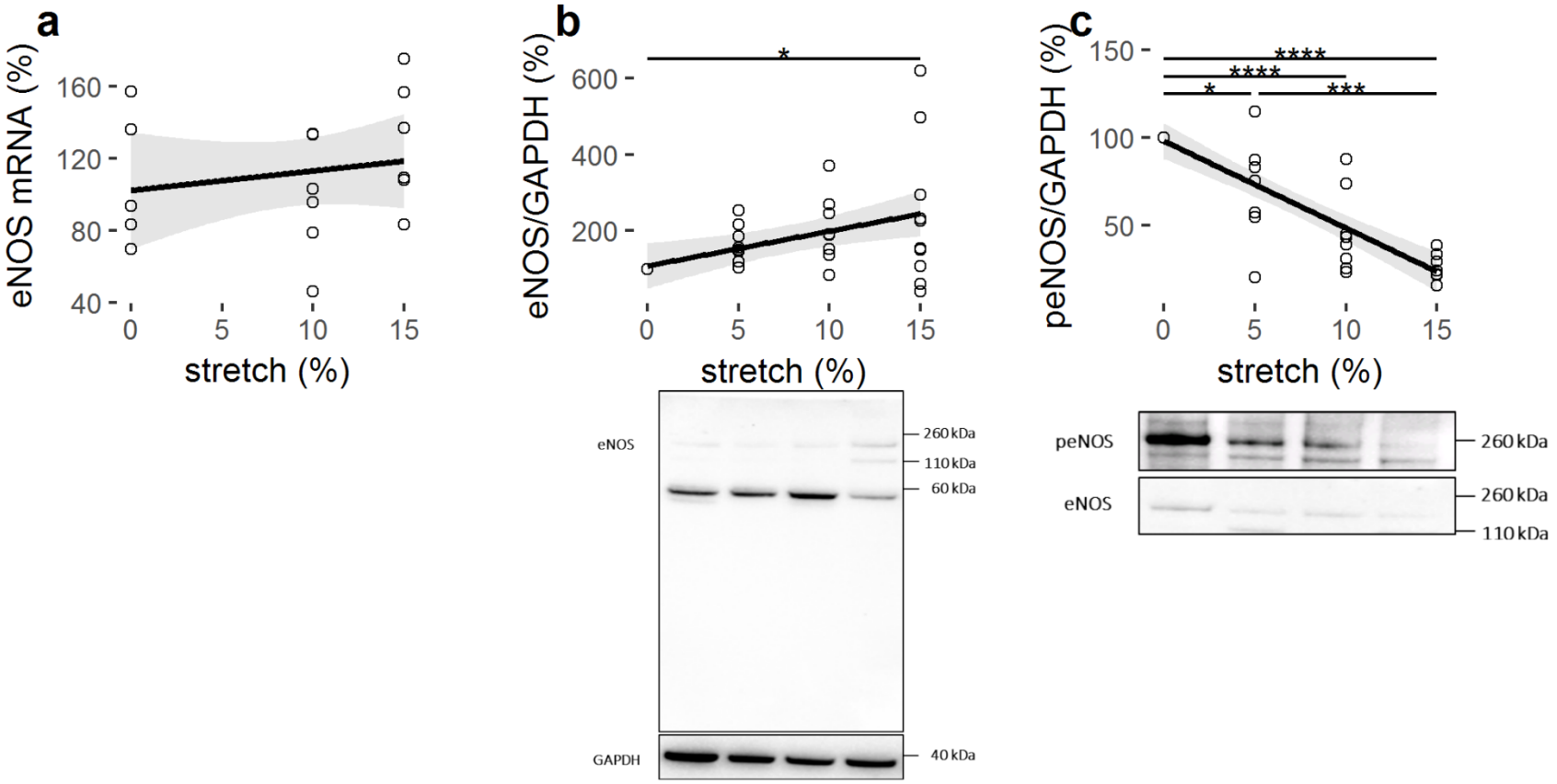

Figure 4.3 Cyclic stretch modulates eNOS expression and phosphorylation in HCMECs. % control mRNA expression (a) densitometric analysis of % control band intensity relative to GAPDH and the representative western blots of protein expression (b) and phosphorylation at S1177 (c) of eNOS in response to cyclic (1 Hz) stretch of HCMECs over 18 hours. ****P<0.0001, ***P<0.001 *P<0.05. n=5-10, analyzed using One-way ANOVA with post-hoc Tukey-corrected multiple comparison tests. Solid line shows the linear regression for the data and the shaded region the 95% confidence interval of the regression (regression statistics in Table 1). Abbreviations: eNOS, endothelial nitric oxide synthase; GAPDH, glyceraldehyde 3-phosphate dehydrogenase; peNOS, phosphorylated eNOS

4.3.4 Cyclic stretch modifies the expression of the inflammatory marker, ICAM-1, in cerebral ECs

ICAM-1 is an inflammatory marker that is regulated by eNOS mediated-NO13. ICAM-1 mRNA expression significantly increased at 10% stretch magnitude (163±13%, $P<0.05$; Figure 4.4) relative to the static control (108±16%) after 18 hours. Protein expression of ICAM-1 was upregulated at cyclic stretch magnitudes of 10% (125±10%, $P<0.05$) and 15% (128±15%, $P<0.05$) compared to the 5% cyclic stretch condition (87±9%; Figure 4.4). Linear regression of ICAM-1 protein expression showed a similar linear trend to that of APP and eNOS, increasing with increased stretch magnitude ($R^2=0.17$, $P<0.05$, Figure 4.4, Table 4.1).

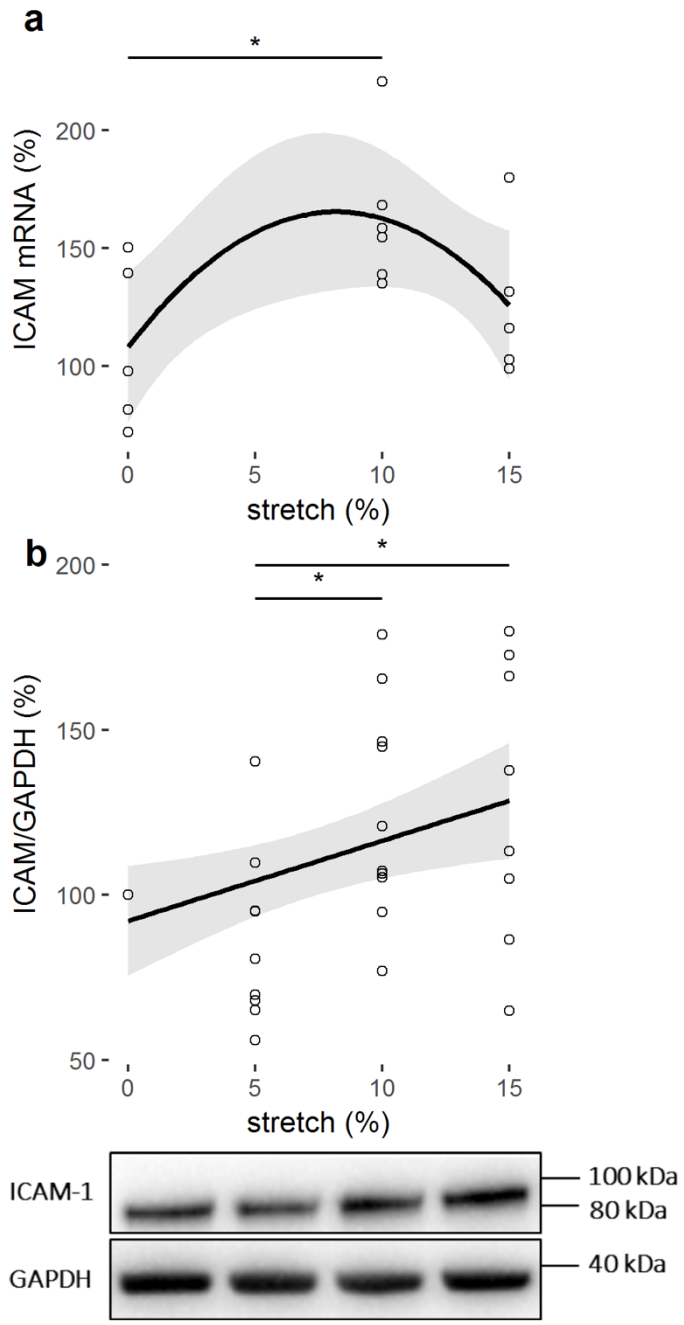

Figure 4.4 Cyclic stretch modulates inflammatory marker ICAM-1 expression. % control mRNA expression (a) and densitometric analysis of % control band intensity relative to GAPDH and the representative western blots of protein expression (b) of ICAM-1 in HCMECs subjected to 18-hour-cyclic (1 Hz) stretch between 0% and 15% magnitude. *P<0.05. Regression in (a), R^2=0.07, P=0.33. n=5-10, analyzed using One-way ANOVA with post-hoc Tukey-corrected multiple comparison tests. Solid line shows the regression fit for the data and the shaded region the 95% confidence interval of the regression (regression statistics in Table 1). Abbreviations: GAPDH, glyceraldehyde 3-phosphate dehydrogenase, ICAM-1, intercellular cell adhesion molecule-1

4.3.5 Long-term cyclic stretch does not significantly affect cell death in cerebral ECs

Since upregulation of APP, eNOS and ICAM-1 protein levels and Aβ42 secretion in response to 18 hours of stretch at 0%,5%,10% or 15% stretch magnitudes could collectively indicate a stress response, lactose dehydrogenase (LDH) activity, as a marker for stressed and dying cells, was measured after EC's had been subjected to the same stretch conditions (Figure 4.5). The range of LDH activity measured in the stretching experiments was 296 to 1620 units/ml. There was no increase in LDH activity with increased stretch magnitude (Figure 4.5, Table 1). The highest singular sample dead cell count was approximately 62,000 cells/ml (Figure 4.5) calculated based on the linear equation of the standard curve. Accordingly, the maximum overall dead cell count approximated to 8% of the initial cell seeding density in the stretching experiments, with the average cell death being much less than 8% (Figure 4.5).

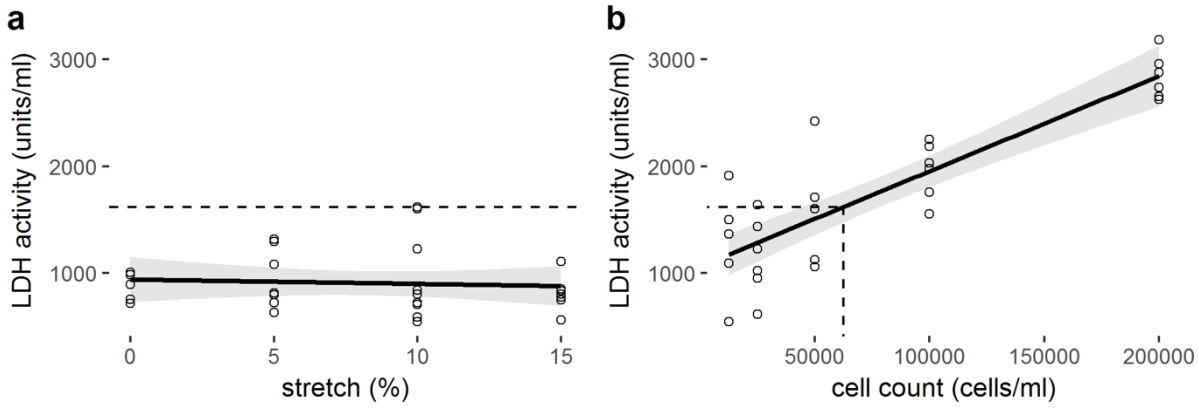

Figure 4.5 LDH activity relative to the stretch magnitude and corresponding cell death. The dashed line indicates maximum LDH activity observed in experiment conditions (a) and the corresponding dead cell count (b), a maximum cell death of 8% of the initial cell seeding density in the stretching experiments with the average cell death being much less than that. n=5-10, analyzed using One-way ANOVA with post-hoc Tukey-corrected multiple comparison tests. Solid line shows the linear regression for the data and the shaded region the 95% confidence interval of the regression (regression statistics in Table 1). Abbreviations: LDH, lactose dehydrogenase

Table 4.1 Regression statistics (linear model) showing changes with respect to increasing cyclic (1 Hz) stretch magnitude from 0 to 15%, as displayed in Figs. 1-5.

	slope	intercept	R^2	p
APP mRNA (%)	9.04	102	0.67	**<0.0001**
APP/GAPDH (%)	11.08	116	0.30	**0.0022**
BACE1/GAPDH (%)	9.70	117	0.29	**0.0023**
Aβ40 (pg/ml)	-0.024	6.9	0.05	0.1998
Aβ42 (pg/ml)	0.028	0.6	0.21	**0.0041**
Aβ42/Aβ40 ratio	0.0043	0.08	0.21	**0.0038**
eNOS mRNA (%)	1.09	102	0.04	0.4542
eNOS/GAPDH (%)	9.11	108	0.21	**0.0055**
peNOS/GAPDH (%)	-4.96	98	0.72	**<0.0001**
ICAM/GAPDH (%)	2.42	92	0.17	**0.0109**
LDH activity (units/ml)	11.79	739	0.04	0.2458

4.4 Discussion

Akt Amyloid deposits, a hallmark of AD, are mainly composed of Aβ aggregates [221]. One of the proposed risk factors for AD is hypertension, which could imply increased cyclic stretch on ECs, particularly, since pulse pressure and large vessel stiffness increases with age [2,224,229]. Based on this knowledge, the current study firstly evaluated the possible effect of increasing cyclic stretch magnitude as a mechanistic stimulus on the expression and processing of APP, the precursor for Aβ, and secreted Aβ levels in a cell culture model of cerebral microvascular ECs. Notably, 5% stretch is considered physiological while 15-20% stretch quoted as pathological [20]. In this study, 20% stretch magnitude was omitted due to substantial cell detachment after 18 hours of stretch, so that a maximal possible magnitude of 15%, which yielded a sufficient protein yield with minimal cell detachment was utilised.

Aβ peptides are cleaved fragments of APP, of which in the normal brain, the accumulation is prevented through adequate regulation of APP processing and clearance [221]. However, in AD, Aβ is accumulated and deposited as Aβ plaques, which is considered to occur via several mechanisms including over-expression of APP, enhanced cleavage of APP to Aβ, and reduced clearance of Aβ [221,230]. APP is cleaved and processed by a number of proteolytic enzymes [221]. The formation of Aβ peptides such as Aβ40 and Aβ42, results predominantly from the cleaving of APP by BACE-1 via the amyloidogenic pathway [221]. Current study showed that increasing the magnitude of cyclic stretch could lead to upregulation of APP expression and amyloidogenic processing enzyme, BACE-1, and Aβ42 secretion (Figure 4.1 & Figure 4.2). The expression of APP was regulated at both mRNA and protein levels (Figure 4.1), which coincided with increased BACE-1 protein expression levels. The upregulation or activation of BACE-1 was indicative of amyloidogenic processing of APP that leads to increased Aβ levels. The amyloid plaques in AD consist of two major isoforms of Aβ, Aβ42 and Aβ40 [231]. The interaction between Aβ42 and Aβ40 has been considered to play a critical role in Aβ deposition [231]. Assessment of Aβ42/Aβ40 ratio has been suggested to be one of the important diagnostic markers for AD pathogenesis [232,233]. To address this, the secreted Aβ40 and 42 levels were investigated. The secretion of Aβ40 did not change significantly although the secretion of Aβ42, which is considered to exhibit higher cellular toxicity compared to other Aβ fragments, proportionally increased with increasing cyclic stretch (Figure 4.2), indicating that Aβ42/Aβ40 ratio was shifted towards Aβ42 (Figure 4.2). Many studies suggested that Aβ42 is the major component of amyloid plaques in AD brains, while Aβ40 is detected only in a subset of plaques [231,234–236]. They explained that the Aβ42 deposition precedes Aβ40 deposition and the initial Aβ42 aggregation does not involve Aβ40 while preferential binding of Aβ42 to extracellular matrix or cell membrane may lead to a high local Aβ42 concentration in the amyloid plaques [231,234–237]. Together, findings of the current study emphasise that

increased cyclic stretch could modulate the expression and processing of APP towards the amyloidogenic pathway, favouring formation of Aβ42.

To the best of our knowledge, the direct effect of cyclic stretch on the expression and processing of APP, and Aβ secretion in cerebral ECs has not been studied before. However, there is considerable evidence supporting the hypothesis that cyclic stretch modifies the expression and/or processing of APP [238]. Traumatic brain injury, in a non-transgenic mouse model, where sudden mechanical stress induces axonal damage, has led to upregulated cerebral APP expression and BACE-1 [238]. A recent study demonstrated a significant correlation between amplitude of retinal vascular pulsatility and neocortical Aβ scores in an elderly cohort including clinical and pre-clinical AD patients [239]. Additionally, hypertension or increased pulse pressure, both of which could lead to elevated vascular pulsatility, are associated with increased risk of pre-symptomatic AD in cognitively normal elderly subjects [2,74]. Angiotensin-II induced hypertension in Tg2576 mice, an AD model in which both circulating and cerebral Aβ is elevated due to a mutation in APP, has resulted in increased vascular amyloid deposition and enhanced BACE-1 mediated-amyloidogenic APP cleavage [3]. Thus, our study substantiates previous observations and suggests that mechanical stretch alters the expression and processing of APP. This adds weight to the hypothesis that increased vascular stretch magnitude, which could be a result of hypertension, or high pulse pressure as is the case in isolated systolic hypertension, may have consequences in terms of cerebral Aβ load. That is, the high pulse pressures generated within the larger vessels in the milieu of hypertension, if transmitted to the vascular beds as increased mechanical stretch, could act as a mechanical switch for the endothelium to overexpress APP and favour APP cleavage into Aβ. Although the present study showed the direct effect of cyclic stretch on the expression of APP and the secretion of Aβ, it was not possible to investigate the clearance of Aβ once released into the supernatant. Of note, the assumption here is that the kinetics of physiological

Aβ clearance remain unchanged such that Aβ would accumulate over time. The physiological and pathophysiological levels of Aβ42 in human circulation are stated to be 50 pM and 4.3 nM respectively [58]. The range of Aβ42 in this study was 0.1-0.4 pM. Although this concentration fell below the physiological level of circulating Aβ42, it would still substantially account for the overall Aβ42 considering that the physiological endothelial milieu would be much larger in scale to the experimental conditions and if it would accumulate over time. Given that the present study was performed over 18 hours in a small number of cells, and that Aβ accumulates over decades in the pathophysiology of AD across a large vascular bed, the amounts reported in this study would be remarkable if it were to accumulate over time. Moreover, physiologically, there are other sources of Aβ42 that contribute to the circulating Aβ42 pool such as neurons. Notably, Aβ40 and Aβ25-35 at nanomolar to micromolar ranges showed a concentration-dependent effect on EC proliferation, thus even lower concentrations of Aβ may have profound effects on EC function, which are key regulators of the blood-brain barrier that is also important in Aβ clearance [240].

The expression of APP is altered at different magnitudes of cyclic stretch (Figure 4.1). An inverse correlation between APP expression and eNOS activity has been reported [103,104,222]. Over-expression of APP in Tg2576 mice has been demonstrated to lead to endothelial dysfunction, thereby mitigating endothelial vasorelaxation with a concomitant decrease in bioavailable NO[222]. Austin *et al.* [103,104] further elaborated a significant role of NO in modulating the expression of APP. In human brain microvascular ECs treated with the NOS inhibitor, N (G)-Nitro-L-Arginine Methyl Ester, and in $eNOS^{-/-}$ mice, it was shown that the expression of APP and BACE-1, and Aβ levels were up-regulated[103]. These effects in $eNOS^{-/-}$ mice were reversed by supplementation with NO by treating the animals with nitroglycerine, which resulted in a marked increase in cyclic guanosine monophosphate (cGMP) levels [104]. An intriguing feedback mechanism between NO bioavailability and Aβ can

be illustrated by these studies along with the study of Rajadas *et al.* [12], which showed that Aβ1–42 treatment caused an upregulation of eNOS expression [12]. This is consistent with a compensatory mechanism dependent on NO bioavailability as increased Aβ may trigger eNOS expression to compensate for the reduced bioavailable NO levels [12].

The present study substantiates the existing evidence that APP and BACE-1 expression and Aβ secretion proportionally increased with stretch and showed similar effects on eNOS expression and phosphorylated eNOS at serine-1177, a common activation site of eNOS that is upstream of endothelial-dependent NO production. Although the overall protein expression of eNOS (Figure 4.3) was increased, the peNOS levels (Figure 4.3) were decreased in response to cyclic stretch. Previous studies have elaborated that cyclic stretch could induce peNOS at S1177 [165,179]. However, these studies were done within 1 hour of stretch in contrast to 18 hours in the current study. Therefore, the results show that, regardless of the overall increase in eNOS expression, the phosphorylation of eNOS at S1177 is downregulated by long-term cyclic stretch that could in turn lead to a decrease in endothelial-dependent NO production, indicative of a dysfunctional endothelium. Consistently, Singh *et al.* [241] also reported that C-reactive protein, a cardiovascular risk marker leading to endothelial dysfunction, causes decreased eNOS activity and NO production by downregulating eNOS phosphorylation in ECs without changing the total eNOS abundance. Of note, the presence of additional bands on total eNOS blots under stretched versus not-stretched conditions further confirmed that cyclic stretch could also modulate the processing of eNOS (Figure 4.3). However, the mRNA expression of eNOS appeared to be unchanged in response to stretch (Figure 4.3), in contrast to the protein expression (Figure 4.3). Many stimuli such as hypoxia could decrease-eNOS stability, and thus the unchanged-eNOS mRNA levels in our study could be explained by the stability of mRNA being compromised due to stretch[242]. Nonetheless, the overall results suggested that eNOS may be pivotal in regulating the expression and processing of APP, since

concomitant fluctuations of APP, Aβ and eNOS protein expression and phosphorylation levels at different levels of stretch indicated a possible compensatory mechanism, consistent with previous findings.

Fluctuations in eNOS expression and phosphorylation due to stretch suggest parallel activation of endothelial inflammatory pathways. ICAM-1 is an inflammatory marker, which can be regulated by NO levels and is also associated with AD-plaques, hence it was also investigated [16,243]. ICAM-1 mRNA was significantly increased at 10% compared to the static control (Figure 4.4), of which the protein levels were upregulated at both 10% and 15% stretch magnitudes compared to the 5% (Figure 4.4). This finding is supported by previous studies that have shown that ICAM-1 expression was upregulated with cyclic stretch [244]. Increased ICAM-1 expression has been associated with AD-plaques [16]. Thus, concomitant ICAM-1 and APP increase after 18 hours of cyclic stretching in the present study suggests that increased APP is associated with increased ICAM-1 expression.

A recent proteomics study that utilised the same approach as the present study, where human cerebral endothelial cells (HCMECs) were stretched for 18 hours at 1 Hz at 5% or 20% stretch magnitudes, revealed that proteins that are related to inflammation and APP were regulated by stretch [212]. Phospholipase-A2-activating-protein that could mediate Aβ-driven-inflammatory responses was downregulated at 5% stretch relative to 0%, implicating the involvement of physiological stretch as a possible inflammatory suppressor [245]. In contrast, at 20% stretch, upregulation of apolipoprotein B-100 (APOB), junctional-adhesion-molecule-A and ELKS/Rab6-interacting/CAST family member-1, a regulator in activating nuclear-factor-kappa-B (NFκB) that elevate ICAM-1 levels, indicated that prolonged-stretch could induce a pro-inflammatory state in ECs [87,246]. Of note, APOB is known to modulate APP metabolism [247]. At 20% stretch, Integrin β-3 (ITGB3), which positively regulates eNOS, increased relative to 0% [240]. ITGB3 is also known to interact with low-density-lipoprotein-

related-receptor-1 that facilitates Aβ clearance [248]. Cyclic adenosine monophosphate (cAMP)-dependent-protein-kinase-catalytic-subunit-β that regulates cAMP-dependent protein kinase activity, which is known to regulate non-amyloidogenic processing of APP, was significantly down-regulated at 20% stretch compared to 5% [249]. Although the present study did not investigate the underlying molecular mechanisms in detail, this proteomic study substantiates possible mechanisms such as aberrant Aβ clearance and cAMP-dependent APP processing, and integrin- and/or NFκB-mediated-eNOS and ICAM-1 signaling, which could be implicated in eventuating deregulation of APP expression, processing and/or clearance and inflammatory responses as seen in the current study. Additionally, decreased eNOS phosphorylation at serine 1177 further corroborates the inflammatory state of the stretched cells.

It is important to note that there are factors inherent to the mechanical stretch system that are unavoidable, which may account for the variability seen in some of the data, and is a limitation of the current study. As this is a mechanical (pneumatic) system, the stretch chambers may not have been stretched to the exact set magnitudes at all times accounting for some level of error. Additionally, one representative control sample that matched the cell passage number closest to all stretch levels out of the 5%,10% or 15% stretch magnitudes was randomly selected to represent the static control for each 5%,10% and 15% set that was run on a gel at a time. This was to be able to compare between the stretch magnitudes, in which case, all samples had to be run simultaneously on the same gel next to each other. This could introduce some level of variability as there are variations between controls from batch to batch. Thus, the above factors could introduce variability within the data. However, importantly, despite the variability introduced by these factors, the recorded effects are statistically significant, and tighter control of these variables or longer time periods of stretching would likely increase the confidence in these significant differences.

4.5 Conclusions

Taken together, the results can be implicated in expanding the existing knowledge on the effect of vascular pulsatility as a mechanical stimulus that modulates endothelial APP, eNOS and ICAM-1 in the context of AD. Modulation of pulsatility of blood microvessels may pose beneficial effects in alleviating the potential deleterious effects on AD progression. Future studies are warranted to further investigate whether the associations between APP, eNOS and ICAM-1 in response to cyclic stretch were directly interdependent.

Chapter 5

Signalling pathways that mediate cerebral endothelial responses to cyclic stretch

Summary—Cyclic stretch modulates amyloid precursor protein (APP) expression and processing and nitric oxide (NO) signalling in endothelial cells (ECs). The serine/threonine-specific kinase, Akt, glycogen synthase kinase-3 (GSK-3) and caveolin-1 are involved in stretch-mediated NO signalling in ECs and Alzheimer's disease (AD) pathology characterised by amyloid-β (Aβ) plaques arising from processed APP. This study sought to investigate the magnitude dependency of mechanical stretch on Akt, GSK-3, caveolin-1 and the APP processing enzyme, a disintegrin and metalloproteinase-10 (ADAM10), and to quantify NO levels in response to stretch in a cerebral EC line since mechanical stretch effects on cerebral ECs are not known in the context of AD. Akt, GSK-3, caveolin-1 and ADAM10 were quantified using western blotting and NO was measured by a NO assay kit. Akt and GSK-3 phosphorylation were downregulated at all stretch magnitudes relative to the static control, ADAM10 increased with a concomitant increase in NO and a decrease in caveolin-1 at the 10% stretch magnitude relative to 5% stretch magnitude. Thus, Akt and GSK-3 phosphorylation are modulated by stretch, although NO signalling is regulated by a different mechanism other than Akt/eNOS signalling. Caveolin-1 is possibly involved in NO production, and NO concentration may in turn regulate ADAM10 and APP processing, at least at the 10% stretch magnitude. Future studies are required to confirm whether Akt/GSK-3 underlie the alterations in APP processing and expression that are shown in Chapter 4, which will provide further understanding of the molecular mechanisms that regulate APP and NO signalling in response to cyclic stretch and, thereby providing evidence supporting vascular contributions towards AD.

5.1 Introduction

Cyclic stretch is a derivative of pulsatile energy exerted on the vasculature by rhythmic contraction and relaxation cycles of the heart and pulse pressure. The pulsatility of vessels is sensed by the cells that align the vascular lumen. These are the endothelial cells (ECs) that form the endothelium, a monolayer of ECs. ECs are crucial in mechanotransduction of mechanical stretch mediated signals in transforming them into biochemical signals that lead to physiological changes such as nitric oxide (NO) production in maintaining vascular homeostasis [165].

Many signalling pathways are involved in the process of mechanotransduction via ECs including phosphatidylinositol-3-OH kinase (PI3K)/Akt [165,250]. PI3K/Akt signalling is known to modulate glycogen synthase kinase (GSK) phosphorylation of GSK-3α and GSK-3β at serine 21 and serine 9 respectively, that leads to inhibition of GSK activity [251–253]. *In vivo* and

ex vivo mechanical stretch studies of the rat myocardium demonstrated that transient mechanical stretch led to GSK-3β inhibition and PI3K dependent Akt activation to mediate cardioprotective effects against cardiac ischemia- reperfusion injury [254]. Cyclic stretch of 12% applied to myotubes resulted in similar effects on Akt and GSK-3β concomitant with an increase in NO production [255]. Additionally, mechanical stretch effect on Akt and GSK-3 activity independent of each other had also been demonstrated [162,165,185,191,192,194,250,256–258].

Involvement of GSK and PI3K/Akt activity is known to be involved in Alzheimer's disease (AD) pathology, whilst GSK activity via PI3K/Akt is known to be modulated by caveolin-1 [17,116,119]. AD is characterised by amyloid-β (Aβ) plaques that are derived from amyloid precursor protein, which is processed by secretases including a disintegrin and metalloproteinase-10 (ADAM10). In transgenic mouse models of AD, GSK-3α mediated both senile plaques and neurofibrillary tangles (NFT) pathogenesis whilst GSK-3β only modulated NFT formation [116]. *In vitro* studies have demonstrated a role of caveolin-1 mediating inhibitory effects on GSK-3 [17,118]. Additionally, caveolin-1 dependent Akt activation in response to mechanical stretch had been reported, showing mechanosensor properties of caveolin-1 [192].

This study sought to investigate the magnitude dependency of mechanical stretch on Akt, GSK-3, caveolin-1, ADAM10, and to quantify NO levels in response to stretch in a cerebral EC line since mechanical stretch effects on cerebral ECs are not known in the context of AD.

5.2 Methods

5.2.1 Culture and stretching conditions

Culture of human microvascular endothelial cell-Simian Virus 40 (HCMEC-SV40; within passage 17-19) and stretching conditions are detailed in Chapter 3 and Chapter 4.

5.2.2 Western blotting

Protein extraction and western blotting procedures are detailed in Chapters 3 and Chapter 4. The primary antibodies utilised in this study were anti-Akt (1:1000; #4691), anti-pAkt at S473 (1:500; #9271), anti- GSK-3α (1:1000; #5676), anti-pGSK-3α at S21 (1:500; #9331), anti-GSK-3β (1:1000; #5676), anti-pGSK-3β at S9 (1:500; #9331), anti-caveolin-1 (1:1000; #3267) and anti-ADAM10 (1:1000; #ab124695), which were detected with anti-rabbit secondary antibody incubation (1:2000; #7074). All antibodies were purchased from Cell Signalling Technologies (Danvers, USA) or Abcam (Melbourne, Australia).

5.2.3 Stripping protocol

Blots were stripped with 0.2 M NaOH solution subsequent of phospho-antibodies and re-probed for total protein bands of corresponding proteins.

5.2.4 NO assay

NO was measured using nitrate/nitrite assay kit (Cayman; cat #: 780001) as per the manufacturer's protocol for quantifying total nitrate and nitrite content in the supernatants. The protein content in the supernatants were quantified using BCA assay and were normalized to 50 µg of total protein prior to performing the assay.

5.2.5 Statistical analysis

Each data point represents an individual experiment and data are represented as mean±SEM analysed using one-way ANOVA with post-hoc Tukey-corrected multiple comparisons performed in GraphPad PRISM software version 7.02. Outliers were identified using the robust regression and outlier removal (ROUT) method (detailed in Motulsky *et al.* [228]) in GraphPad PRISM with a Q value set at 10% that defines the threshold for outliers. % control

protein expression or phosphorylation were treated as independent variables and % stretch was treated as the independent variable.

5.3 Results

5.3.1 Cyclic stretch downregulates Akt phosphorylation at S473

Due to the involvement of Akt phosphorylation in response to stretch, it was first investigated whether stretch influences Akt in the cerebral EC line, HCMEC-SV40. Followed by 18 hours of stretching at 1 Hz, Akt expression did not change significantly in HCMECs at any of the stretch magnitudes that had been tested (Figure 5.1). However, phosphorylation of Akt at its activation site, S473, was reduced significantly at 5% (36±7%, $P<0.0001$), 10% (44±10%, $P<0.0001$) and 15% (42±10%, $P<0.0001$) stretch compared to 0% static control (100%; Figure 5.1).

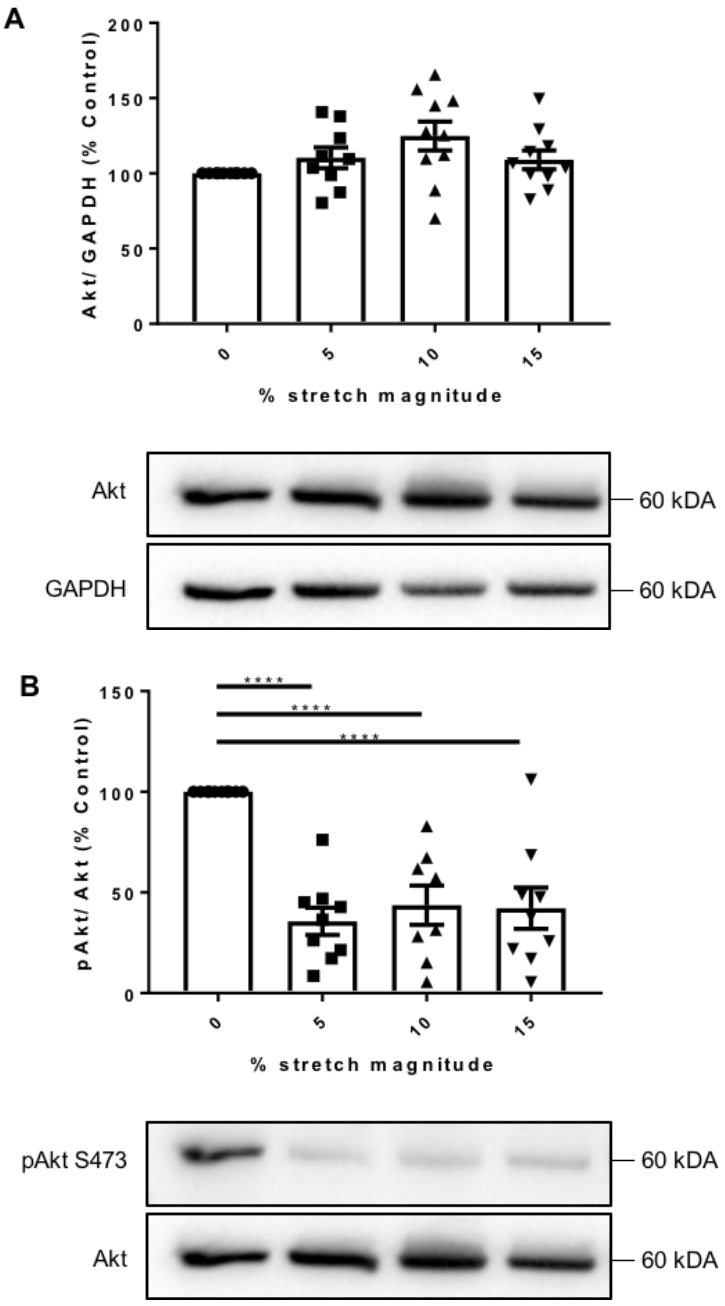

Figure 5.1 Effect of cyclic stretch on Akt in HCMEC-SV40. 18 hours of cyclic stretch at 1Hz did not change the Akt expression at any magnitude (A) although Akt phosphorylation at S473 (B) was significantly downregulated at all stretch magnitudes. Representative western blot bands are shown below the bar graphs. ****P<0.0001, n=7-10, analysed using One-way ANOVA with post-hoc Tukey-corrected multiple comparison tests. Abbreviations: GAPDH, glyceraldehyde 3-phosphate dehydrogenase; pAkt, phosphorylated Akt

5.3.2 Cyclic stretch modulates GSK-3α and GSK-3β

GSK-3 expression and phosphorylation at the relevant sites were next investigated since it is known that Akt phosphorylation, which was altered in response to stretch in HCMECs (Figure 5.2), could regulate GSK-3 activity [251–253]. 18 hours of stretching did not change the expression of GSK-3α in HCMECs. However, stretching resulted in a significant reduction in GSK-3β expression at all stretch magnitudes tested, 5% (53±8%, $P<0.01$), 10% (64±10%; $P<0.05$) and 15% (66±13%; $P<0.05$) compared to the 0% static control (100%; (Figure 5.2). Nonetheless, the phosphorylation of GSK-3 was downregulated at both pGSK-3α/S21 and pGSK-3β/S9 at 5% (pGSK-3α: 57±10%, $P<0.01$; pGSK-3β: 42±9%, $P<0.0001$), 10% (pGSK-3α: 49±9%, $P<0.001$; pGSK-3β: 42±10%, $P<0.0001$) and 15% (pGSK-3α: 45±10%, $P<0.001$; pGSK-3β: 25±5%, $P<0.0001$) compared to the 0% static control (100%; Figure 5.2).

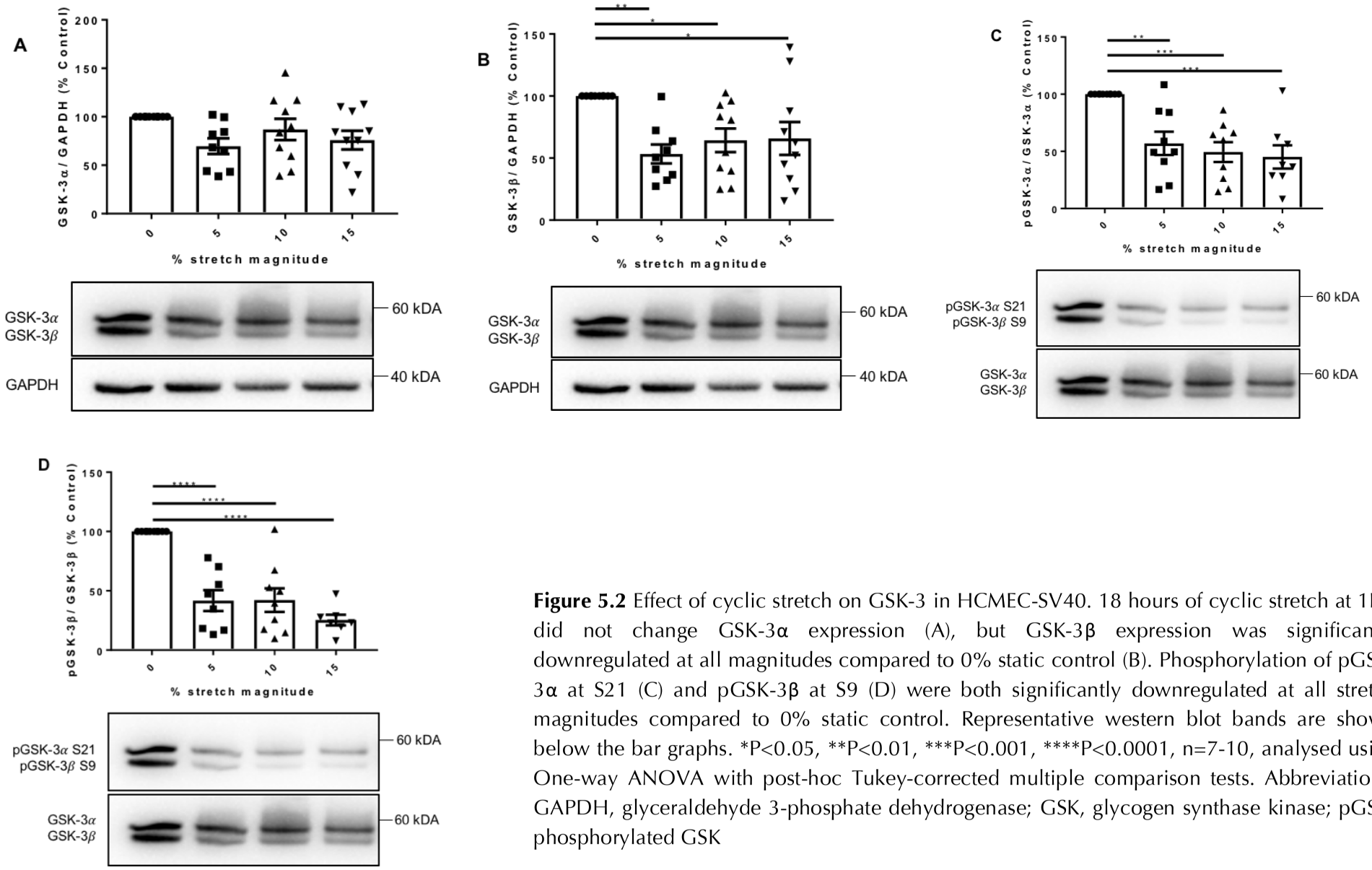

Figure 5.2 Effect of cyclic stretch on GSK-3 in HCMEC-SV40. 18 hours of cyclic stretch at 1Hz did not change GSK-3α expression (A), but GSK-3β expression was significantly downregulated at all magnitudes compared to 0% static control (B). Phosphorylation of pGSK-3α at S21 (C) and pGSK-3β at S9 (D) were both significantly downregulated at all stretch magnitudes compared to 0% static control. Representative western blot bands are shown below the bar graphs. *P<0.05, **P<0.01, ***P<0.001, ****P<0.0001, n=7-10, analysed using One-way ANOVA with post-hoc Tukey-corrected multiple comparison tests. Abbreviations: GAPDH, glyceraldehyde 3-phosphate dehydrogenase; GSK, glycogen synthase kinase; pGSK, phosphorylated GSK

5.3.3 Cyclic stretch alters NO production

Akt/GSK-3β is known to modulate endothelial NO production, and eNOS phosphorylation at S1177 was downregulated in response to stretch in HCMECs (Chapter 4), hence NO production was next investigated in response to different magnitudes of stretch in HCMECs[255] (Figure 5.3). NO concentration was significantly higher at 10% stretch magnitude (0.046±0.003 μM/μg) compared to the 5% stretch magnitude (0.033±0.003 μM/μg, P<0.05; Figure **5.3**).

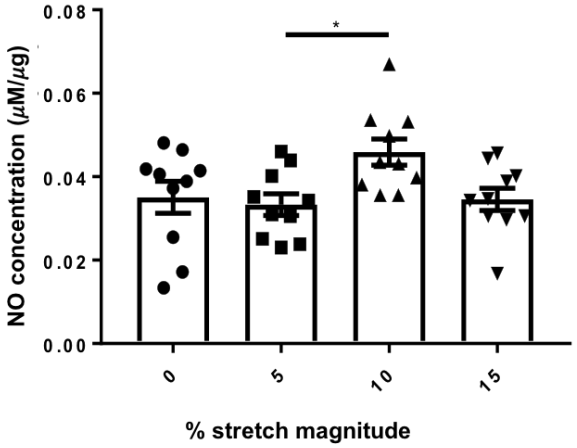

Figure 5.3 Effect of cyclic stretch on endothelial NO production. NO production at 10% stretch magnitude after HCMECs had been stretched for 18 hours at 1 Hz was significantly higher than that at 5% stretch magnitude. *P<0.05, n=10, analysed using One-way ANOVA with post-hoc Tukey-corrected multiple comparison tests. Abbreviations: NO, nitric oxide

5.3.4 Cyclic stretch modulates caveolin-1

GSK-3 activity via PI3K/Akt is known to be modulated by caveolin-1[119]. Stretching altered GSK-3 expression and phosphorylation (Figure 5.2). Therefore caveolin-1 expression in response to stretch was also studied. Caveolin-1 expression at 5% stretch magnitude (299±82%) was significantly increased compared to 10% stretch magnitude (118±25%, P<0.05) and 0% static control (100%, P<0.05; Figure 5.4).

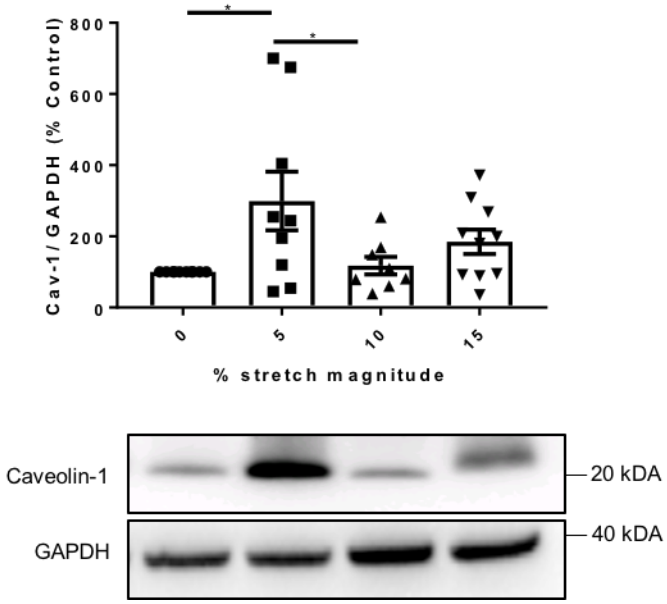

Figure 5.4 Effect of cyclic stretch on caveolin-1. Caveolin-1 expression significantly increased at 5% stretch magnitude compared to 10% stretch and 0% stretch magnitudes after 18 hours of 5%, 10%, 15% or 0% stretch at 1Hz. Representative western blot bands are shown below the bar graph. *P<0.05, n=7-10, analysed using One-way ANOVA with post-hoc Tukey-corrected multiple comparison tests. Abbreviations: Cav-1, caveolin-1; GAPDH, glyceraldehyde 3-phosphate dehydrogenase

5.3.5 Cyclic stretch modulates pro-ADAM10

The APP processing enzyme, ADAM10 was next evaluated in response to stretch. No bands were observed at the mature ADAM10, which is approximately 65 KDa. However, pro-ADAM10 bands that appeared at approximately 84 KDa, which is indicative of ADAM10 expression were quantified. Level of expression of pro-ADAM10 at the 10% stretch magnitude was upregulated significantly compared to 5% (129±10%, P<0.05), 15% (122±17%, P<0.05), and 0% static control (100%, P<0.01; Figure 5.5).

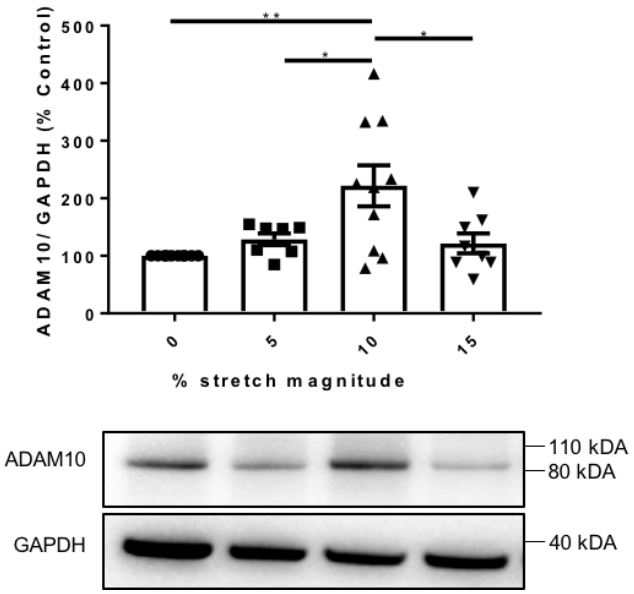

Figure 5.5 Effect of cyclic stretch on ADAM10. 18 hours of stretch at 5%, 10%, 15% or 0% at a frequency of 1Hz resulted in a significant increase in pre-ADAM10 compared to 15% stretch magnitude and the 0% static control. Representative western blot bands are shown below the bar graph. *P<0.05, **P<0.01, n=7-10, analysed using One-way ANOVA with post-hoc Tukey-corrected multiple comparison tests. Abbreviations: ADAM10, A Disintegrin and metalloproteinase domain-containing protein 10; GAPDH, glyceraldehyde 3-phosphate dehydrogenase

5.4 Discussion

Akt expression and/or phosphorylation has been implicated in stretch induced changes in a number of different cell types including ECs [165,250,259]. In the present study, Akt phosphorylation at S473 was shown to be downregulated by stretch without affecting the total Akt levels (Figure 5.1). However, in human umbilical vein ECs (HUVECs) stretched for a total of 120 minutes at stretch magnitudes of 20-50%, an increase in Akt phosphorylation at S473 after 30 minutes of stretch was evident, which was attenuated by the Akt inhibitor, LY294002 [162]. This was also concomitant with an increase in NO production and was decreased in the presence of LY294002 [162]. However, this effect was not observed at 15 minutes of stretching, which was shown to be a time-dependent activation of Akt by stretch in regulating NO

production [162]. Similar results on Akt phosphorylation were reported in a human intestinal epithelial cell line in response to 10% stretch at 5 cycles/minute for 60 minutes and in bovine arterial endothelial cells exposed to 20 minutes of 20% stretch at 1 Hz [165,186]. The reduction in Akt phosphorylation in the present study as opposed to increased Akt phosphorylation in those previous studies could be explained by the fact that the present study was conducted for a longer 18-hour period rather than within 120 minutes in the previous studies. Furthermore, since it is reported that Akt phosphorylation is regulated in a time dependent manner by stretch, the results presented demonstrate that prolonged stretch could negatively regulate Akt phosphorylation (Figure 5.1).

Akt phosphorylation is known to modulate GSK-3 activity by phosphorylating GSK-3 at S21 and S9 respectively of GSK-3α and GSK-3β, leading to GSK-3 inhibition [251–253]. The present study showed significant downregulation of GSK-3 activity in response to stretch in HCMECs concomitant with downregulation of pAkt (Figure 5.1 & Figure 5.2). Thus, loss of Akt phosphorylation may have eventuated a decrease in GSK-3 phosphorylation, thereby increasing GSK-3 activity.

A previous study demonstrated that in HUVECs, Akt phosphorylation was downregulated whilst the downstream Akt substrates, eNOS and GSK-3β were also underphosphorylated in the presence of Aβ [108]. This had resulted in a reduction in NO production [108]. Consistent with this study [108], Chapter 4 (based on the recent publication [19]), a study conducted under the same conditions as the present study, reported that cyclic stretch mediated increases in Aβ levels in HCMECs concomitant with a reduction in eNOS phosphorylation at S1177, although the level of NO was not reported. eNOS phosphorylation at S1177 was downregulated by stretch (Chapter 4, based on the recent publication [19]) in HCMECs, with a stretch mediated reduction in Akt phosphorylation as demonstrated in the present study. Since it is known that eNOS phosphorylation at S1177 could be regulated by phosphorylation

of Akt [162,165,250], these results together indicate that prolonged stretch of HCMECs could downregulate Akt by possibly altering Aβ levels (Chapter 4) [19], thereby causing a reduction in S1177 phosphorylation of eNOS. However, the present study found that NO production was increased at the 10% stretch magnitude compared to the 5% stretch magnitude after 18 hours of stretching at 1Hz, with no significant changes between other magnitudes (Figure 5.3). Taken together, results suggest that downregulation of phosphorylated eNOS at S1177 in response to cyclic stretch (Chapter 4) [19], is a downstream effect of reduced Akt and GSK-3 phosphorylation, consequent of increased Aβ levels mediated by stretch as reported in Chapter 4 [19]. However, the NO levels were maintained essentially the same. Therefore, the results reveal that in HCMECs, long-term stretch (18 hours) could regulate NO levels via a different pathway other than the Akt/GSK-3/eNOS signalling cascade, such as the protein kinase A (PKA) pathway, which is reported to regulate eNOS activation in response to stretch in HUVECs [162]. It is also possible that another phosphorylation site of eNOS, serine 633, which is known to be regulated by mechanical stretch activates eNOS and regulate NO levels, in a PKA-dependent manner [162]. Additionally, stretch is known to alter intracellular calcium levels via stretch activated channels to activate NO production through directly modulating calcium/calmodulin signalling, thus could be possibly involved to mediate the increase in NO production in the present study [165].

The results presented here show that GSK-3α and GSK-3β are differentially regulated by stretch. This is because GSK-3α expression did not change although the phosphorylation did, after HCMECs were subjected to 18 hours of stretch, in contrast to GSK-3β of which both expression and phosphorylation were downregulated by the same regimen of stretch (Figure 5.2). These results show that GSK-3α is regulated by mechanical stretch post-translationally, whilst GSK-3β is regulated at the transcriptional level or both.

GSK-3 activity via PI3K/Akt is reported to be modulated by caveolin-1 in astrocytes in regulating glycogen content whilst caveolin-1 led to inhibitory effects on GSK-3 activity [17,118,119]. Additionally, caveolin-1 dependent Akt activation in response to mechanical stretch has been reported, demonstrating a role of caveolin-1 as a mechanosensor [192]. Caveolin-1 expression at the 5% stretch magnitude was upregulated compared to both static control and the 10% stretch magnitude in HCMECs exposed to 18 hours of stretching at 1 Hz in the current study. The GSK-3 activity however, was sustained regardless of caveolin-1 expression, as the phosphorylation of both GSK-3α and GSK-3β remained downregulated by stretch at all magnitudes, as opposed to caveolin-1, which was increased only at the 5% magnitude (Figure 5.2 & Figure 5.4). These results suggest that GSK-3 activity could most likely to be regulated by Akt phosphorylation alone independent of caveolin-1, since the Akt phosphorylation was downregulated at all stretch magnitudes (Figure 5.1, Figure 5.2 & Figure 5.4). Nevertheless, caveolin-1 expression could have implications on eNOS-mediated NO production, since the significant increase in caveolin-1 expression at 5% stretch magnitude compared to 10% stretch magnitude coincided with a significant increase in NO production at 10% stretch magnitude compared to 5% stretch magnitude with no changes at 15% stretch (Figure 5.3 & Figure 5.4). In bovine aortic endothelial cells, exposure to shear stress in the range of 5-100 dynes/cm^2 increased caveolin-1 protein levels leading to an increase in eNOS activation only in the presence of 50 μM H_2O_2 [98]. Since this study demonstrated the effect of caveolin-1 expression on NO production mediated by shear stress only in the presence of H_2O_2, elaborating a role of oxidative stress combined with shear stress in regulating eNOS activation caveolin-1 dependently, in the present study, caveolin-1 may negatively regulate eNOS activity possibly due to an absence of oxidative stress that was required for localisation of eNOS[98]. This hypothesis could be supported by the lactose dehydrogenase (LDH) activity in response to stretch presented in Chapter 4 [19], since LDH activity did not change

significantly in response to stretch, which indicates that the cells were not under oxidative stress.

Both GSK-3α and GSK-3β have implications in AD pathology [17,116]. In primary neurons from soluble-APPα (sAPPα) over expressing mice and in SHSY5Y neuroblastoma cells treated with 0–25 nM sAPPα for 12 hours, sAPPα inhibited GSK-3β by phosphorylating GSK-3β at S9 [260]. Similar results were demonstrated in SHSY5Y cells over-expressing β-secretase 1 (BACE-1), whilst in HeLa cells over-expressing human tau, in addition to the inhibitory effect on GSK3β activity via phosphorylation at S9, tau phosphorylation was also reduced [260]. BACE-1 inhibition also led to loss of GSK-3β activity as indicated by increased pGSK-3β at S9 [260]. Furthermore, in AD models over-expressing sAPPα, tau phosphorylation and Aβ levels were reduced [260,261]. Therefore, sAPPα, which is a downstream cleavage product of APP in the non-amyloidogenic pathway after being processed by ADAM10, and BACE-1 inhibition, regulated GSK-3β, thereby regulating Aβ and tau levels, the central players modulating AD pathophysiology. These studies indicate the relevance of including the effect of stretch on sAPPα in future studies, to identify whether stretch-mediated responses are mediated by reduced sAPPα.

Chapter 4 (recent publication [19]), reported that APP expression at both 10% and 15% stretch magnitudes relative to the static control, with a significant upregulation of Aβ42 at 15% stretch magnitude compared to the static control. Additionally, the APP processing enzyme that cleaves APP towards amyloidogenic processing of APP, BACE-1, also increased significantly at 10% and 15% stretch magnitudes compared to the static control (Chapter 4). In this study, the APP processing enzyme that cleaves APP towards non-amyloidogenic pathway, ADAM10 was investigated in response to stretch, with the same study design as of chapter 4. Although the mature ADAM10 approximating to 65 KDa was not apparent, the

pro-ADAM10 band approximating to 84 KDa was apparent and thus was quantified (Figure 5.5). With the assumption that the pro-ADAM10 would turn into mature ADAM10, the significant upregulation of pro-ADAM10 at the 10% stretch magnitude relative to 5%, 15% and 0% stretch magnitudes in the present study show that stretch modulated ADAM10 expression, which could potentially be a compensatory mechanism in regulating Aβ homeostasis (Figure 5.5). Additionally, it is known that NO reservoirs could bi-directionally regulate BACE-1 and ADAM10 mediated APP processing depending upon NO concentration [262]. Hence, regardless of the upregulation of BACE-1 at the 10% stretch magnitude, Aβ42 levels did not change significantly at 10% (Chapter 4 [19]), possibly due to an increase in ADAM10 expression and increase in NO at 10% stretch magnitude (Figure 5.3 & Figure 5.5). However, the prevalence of increased Aβ42 at the 15% magnitude indicate that BACE-1 (Chapter 4) overwhelmed the effect of ADAM10 at the higher magnitude of stretch (Figure 5.5). This increase in BACE-1 levels may have been a consequence of sustained GSK-3 activity as indicated by reduced pGSK-3 levels at all stretch magnitudes. Therefore, overall results collectively corroborated previous studies whereby stretch of HCMECs led to increases in APP and BACE-1 and decreases in pGSK-3 phosphorylation at 10% and 15% stretch magnitudes concomitant with an upregulation of Aβ42 secretion at 15% stretch magnitude, and ADAM10 at the 10% stretch magnitude (Figure 5.5). Therefore, prolonged stretch of HCMECs may regulate ADAM-10 levels, favouring BACE-1 mediated APP processing to increase amyloidogenic processing of APP, thereby elevating Aβ levels at the higher magnitude of stretch.

5.5 Conclusions

Cyclic stretch downregulated phosphorylation of Akt, GSK and eNOS (Chapter 4), although it did not result in a reduction in NO, suggesting that eNOS is regulated by prolonged stretch by a different mechanism other than Akt/GSK-3. Possible mechanisms for the production of

NO in response to cyclic stretch include eNOS phosphorylation at a different site other than S1177, and increased calcium signalling that can directly stimulate eNOS-mediated NO production. GSK-3 and Akt phosphorylation were downregulated at all magnitudes of stretch concomitant with an increase in APP, BACE-1 and Aβ42 (Chapter 4), thus Akt and GSK-3 may play regulatory roles in eventuating these changes (Figure 5.6). At the 10% stretch magnitude, NO level increased with an upregulation of ADAM10 without a significant increase in Aβ regardless of the significant upregulation of BACE-1, thus NO-dependent ADAM10 mediated APP processing may serve as a compensatory mechanism to maintain Aβ homeostasis in response to stretch magnitudes less than 15%. However, whether these observations are dependent on these regulatory mechanisms requires further investigation.

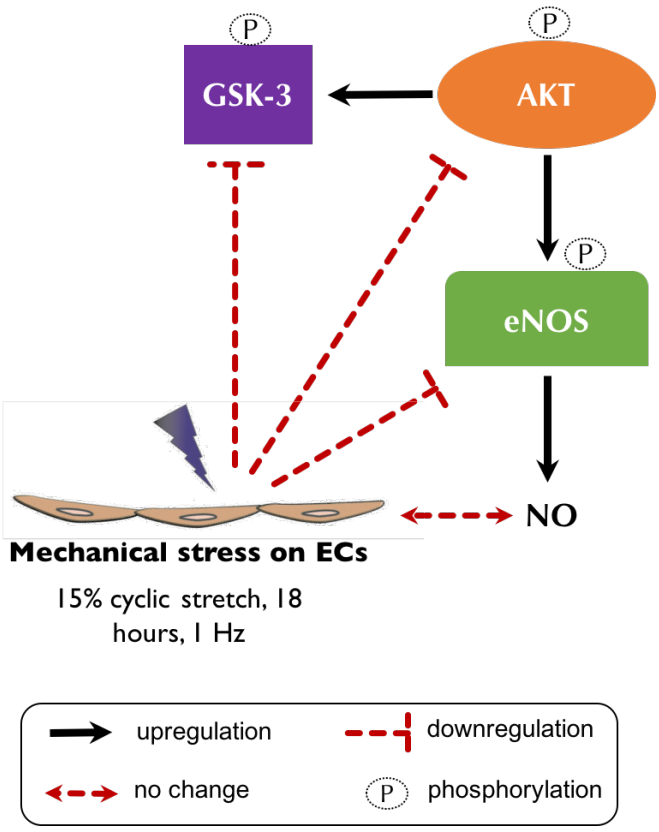

Figure 5.6 Schematic representation of summarised stretch mediated changes in AKT/GSK/eNOS signalling presented in the current study. Phosphorylation of Akt at S473 activates eNOS by phosphorylation at S1177 that leads to NO production, and downregulates GSK activity by phosphorylating GSK-3α at S21 and GSK-3β at S9. Cyclic stretching for 18 hours at 1 Hz at a magnitude of 15% downregulated pGSK-3α and pGSK-3β, pAkt and peNOS,

with no change in NO levels. Results suggest that cyclic stretch of ECs activated GSK-3 via downregulating pAkt, that in turn led to a decrease in peNOS. No change in NO levels indicated a different mechanism other than Akt/GSK-3 signalling that modulated NO levels. Abbreviations: ECs, endothelial cells; eNOS, endothelial nitric oxide synthase; GSK, glycogen kinase synthase; NO, nitric oxide

Chapter 6

Effect of endothelial cell passaging and cyclic stretch on APP expression, amyloid secretion, and NO signalling

Summary—Vascular ageing and vascular pulsatility are implicated in Alzheimer's disease (AD). Amyloid precursor protein (APP) that is cleaved by secretases such as a disintegrin and metalloproteinase-10 (ADAM10) and β secretase-1 (BACE-1) to form AD-plaques, is associated with endothelial nitric oxide synthase (eNOS) signalling that leads to nitric oxide (NO) production. The inflammatory marker, intercellular cell adhesion molecule-2 (ICAM-1), caveolin-1, the serine/threonine-specific kinase, Akt, and glycogen synthase kinase-3 (GSK-3) are associated with endothelial NO signalling and AD. This study aimed to investigate the effect of ECpassaging in the presence of cyclic stretch by comparing human cerebral microvascular endothelial cells of early and late passages exposed to 18 hours of 15% of cyclic stretch (1 Hz), on APP, ADAM10, BACE-1, Aβ42 secretion, eNOS, NO production, ICAM-1, Akt, caveolin-1 and GSK. APP, ADAM10, BACE-1, eNOS, phosphorylated eNOS, ICAM-1, Akt, caveolin-1 and GSK-3 were quantified using western blotting while Aβ42 and NO were measured by an ELISA or NO assay kit. Cyclic stretch appeared to induce senescent characteristics in late passage HCMECs. Cyclic stretch differentially modulated the expression and/or phosphorylation of some proteins studied in ECs at higher passages compared to ECs at lower passages. These include, APP, BACE-1, eNOS, ICAM-1, caveolin-1, GSK-3α and GSK-3β. Additionally, Aβ42 secretion and NO production in response to cyclic stretch also differed between old and naïve ECs. Taken together, the results indicate a potential role of cell senescence and vascular ageing and vascular pulsatility in modulating these factors in the endothelium. The results implicate how vascular pulsatility could modulate differential signalling pathways and EC characteristics due to vascular ageing present in the milieu of AD. Thus, further studies will confirm whether these responses are mediated by EC senescence, and molecular pathways involved in mediating altered APP processing in response to stretch in late passage ECs compared to early passage ECs.

6.1 Introduction

Amyloid plaques are a key characteristic of Alzheimer's disease (AD), and are derived from proteolytic processing of amyloid precursor protein (APP) by secretases including β-secretase 1 (BACE-1) and a disintegrin and metalloproteinase-10 (ADAM10) [261]. Ageing is a non-modifiable risk factor for many chronic diseases including AD [1]. In the United States, 96% of AD cases were reported in individuals older than 65 years of age [1]. Whilst age is the greatest non modifiable risk factor for AD, hypertension is amongst the common modifiable risk factors for AD, as stated in Alzheimer's facts and figures 2017 report compiled and published by the Alzheimer's Association [1,263].

Hypertension is shown to be associated with AD, and elevated pulse pressure, which could be a consequence of hypertension, is also demonstrated to be associated with AD in patient cohorts [3,4,6,101]. High pulse pressure and pulsatility index, suggestive of increased large artery stiffness and reduced vessel distensibility, are associated with AD, lower memory scores, increased amyloid burden and cerebral microvascular damage [64,74]. Large artery stiffness, which is associated with compromised vessel compliance, is a cumulative factor with ageing, and is associated with endothelial dysfunction that is characterised by diminished endothelium-dependent vasodilation [73,264,265]. Endothelial vasodilation is mediated by nitric oxide (NO) via the enzyme endothelial NO synthase (eNOS) [265].

Regulation of eNOS expression and phosphorylation by mechanical forces such as pulsatile stretch and shear stress resultant of haemodynamics within blood vessels has been demonstrated [162,163,165–167,184,266,267]. NO production mediated by eNOS is known to be modulated by the serine/threonine-specific kinase, Akt, whilst glycogen synthase kinase-3 (GSK-3) is regulated by Akt [165,250–253]. NO regulates inflammatory markers such intercellular cell adhesion molecule-1 (ICAM-1), which is also known to be present surrounding AD plaques [16,268]. eNOS, NO, Akt, GSK-3 and ICAM-1 are involved in AD pathophysiology and are known to be modulated by stretch [17,116,119,153,162,165,185,191,192,194,205,250,256–258]. eNOS is bound to caveolin-1, which is present within caveolar structures in the plasma membrane, in its inactive form, and caveolin-1 is known to be involved in mechanotransduction [98,192].

A recent study demonstrated that APP processing is altered between early and late passage cells in primary human brain microvascular endothelial cells (BMECs) [21]. In late passage senescent BMECs, APP expression and secreted soluble APPα decreased, with concomitant increases in BACE-1 and Aβ40 compared to early passage BMECs, indicating a contributory role of EC senescence towards amyloidogenic processing [21]. However, the effect of endothelial

cell senescence in the presence of cyclic stretch on APP, BACE-1, ADAM10, eNOS, Akt, GSK-3, ICAM-1 or caveolin-1 has not been studied.

This study aimed to investigate the effect of cell passaging in the presence of cyclic stretch by comparing human cerebral microvascular endothelial cell line-SV40 (HCMEC-SV40) of early and late passages exposed to 18 hours of 15% of cyclic stretch (1 Hz), on APP, ADAM10, BACE-1, Aβ42 secretion, eNOS, NO production, ICAM-1, Akt, caveolin-1 and GSK.

6.2 Methods

All methodological approaches including culture conditions are detailed in Chapters 3, 4, and 5. HCMEC-SV40 were subjected to 18 hours of stretching at 1 Hz and were compared between 7-10 passages and 17-19 passages representative of naïve and mature cerebral ECs respectively. All data presented in this thesis that were acquired at 15% stretch magnitude and had been normalised to their corresponding static control as % control values, were divided according to the passage number and analysed in this chapter to detect any passage effects.

6.2.1 Statistical analysis

Each data point represents an individual experiment and data are represented as mean±SEM analysed using unpaired t-tests performed in GraphPad PRISM software version 7.02. Outliers were identified using the robust regression and outlier removal (ROUT) method (detailed in Motulsky *et al.* [228]) in GraphPad PRISM with a Q value set at 10% that defines the threshold for outliers.

6.3 Results

6.3.1 Effect of cyclic stretch on the morphology in early passage HCMECs compared to HCMECs in late passages

The morphology of HCMECs before and after cyclic stretch were examined in early and late passage HCMECs (Figure 6.1). Representative micrographs of HCMECs at early and late passages are shown in Figure 6.1, of passage 7 and passage 18 respectively. The cells were checked at exponential growth stage. The average cell diameter was measured to be approximately 2-3 μM both before and after stretch in early and late passage cells. The typical polygonal morphology was apparent prior to stretching of both early and late passage cells, although the ECs at the late passage showed relatively more elongated morphology compared to ECs at the early passage after being subjected to 18 hours of cyclic stretching (1 Hz; Figure 6.1).

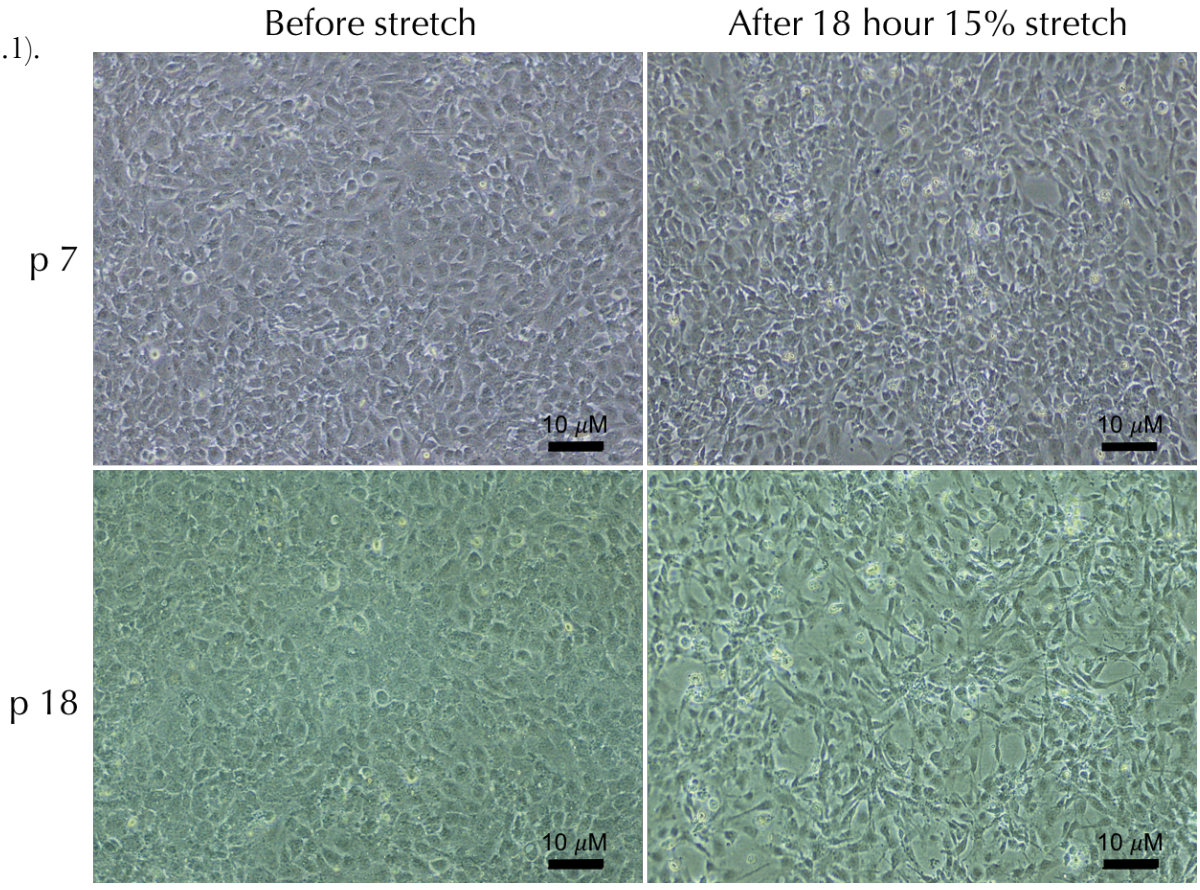

Figure 6.1 Representative micrographs showing the effect of cyclic stretch on the morphology of HCMECs in early passages compared to HCMECs in late passages. Early (passage 7) and late (passage 18) passage cell morphology prior to stretching appeared similar. However, late

passage HCMECs appeared to relatively more elongated after being subjected to 18 hours of stretching (1 Hz) compared to that of early passage HCMECs. Scale bar= 10 μM. Abbreviations: HCMEC, human cerebral microvascular cell line-SV40

6.3.2 Cyclic stretch differentially modulates APP and BACE-1 expression, and secreted Aβ42 in late passage HCMECs compared to HCMECs in early passages

Old age is the greatest non-modifiable risk factor for AD, which is characterised by Aβ plaques [1,261]. APP becomes cleaved by secretases including BACE-1 and ADAM10 [1,261]. To investigate whether there are differences in expression of APP and APP processing enzymes, BACE-1 and ADAM10, in response to 15% cyclic stretch that prolonged for 18 at 1 Hz hours, between mature cells and naïve cells, ECs were subjected to stretch at early (7-9) or late (17-19) passages. Both APP expression and BACE-1 expression were significantly higher in late passage ECs compared to early passage ECs after being exposed to cyclic stretch (15%, 1Hz) for 18 hours (Figure 6.2). APP expression was higher in the mature cells (243±37%, $P<0.001$) than in the naïve cells (124±12%) approximately by 2-fold (Figure 6.2). BACE-1 expression was higher in the late passage cells (221±51%, $P<0.01$) than in the early passage cells (64±6%) approximately by 3-fold (Figure 6.2). No significant changes in ADAM10 were detected (Figure 6.2). Consistent with APP and BACE-1 expression, secreted Aβ42 in the late passage cells (1.0±0.12 pg/ml, $P<0.01$) was significantly higher than that of early passage cells by 2-fold (0.5±0.01 pg/ml; Figure 6.2).

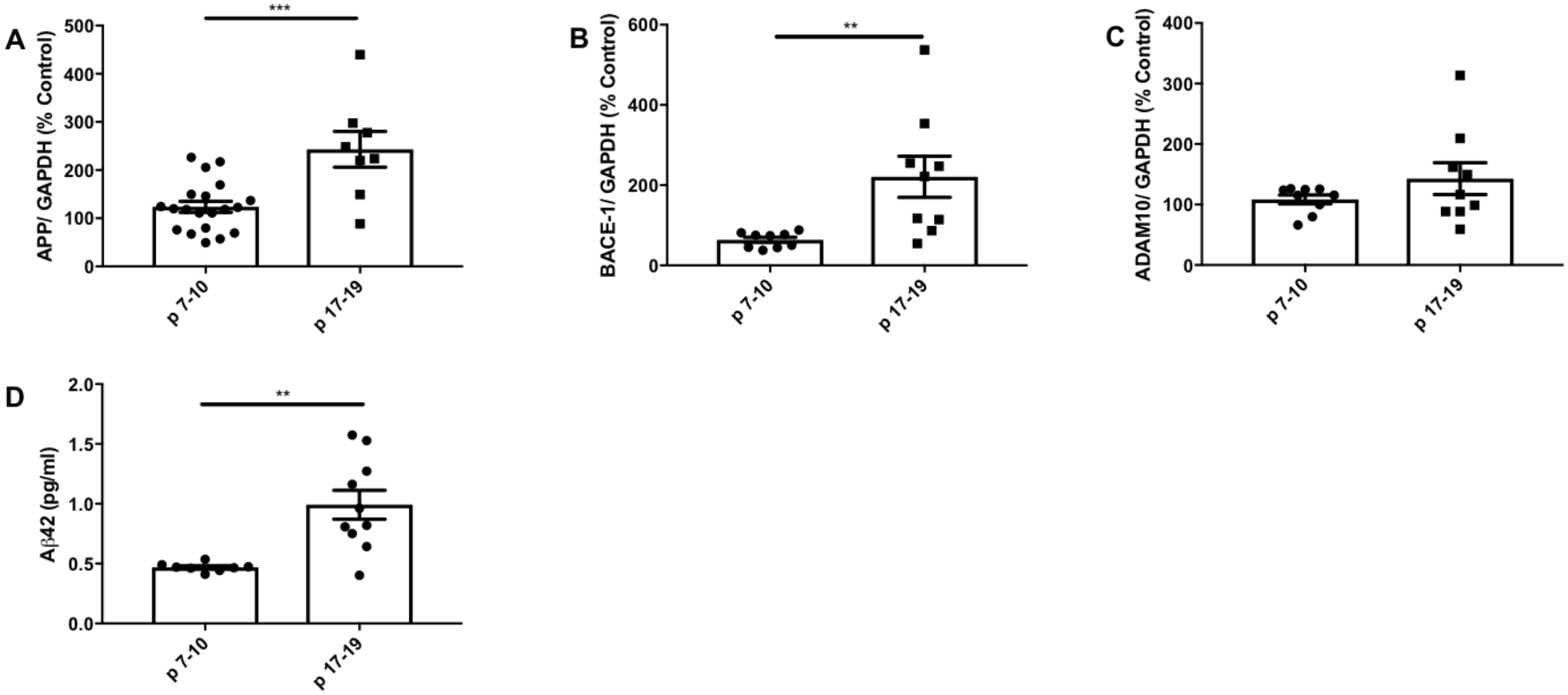

Figure 6.2 Effect of passage number of HCMECs on APP, BACE-1 and ADAM10 in response to cyclic stretch. Expression of APP (A), ADAM10 (B) and BACE-1 (C), and Aβ42 secretion (D) after 18 hours of stretch at 1 Hz in late passage (17-19 passages) compared to early passage (7-9 passages) HCMECs. ***P<0.001, **P<0.01, n=8-20, analysed using unpaired t-tests (two-tailed). Abbreviations: Aβ, amyloid-beta; ADAM10, A Disintegrin and metalloproteinase domain-containing protein 10; APP, amyloid precursor protein; BACE-1, β secretase-1; GAPDH, glyceraldehyde 3-phosphate dehydrogenase

6.3.3 Cyclic stretch differentially modulates eNOS and ICAM-1 expression, and NO production in late passage HCMECs compared to HCMECs in early passages

eNOS signalling and inflammation are involved in AD [16,268], thus eNOS expression, phosphorylation at S1177, and NO production, and the inflammatory marker, ICAM-1, were investigated in HCMECs exposed to 18 hours of cyclic stretch (15%, 1Hz), and responses were compared between early (7-9) and late (17-19) passages. The expression of eNOS, NO production and ICAM-1 were significantly higher in the late passage HCMECs than in the early passage HCMECs, although no changes were detected in the level of phosphorylation of eNOS between the two cohorts (Figure 6.3). eNOS expression was higher in the late passage cells (248±66%, $P<0.001$) than in the early passage cells by approximately 3-fold (85±8%; (Figure 6.3). NO production was also significantly higher in the early passage cells (0.088±0.011 µM/µg, $P<0.01$) than in the late passage cells by approximately 3-fold (0.035±0.003 µM/µg; (Figure 6.3). Similarly, ICAM-1 expression was significantly higher in the late passage cells (109±17%, $P<0.01$) than in the early passage cells by approximately 2-fold (66±7%; Figure 6.3).

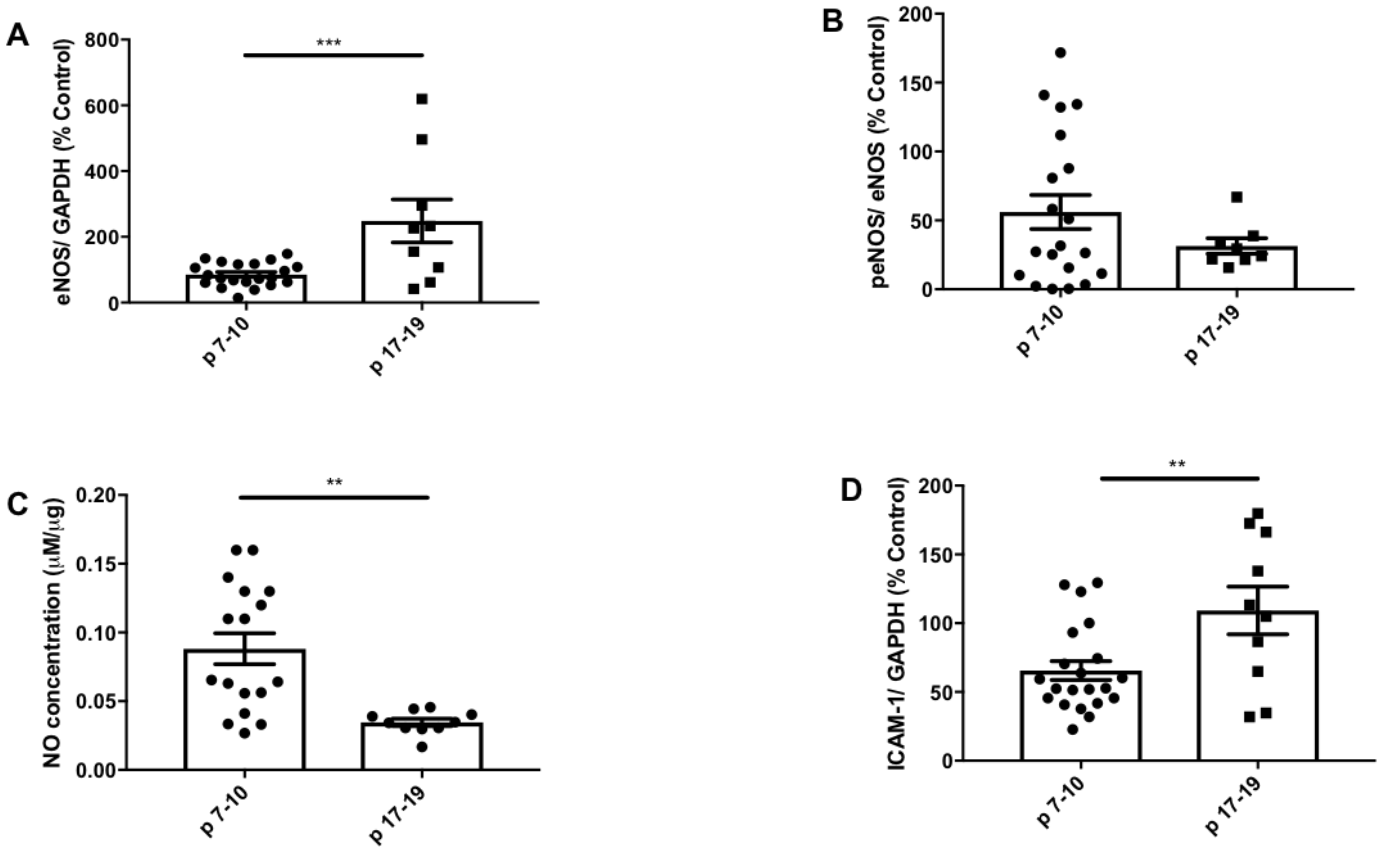

Figure 6.3 Effect of passage number of HCMECs on eNOS, peNOS, NO and ICAM-1 in response to cyclic stretch. Expression of eNOS (A), phosphorylation of eNOS at S1177 (B), NO production (C), and ICAM-1 expression (D) after 18 hours of stretch at 1 Hz in late passage (17-19 passages) compared to early passage (7-9 passages) HCMECs. ***P<0.001, **P<0.01, n=8-21, analysed using unpaired t-tests (two-tailed). Abbreviations: eNOS, endothelial nitric oxide synthase; GAPDH, glyceraldehyde 3-phosphate dehydrogenase; ICAM-1, intercellular cell adhesion molecule-1; NO, nitric oxide; peNOS, phosphorylated eNOS

6.3.4 Cyclic stretch differentially modulates caveolin-1 expression in late passage HCMECs compared to HCMECs in early passages

To explore regulatory mechanisms underlying eNOS signalling, Akt expression and phosphorylation of Akt S473, and caveolin-1, were investigated. Akt expression or phosphorylation of Akt at S473 did not change significantly in response to 18 hours of 15% stretch between early passage and late passage HCMECs (Figure 6.4). However, caveolin-1 expression was significantly higher in the late passage cells (185±34%, $P<0.05$) than in the early passage cells by approximately 2-fold (78±19%; Figure 6.4).

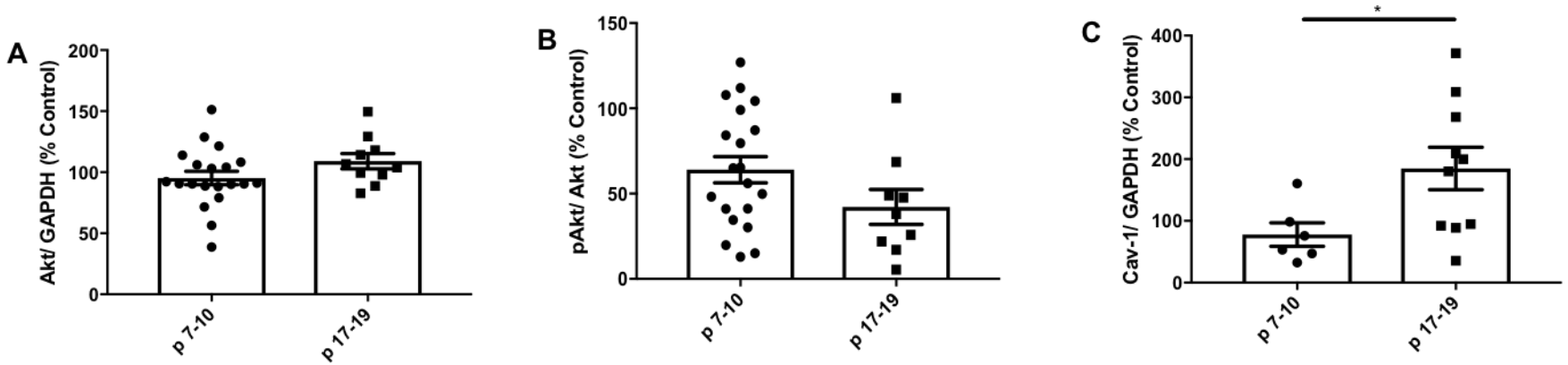

Figure 6.4 Effect of passage number of HCMECs on Akt, phosphorylation of Akt and caveolin-1 in response to cyclic stretch. Expression of Akt (A), phosphorylation of Akt at S473 (B) and caveolin-1 expression (C) after 18 hours of stretch at 1 Hz in late passage (17-19 passages) compared to early passage (7-9 passages) HCMECs. *P<0.05, n=6-20, analysed using unpaired t-tests (two-tailed). Abbreviations: Cav-1, caveolin-1; GAPDH, glyceraldehyde 3-phosphate dehydrogenase; pAkt, phosphorylated Akt

6.3.5 Cyclic stretch differentially modulates GSK-3α and GSK-3β in late passage HCMECs compared to HCMECs in early passages

One of the downstream targets of Akt activation, and an enzyme involved in AD, GSK-3, was also investigated. The expression of GSK-3α did not change significantly although phosphorylation of GSK-3α decreased significantly in late passage cells (45±10%, $P<0.01$) compared to early passage cells (142±18%; Figure 6.5). However, both expression (66±13%, $P<0.05$, approximately 1.4-fold) and phosphorylation (33±9%, $P<0.001$, approximately 3-fold) of GSK-3β in late passage cells, were decreased compared to expression (90±3%) and phosphorylation (97±9%) of GSK-3β in early passage cells Figure 6.5).

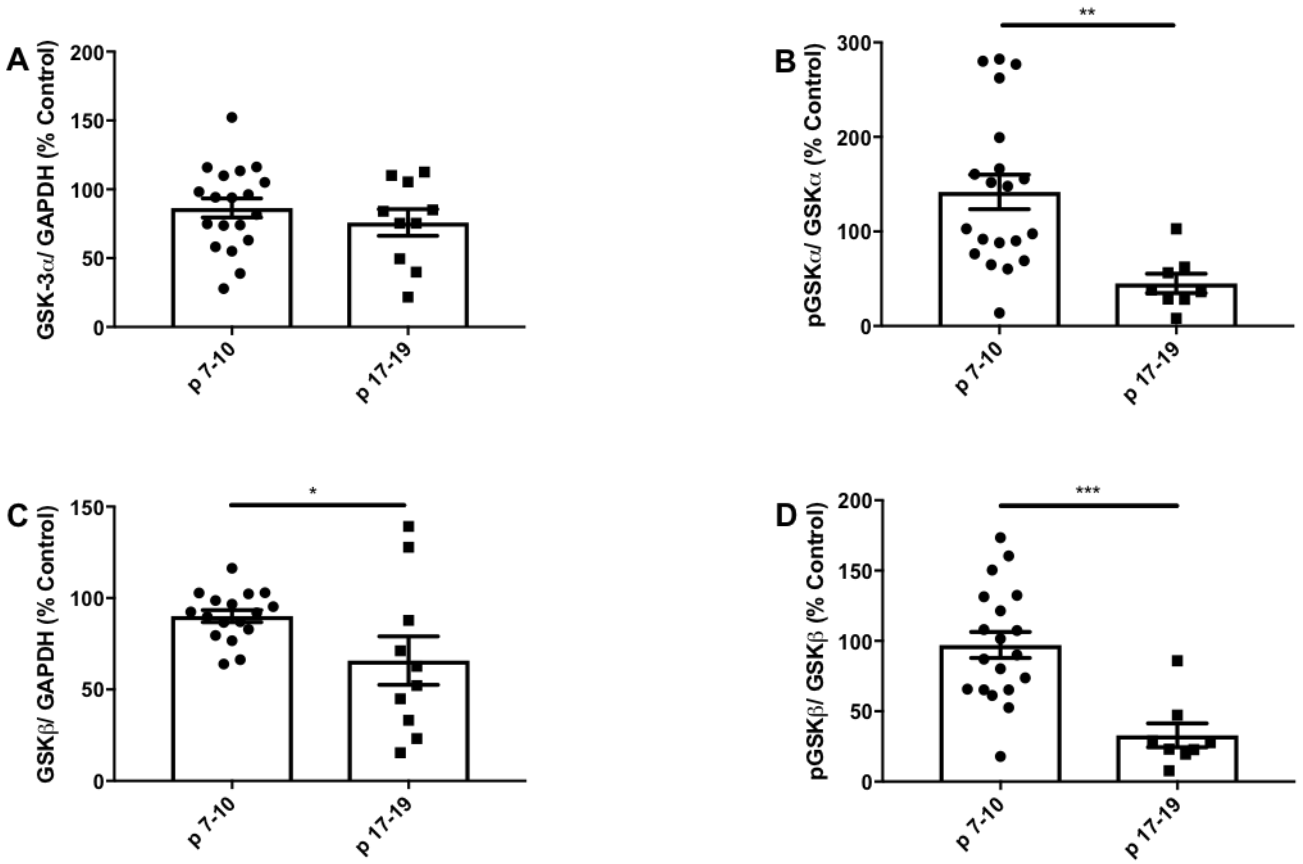

Figure 6.5 Effect of passage number of HCMECs on GSK-3α and GSK-3β in response to cyclic stretch. Expression of GSK-3α (A), phosphorylation of GSK-3α at S21 (B), expression of GSK-3β (C), and phosphorylation of GSK-3β at S9 (D) after 18 hours of stretch at 1 Hz in late passage (17-19 passages) compared to early passage (7-9 passages) HCMECs. ***P<0.001, **P<0.01, *P<0.05, n=8-20, analysed using unpaired t-tests (two-tailed). Abbreviations: GAPDH, glyceraldehyde 3-phosphate dehydrogenase; GSK, glycogen synthase kinase; pGSK, phosphorylated GSK

6.4 Discussion

According to the AD Facts and Figures 2017 report issued by the Alzheimer's Association, ageing is the greatest non-modifiable risk factor for AD, whilst hypertension, pulse pressure and large artery stiffening are vascular risk factors for AD [1]. Based on these, the novel concept presented throughout this thesis, the effect of endothelial pulsatility was investigated including the effect of endothelial ageing by means of late or early passage HCMECs. The preceding two Chapters showed that prolonged (18 hours) cyclic stretch differentially modulate expression of APP, BACE-1, ADAM10, eNOS, ICAM-1, caveolin-1, Akt and GSK, Aβ42 secretion and NO production at different stretch magnitudes in HCMECs. In the present study, the highest stretch magnitude that was optimised in this thesis, 15% (to detect maximal stretch effect), was selected to investigate whether there is an effect of passage number, thereby simulating the effect of endothelial ageing.

Endothelial cell senescence can be characterised by different factors including the cell morphology [214]. The typical polygonal morphology of HCMECs after being subjected to 18 hours of cyclic stretching at 1 Hz in late passage cells appeared to be elongated compared to the cells at early passage (Figure 6.1), possibly indicating that cyclic stretch induces senescent characteristics in ECs. Interestingly, the present study demonstrated that at higher passages, cerebral ECs exposed to cyclic stretch have higher APP expression, BACE-1 expression, and Aβ42 secretion than ECs exposed to cyclic stretch that were at lower passages (Figure 6.2), which is consistent with the ageing effect observed in AD. It was reported that the passage number of cells could have profound effects on expression profiles of mRNA and protein [269–271]. Additionally, the recent study by Sun *et al.* [21] indicated that in BMECs APP expression and processing along with the expression of the APP processing enzyme, BACE-1 were altered significantly between early and late passage ECs, showing a role of EC senescence in mediating amyloidogenic processing of APP [21]. Data presented in this study are normalised

against the corresponding static control of the stretched cells at 15%, thereby isolating the effect of cyclic stretch alone. Thus, the data demonstrate the effect of cyclic stretch on the proteins studied, in ECs at higher passages compared to ECs that are at lower passages, rather than the effect of ageing on the endogenous levels of the proteins studied. It is shown here that the same magnitude of stretch could substantially potentiate APP processing towards amyloidogenic processing of APP in aged cells as APP, BACE-1 and Aβ42 were greater in the cells that were at higher passages compared to the cells that were at lower passages (Figure 6.2). Taken together, the data show that cyclic stretch promotes amyloidogenic processing of APP expression in aged cells that are at late passages compared to cells at early passages, illustrating a possible role of endothelial ageing and vascular pulsatility in AD plaque formation, consistent with the study by Sun *et al.* [21].

In human umbilical vein endothelial cells, eNOS phosphorylation at S1177 and NO production was demonstrated to be reduced with increasing passage number [269]. The present study demonstrates that there were no substantial changes in eNOS phosphorylation at S1177 in response to stretch between lower and higher passages of HCMECs, although the eNOS expression and NO production were significantly altered between lower and higher passages (Figure 6.3). Although the data presented here do not show the differences in endogenous eNOS or NO levels as stated above, NO production was shown to be decreased at higher passages than at lower passages in response to cyclic stretch indicating a role of vascular ageing (consistent with studies by Lee *et al.* [269]) and vascular pulsatility in modulating NO levels independent of phosphorylation of eNOS at S1177 (Figure 6.3).

The notion that the reduction of NO was independent of peNOS can be further supported by the Akt results, as Akt phosphorylation, which is upstream of phosphorylation of eNOS at S1177 did not change as well (Figure 6.4). The NO depletion could be attributed to increased caveolin-1 levels, which could indicate inactive eNOS, since eNOS is bound to caveolin-1

present in the plasma membrane, in its inactive form (Figure 6.4) [99]. The increase in caveolin-1 could also serve as a protective mechanism against mechanical rupture of the endothelial membrane due to the involvement of caveolin-1 in mechanotransduction and preserving the cell membrane [272]. Thus, cyclic stretch could trigger caveolin-1 expression, a potential protective mechanism to preserve the EC membrane from rupture in response to cyclic stretch and that could also inactivate eNOS, thereby, decreasing NO reservoirs.

Pulmonary ECs (passage numbers 5-7) subjected to 18% cyclic stretch for 48-72 hours (25 cycles/minute) resulted in increased ICAM-1 expression indicative of activation of endothelial inflammation [244]. Consistently, HCMECs subjected to 18 hours of 15% stretch (60 cycles/minute) resulted in an increase in ICAM-1 expression as demonstrated in Chapter 4. The present study showed that there is a passage effect such that the effect of stretch on ICAM-1 expression in HCMECs at higher passages is different from that at lower passages, showing an incremental effect in older cells (Figure 6.3). The results implicate that vascular pulsatility could differentially activate inflammatory signalling in aged ECs compared to naïve ECs.

GSK-3α and GSK-3β, both are associated with AD [114–116]. The present study showed that cyclic stretch decreased inhibitory phosphorylation of both GSK-3α and GSK-3β, at S21 and S9 respectively in HCMECs at higher passages than in HCMECs at lower passages (Figure6.5). Additionally, the expression of GSK-3β was also regulated by stretch differentially between higher and lower passages, such that ECs at higher passages having reduced GSK-3β expression compared to ECs at lower passages (Figure 6.5). These results suggest that reduction in GSK-3β phosphorylation is a consequence of reduction of GSK-3β expression as stated in Chapter 5, and the present study shows that this effect is prominent in ECs that were at higher passages than in the ECs at lower passages (Figure 6.5). GSK-3α however, appears to be regulated at the post-translational level by cyclic stretch in ECs as demonstrated in

Chapter 5, and this is also altered between passages such that at higher passages, GSK-3α phosphorylation is decreased significantly, indicating GSK-3α activation, compared to ECs at lower passages (Figure 6.5).

Kirouac *et al.* [114] demonstrated that APP expression and Aβ42 facilitated GSK activation and aberrant cell cycle signalling by activating Ras and extracellular signal-regulate kinase 1/2 (ERK 1/2) in neurons. This was also recapitulated in human AD brain tissue [114]. Additionally, Aβ42 was shown to increase APP phosphorylation at Thr668, which could lead to increased BACE-1 processing of APP [114,273]. The results presented in this study corroborate these findings on APP, Aβ42 and GSK activation in ECs that are at higher passages as opposed to ECs that are at lower passages (Figure 6.2 & Figure 6.5). Therefore, cyclic stretch in aged ECs may lead to an increase in APP and BACE-1, which in turn may lead to activation of GSK, that facilitates APP phosphorylation at Thr668, leading to increased amyloidogenic processing and enhanced Aβ42. Elevated Aβ42 could in turn act as a positive feedback loop that further facilitates amyloidogenic processing of APP. Future studies are warranted to investigate the possible involvement of Ras/ERK signalling pathway to confirm these plausible mechanisms. Additionally, whether these studies were related to senescence needs to be confirmed by characterising EC senescent specific markers such as β-galactosidase, although the morphological change in response to cyclic stretch of late passage HCMECs appeared to have a senescent appearance (Figure 6.1) [21]. Thus, future studies investigating whether cyclic stretch could be a stimulus for EC senescence would also be useful.

6.5 Conclusions

Cyclic stretch appeared to induce senescent characteristics in late passage HCMECs, which requires to be confirmed by further analysis of specific markers of EC senescence. Cyclic stretch differentially modulated the expression and/or phosphorylation of some proteins

studied in ECs at higher passages compared to ECs at lower passages. These include, APP, BACE-1, eNOS, ICAM-1, caveolin-1, GSK-3α and GSK-3β. Additionally, Aβ42 secretion and NO production in response to cyclic stretch also differed between old and naïve ECs. Taken together, the results indicate a role of vascular ageing and vascular pulsatility in modulating these factors in the endothelium. The results implicate how vascular pulsatility could modulate differential signalling pathways due to vascular ageing present in the milieu of AD. Thus, further studies will confirm molecular pathways involved such as Ras/ERK signalling in mediating such responses.

Chapter 7

Effect of cyclic stretch in cerebral endothelial cells pre-exposed to Aβ

Summary—Amyloid plaques are a hallmark of Alzheimer's disease (AD), which consist of amyloid β (Aβ) peptides that are proteolytic cleavage products of amyloid precursor protein (APP). Cyclic stretch modulates APP expression and processing and nitric oxide (NO) signalling in cerebral endothelial cells (ECs). The serine/threonine-specific kinase, Akt, glycogen synthase kinase-3 (GSK-3) and intercellular cell adhesion molecule-1 (ICAM-1) are associated with NO signalling in ECs, and AD pathology. This study aimed to investigate the combinatory effect of exogenous Aβ due to the presence of Aβ in the milieu of AD, and mechanical cyclic stretch on APP, Aβ and APP processing enzymes, β-secretase-1 (BACE-1) and a disintegrin and metalloproteinase-10 (ADAM10), proteins associated with eNOS signalling, Akt, GSK-3, ICAM-1 and NO in a cerebral EC line. APP, ADAM10, BACE-1, eNOS, phosphorylated eNOS, Akt, GSK-3 caveolin-1 and ICAM-1 were quantified using western blotting while Aβ42 and NO were measured by an ELISA or NO assay kit. Aβ pre-treatment did not appear to have any additional effects, though the effect of stretch on APP, ADAM10 and caveolin-1 was consistent with data reported in all previous chapters. Effect of stretch on BACE-1, Aβ42 secretion, NO production, Akt, GSK-3 and ICAM-1 consistently demonstrated a role of cell passaging that is reported in Chapter 6. Thus, HCMECs in early passages may regulate APP processing and NO production differently to late passages, in response to cyclic stretch. Long term stretch consistently potentiated NO production, which in early passage HCMECs may mediate non-amyloidogenic processing of APP. Nonetheless, Aβ pre-treatment substantially increased secreted Aβ42 levels overwhelming the stretch mediated downregulation of Aβ42 secretion, thus showing a possible role of exogenous Aβ in triggering further Aβ42 secretion, thus a potential role of Aβ in exacerbation of Aβ pathologies in AD.

7.1 Introduction

Amyloid precursor (APP) gives rise to the amyloid β (Aβ) peptide that aggregates to form Aβ plaques, characteristic of Alzheimer's disease (AD) [46,274,275]. Hypertension is a risk factor associated with AD [3,4]. Higher pulsatility index and pulse pressure, indicative of increased large artery stiffness and reduced vessel compliance, are associated with AD, lower memory scores, increased amyloid burden and cerebral microvascular damage [64,74]. These findings together suggest a significant role of mechanical stretch in the pathophysiology of AD since hypertension and elevated pulse pressure could impose increased circumferential stretch on the vessel wall.

Vascular stretch could directly modulate endothelial cell responses such as production of nitric oxide (NO), which is an important second messenger and a mediator of vasodilation facilitated by the enzyme, endothelial NO synthase (eNOS) [168,169,276]. Regulation of eNOS expression and phosphorylation by mechanical forces such as pulsatile stretch and shear stress resultant of haemodynamics within blood vessels [162,163,165–167,184,266,267]. Importantly, NO signalling is known to modulate APP processing, and lead to Aβ generation that enable Aβ plaque formation in AD [18,262,275]. In human brain microvascular endothelial cells (BMECs), eNOS inhibition using N(G)-Nitro-L-Arginine Methyl Ester (L-NAME) markedly increased APP, BACE-1 and Aβ levels, which was recapitulated in late middle aged-eNOS knockout mice compared to control mice [18]. NO supplementation in eNOS null mice by treating the animals with nitroglycerine attenuated these effects [104]. Moreover, NO concentration bi-directionally regulated APP processing such that increased NO levels by sodium nitroprusside (SNP) in the range of 10 and 20 μM mediating amyloidogenic processing, whereas NO levels mediated by physiological SNP concentrations in the range of 0.01 and 0.1 μM leading to non-amyloidogenic processing in SH-SY5Y neuroblastoma cells stably transfected with wild-type APPwt695 [262]. These studies elaborated a role of NO in modulating APP processing and Aβ levels.

NO production via eNOS is known to be modulated by the serine/threonine-specific kinase, Akt while glycogen synthase kinase-3 (GSK-3) is regulated by Akt [165,250–253]. Akt activation by cyclic stretch has been reported, dependent upon caveolin-1, a protein involved in eNOS activation [97–99,192]. NO could regulate inflammatory markers such as intercellular cell adhesion molecule-1 (ICAM-1) [268]. All these factors are involved in AD pathophysiology and are known to be modulated by stretch [17,116,119,153,162,165,185,191,192,194,205,250,256–258192]. However, effect of cyclic stretch in the presence of exogenous Aβ has not been studied in a cerebral endothelial cell line.

This study aimed to investigate the combinatory effect of exogenous Aβ and mechanical cyclic stretch on APP, Aβ and APP processing enzymes, BACE-1, a disintegrin and metalloproteinase-10 (ADAM10), proteins associated with eNOS signalling, Akt, GSK-3, ICAM-1 and NO in a cerebral EC line since mechanical stretch effects on cerebral ECs in the presence of exogenous Aβ on these signalling molecules are not known in the context of AD.

7.2 Methods

All methodological approaches including culture conditions are detailed in Chapters 3, 4, and 5. HCMEC-SV40 used in this experiment were between 7-10 passages.

7.2.1 Aβ treatment

HCMECs were pre-treated with 150 nM Aβ42 (#AMP42-1, EZBiolab, USA) peptide for 6 hours followed by application of 15% stretch for 18 hours after replenishing culture media. The treatment conditions such as the concentration of Aβ42 and time duration were optimised based on a previous study showing Aβ cytotoxicity in ECs [277].

7.2.2 Statistical analysis

Each data point represents an individual experiment and data are represented as mean±SEM analysed using one-way ANOVA (Repeated Measures or Ordinary) with post-hoc Tukey-corrected multiple comparisons performed in GraphPad PRISM software version 7.02. Paired or unpaired t-test (two-tailed) comparisons were made between groups and reported in the relevant results sections to emphasise statistically underpowered studies, of which the graphs are shown in an appendix. Outliers were identified using the robust regression and outlier removal (ROUT) method (detailed in Motulsky *et al.* [228]) in GraphPad PRISM with a Q value that defines the threshold for outliers set at 10%.

7.3 Results

7.3.1 Effect of cyclic stretch in the presence of exogenous Aβ on APP expression and processing

Aβ is present in the milieu of AD [274] while vascular risk factors of AD such as hypertension and elevated pulse pressure could lead to increased vessel stretch, thus the effect of pulsatility in the presence of Aβ pre-treatment was investigated in the cerebral EC line, HCMEC-SV40. Followed by 18 hours of stretching at 1 Hz, APP and BACE-1 expression were altered with no significant changes in ADAM10 expression (Figure 7.1). APP expression was significantly higher at the 15% stretch magnitude (126±5%) compared to static control (100%, $P<0.05$). A paired t-test (two-tailed) showed that APP expression was also higher in the cells that had been stretched with the Aβ pre-treatment (167±20%) compared to static cells as well (100%, $P<0.05$; Appendix).

BACE-1 expression significantly increased in Aβ pre-treated static cells (124±11%) compared to both Aβ pre-treated (67±7%, $P<0.01$) and untreated (56±7%, $P<0.01$) cells that had been stretched for 18 hours at a stretch magnitude of 15% (Figure 7.1). Additionally, 18 hours of stretching of the cells at 15% in the presence (67±7%, $P<0.01$) or absence (56±7%, $P<0.01$) of Aβ pre-treatment decreased the BACE-1 expression compared to the static vehicle control (100%).

Aβ pre-treatment has led to significant increases in Aβ2 secretion with (51±8 pg/ml) or without (47±5%) the 15% stretch regimen compared to both static control (0.6±0.03 pg/ml, $P<0.0001$) and cells that had been stretched for 18 hours at 15% stretch magnitude (0.5±0.01 pg/ml, $P<0.0001$; Figure 7.1). A paired t-test (two-tailed) performed between the cells that had been stretched and static vehicle control showed a significant decrease in Aβ2 secretion in stretched cells (0.5±0.01 pg/ml, $P<0.05$) compared to static cells (0.6±0.03 pg/ml; Appendix).

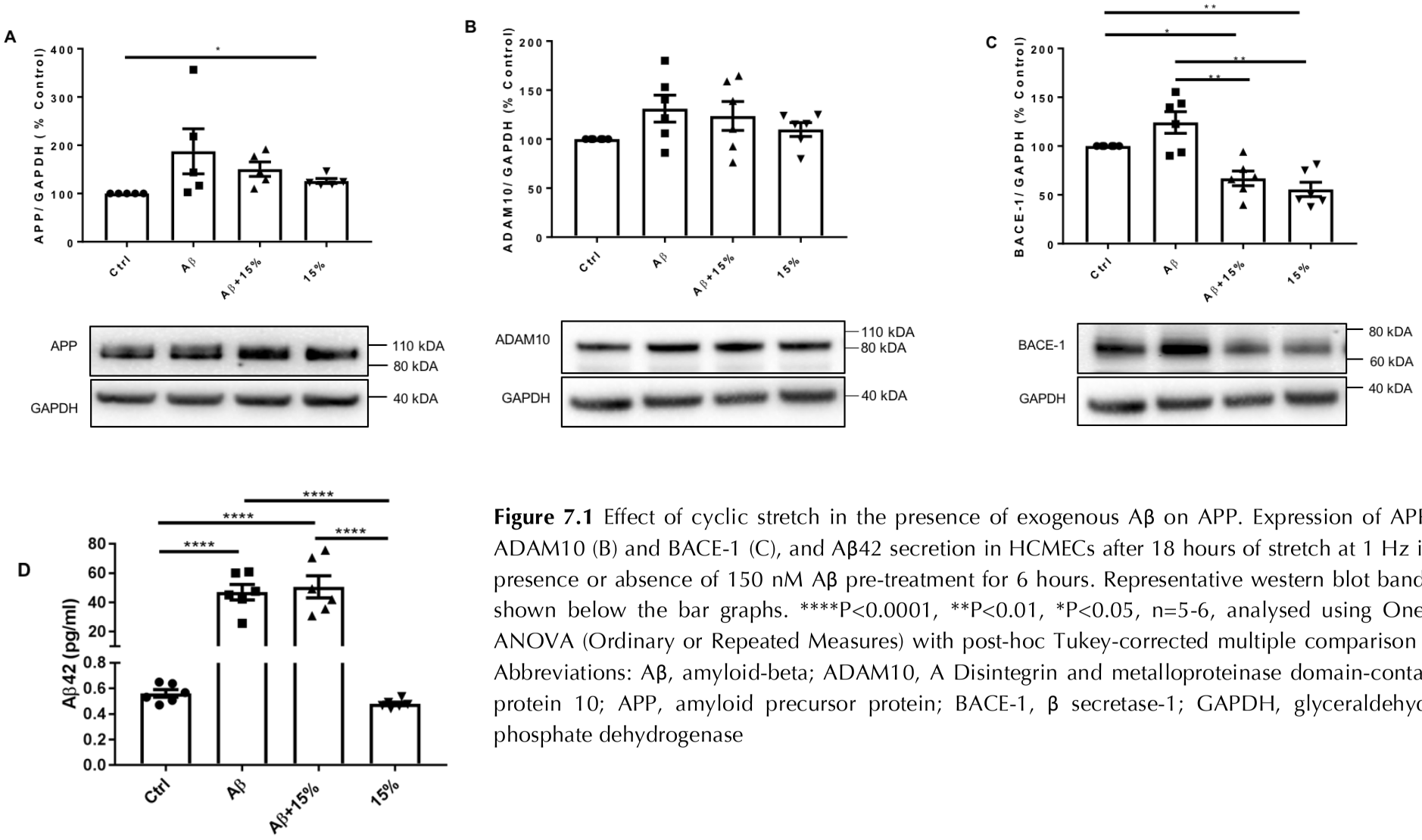

Figure 7.1 Effect of cyclic stretch in the presence of exogenous Aβ on APP. Expression of APP (A), ADAM10 (B) and BACE-1 (C), and Aβ42 secretion in HCMECs after 18 hours of stretch at 1 Hz in the presence or absence of 150 nM Aβ pre-treatment for 6 hours. Representative western blot bands are shown below the bar graphs. ****P<0.0001, **P<0.01, *P<0.05, n=5-6, analysed using One-way ANOVA (Ordinary or Repeated Measures) with post-hoc Tukey-corrected multiple comparison tests. Abbreviations: Aβ, amyloid-beta; ADAM10, A Disintegrin and metalloproteinase domain-containing protein 10; APP, amyloid precursor protein; BACE-1, β secretase-1; GAPDH, glyceraldehyde 3-phosphate dehydrogenase

7.3.2 Effect of cyclic stretch on NO signalling in the presence of exogenous Aβ

To investigate whether NO signalling is altered in response to cyclic stretch in the presence or absence of Aβ, eNOS expression, eNOS phosphorylation and NO production were investigated. Followed by 18 hours of stretching with or without 150 nM Aβ pre-treatment, eNOS expression or eNOS phosphorylation at S1177 did not change significantly (Figure 7.2). However, an unpaired t-test (two-tailed) showed that peNOS was significantly downregulated in stretched cells (49±20%) compared to static cells (100%, $P<0.05$; Appendix). Additionally, paired t-test (two-tailed) showed that the level of peNOS was significantly increased in Aβ pre-treated static cells compared to cell that had been stretched (49±20%, $P<0.05$; Appendix).

NO production however, was significantly higher at 15% stretch either in the presence (0.15±0.01 μM/μg) or absence (0.13±0.01 μM/μg) of Aβ pre-treatment relative to the vehicle treated static control (0.07±0.01 μM/μg, $P<0.0001$; Figure 7.2). Additionally, Aβ pre-treated static control (0.09±0.004 μM/μg, $P<0.0001$) had a significantly lower NO level compared to stretched cells with (0.15±0.01 μM/μg, $P<0.0001$) or without (0.13±0.01 μM/μg, $P<0.01$) Aβ pre-treatment (Figure 7.2).

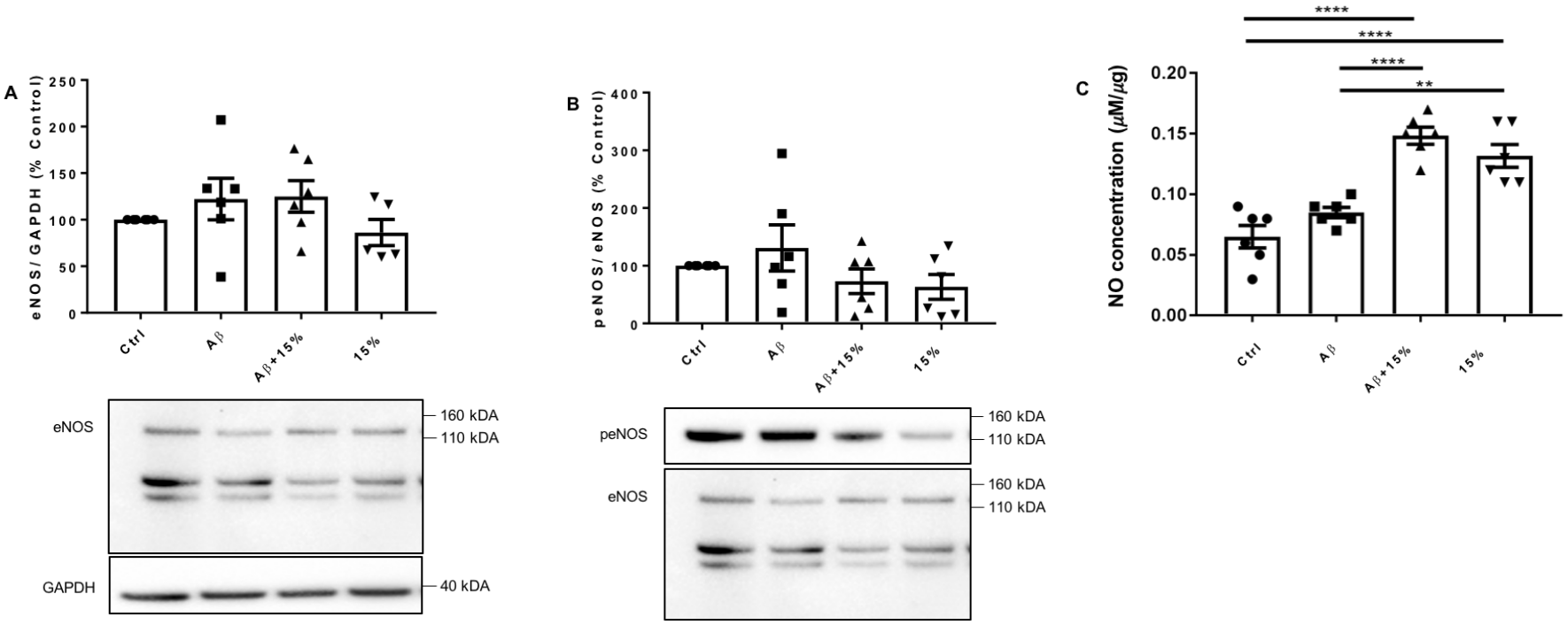

Figure 7.2 Effect of cyclic stretch in the presence of exogenous Aβ on eNOS. Expression of eNOS (A), phosphorylation of eNOS at S1177 (B), and NO production (C) in HCMECs after 18 hours of stretch at 1 Hz in the presence or absence of 150 nM Aβ pre-treatment for 6 hours. Representative western blot bands are shown below the bar graphs. ****P<0.0001, **P<0.01, n=5-6, analysed using One-way ANOVA (Ordinary or Repeated Measures) with post-hoc Tukey-corrected multiple comparison tests. Abbreviations: eNOS; endothelial nitric oxide synthase; GAPDH, glyceraldehyde 3-phosphate dehydrogenase**;** NO, nitric oxide; peNOS, phosphorylated eNOS

7.3.3 Effect of cyclic stretch in the presence of exogenous Aβ on Akt

To explore regulatory mechanisms underlying eNOS mediated-NO production, Akt expression and phosphorylation of Akt S473, were investigated. Akt expression or phosphorylation of Akt at S473 did not change significantly in response to 18 hours of 15% stretch or Aβ pre-treatment alone or combined when compared with an ANOVA and post-hoc Tukey corrected multiple correction tests (Figure 7.3). However, an unpaired t-test (two-tailed) showed that pAkt levels were significantly decreased in stretched cells (59±16%) compared to static vehicle control (100%, $P<0.05$; Appendix).

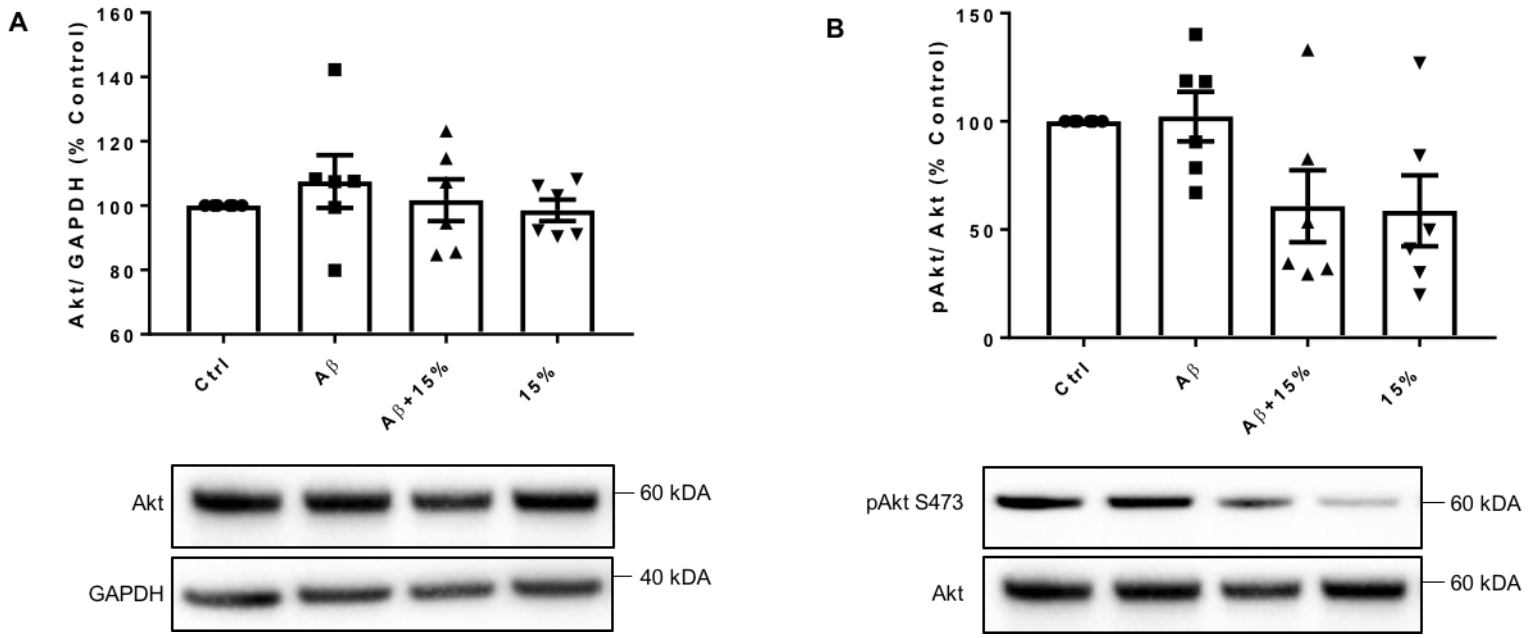

Figure 7.3 Effect of cyclic stretch in the presence of exogenous Aβ on Akt. Expression of Akt (A) and phosphorylation of Akt at S473 (B) in HCMECs after 18 hours of stretch at 1 Hz in the presence or absence of 150 nM Aβ pre-treatment for 6 hours. Representative western blot bands are shown below the bar graphs. n=6, analysed using One-way ANOVA (Repeated Measures) with post-hoc Tukey-corrected multiple comparison tests. Abbreviations: GAPDH, glyceraldehyde 3-phosphate dehydrogenase**;** pAkt, phosphorylated Akt

7.3.4 Effect of cyclic stretch in the presence of exogenous Aβ on GSK-3α and GSK-3β

Downstream target of Akt activation, GSK-3 was also investigated. 18 hours of stretching with or without Aβ pre-treatment did not change the expression of GSK-3α, GSK-3β or phosphorylation of GSK-3α phosphorylation at S21 or GSK-3β at S9 in HCMECs (Figure 7.4).

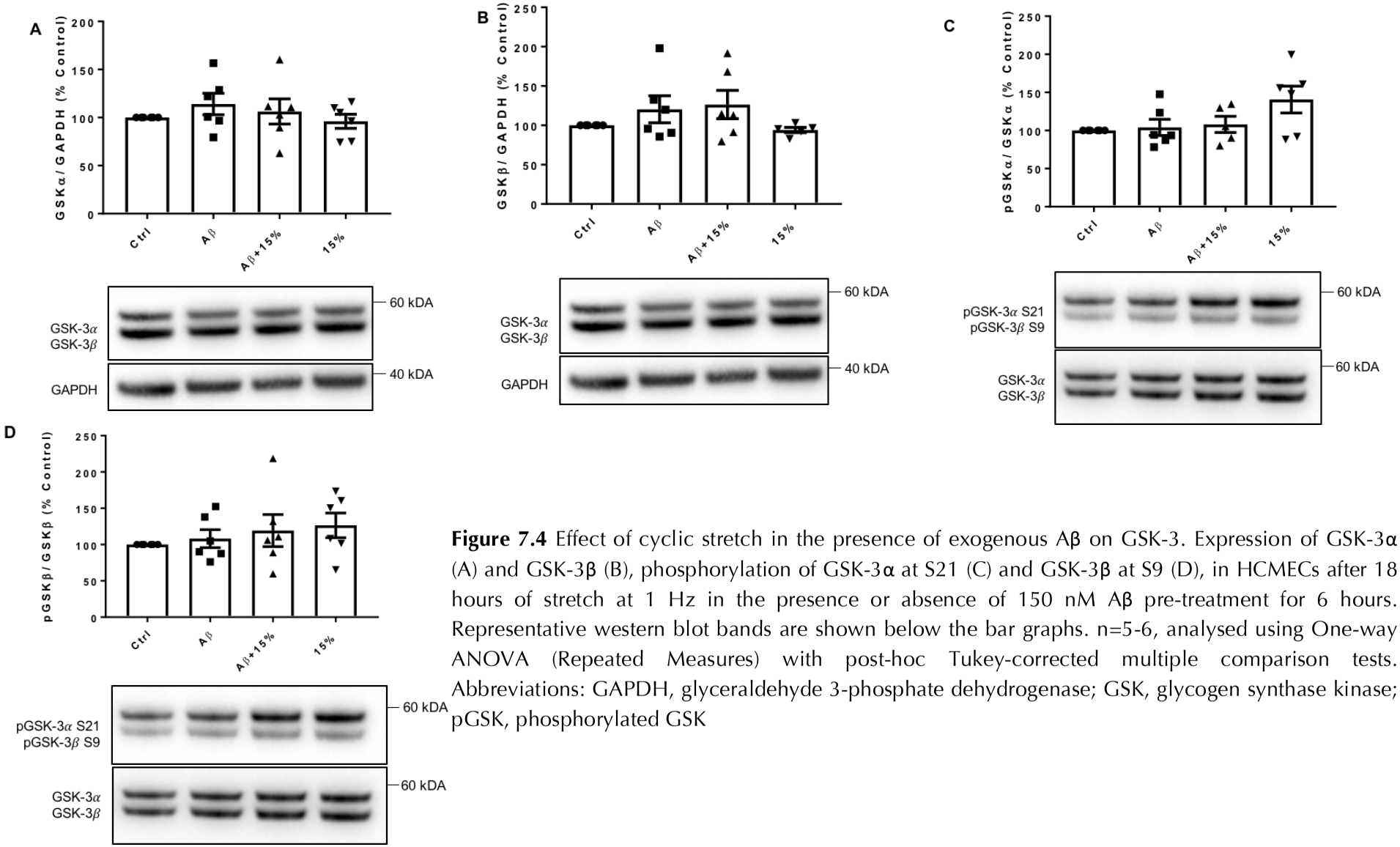

Figure 7.4 Effect of cyclic stretch in the presence of exogenous Aβ on GSK-3. Expression of GSK-3α (A) and GSK-3β (B), phosphorylation of GSK-3α at S21 (C) and GSK-3β at S9 (D), in HCMECs after 18 hours of stretch at 1 Hz in the presence or absence of 150 nM Aβ pre-treatment for 6 hours. Representative western blot bands are shown below the bar graphs. n=5-6, analysed using One-way ANOVA (Repeated Measures) with post-hoc Tukey-corrected multiple comparison tests. Abbreviations: GAPDH, glyceraldehyde 3-phosphate dehydrogenase; GSK, glycogen synthase kinase; pGSK, phosphorylated GSK

7.3.5 Effect of cyclic stretch in the presence of exogenous Aβ on caveolin-1 and ICAM-1

A regulatory protein involved in eNOS activation, caveolin-1, and an inflammatory marker involved in NO-mediated signalling, ICAM-1 were next investigated. No changes in caveolin-1 were observed under any condition. ICAM-1 was significantly increased in Aβ pre-treated static cells (135±20%) compared to cells that had been stretched for 18 hours at 15% with (71±14%, $P<0.01$) or without (57±6%, $P<0.05$) Aβ pre-treatment (Figure 7.5). Cells that had been stretched without Aβ (57±6%) had significantly lower ICAM-1 levels compared to the static vehicle control (100%, $P<0.01$; Figure 7.5).

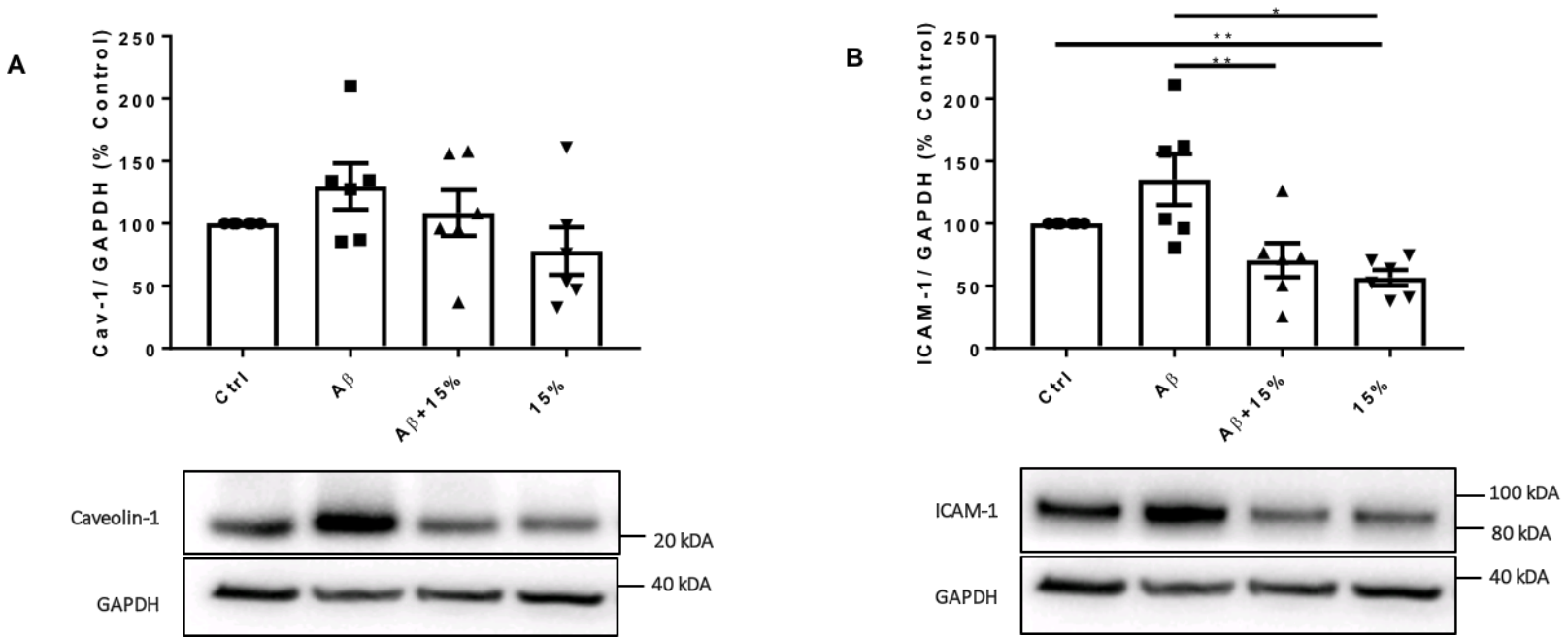

Figure 7.5 Effect of cyclic stretch in the presence of exogenous Aβ on caveolin-1 and ICAM-1 expression. Expression of caveolin-1 (A) and ICAM-1 (B) in HCMECs after 18 hours of stretch at 1 Hz in the presence or absence of 150 nM Aβ pre-treatment for 6 hours. Representative western blot bands are shown below the bar graphs. **P<0.01, *P<0.05, n=6, analysed using One-way ANOVA (Repeated Measures) with post-hoc Tukey-corrected multiple comparison tests. Abbreviations: Cav-1; caveoli-1, GAPDH, glyceraldehyde 3-phosphate dehydrogenase; ICAM-1, intercellular cell adhesion molecule-1

7.4 Discussion

Owing to the involvement of vascular factors such as hypertension, elevated pulse pressure and large artery stiffness that could in turn induce increased mechanical stretch on the vascular wall, and the presence of Aβ in AD pathophysiology, the current study combined the effect of pulsatility and Aβ, to investigate stretch-mediated changes in AD in a cerebral EC line. The effect of stretch on APP expression is consistently observed as reported in Chapter 4 (and the recent publication) [19] and Chapter 6, since APP expression was significantly elevated at the end of 18 hours of stretching period at a magnitude of 15% (Figure 7.1). Pre-exposure to Aβ did not have any significant additional effects on APP expression, except that the significant increase in APP after stretching was not observed in the presence of the pre-Aβ treatment although there was a non-significant trend of a slight incremental effect (Figure 7.1). However, the effect of stretch on APP expression was still present even with the Aβ pre-treatment, when the two groups are compared with a t-test rather than by an ANOVA with post-hoc Tukey multiple comparison tests (Figure 7.1 & appendix), implying that the study was statistically underpowered to show the effect. The consistent upregulation of APP expression mediated by 15% stretch indicate that cyclic stretch upregulates APP expression in HCMECs.

The expression of the APP processing enzyme towards amyloidogenic APP processing, BACE-1, was downregulated by stretch with or without Aβ pre-treatment compared to both static vehicle control and Aβ pre-treated static control (Figure 7.1). The stretch effect of the current study is contradistinction to the results of Chapter 4 [19], which is explained by the passaging effect shown in Chapter 6. As demonstrated and discussed in Chapter 6, the differences in passage numbers (passage 7-9 in the present study versus passage 17-19 in Chapter 4) in the two studies, can significantly affect BACE-1 expression, such that HCMECs at early passages regulating BACE-1 expression differently to those cells that are in late

passages. This is supported by many previous studies showing differences in gene and protein expression profiles at early passages relative to late passages, and a recent study that demonstrated that in human brain microvascular endothelial cells (BMECs) APP processing altered between early and late passage cells [21,278–282]. These findings also suggest that in early passage cells (as in the present study), cyclic stretch mediates non-amyloidogenic processing of APP by downregulating BACE-1, in contrast to cells that are in late passages, that mediate amyloidogenic processing of APP by upregulating BACE-1, as shown in Chapter 4 [19]. No changes were seen in ADAM10 expression under any treatment (Figure 7.1). No change in ADAM10 expression in response to 15% stretch for 18 hours is consistent with Chapter 5 and Chapter 6. These consistent results suggest that stretch does not regulate ADAM10 expression at the 15% magnitude. However, secreted Aβ42 levels in the culture supernatants were significantly upregulated in the presence of the Aβ pre-treatment in static and stretched ECs, although there were no additional effects with stretch, since there was no difference between Aβ pre-treated static control group and the Aβ pre-treated-stretched group (Figure 7.1). Nonetheless, the significant upregulation of Aβ42 secretion in Aβ pre-treated groups compared to both stretched and static ECs indicated that Aβ pre-treatment can upregulate Aβ42 secretion, and that the decreasing effect of cyclic stretch on Aβ42 secretion (shown by a paired t-test between the two groups; appendix), was overwhelmed subsequent to Aβ pre-treatment, thereby showing a possible role of exogenous Aβ that triggers Aβ42 secretion. Changes in tight junction formation in BMECs in response to Aβ treatment and mechanical forces including circumferential stretch have been reported [283,284]. Additionally, treatment with Aβ42 fibrils in Hep-1 cell line has resulted in increased $A\beta_{1-40}$ levels [12]. In line with these studies, Aβ pre-treatment in the present study may regulate HCMECs in favour of further Aβ42 secretion due to alterations in tight junctions in ECs in response to stretch that in turn affect Aβ42 clearance into the culture media. However, the possibility that the source of the upregulated Aβ42 levels in the treated groups comes from the treatment itself cannot be ruled

out. In addition, the Aβ42 secretion in cells that had been exposed to 15% stretch alone was downregulated compared to control cells as shown by the t-test results (Appendix), indicating that in HCMECs at early passages, Aβ42 secretion in response to cyclic stretch is differentially regulated compared to HCMECs at late passages, consistently showing a possible role of EC senescence or multiple passaging in APP processing as discussed and shown in Chapter 6. Moreover, decreased Aβ42 secretion along with reduced BACE-1 suggest that HCMECs in early passages (as in the present study) regulate APP processing towards non-amyloidogenic pathway compared to late passage HCMECs that showed amyloidogenic processing of APP (Chapter 4) [19].

The physiological and pathophysiological levels of Aβ42 in the human circulation are stated to be 50 pM and 4.3 nM respectively [58]. The range of average Aβ42 levels in Aβ treated groups were 10-11 pM (equivalent to 47-50 pg/ml as reported in the results section) in the current study. Since there were no additional effects of Aβ pre-treatment with stretch, a higher concentration of Aβ might provide a better representation of the AD pathological milieu, thus giving more pronounced effects, although at the levels of Aβ42 detected in the present study also appeared to have affected Aβ42 secretion.

There was a significant difference in NO production between the Aβ pre-treated static control and Aβ pre-treated stretched cells, showing an incremental effect of prolonged cyclic stretch on NO production in HCMECs (Figure 7.2). Aβ pre-treatment did not have any additional statistically significant effects indicating that Aβ in the concentrations present in this study does not regulate NO production, although there was a non-significant trend towards increased NO production with Aβ pre-treatment (Figure 7.2). However, the present study indicated that NO production in response to long term stretch is unlikely to be mediated by eNOS phosphorylation at S1177 as the eNOS phosphorylation at this site did not coincide with NO levels in this study, and in Chapters 4 [19] and 5 (Figure 7.2). Caveolin-1 did not

change in response to 18 hours of 15% stretching as reported in Chapter 5, indicating that 15% stretch for 18 hours does not potentiate caveolin-1 in HCMECs (Figure 7.5), although acute mechanical stretch studies performed within 1 hour of stretching showed altered caveolin-1 mediated signalling, prolonged stretch may not mediate such changes [192–194].

NO is known to modulate ICAM-1 signalling whilst mechanical stretch is known to upregulate ICAM-1 [160,202–205]. The present study showed ICAM-1 downregulation in response to 18 hours of stretch (Figure 7.5), another distinct finding to that in Chapter 4, which reported increased ICAM-1 expression in response 15% stretch. Chapter 6 showed that there is a passaging effect on ICAM-1 expression such that late passage HCMECs (as in the Chapter 4 [19]) having significantly higher ICAM-1 levels than HCMECs at early passages (as in the present study). These results indicate elevated inflammatory signalling consequent of cyclic stretch, in late passage cells compared to early passage cells, showing a role of cell senescence. Additionally, ICAM-1 exists in a soluble form, which is released into the supernatant, and is shown to be increased in response to stretch [203]. It can be suggested that at early passages of HCMECs, ICAM-1 is released into the supernatant in the soluble form; this will need to be studied in future experiments.

Consistent with results in Chapter 5, cyclic stretch downregulated pAkt as demonstrated by an unpaired t-test (Appendix), without any additional effect with the Aβ pre-treatment (Figure 7.3). However, no effects were shown on GSK-3β, pGSK-3β, GSK-3α or pGSK-3 α in response to stretch (Figure 7.4), although results in Chapter 5 showed that stretch downregulate GSK-3β, pGSK-3β or pGSK-3 α. This is consistent with Chapter 6, that showed a passage effect on these proteins, thus collectively, the results suggest that in early passage HCMECs (as in the present study) GSK-3 is regulated differentially to that of late passage HCMECs (as in Chapter 5) in response to cyclic stretch. As discussed in Chapter 6, multiple passaging could give rise to differential cell signalling due differences in gene and

protein expression as previous reported and cell senescence could play a role in EC protein expression levels [21,278–282].

In summary, the results of APP expression, BACE-1 and Aβ42 secretion suggested that APP is processed differently in response to stretch at lower passages (as in the present study) compared to higher passages of HCMECs (as of Chapters 4 and 5). These results indicate a possible regulatory role of EC senescence in APP processing as recently reported by Sun *et al.* [21], emphasising the relevance of investigating soluble APPα, which is known to exert neuroprotective effects in AD, and could explain the unaltered Aβ42 secretion in the present study (Figure 7.1) [116]. NO in response to stretch could be altered leading to differential processing of APP dependent upon NO concentration since NO bioavailability was demonstrated to regulate APP processing bi-directionally [262]. Increased NO levels in the range of 10 and 20 μM mediated amyloidogenic processing, whereas physiological NO levels in the range of 0.01 and 0.1 μM leading to non-amyloidogenic processing in SH-SY5Y neuroblastoma cells stably transfected with wild-type APPwt695 treated with sodium nitroprusside, a potent NO donor [262]. The present study found average NO concentrations in the range of 0.13-0.15 μM after stretching for 18 hours at a stretch magnitude of 15%. These results could be consistent with non-amyloidogenic processing of APP, thus showing the need for investigating APPα in future studies.

7.5 Conclusions

Effect of cyclic stretch was consistently shown on APP expression, eNOS and Akt phosphorylation, and NO production, with no substantial changes in the presence or absence of Aβ pre-treatment. However, Aβ pre-treatment substantially increased secreted Aβ42 levels overwhelming the stretch mediated downregulation of Aβ42 secretion, thus indicating that exogenous Aβ may trigger further Aβ42 secretion and a role of Aβ in exacerbation of Aβ

pathologies in AD. Effect of cyclic stretch on BACE-1 expression, Aβ42 secretion, and GSK-3 expression and phosphorylation in early passage HCMECs, were different to the effect of cyclic stretch reported in Chapters 4 and 5 that were investigated in late passage HCMECs, consistently showing a combinatory effect of EC passaging and cyclic stretch as reported in Chapter 6. Investigation of NO dependency on non-amyloidogenic APP processing appear to be relevant in future studies. Some of the results becoming statistically significant only when compared using t-tests indicate that the studies are underpowered to show the effects, thus repetition of the experiments are required to confirm these results.

7.6 Appendix

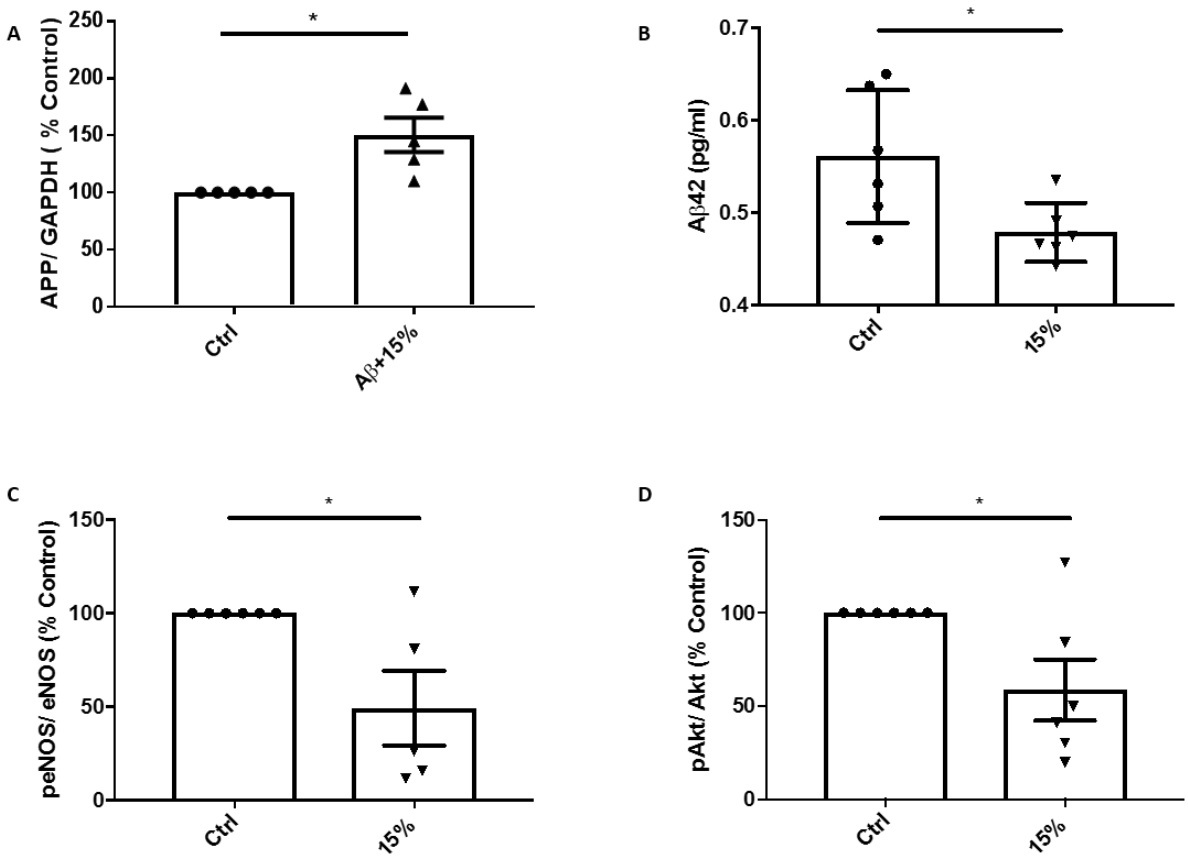

Figure 7.6 Paired or unpaired t-test results of APP expression (A), Aβ42 secretion (B), eNOS phosphorylation (C), and Akt phosphorylation (D) in response to 15% stretch in HCMECs. *P<0.05, n=5-6. Abbreviations: Aβ, amyloid-beta; APP, amyloid precursor protein; pAkt; phosphorylated Akt; peNOS, phosphorylated endothelial nitric oxide synthase

Chapter 8

Effect of cyclic stretch and glycosphingolipid inhibition on cerebral endothelial cells

Summary—Elevated pulsatility of arterial pressure and deregulation of ceramide and nitric oxide (NO) metabolism are independently associated with Alzheimer's disease (AD). AD is characterised by amyloid β (Aβ) deposits that are aggregates of Aβ peptides that are cleaved off amyloid precursor protein (APP). Glycosphingolipid inhibitors that inhibit the enzyme glucosylceramide synthase by blocking ceramide glycosylation are known to increase γ secretase-mediated-Aβ release. This study investigates whether pulsatile stretch of human cerebral microvascular endothelial cells (HCMECs) pre-treated with the glycosphingolipid inhibitor, D-PDMP, that inhibits both lactosyl- and glucosyl- ceramide synthases, alters expression and/or phosphorylation of APP and eNOS, Aβ42 secretion, NO production, and expression and phosphorylation of regulatory proteins associated with eNOS activity such as serine/threonine-specific kinase, Akt, glycogen synthase kinase-3 (GSK-3) and intercellular cell adhesion molecule-1 ICAM-1. APP expression significantly increased in response to stretch in ECs pre-treated with D-PDMP compared to those that have been stretched without pre-treatment. eNOS phosphorylation was down-regulated in ECs subjected to stretch compared to vehicle control and PDMP-treated-static control. In ECs pre-treated with D-PDMP prior to stretch, phospho-eNOS levels significantly decreased compared to vehicle control, D-PDMP-treated-static control and stretched cells pre-treated with D-PDMP. APP expression increased in cerebral ECs pre-exposed to D-PDMP after being exposed to cyclic stretch. In conclusion, eNOS phosphorylation was down-regulated by cyclic stretch. D-PDMP pre-treatment appeared to have a restoring effect on peNOS. Glucosyl and/or lactosyl ceramide synthases may have regulatory roles in modulating APP expression and NO signaling in ECs and may have implications on Aβ load, NO production and related vascular pathologies in the context of AD.

8.1 Introduction

Amyloid precursor protein (APP) becomes cleaved by proteolytic enzymes that leads to amyloid β (Aβ) peptides, which aggregate to form Aβ plaques, characteristic of Alzheimer's disease (AD) [46,274,275]. Sphingolipid homeostasis is implicated in AD pathology [132]. Ceramide forms the backbone of complex sphingolipids such as sphingomyelin and glycosphingolipids, which are abundantly present in the brain and modulate structural support and function of membrane-associated proteins, and cell signaling [130,131]. Sphingomyelin synthases synthesise sphingomyelin from ceramide while sphingomyelinases catabolise sphingomyelin back into ceramide. Lactosyl and glucosyl ceramide synthases contribute towards the generation of glycosphingolipids, precursor for gangliosides.

Elevated acid sphingomyelinase and acid ceramidase expression in AD brain samples

correlated with reduced sphingomyelin and elevated of ceramide levels [135]. In an AD cell model, deregulation of ceramide species was demonstrated, where the simplest ganglioside, GM3, lactosylceramide, the precursor of GM3, and ganglioside GD1a have increased significantly relative to those of the wild type H4 cells [137]. While ceramide is known to drive neuronal apoptosis, ceramide associated enzymes such as acid sphingomyelinases and lactosyl ceramide synthases are known to regulate intracellular adhesion molecule-1 (ICAM-1), a marker of microvascular injury implicated in AD [135,143–145]. Glycosphingolipid inhibitors including the synthetic ceramide analogue dl-threo-1-phenyl-2-decanoylamino-3-morpholino-1-propanol (D-PDMP), that inhibit the enzyme glucosylceramide synthase (Figure 8.1) by blocking ceramide glycosylation are known to increase γ secretase-mediated-Aβ release [138].

Hypertension is a risk factor for AD whilst higher pulsatility index and pulse pressure, indicative of increased large artery stiffness and reduced vessel compliance, are associated with AD [3,4,64,74]. Nitric oxide (NO) signalling is known to modulate APP processing and to lead to Aβ generation that enables Aβ plaque formation in AD whilst NO is known to be modulated by mechanical stretch of endothelial cells (ECs), which is mediated by endothelial NO synthase (eNOS) [18,165,262,275]. These findings together indicate a possible role of mechanical stretch and NO signalling in the pathophysiology of AD due to increased circumferential stretch of the vessel wall consequent of hypertension and elevated pulse pressure.

Taken together, elevated pulsatility of arterial pressure and deregulation of ceramide and NO metabolism are independently associated with AD [18,74,138]. This study investigates whether pulsatile stretch of human cerebral microvascular endothelial cells (HCMECs) pre-treated with the glycosphingolipid inhibitor, D-PDMP alters expression and/or phosphorylation of APP and eNOS, Aβ42 secretion, NO production, and expression and phosphorylation of regulatory proteins associated with eNOS activity such as serine/threonine-specific kinase, Akt, glycogen synthase kinase-3 (GSK-3) and ICAM-1 [165,250–253].

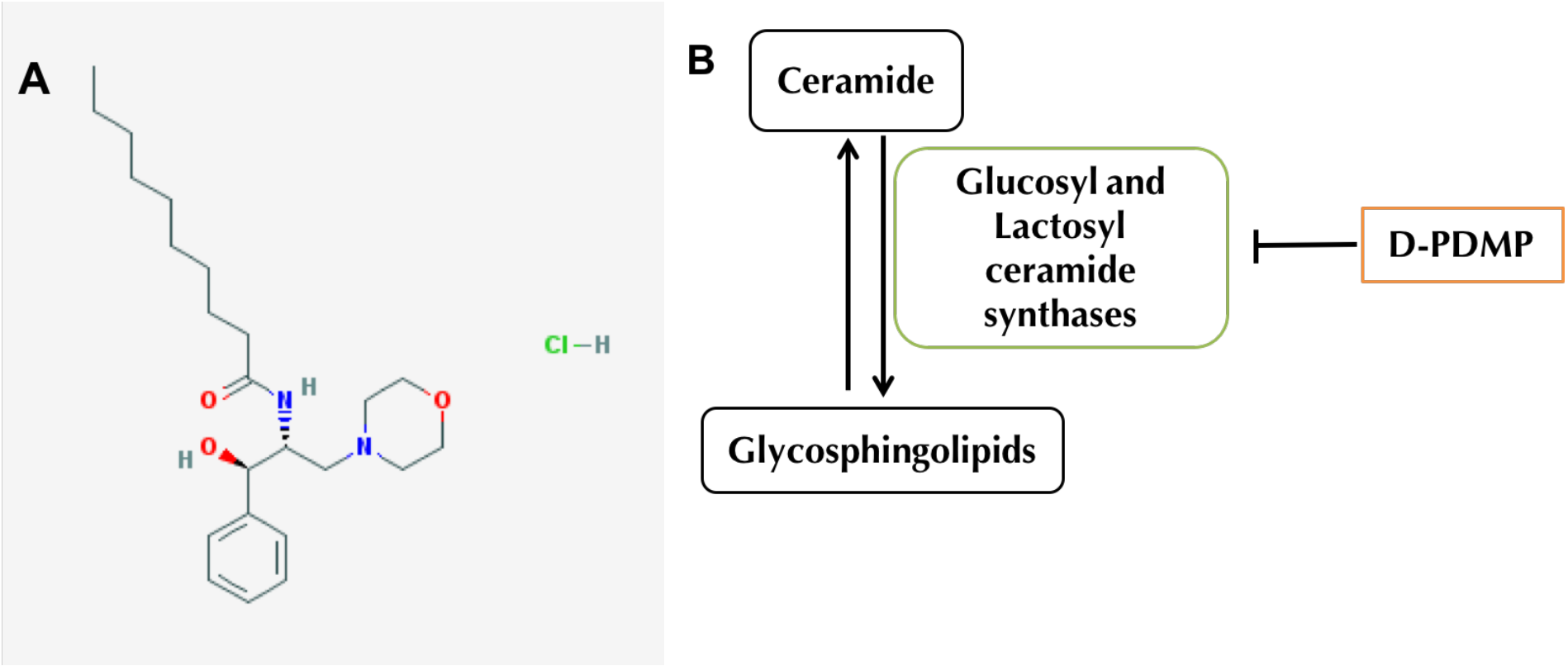

Figure 8.1 Structure of D-PDMP and its action in the ceramide pathway. Chemical structure of D-PDMP (A) and a brief overview of its action (B) Ceramide is the precursor molecule for complex glycosphingolipids, and is converted into glycosphingolipids by the action of gulcosyl and lactosyl ceramide synthases. D-PDMP inhibits the action of glucosyl and lactosyl ceramide synthases. Abbreviations: D-PDMP, dl-threo-1-phenyl-2-decanoylamino-3-morpholino-1-propanol. Chemical structure taken from Pubchem database, CID=16219895.

8.2 Methods

All methodological approaches including culture conditions are detailed in Chapters 3, 4, and 5. HCMEC-SV40 used in this experiment were between 7-9 passages.

8.2.1 D-PDMP treatment

HCMECs were pre-treated with 20 μM D-PDMP (Cat. No. 1756, AdeLab scientific) prepared in sterile 1x phosphate buffered saline 2 hours followed by application of 15% stretch for 18 hours after replenishing culture media. The treatment criteria were selected based on a previous publication in ECs [145].

8.2.2 Statistical analysis

Each data point represents an individual experiment and data are represented as mean±SEM analysed using one-way ANOVA (Repeated Measures or Ordinary) with post-hoc Tukey-corrected multiple comparisons performed in GraphPad PRISM software version 7.02. Paired or unpaired t-test (two-tailed) comparisons were made between groups and reported in the relevant results sections to emphasise statistically underpowered studies, of which the graphs are shown in an appendix. Outliers were identified using the robust regression and outlier removal (ROUT) method (detailed in Motulsky *et al.* [228]) in GraphPad PRISM with a Q value set at 10% that defines the threshold for outliers.

8.3 Results

8.3.1 Effect of cyclic stretch and glycosphingolipid inhibition on APP expression and Aβ42 secretion

Ceramide homeostasis is implicated in AD [132], whilst the vascular risk factors of AD such as hypertension and elevated pulse pressure could lead to increased vessel stretch. Thus, the effect of pulsatility and glycosphingolipid inhibition was investigated in the cerebral EC line,

HCMEC-SV40. Followed by 18 hours of stretching at 1 Hz, APP expression increased significantly in stretched HCMECs pre-treated with D-PDMP (170±27%, $P<0.01$) relative to cells that had been stretched without the pre-treatment (115±23%; Figure 8.2). A slight, but not significant increase in APP expression at 15% stretch magnitude (115±23%) was evident compared to the static control (100%). The optical density units (ODU) at 450 nm, which is indicative of Aβ42 secretion, of stretched cells with no pre-treatment (0.131±0.005 ODU) was decreased compared to both pre-treated cells that had been stretched (0.149±0.006 ODU, $P<0.05$), and vehicle static control (0.147±0.003 ODU; $P<0.01$; Figure 8.2).

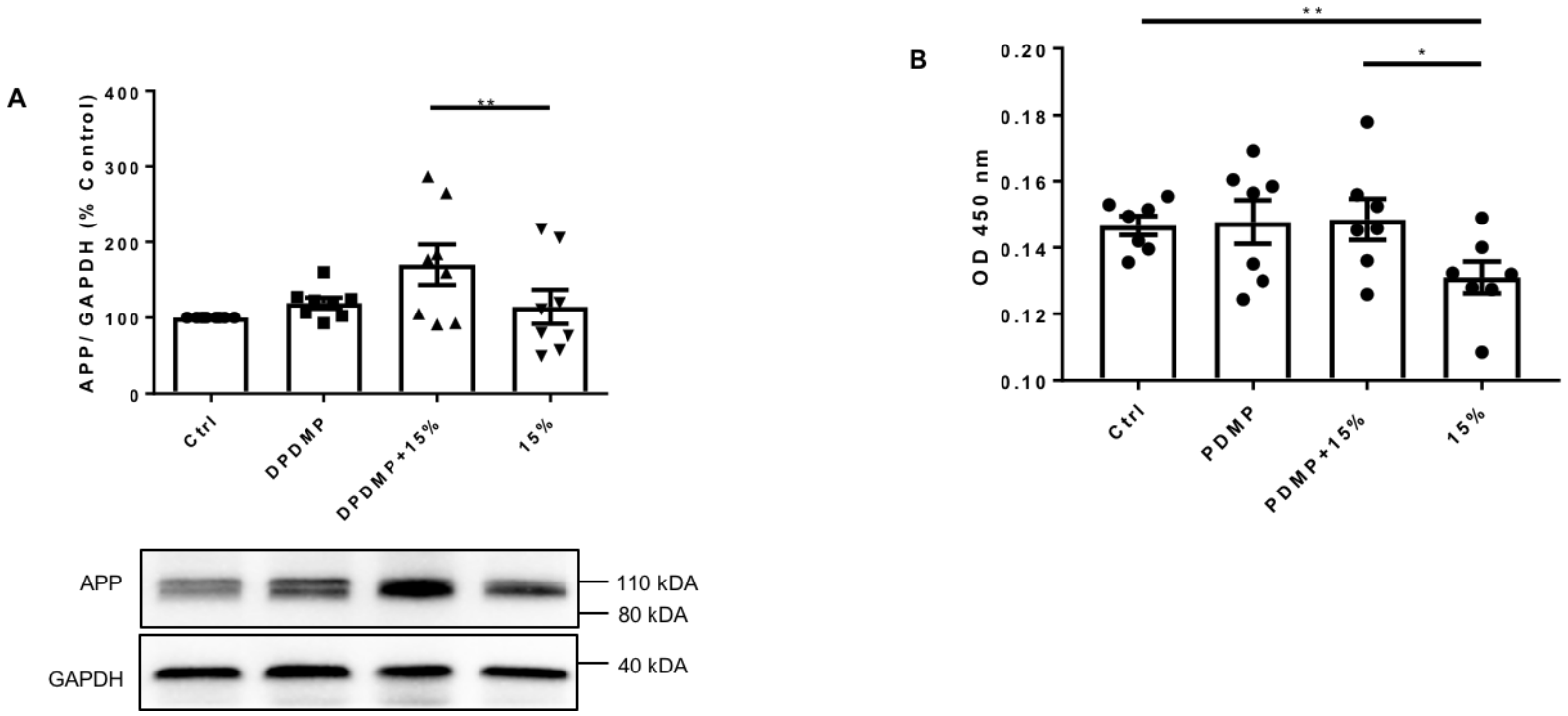

Figure 8.2 Effect of cyclic stretch and glycosphingolipid inhibition on APP and Aβ. Expression of APP (A), and optical density at 450 nm representative of Aβ42 secretion in HCMECs after 18 hours of stretch at 1 Hz pre-treated with or without 20 μM D-PDMP pre-treatment. Representative western blot bands are shown below the bar graphs. **P<0.01, *P<0.05, n=7-8, analysed using Repeated Measures-One-way ANOVA with post-hoc Tukey-corrected multiple comparison tests. Abbreviations: Aβ, amyloid-beta; D-PDMP, dl-threo-1-phenyl-2-decanoylamino-3-morpholino-1-propanol; GAPDH, glyceraldehyde 3-phosphate dehydrogenase

8.3.2 Effect of cyclic stretch and glycosphingolipid inhibition on NO signalling

To investigate whether NO signalling is altered in cells that had been stretched with or without D-PDMP pre-treatment, eNOS expression, eNOS phosphorylation and NO production were next investigated. Followed by 18 hours of stretching with or without 20 μM D-PDMP, eNOS expression did not change. However, eNOS phosphorylation at S1177 was downregulated significantly in cells that had been stretched without the D-PDMP pre-treatment (10±4%) compared to vehicle static control (100%; $P<0.0001$) and D-PDMP treated static control (107±17%; $P<0.01$; Figure 8.3). Similarly, downregulation of eNOS phosphorylation at S1177 was evident in stretched cells with the D-PDMP pre-treatment (40±15%) as well, compared to both vehicle static control (100%; $P<0.05$) and D-PDMP treated static control (107±17%; $P<0.01$; Figure 8.3). There was a non-significant increasing trend in eNOS phosphorylation in stretched cells with the D-PDMP pre-treatment (40±15%) compared to stretched cells without the pre-treatment (10±4%; Figure 8.3) when compared using One-way ANOVA with post-hoc Tukey corrected multiple comparisons. However, a paired t-test between the two groups, D-PDMP pre-treated with stretch (40±15%) and stretch alone (10±4%) detected that D-PDMP pre-treated group had significantly higher phospho-eNOS levels ($P<0.05$; Appendix).

NO production however, did not change significantly under any condition when analysed using One-way ANOVA with post-hoc Tukey corrected multiple comparisons (Figure 8.3). However, paired t-tests between the stretched cells with no pre-treatment (0.051±0.005 μM/μg) and, vehicle treated static cells (0.041±0.003 μM/μg) or D-PDMP-pre-treated static cells (0.040±0.002 μM/μg), showed that stretched cells had significantly higher NO levels relative to either of the static cell groups ($P<0.05$; Appendix).

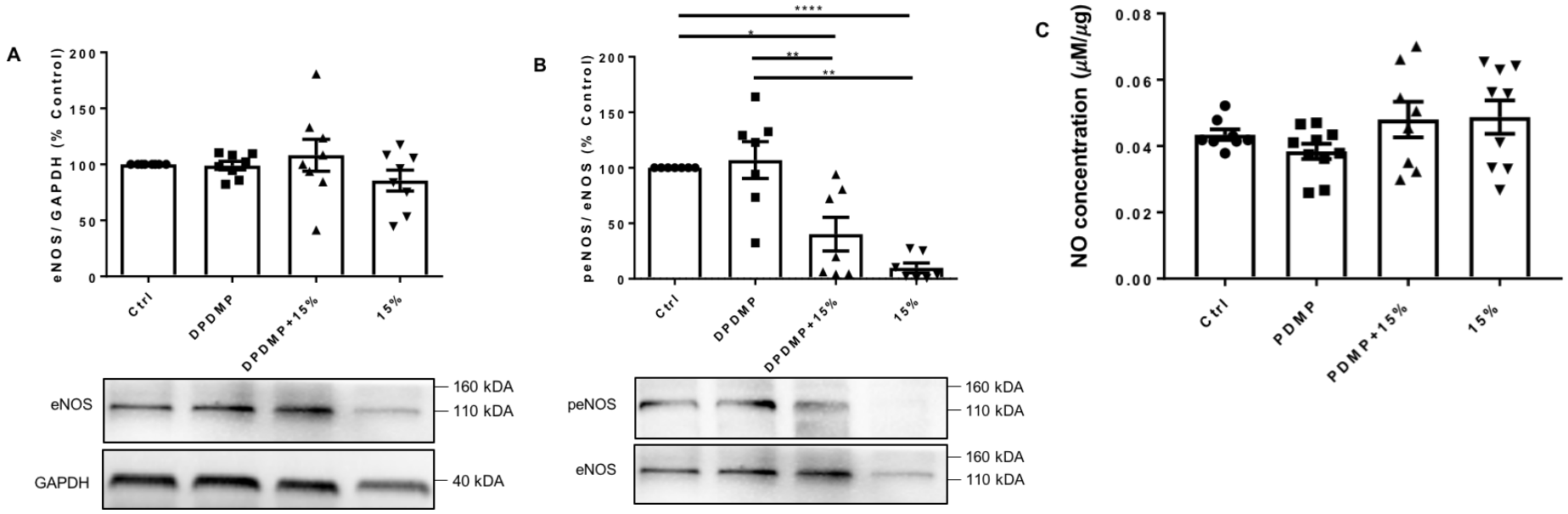

Figure 8.3 Effect of cyclic stretch and glycosphingolipid inhibition on eNOS and NO. Expression of eNOS (A), phosphorylation of eNOS at S1177 (B), and NO production (C) in HCMECs after 18 hours of stretch at 1 Hz with or without 20 μM D-PDMP pre-treatment. Representative western blot bands are shown below the bar graphs. ****P<0.0001, **P<0.01, *P<0.05, n=7-10, analysed using Repeated Measures- or Ordinary- One-way ANOVA with post-hoc Tukey-corrected multiple comparison tests. Abbreviations: D-PDMP, dl-threo-1-phenyl-2-decanoylamino-3-morpholino-1-propanol; eNOS, endothelial nitric oxide synthase; GAPDH, glyceraldehyde 3-phosphate dehydrogenase; NO, nitric oxide; peNOS, phosphorylated eNOS

8.3.3 Effect of cyclic stretch and glycosphingolipid inhibition on Akt

To explore regulatory mechanisms underlying eNOS mediated-NO production, Akt expression and phosphorylation of Akt S473, were investigated. Akt expression did not change under any condition (Figure 8.4). However, Akt phosphorylation at S473 significantly decreased in HCMECs in response to 18 hours of 15% stretch without D-PDMP pre-treatment (75±11%) compared to D-PDMP pre-treated static cells (117±5%, $P<0.05$; Figure 8.4). Additionally, in HCMECs stretched with the pre-treatment of D-PDMP (66±9%), Akt phosphorylation at S473 was significantly downregulated compared to both vehicle treated (100%, $P<0.05$) and D-PDMP treated (117±5%, $P<0.01$) static controls (Figure 8.4). Akt phosphorylation was significantly higher in D-PDMP treated static cells (117±5%) compared to vehicle treated static cells (100%, $P<0.05$) when analysed using a paired t-test (Appendix). Akt phosphorylation was downregulated at the 15% stretch magnitude (75±11%) relative to the static control (100%, $P<0.05$) when compared using an unpaired t-test (Appendix).

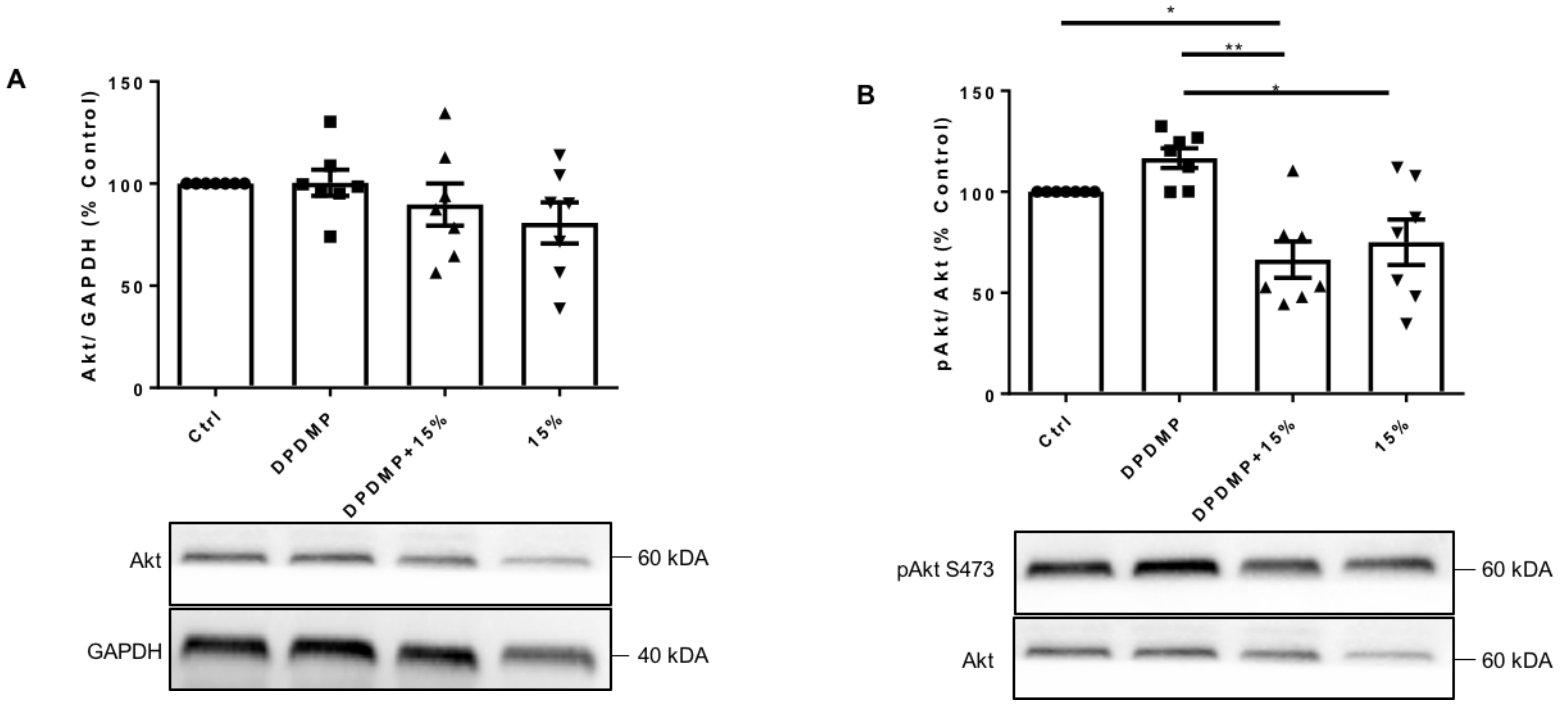

Figure 8.4 Effect of cyclic stretch and glycosphingolipid inhibition on Akt. Expression of Akt (A) and phosphorylation of Akt at S473 (B) in HCMECs after 18 hours of stretch at 1 Hz with or without 20 μM D-PDMP pre-treatment. Representative western blot bands are shown below the bar graphs. **P<0.01, *P<0.05, n=7, analysed using Repeated Measures-One-way ANOVA with post-hoc Tukey-corrected multiple comparison tests. Abbreviations: D-PDMP, dl-threo-1-phenyl-2-decanoylamino-3-morpholino-1-propanol; GAPDH, glyceraldehyde 3-phosphate dehydrogenase; pAkt, phosphorylated Akt

8.3.4 Effect of cyclic stretch and glycosphingolipid inhibition on GSK-3α and GSK-3β

Downstream target of Akt activation, GSK-3 was also investigated in response to stretch and glycosphingolipid inhibition. 18 hours of stretching with or without D-PDMP pre-treatment did not change the expression of GSK-3α, GSK-3β or phosphorylation of GSK-3α phosphorylation at S21 or GSK-3β at S9 in HCMECs (Figure 8.5).

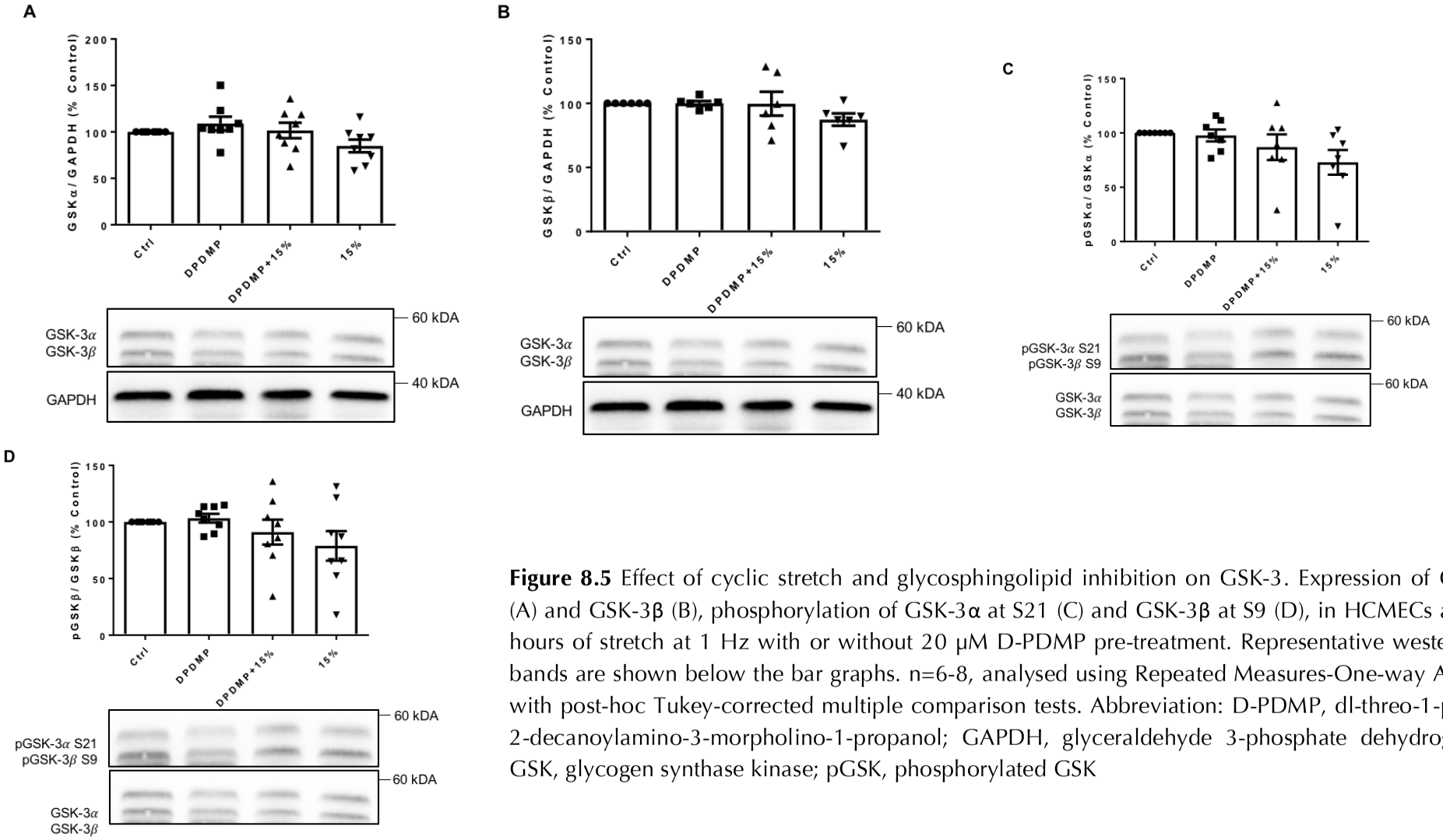

Figure 8.5 Effect of cyclic stretch and glycosphingolipid inhibition on GSK-3. Expression of GSK-3α (A) and GSK-3β (B), phosphorylation of GSK-3α at S21 (C) and GSK-3β at S9 (D), in HCMECs after 18 hours of stretch at 1 Hz with or without 20 μM D-PDMP pre-treatment. Representative western blot bands are shown below the bar graphs. n=6-8, analysed using Repeated Measures-One-way ANOVA with post-hoc Tukey-corrected multiple comparison tests. Abbreviation: D-PDMP, dl-threo-1-phenyl-2-decanoylamino-3-morpholino-1-propanol; GAPDH, glyceraldehyde 3-phosphate dehydrogenase; GSK, glycogen synthase kinase; pGSK, phosphorylated GSK

8.3.5 Effect of cyclic stretch and glycosphingolipid inhibition on ICAM-1

The inflammatory marker involved in NO-mediated signalling, ICAM-1 was next investigated. ICAM-1 was significantly increased in D-PDMP pre-treated static cells (120±14%) compared to cells that had been stretched for 18 hours at 15% with (57±4%, P<0.05) or without (53±3%, P<0.05) D-PDMP pre-treatment. Cells that had been stretched with (57±%4, P<0.001) or without D-PDMP (53±3%, P<0.0001) had significantly lower ICAM-1 levels compared to the static vehicle control (100%; Figure 8.6).

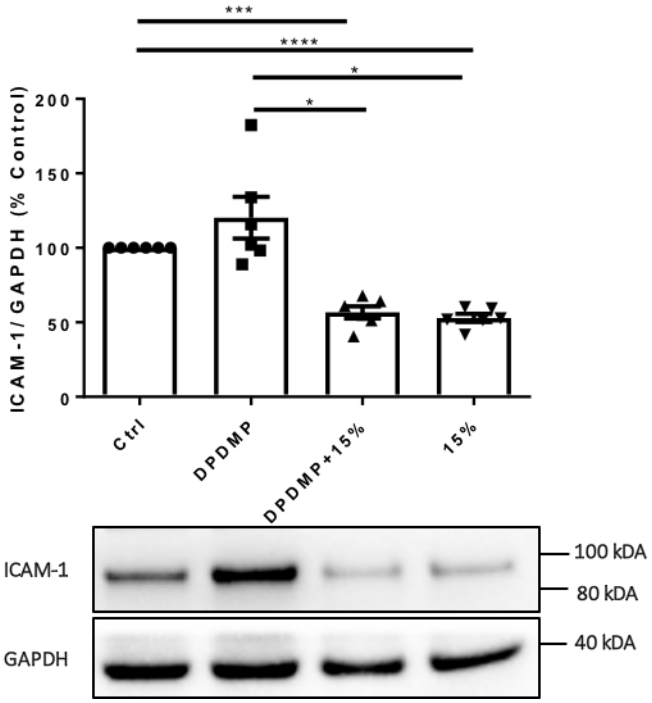

Figure 8.6 Effect of cyclic stretch and glycosphingolipid inhibition on ICAM-1 expression. Expression of ICAM-1 in HCMECs after 18 hours of stretch at 1 Hz with or without 20 μM D-PDMP pre-treatment. Representative western blot bands are shown below the bar graphs. ****P<0.0001, **P<0.001, *P<0.05, n=6, analysed using Repeated Measures-One-way ANOVA with post-hoc Tukey-corrected multiple comparison test. Abbreviations: D-PDMP, dl-threo-1-phenyl-2-decanoylamino-3-morpholino-1-propanol; GAPDH, glyceraldehyde 3-phosphate dehydrogenase; ICAM-1, intercellular cell adhesion molecule-1

8.4 Discussion

Glycosphingolipids are involved in AD whilst pulsatility is a potential culprit that could play a pathological role since vascular factors for AD such as hypertension, elevated pulse pressure

and large artery stiffness could in turn imply increased mechanical stretch on the vascular wall leading to deleterious effects on ECs [18,74,135,137,138]. Thus, the current study combined the effect of pulsatility and glycosphingolipid inhibition, to investigate stretch-mediated changes in protein expression and signalling, and the relevance of glycosphingolipids associated with AD in a cerebral EC line. One of the main findings of this study is that D-PDMP pre-treatment upregulated APP expression only when the cells were under stretch compared to cells that had been stretched without pre-treatment (Figure 8.2). This was consistent with an upregulation of Aβ42 secretion indicated by the increased OD of stretched cells with pre-treatment compared to stretched cells without pre-treatment (Figure 8.1). This is consistent with a previous study that showed increased γ-secretase-mediated-Aβ release in response to D-PDMP treatment [138]. γ-secretases cleave APP to generate Aβ peptides that aggregate to form AD plaques [285]. In HEK293 cells stably expressing the Swedish mutant of APP or Neuro2a cells, that were treated with 10 μM D-PDMP for 24 hours, a marked increase in secreted Aβ42 concomitant with an increase in γ-secretase activity were reported [138]. In contrast, in Chinese Hamster Ovary cells stably expressing human APP, 48 hours of D-PDMP treatment at 15 μM resulted in reduced Aβ levels [139]. Similarly, Tamboli *et al.* [141] reported that 48 hours of 10 μM D-PDMP reduced soluble APP and decreased endogenous Aβ in HEK293 and HeLa cells, or SHSY5Y respectively [141]. Additionally, APP maturation in the secretory pathway and its expression at the cell surface was also affected by D-PDMP treatment [141]. These results were suggested to be due to lack of access to APP by β-secretase 1 (BACE-1) consequent of glycosphingolipid depletion or altered secretase processing of APP [141]. This study also reported that in HEK293 cells, 2 hours of 25 μM D-PDMP did not alter glycosphingolipid levels significantly and that these effects could not be replicated in transfected cells [141]. Collectively, these studies suggest that cell type and treatment duration could have distinct effects on APP and Aβ secretion. The present study included a 20 μM pre-treatment for 2 hours with D-PDMP followed by 18 hours of cyclic stretching at a frequency of 1 Hz and a

magnitude of 15%. The results showed a significant increase in both APP expression and Aβ42 secretion indicating that cyclic stretch could have additive effects towards amyloidogenic processing of APP combined with brief glycosphingolipid inhibition. Additionally, mechanical stretch is reported to cause increased glycosphingolipid turnover in myoblasts stretched on silicon chambers at 1 Hz for 15 minutes whilst a brief stretch of myoblasts for 1 minute at 1 Hz was shown to reduce glycosphingolipid packing [196]. Since D-PDMP inhibits glycosphingolipid formation, this means that the ceramide homeostasis is disturbed leading to ceramide accumulation. Ceramide is known to stabilise BACE-1 and increase Aβ [142]. Taken together, prolonged stretch of cerebral ECs pre-conditioned with a brief D-PDMP treatment may trigger further ceramide accumulation leading to increased Aβ. The results can be implicated in modulating glycosphingolipid levels to regulate endothelial Aβ. Investigating soluble APP and secretases including both BACE-1, and the effect of stretch in the presence of exogenous ceramide in future studies will provide insights into mechanisms how these novel effects are mediated.

The effect of stretch on APP expression that was consistently shown in previous chapters was observed only as a non-significant trend in this study possibly due to the current study being statistically under powered. However, the mean APP expression was still consistent such that APP expression in cells under stretch was higher than that in static cells (Figure 8.2), showing that stretch regulates cerebral endothelial APP expression, a novel finding that is presented throughout this thesis. Nonetheless, the present study showed a significant downregulation of Aβ42 secretion as indicated by the decreased OD at 15% stretch compared to static cells (Figure 8.2), which is consistent with the results presented in Chapter 7. Data presented in Chapter 7 where the cell passages were within 7-9, hence comparable to this study, showed the same effect in cells under 15% stretch for 18 hours compared to static cells. Taken together, the present study and the data presented in Chapter 7, support the results presented

in Chapter 6 that showed that at lower passages (passage 7-9) HCMECs respond to cyclic stretch differently compared to higher passages (passage 17-19) in terms of APP processing. Furthermore, the findings in the present study together with Chapter 7 showing a significant downregulation of Aβ42 secretion and BACE-1 (as shown in Chapter 7) in response to 18 hours of 15% stretch compared to static cells in early passage HCMECs, suggest that at lower passages, HCMECs undergo non-amyloidogenic processing of APP, whereas at higher passages, they undergo amyloidogenic processing of APP (as presented in Chapter 4 and in the recent publication [19]) in response to the same stretch stimulus. This is consistent with a possible role of ageing or multiple passaging on APP processing in HCMECs, and these findings could inform further studies in investigations involving brain EC senescence and AD.

NO production was found to modulate APP processing and Aβ secretion [18,262,275]. Consistent with previous chapters showing significant increases in NO levels in response to 15% stretch, the present study showed increased NO concentrations in response to 18 hours of cyclic stretching (1 Hz) at 15% compared to both D-PDMP pre-treated and vehicle treated static cells (Figure 8.3). As discussed in Chapter 7, NO in response to stretch could be altered leading to differential processing of APP since NO bioavailability was demonstrated to regulate APP processing bi-directionally [262]. NO levels produced by the potent NO donor, sodium nitroprusside (SNP) in the range of 10 and 20 μM mediated amyloidogenic processing, whereas physiological SNP levels in the range of 0.01 and 0.1 μM leading to non-amyloidogenic processing in SH-SY5Y neuroblastoma cells stably transfected with wild-type APPwt695 [262]. The present study found average NO concentrations approximated to 0.1 μM after stretching for 18 hours at a stretch magnitude of 15%, similarly to the concentrations found in Chapters 5, 6 and 7. These results indicate non-amyloidogenic processing of APP, thus showing the need for investigating APPα in future studies under these conditions.

eNOS phosphorylation at S1177, a regulatory site that potentiates NO was also studied to investigate phosphorylation as a possible mechanism that underlies the NO production. The levels of peNOS were significantly downregulated by 15% stretch for 18 hours, which is consistent with all previous chapters, whilst the D-PDMP treatment had a restoring effect on peNOS in cells under stretch as indicated by a paired t-test between the two groups (Appendix). However, the decreased eNOS phosphorylation at this site in stretched cells or the restored phospho-eNOS levels in stretched cells with D-PDMP treatment did not coincide with alterations in NO levels as consistently shown in this study and in the data presented in previous chapters, reiterating that NO production in response to long term stretch is unlikely to be mediated by eNOS phosphorylation at S1177 (Figure 8.3). Nonetheless, glycosphingolipid inhibition may preserve eNOS phosphorylation at S1177 in cerebral ECs under stress such as cyclic stretch.

In addition to eNOS phosphorylation at S1177, Akt phosphorylation at S473, a regulatory mechanism that mediates phospho-eNOS at S1177 was also downregulated by stretch (which is consistent with all previous chapters), regardless of the D-PDMP pre-treatment relative to the D-PDMP pre-treated static cells (Figure 8.4). D-PDMP pre-treated static cells had higher pAkt compared to vehicle treated static cells when analysed using a paired t-test, which was downregulated after 18 hours of cyclic stretching at 15% (Figure 8.4). The results demonstrate that long term cyclic stretch downregulates pAkt, thus the downstream effect of reduced eNOS phosphorylation could be mediated by Akt phosphorylation at S473.

GSK-3, another downstream target of Akt phosphorylation was also investigated, of which phosphorylation could coincide with increased pAkt and vice versa. Cyclic stretching did not affect GSK-3β, pGSK-3β, GSK-3α or pGSK-3α (Figure 8.5), as consistently reported in Chapter 7, of which the findings are comparable to the present study as the experimental design utilised was the same as the present study as opposed to Chapter 4 and Chapter 5. As

discussed in Chapter 6, multiple passaging could give rise to differential cell signalling due differences in gene and protein expression as previously reported, thus explaining the contradistinctions between the chapters [278–282].

In line with this, ICAM-1, which is known to be modulated by NO and mechanical stretch, was downregulated in the present study in response to stretch consistent with the results presented in Chapter 7, whilst Chapter 4 showed upregulation of ICAM-1 in response to the same stretch regimen, demonstrating a passaging effect on ICAM-1 expression in HCMECs in response to stretch, which is reported in Chapter 6 [160,202–205]. However, whether this downregulation of ICAM-1 expression coincides with altered levels of soluble ICAM-1 levels should be further studied since it is known that soluble ICAM-1 was shown to be increased in response to stretch [203]. Thus, the present study suggests that at early passages of HCMECs, ICAM-1 may be released into the supernatant in the soluble form.

8.5 Conclusions

Effect of cyclic stretch was consistently shown on APP expression and NO production as previous chapters. D-PDMP pre-treatment significantly increased APP expression when combined with stretch compared to the stretch alone group, signifying a role of glycosphingolipids in modulating APP expression in cerebral ECs under stretch. The effect of stretch on Aβ42 secretion, ICAM-1 expression and GSK-3 expression and/or phosphorylation, were similar to findings reported in Chapters 6 and 7, although it was in contradistinction with Chapter 4 and 5, which could be explained by the differences in the passage numbers between the studies that could in turn affect these signalling molecules as discussed in Chapter 6. Investigating ceramide levels in mediating altered APP processing appear to be important in understanding the underlying mechanisms and pathways that may affect the stretch-mediated changes in cerebral ECs in the presence of the D-PDMP pre-

treatment. Glucosyl and/or lactosyl ceramide synthases may have regulatory roles in modulating APP expression and NO signaling in ECs and may have implications on Aβ load (Figure 8.7), NO production and related vascular pathologies in the context of AD.

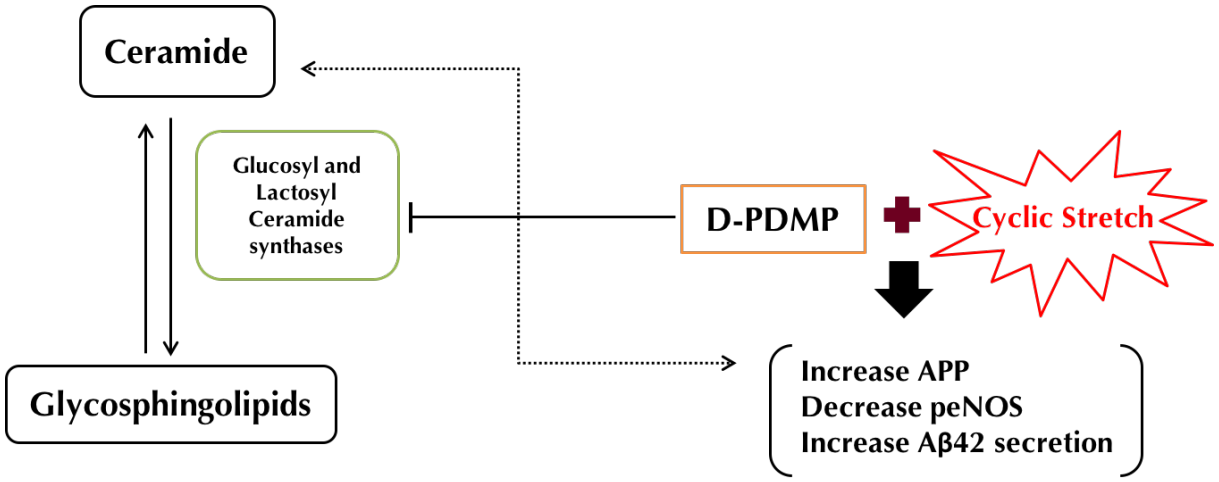

Figure 8.7 Summary of main conclusions of this study. D-PDMP pre-treatment increased APP expression, Aβ42 secretion with a concomitant decrease in phosphorylation of eNOS at S1177 in HCMECs exposed to 18 hours of 15% cyclic stretch (1 Hz). Results indicate a possible role of accumulation of ceramide in mediating these responses as glycosphingolipid inhibition using D-PDMP may shift the ceramide homeostasis towards ceramide. Abbreviations: Aβ42, amyloid beta 42; APP, amyloid precursor protein; D-PDMP, dl-threo-1-phenyl-2-decanoylamino-3-morpholino-1-propanol; peNOS, phosphorylated endothelial nitric oxide synthase

8.6 Appendix

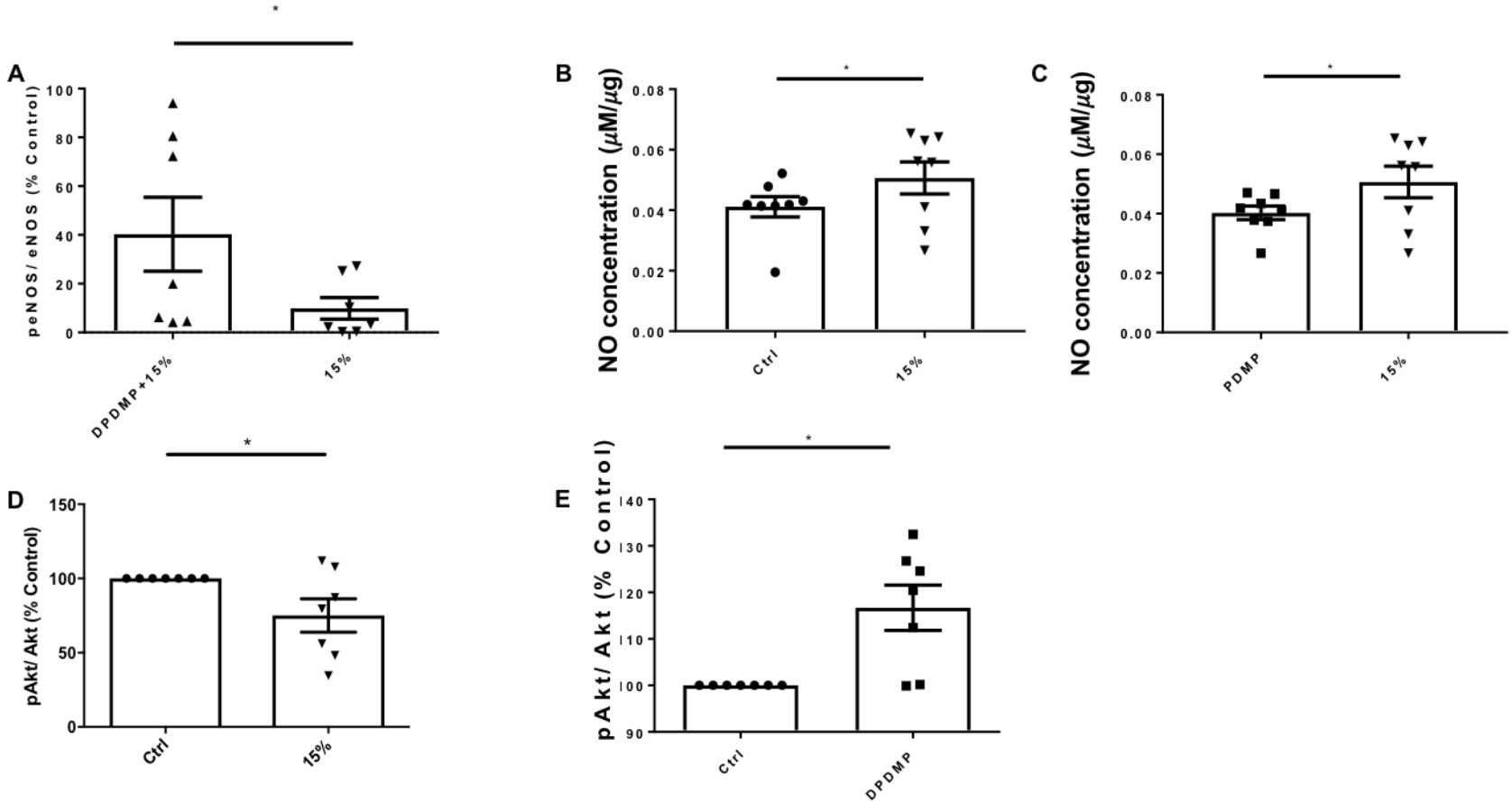

Figure 8.8 Paired or unpaired t-test results of eNOS phosphorylation (A), NO (B-C) and phosphorylation of Akt (D-E) in response to 15% stretch and/or D-PDMP treatment in HCMECs. *P<0.05, n=7-8. Abbreviations: D-PDMP, dl-threo-1-phenyl-2-decanoylamino-3-morpholino-1-propanol; GAPDH, glyceraldehyde 3-phosphate dehydrogenase; NO, nitric oxide; pAkt, phosphorylated Akt; peNOS, phosphorylated endothelial nitric oxide synthase

Chapter 9

A preliminary study of the effect of a high salt diet on APP processing, eNOS signalling and aortic stiffness

Summary—Hypertension is a risk factor for Alzheimer's disease (AD), which is characterised by amyloid precursor protein (APP) mediated Aβ pathologies. Consumption of a high salt diet is known to induce hypertension, and is associated with arterial stiffness, altered endothelial nitric oxide synthase (eNOS) signalling, and AD. The present study investigates whether a high salt diet affects APP processing and NO signalling, and markers of aortic stiffness in Sprague-Dawley (SD) rats treated with a high salt diet, and whether anti-hypertensive therapy could compensate for any negative effects that a high salt diet may induce. High salt (HS)-treated rats had increased levels of processed APP regardless of anti-hypertensive therapy, which was corroborated by qualitative immunofluorescence of brain sections showing positive Aβ staining. The phosphorylation of eNOS at S1177 or the expression of caveolin-1 did not change significantly. Arterial stiffness parameters, including pulse pressure amplification and pulse wave velocity increased in HS and HS rats treated with the anti-hypertensive drug, showing a blood pressure independent effect that a high salt diet induced. High salt diet-induced arterial stiffness may have implications in amyloid processing in the brain and cognitive effects, and alleviating arterial stiffness may have beneficial effects on AD progression.

9.1 Introduction

Hypertension is a risk factor for Alzheimer's disease (AD) whilst high pulsatility index and pulse pressure, indicative of increased large artery stiffness and reduced vessel compliance, are associated with AD [3,4,64,74]. A diet high in salt is reported to be associated with hypertension, arterial stiffness, altered cerebral blood flow and AD and/or cognitive deficits [24,286–288].

In 2 months old Sprague-Dawley rats treated with a high salt diet (9% NaCl), compared to control rats that were fed a low salt diet (0.26% NaCl) for 9 weeks, a marked increase in systolic blood pressure, decrease in cerebral blood flow and spatial memory deficits were demonstrated [24]. This is consistent with a role of high salt diet-induced hypertension in dementia [24]. In line with this, another study showed that in cultured human embryonic kidney (HEK) cell line, HEK293 that overexpressed APP or C99 fragment, an additional supplementation of 40 mM NaCl added into the normal culture media that was incubated for 24 hours, upregulated Aβ 40 and Aβ 42 secretion compared to cells that did not receive the additional salt supplementation [289]. This was coincident with a decrease in Aβ clearance [289]. However, double transgenic mice harbouring the APPswe, and PSEN1 mutations, and

control littermates fed with a high salt (4%) diet started at 2 months of age that continued for 3 months showed increased cerebral blood flow compared to low salt (0.08%) fed animals concomitant with reductions in Aβ plaques [290]. These studies showed a significant role of salt consumption in the pathogenesis of AD and vascular parameters such as cerebral blood flow, and Aβ. A recent study by Iadecola *et al.* [288] demonstrated that a high salt diet (4-8 % NaCl compared to a normal diet containing 0.5% NaCl for up to 24 weeks) resulted in reduced cerebral blood flow and cognitive impairment, independent of blood pressure, and, subsequent to endothelial dysfunction due to altered nitric oxide (NO) levels mediated by endothelial NO synthase (eNOS) [288].

NO signalling is known to modulate amyloid precursor protein (APP) that enables generation of Aβ plaques that characterises AD, and the enzyme eNOS is the key mediator of NO in the endothelium [18,262,275]. Inhibition of eNOS is demonstrated to elevate aortic stiffness in rats, and NO is well known to modulate vessel distensibility [264,265]. Activation of eNOS is also responsible for regulating blood pressure [170]. Inactive eNOS is bound to caveolae present in the plasma membrane, and eNOS activity is considered to be inhibited or regulated by the caveolae coating transmembrane protein, caveolin-1 [97–99]. In summary, NO is associated with arterial stiffness and hypertension, and, the enzyme that predominantly mediates endothelial NO, eNOS, is known to be involved in both these associations.

This study investigates whether a high salt diet affects APP processing and NO signalling and pulse pressure amplification and pulse wave velocity as markers of aortic stiffness in Sprague-Dawley (SD) rats treated with a high salt diet, and, whether anti-hypertensive therapy could compensate for any negative effects that a high salt diet may induce.

9.2 Methods

9.2.1 Animals

All experimental procedures were approved by the Macquarie University Animal Ethics Committee and were carried out in accordance with the guidelines of the National Health and Medical Research Council of Australia. A total of 24 male SD rats, which were obtained from the Animal Research Centre, Perth, Western Australia were housed at Macquarie University from 4 weeks of age. The rats were divided into three groups: control (n=8); high-salt diet (HS, n=8); high-salt diet with antihypertensive therapy (HST, n=8). All rats had *ad-libitum* access to chow and drinking water. The two groups assigned to an increased salt diet had chow with an 8% NaCl concentration (Specialty Feeds, SF03-10 rodent diet, 8% salt modification of AIN93G rodent diet) and the control group was fed an equivalent diet but with a normal salt content for a rodent diet of 0.26% NaCl (Specialty Feeds, AIN93G standard rodent diet). Animals assigned to the high salt diet with antihypertensive treatment group received subcutaneous injections every second day of the calcium channel blocker, amlodipine besylate (5 mg/kg/day), in peanut oil (amlodipine besylate concentration 15 mg/ml) starting from 5 weeks of age. All other animals were given subcutaneous injections of equivalent volume of the vehicle every second day. At 10 and 13 weeks of age, the water and food consumption were measured by housing the animals in metabolic cages for a 24 hour period. Weight and nose to rump length was measured every second day throughout the study.

Weekly measurements of systolic blood pressure were measured non-invasively using tail-cuff method. BP measurements are not reported for the animals at 4 to 5 weeks of age as readings were unreliable due to the size of the cuffs relative to the tail circumference, and as the rats had not become conditioned to the procedure at the time.

Animals were sacrificed (urethane anaesthesia, urethane 1.3 g/kg, 0.1 g/ml in 0.9\% saline, intraperitoneal injection) at 14 to 17 weeks of age, and the brains were harvested and halved for western blotting and histological analysis.

9.2.2 *In-vivo* measurement of cardiovascular parameters

Heart rate was monitored via electrocardiogram leads whilst a tracheal tube was inserted to ensure a free airway throughout the procedure. The animal was free breathing with the air supplemented with supplied oxygen.

For measurement of pressure within the thoracic aorta and the abdominal aorta of the rats, pressure catheters (Scisense catheter diameter 1.6 F) were introduced via the carotid and femoral arteries respectively. With all instrumentation in place (Figure 9.1), blood pressure was raised and lowered using intravenous infusion of phenylephrine and sodium nitroprusside (both 30 µg/ml at an infusion rate of 30 µg/kg/min) for measurement of aortic stiffness across a physiological range of mean arterial pressure (60-150 mmHg), as previously described [291]. Invasive *in-vivo* data was acquired at 10 kHz using a CED 1401 data acquisition system (Cambridge Electronic Design, UK). Aortic pulse pressure amplification and pulse wave velocity, for which the required vascular parameters were measured as illustrated in (Figure 9.1) and, which were calculated as shown in Equation 9.1 and 9.2, where pulse pressure denotes the ratio between pulse pressures measured in the thoracic aorta and the abdominal aorta whilst pulse wave velocity (metres/second) denotes the distance between the pressure probes and the transit time, where the transit time was measured from the diastolic feet of the pressure wave at the two sites, the foot defined as the peak of the second derivative of pressure.

Pulse pressure amplification = PP abdominal/ PP thoracic 9.1

Pulse wave velocity (m/s) = distance (m)/ transit time (s) 9.2

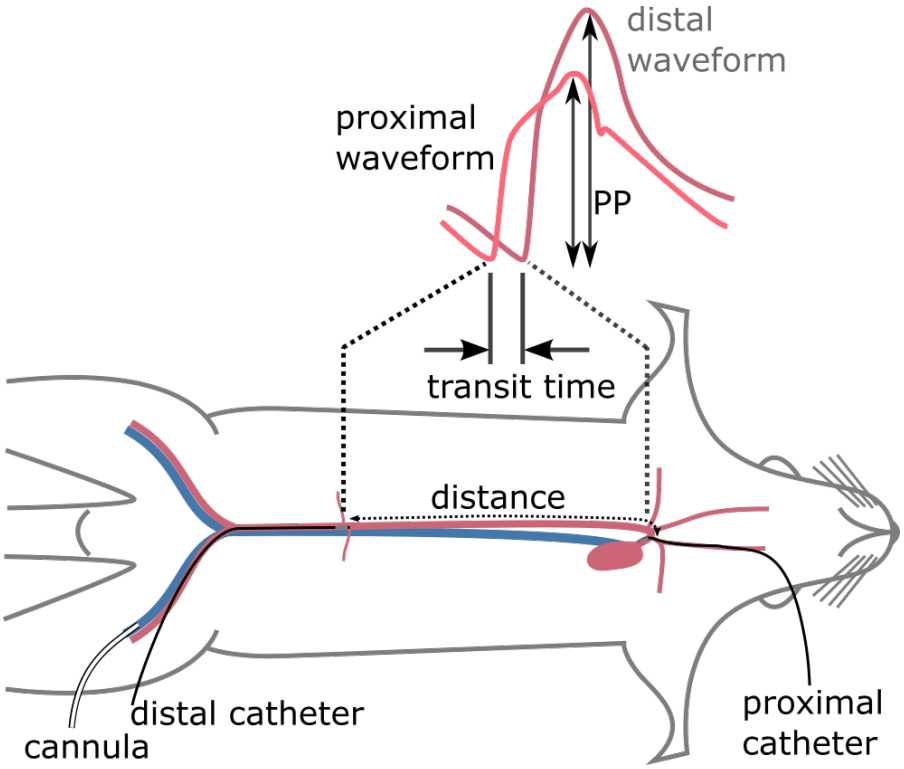

Figure 9.1 An illustration of how the *in vivo* vascular parameters were measured. For measurement of pressure within the thoracic aorta and the abdominal aorta of the rats, pressure catheters were introduced via the carotid and femoral arteries respectively. Aortic pulse pressure amplification was calculated as the ratio of the thoracic aortic pulse pressure to the abdominal aortic pulse pressure. Aortic pulse wave velocity was calculated as the distance between the pressure sensors divided by the transit time, where the transit time was measured from the diastolic feet of the pressure wave at the two sites, the foot defined as the peak of the second derivative of pressure.

9.2.3 Western blotting

One half of the brain was snap frozen in liquid nitrogen and stored fresh at -80 ^{0}C for western blotting. The frozen brain tissue was placed in radioimmunoprecipitation assay lysis buffer (50 mM Tris-hydrochloride, pH 7.4, 150 mM sodium chloride, 5 mM EDTA, 10 mM sodium fluoride, 10 mM sodium pyrophosphate, 1% IGEPAL CA-630, 0.5% sodium deoxycholate (SDS), 0.1% sodium dodecyl sulfate, phosphatase inhibitor; 1 tablet/ 10 ml (PhosSTOP,

Sigma) with protease inhibitor 10 µl/ml (P8340, Sigma) added immediately prior to lysis. Samples were lysed and the protein bands were transferred to nitrocellulose membranes (Life Technologies) after resolution on the SDS-polyacrylamide gel electrophoresis (PAGE) electrophoresis as previously described [292]. Equal amounts of tissue lysates (50 µg) were mixed with 4x NuPAGE sample buffer (Life Technologies) and were heated at 44 ^{0}C for 10 minutes before loading on 10% NuPAGE® Novex® Bis-Tris gels. The nitrocellulose membranes were blocked in 5% skim milk buffer in tris buffered saline-Tween (TBST; 20 mM tris-HCl, pH 7.4, 0.5 M NaCl, 0.1% Tween 20) to be probed with anti-APP (1: 1000; Covance), anti-eNOS (1: 250; Cell Signaling Technologies), anti-phospho-eNOS (peNOS) at serine 1177 (1: 1000; Cell Signaling Technologies), anti-GAPDH (1: 1000; ABCAM) or antibodies followed by incubating with secondary antibodies (1:2000; Cell Signaling Technologies or R & D) as previously described [227]. The western blot membranes were cut as required, to avoid higher molecular weight bands from interfering detection of weak bands. The blots were developed using Clarity™ Western ECL Substrate Kit (Bio-Rad) according to the manufacturers protocol. The protein bands were quantified using the Image Lab 5.1 software within the linear range of detection as % change in density or relative % control (Bio-Rad Labs. Inc).

9.2.4 Tissue processing and sectioning

The remaining half of the brain was placed in 10% paraformaldehyde in phosphate buffered saline solution (pH 6.9) to be fixed for up to 48 hours, which was cryoprotected in 30% sucrose solution [292]. The fixed brain tissue samples were embedded in OCT and sectioned (thickness: 10-15 µm) using a cryostat (Leica). Coronal sections were surgically excised from the brain, between the stereotaxic coordinates bregma: 4.68mm to 2.76 mm and interaural 13.68 mm to 11.76 mm, and between the stereotaxic coordinates bregma: -5.28 mm to -9.36 mm and interaural +3.72 mm to -0.36 mm (Figure 9.2; Paxinos and Watson [293]). The coronal

sections from these regions are respectively referred to as frontal cortex (FC) and hippocampal (HC) regions throughout the chapter.

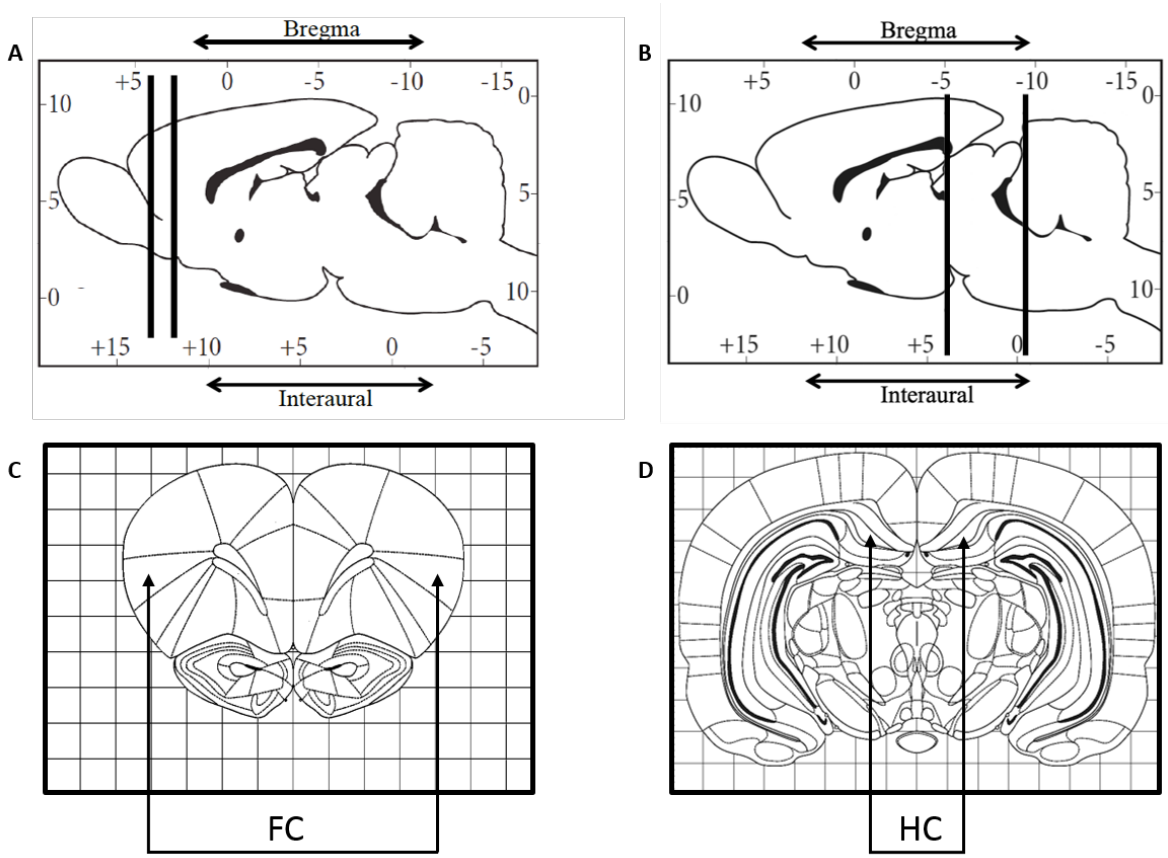

Figure 9.2 Diagrammatical representation of FC and HC regions of the rat brain in representative coronal sections. (A) The two vertical lines indicate approximate stereotaxic coordinates of the coronal sections of the two different regions of the rat brain; bregma: 4.68 mm to 2.76 mm and interaural 13.68 mm to 11.76 mm (A), and bregma: -5.28 mm to -9.36 mm and interaural +3.72 mm to -0.36 mm (B). (C) and (D) represent coronal sections taken within the two specified regions respectively, including the FC and HC regions as pointed by the arrows (Modified from Paxinos and Watson [293]). Abbreviations: FC, frontal cortex, HC, hippocampal

9.2.5 Hematoxylin and eosin (H and E) staining

Representative tissue sections were stained using H & E staining protocol as previously described [294]. Tissue sections were dehydrated in an oven at 37 ^{0}C for 15 minutes. Rehydration with 100% ethanol (twice/3 minutes each), 95% ethanol (twice/3 minutes each) and 70% ethanol (once/3minutes) was followed with a brief rising step (5 minutes) with

distilled water. The sections were stained with Harris Hematoxylin (Sigma, HHS-32) for 6 minutes, and rinsed under running tap water for 10 minutes, which was followed by 0.25% (v/v) hydrochloric acid in 95% ethanol acid-alcohol decolourisation for approximately 1 second. The slides were then immersed in 1.36% (w/v) lithium carbonate in distilled water (for approximately 3 seconds), followed by a 5-minute wash under running tap water, and counterstaining with Eosin (0.1% v/v) / Phloxin B (0.01% v/v) for approximately 15 seconds. The slides were dehydrated in ethanol in the reverse order from the initial rehydration step, excluding the 70% ethanol incubation, to be cleared in histolene I and II solutions (5 minutes in each). All steps excluding the washing steps in running tap water were performed in a fume hood. Finally, the slides were mounted with Cytoseal mounting medium and then were left overnight in a fume hood to be imaged with the Zeiss fluorescent microscope under bright field setting (Zeiss Imager.z1).

9.2.6 Immunofluorescence

Immunohistochemical procedures were performed as previously described with minor modifications [295,296]. Briefly, tissue sections were blocked with 10% (v/v) goat serum prepared in 1x tris-buffered-saline (TBS; pH 7.4; Sigma), 0.025% Trition X 100 (Amresco, USA) and 0.3 M glycine (Sigma) for 1 hour at room temperature, followed by anti-APP (1:1000 in 1 x TBS, with 1% goat serum and 0.025% Triton X 100; Covance) primary antibody incubation overnight at 4 ^{0}C. Goat anti-mouse Cy3-conjugated secondary antibody incubation was followed, for 2 hours at room temperature. The sections were mounted with DAKO (Dako, Denmark) mounting medium to be imaged using Zeiss fluorescent microscope (Zeiss Imager.z1) under channels for Cyanine 3 (Cy3) filter settings. Images were taken and processed through the Carl Zeiss ZEN software (Blue edition, version 2.3). All images were processed similarly to enhance image quality.

9.2.7 Statistical analysis

The water and food intake and body mass index (BMI) and systolic blood pressure measurements were analysed using ANOVA with post-hoc Bonferroni corrected multiple comparisons using R statistical package. Robust-ANCOVA with post-hoc Bonferroni corrected multiple comparisons were used to analyse the mean±SEM of pulse pressure amplification and pulse wave velocity parameters using R statistical package.

Each data point shown in densitometric analysis of the western blot band intensity represents an individual experiment and data are represented as mean±SEM analysed using ordinary one-way ANOVA with post-hoc Tukey-corrected multiple comparisons or unpaired t-tests (two-tailed), performed in GraphPad PRISM software version 7.02. Unpaired t-test (two-tailed) comparisons were made between groups and reported in the relevant results sections to emphasise statistically underpowered studies, of which the graphs are shown in an appendix. Outliers were identified using the robust regression and outlier removal (ROUT) method (detailed in Motulsky *et al.* [228]) in GraphPad PRISM with a Q value set at 10% that defines the threshold for outliers.

9.3 Results

9.3.1 Effect of a high salt diet on food and water intake of SD rats

Food and water intake were measured at 10 and 13 weeks of age. The food intake was lower in the HST group at 10 weeks of age compared to control the group ($P<0.05$), whilst the water intake was higher in both HS and HST groups compared to the control group ($P<0.001$) both at 10 and 13 weeks of age as shown by the box plots (Figure 9.3). The body mass index (BMI) of both HS and HST groups was relatively lower than the control groups ($P<0.001$; (Figure 9.3).

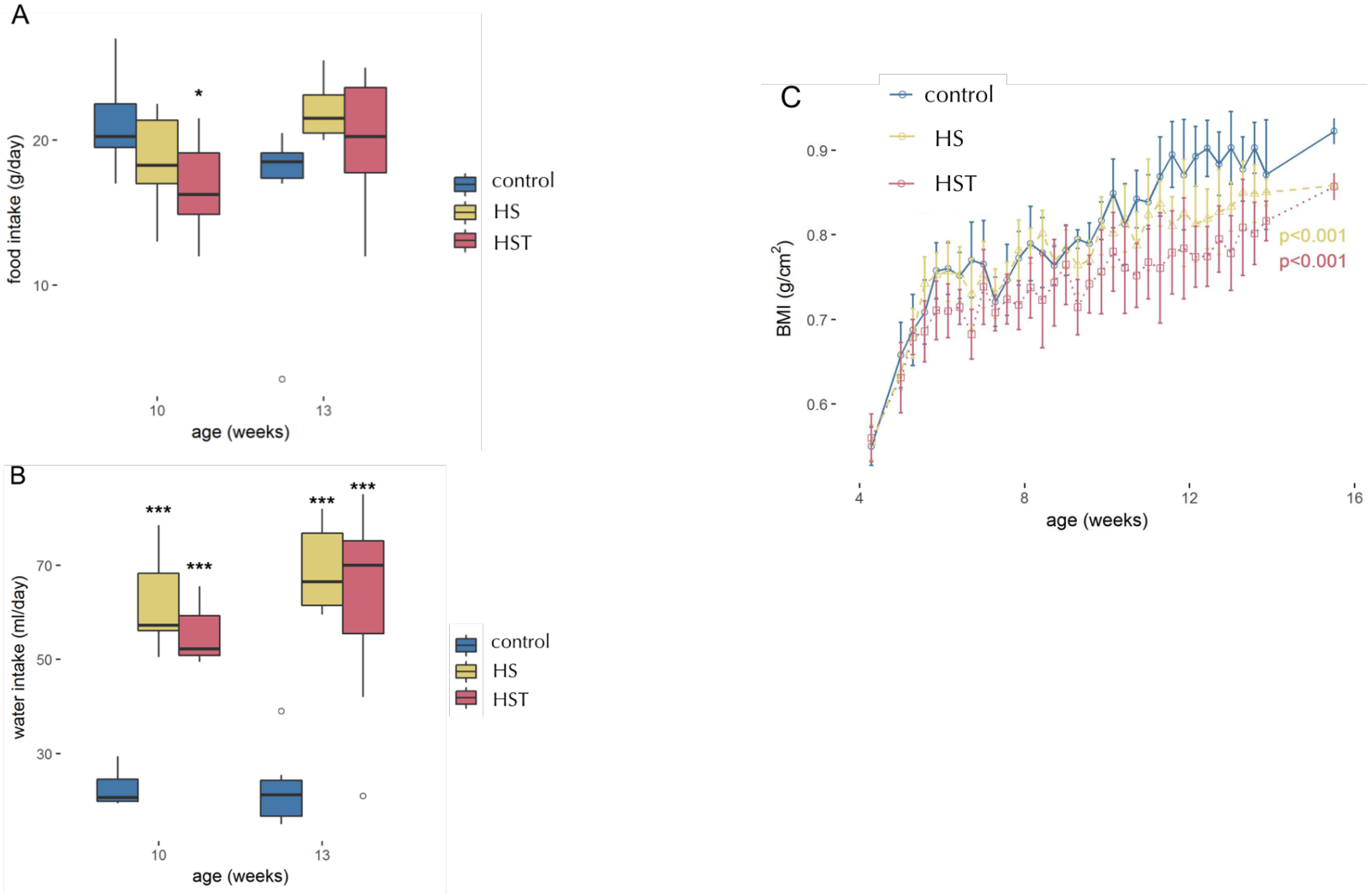

Figure 9.3 Water and food intake and BMI of SD rats in response to a high salt diet. Food intake (A), water intake (B) and BMI (C) of the SD rats assigned to control, HS and HST groups. ***P<0.001, *P<0.05 Vs control, analysed using Ordinary-One-way ANOVA with post-hoc Bonferroni-corrected multiple comparison tests. Abbreviations: BMI, body mass index, HS, high salt, HST, high salt treated with an anti-hypertensive, SD, Sprague-Dawley

9.3.2 Tissue integrity

Tissue integrity was checked using H & E staining of representative tissue sections from SD rats belonging to control, HS and HST groups, prior to immunostaining in order to ensure that the tissue quality was sufficient to proceed to immunofluorescent staining. Nuclear structures and other cytoplasmic structures were shown to be similar between the groups (Figure 9.4).

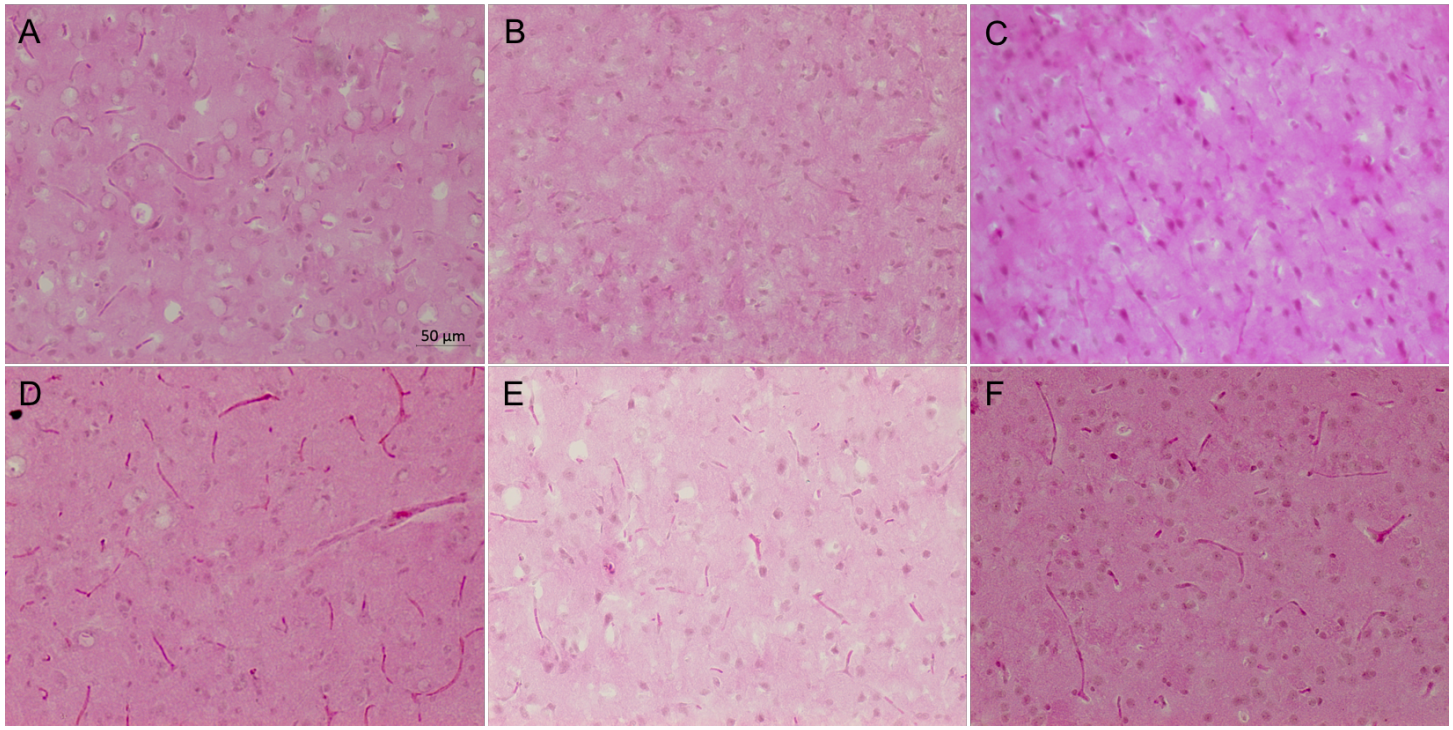

Figure 9.4 H & E staining to check for qualitative tissue integrity. Representative micrographs of H & E staining of rat brain tissue sections including HC (upper panel), and FC (lower panel), regions of control (A & D), HS (B & E) and HST (C & F) SD rats. Abbreviations: FC, frontal cortex, HC, hippocampal, HS, high salt, HST, high salt treated with an anti-hypertensive.

9.3.3 Effect of a high salt diet on APP processing and Aβ

A high salt diet has been shown to play a role in dementia [24,288], thus it was investigated whether APP and Aβ, which are involved in Alzheimer's dementia were affected by a high salt diet. Two bands indicative of processed-APP approximating to 30 and 60 KDa were detected in western blots of the brain tissue lysates. Both HS (167±28%) and HST (222±4%) groups had elevated amounts of processed APP as quantified with the 30 KDa band, compared to the untreated control animal brains (100±8%; Figure 9.5). A slight, but not significant increase in APP band at 60 KDa in the HS treated group compared to the control animal group was present when compared with an ANOVA test with post-hoc Tukey corrected multiple comparisons (Figure 9.5). However, the APP fragment intensity of the band appearing approximately at 60 kDa was significantly increased in the HST group (129±11%, $P<0.05$) compared to the control group (100±7%) when compared with a two-tailed unpaired t-test (appendix).

6E10 positive immunofluorescence of representative HC and FC regions of HS and HST groups showed higher immunofluorescence intensity relative to the control rats in both regions, indicative of elevated Aβ levels (Figure 9.5).

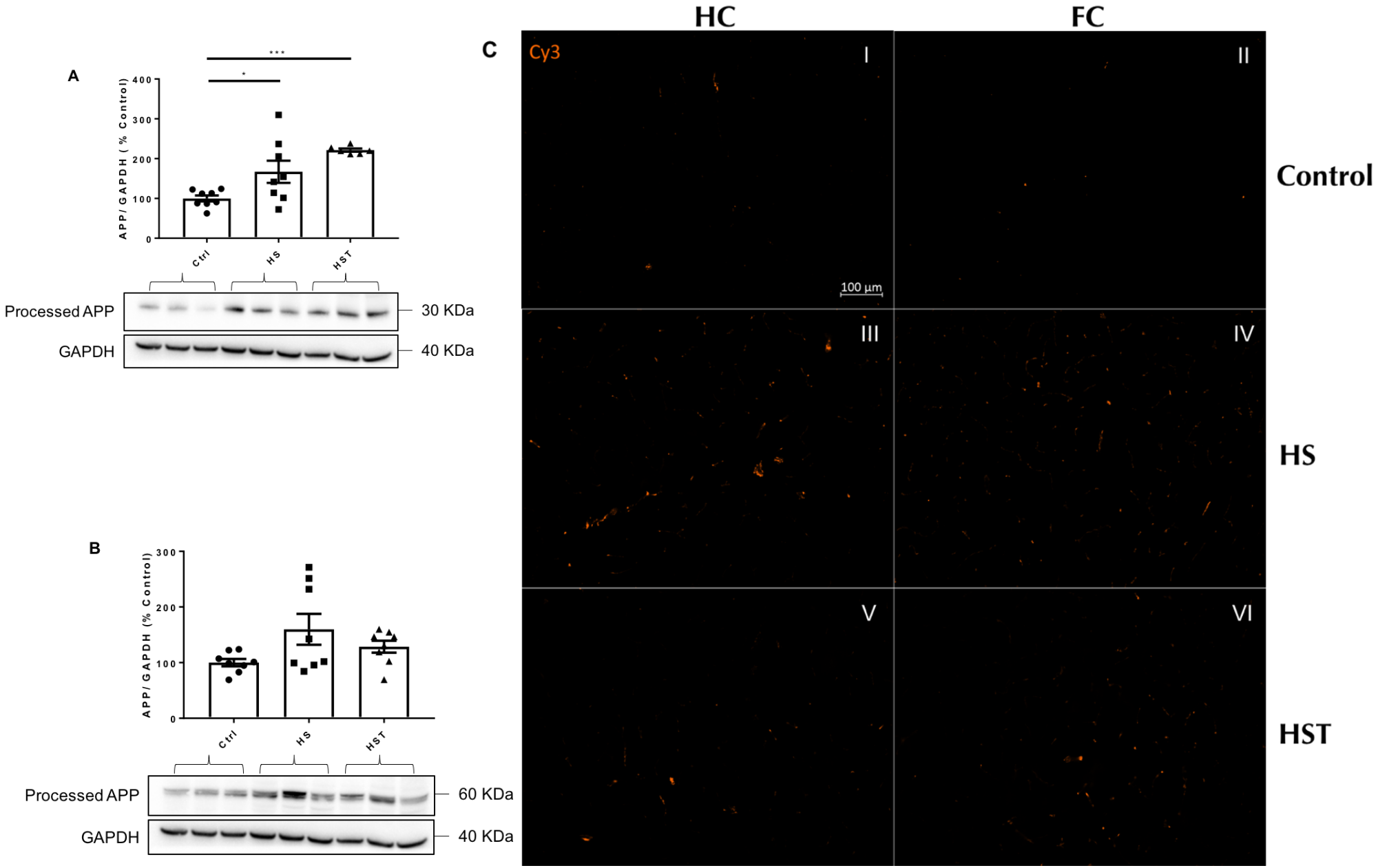
A
***
*
APP/ GAPDH (% Control)
400
300
200
100
0
Ctrl
HS
HST
Processed APP
30 KDa
GAPDH
40 KDa
B
APP/ GAPDH (% Control)
300
200
100
0
Ctrl
HS
HST
Processed APP
60 KDa
GAPDH
40 KDa
C
HC
FC
Cy3
I
II
100 µm
III
IV
V
VI
Control
HS
HST

Figure 9.5 Effect of a high salt diet on APP processing and Aβ. Two different bands and representative western blots (n=6-8) showing processed APP in the soluble fraction approximating to 30 KDa (A) and 60 KDa (B) in control HS and HST SD rat brain tissue, and representative micrographs (n=1) of 6E10 immunofluorescence of rat brain tissue (C). Left hand panel show tissue sections including HC, and right hand panel show tissue sections including FC, of control (I-II), HS (III-IV) and HST (V-VI) SD rats. The intensity of immunofluorescence indicates 6E10 positive staining for insoluble Aβ. ***P<0.001, *P<0.05, analysed using Ordinary-One-way ANOVA with post-hoc Tukey-corrected multiple comparison tests. Abbreviations: APP; amyloid precursor protein; FC, frontal cortex, GAPDH, glyceraldehyde 3-phosphate dehydrogenase; HC, hippocampal, HS, high salt, HST, high salt treated with an anti-hypertensive.

9.3.4 Effect of a high salt diet on eNOS and caveolin-1

The expression of eNOS and caveolin-1 or phosphorylation of eNOS at its activation site S1177 did not change significantly when compared with ordinary ANOVA tests with post hoc Tukey corrected multiple comparisons (Figure 9.6). However, a two-tailed unpaired t-test between control and HST groups showed a significant increase in peNOS in HST rats (145±16%, $P<0.05$) compared to control (100±10%) rats (appendix).

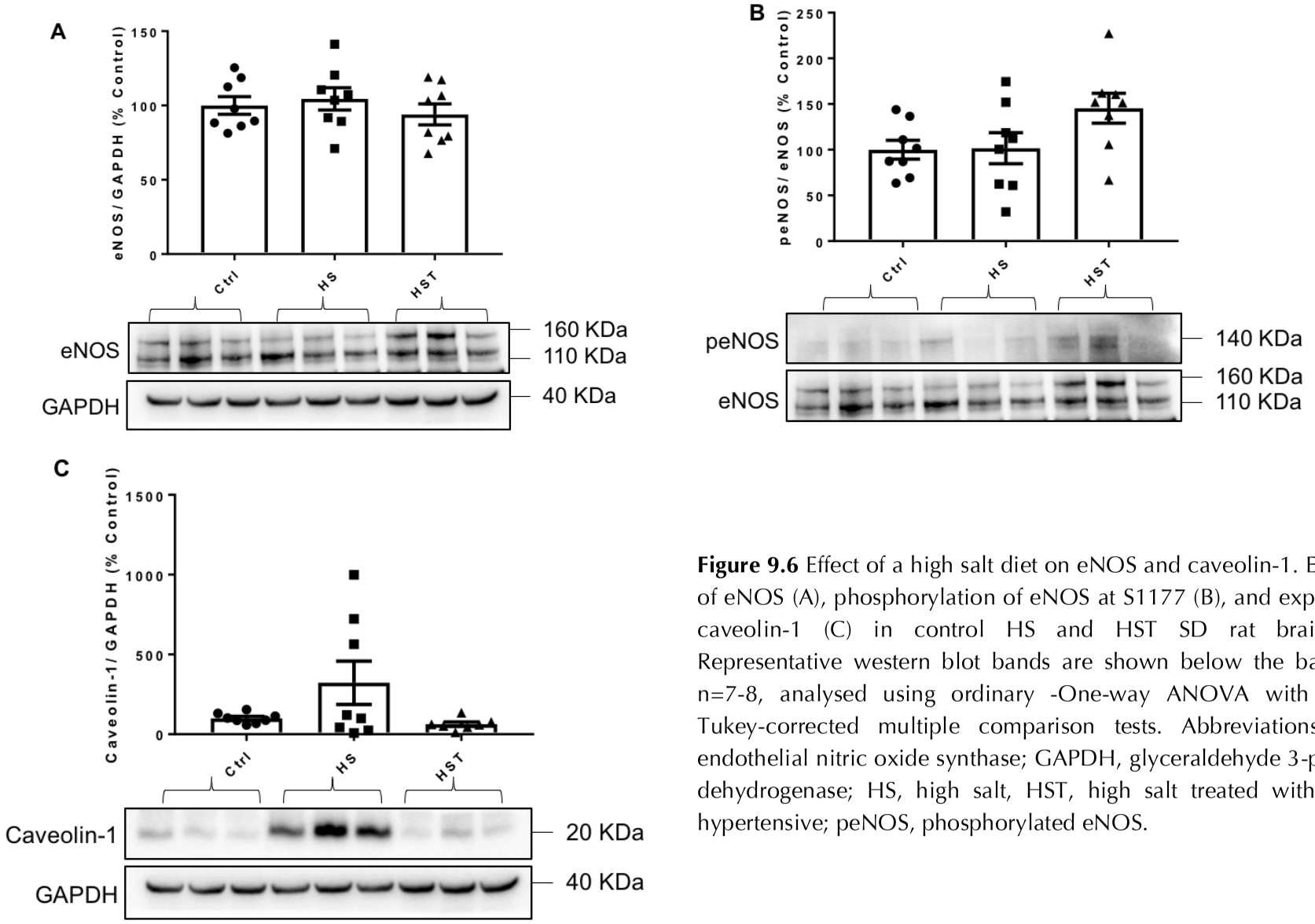

Figure 9.6 Effect of a high salt diet on eNOS and caveolin-1. Expression of eNOS (A), phosphorylation of eNOS at S1177 (B), and expression of caveolin-1 (C) in control HS and HST SD rat brain tissue. Representative western blot bands are shown below the bar graphs. n=7-8, analysed using ordinary -One-way ANOVA with post-hoc Tukey-corrected multiple comparison tests. Abbreviations: eNOS, endothelial nitric oxide synthase; GAPDH, glyceraldehyde 3-phosphate dehydrogenase; HS, high salt, HST, high salt treated with an anti-hypertensive; peNOS, phosphorylated eNOS.

9.3.5 Effect of a high salt diet on vascular stiffness parameters

The conscious systolic blood pressure was marginally increased in the HS group (125±12 mmHg) relative to control rats (117±13 mmHg), which was normalised by the anti-hypertensive treatment in the HST group (112±13 mmHg, $P<0.01$; Figure 9.7).

Aortic pulse pressure amplification and pulse wave velocity were measured as markers of aortic stiffness. Rats both in the HS group and HST group had increased aortic pulse pressure amplification and aortic pulse wave velocity compared to the control SD rats ($P<0.001$; Figure 9.7).

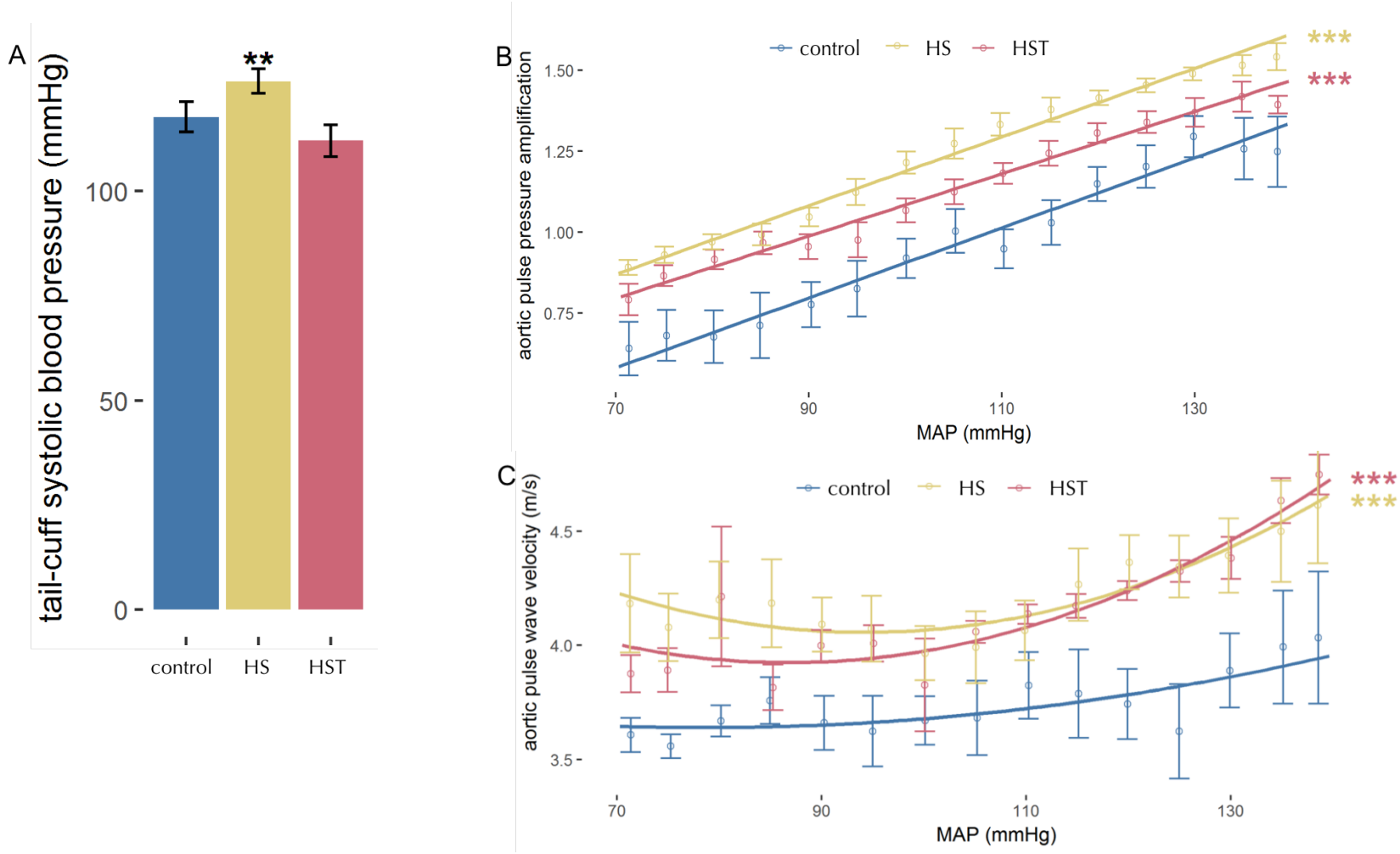

Figure 9.7 Effect of a high salt diet on parameters of vascular stiffness in SD rats. Averaged SBP (A), and aortic pulse pressure amplification (B) and aortic pulse wave velocity (C) of SD rats assigned to control, HS and HST groups. ***P<0.001, **P<0.01 Vs control, analysed using Robust-ANCOVA with post-hoc Bonferroni-corrected multiple comparison tests. Abbreviations: HS, high salt, HST, high salt treated with an anti-hypertensive, MAP, mean arterial pressure, SD, Sprague-Dawley

9.4 Discussion

A diet high in salt is demonstrated to play a role in eventuating cognitive effects, and altered cerebrovascular parameters such as cerebral blood flow and endothelial dysfunction, and inducing vascular stiffness [24,286–288]. The present study investigated whether consuming a high salt diet (8%) compared to a normal diet (0.26%) could lead to altered APP processing as seen in AD, and eNOS signalling, and expression of caveolin-1, a regulatory protein associated with eNOS, since endothelial dysfunction is known to be caused by a high salt diet in rats [288]. Additionally, aortic pulse pressure amplification and pulse wave velocity were measured as markers of arterial stiffness. The H & E staining, confirmed the integrity of the tissue sections prior to immunostaining whilst western blotting and immunofluorescence were performed to analyse protein expression and Aβ levels respectively (Figure 9.4 & Figure 9.5). Dietary intervention appeared to significantly affect the food intake in the HST group initially at 10 weeks of age, although was not present at the later time point (Figure 9.3). Additionally, the water intake was markedly increased with a significant decrease in BMI. Collectively, these results emphasise the impact of dietary interventions in metabolic changes.

One of the most significant findings of this study is that a high salt diet resulted in altered APP processing. This was shown by the increased levels of processed APP fragments in the high salt treated groups irrespective of the anti-hypertensive therapy since both HS and HST groups had higher band intensity compared to the normal control group (Figure 9.5). The band that appeared around 30 kDa was significantly higher in the HS and HST groups compared to rats on the control diet, although the band that appeared approximating to 60 kDa only showed a non-significant increasing trend (Figure 9.5). However, the APP fragment intensity of the band appearing approximately at 60 kDa was significantly increased in the HST group compared to the control group when compared with an unpaired t-test (Appendix). APP is proteolytically cleaved by several different secretases to produce different fragments of

processed APP [221,261]. Previous studies have shown APP bands appearing at different sizes including approximate band sizes of 30 and 60 kDa, indicative of processed APP fragments or soluble Aβ oligomers, using 6E10 monoclonal antibody in western blotting, as in the present study [40,297,298]. However, the present study did not include any exogenous treatment with Aβ or animal models that had elevated Aβ levels, thus it is unlikely that the bands are representative of Aβ oligomers, since the levels of endogenous Aβ are unlikely to appear in the soluble fraction. Therefore, the intense bands appearing in the high salt treated groups compared to the rats on a control diet provided qualitative evidence of differential APP processing induced by a high salt diet. The western blot results were further supported by the qualitative appearance of the immunofluorescence present in the stained brain tissue (Figure 9.5). Both HS and HST groups had higher immunofluorescence with 6E10 staining compared to the control rats corroborating the western blot data in both regions of the brain (Figure 9.5). As stated in Alzheimer's Facts and Figures 2017 report of the Alzheimer's Association, the most common initial clinical symptom of AD, an inability to retain new information, is due to neurons responsible for retaining new information are damaged at first such as in the hippocampus, with gradual progression towards the other regions of the brain such as the frontal cortex, which in turn proceed to other clinical symptoms such as agitation and sleeplessness, during AD progression [1]. Additionally, previous studies have shown that high salt intake could induce cognitive deficits [24,288]. The stereotaxic coordinates bregma: -5.28 mm to -9.36 mm and interaural +3.72 mm to -0.36 mm, and bregma: 4.68mm to 2.76 mm, and interaural 13.68 mm to 11.76 mm, denote regions of the brain towards the back of the brain including HC, and towards the front of the brain including the FC, respectively (Figure 9.2). The intensity of the immunofluorescence of the representative coronal section from towards the back of the brain (bregma: -5.28 mm to -9.36 mm and interaural +3.72 mm to -0.36 mm; Figure 9.2) was relatively higher than that of the coronal section representative of the front of the brain (bregma: 4.68mm to 2.76 mm, and interaural 13.68 mm to 11.76 mm; Figure 9.2).

Thus, this study provides preliminary evidence to indicate early AD pathology in the brain due to high salt intake showing amyloid pathologies.

High salt consumption is known to increase blood pressure, and hypertension is a risk factor for AD [3,24]. Altered APP processing in aged spontaneously hypertensive rats (SHR) had been demonstrated (Figure 9.8) [299]. Of note, the high salt treatment in the present study did not induce hypertension, but only a slight increase in systolic pressure (Figure 9.7) consistent with studies by Iadecola *et al.* [288]. Thus, the results indicate that the changes in altered levels of processed APP is an effect induced by high salt intake largely independent of high blood pressure.

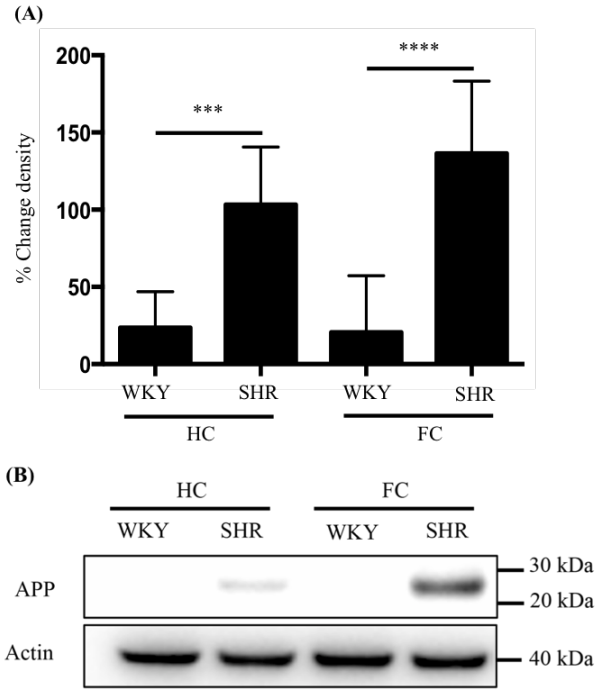

Figure 9.8 APP processing is altered between SHR and WKY rats. Data shown represents mean ± SD for SHR (n=3); ***P<0.001, P****<0.0001 compared to WKY (n=3) by two-way ANOVA with post-hoc Bonferroni-corrected multiple comparison tests. (B) Representative western blots demonstrating altered APP processing (upper panels) in hippocampal and frontal cortical regions of WKY and SHR. The lower portion of the membrane was probed with Actin (lower panels) for normalization. Protein standards for 40, 30 and 20 kDa are shown. Abbreviations: APP, Amyloid precursor protein; FC, frontal cortex; HC, hippocampus; SHR, spontaneously hypertensive rat; WKY, Wistar-Kyoto rat. (Data from Gangoda [299]).

One of the possible factors that could mediate altered APP processing independent of blood pressure is large artery stiffness, since large artery stiffness is implicated in AD, hypertension and high salt intake [25,85]. The implication of a high salt intake is well characterised in terms of vascular effects such as endothelial dysfunction and arterial stiffness [25,288,300,301]. Pulse pressure, a marker of arterial stiffness was demonstrated to be associated with AD and dementia in old adults as reported in a longitudinal community based study in persons aged 75 years and above [6]. These associations emphasised a possible role of arterial stiffening in AD. In Chapter 4 (based on the publication [19]), it was reported that cerebral endothelial pulsatility, that could originate from increased pulse pressures within blood vessels, leads to increased amyloidogenic processing of APP. Since elevated endothelial pulsatility is a resultant of increased pulse pressure, and elevated pulse pressure is a marker of arterial stiffening, this finding further elaborates a potential involvement of arterial stiffening in modulating APP processing. Moreover, the amplitude of retinal arterial pulsations, which could also be a consequence of large artery stiffness, was shown to positively correlate with neocortical Aβ scores in a preclinical AD cohort consisting of persons aged 79 ± 5 years [239]. Consistent with these findings, in the participants of the community-based Reykjavik study who had no history of stroke, transient ischaemic attack or dementia, pulsatility index, carotid-femoral pulse wave velocity and carotid pulse pressure, all of which are indices of arterial stiffness, were associated with lower memory scores and impaired executive function [8]. The HS and HST groups in the present study had higher pulse pressure amplification and pulse wave velocity parameters compared to the control rats indicative of increased arterial stiffening (Figure 9.7), supporting the presented hypothesis that vascular remodeling could mediate altered APP processing, though further studies are required to prove this hypothesis. This hypothesis can be further supported by the fact that arterial stiffening is also incremental with age, which is the key non-modifiable risk factor for AD [1,302].

High salt intake is also known to induce endothelial dysfunction mediated by compromised NO signalling via eNOS concomitant with cognitive deficits [288]. This recent study demonstrated that a high salt diet induced an increase in interlukin-17 (IL-17) mediated by a T helper cell-17 response in the gut that in turn has led to increased inhibitory phosphorylation of eNOS at Thr495 via Rho kinase [288]. The inhibitory eNOS phosphorylation coincided with decreased NO, endothelial dysfunction, reduced cerebral blood flow and cognitive deficits in high salt fed rats [288]. This study also reported that there were no significant changes in eNOS phosphorylation at S1177 [288]. Consistent with this, the present study also showed no changes in eNOS expression or phosphorylation at S1177 in the HS group compared to the control rats (Figure 9.6). Since this study reported a reduction of eNOS mediated NO due to an increase in inhibitory phosphorylation of eNOS at Thr495, it cannot be ruled out in the present study as well. However, there was a significant increase in peNOS in the HST rats relative to the control rats when analysed using an unpaired t-test (appendix) indicative of active eNOS, showing that anti-hypertensive therapy could enhance eNOS phosphorylation at S1177. The results being significant only when compared with a t-test showed that the study is underpowered to show the effect, thus needs to be repeated to confirm this result.

Collectively, previous studies showing that arterial stiffness is related to AD and possibility of involvement of arterial stiffness in APP processing and mediating cognitive effects, and the recent study demonstrating gut-brain axis linking the effect of a high salt diet that induced an inflammatory response in the gut, which in turn resulted in neurovascular and cognitive effects [288], show the multi-factorial nature of AD pathology.

9.5 Conclusions

A high salt diet in SD rats induced altered APP processing independent of anti-hypertensive therapy and this effect was independent of high blood pressure relative to control diet fed SD rats. The immunofluorescence results of 6E10 staining for Aβ corroborated the western blot results showing possible amyloidogenic processing of APP. Both pulse pressure amplification and pulse wave velocity increased in the HS and HST groups, thus showing that a high salt diet induces large artery stiffness independent of blood pressure. Further studies are required to confirm the immunofluorescence data and eNOS phosphorylation. A high salt induced alterations in arterial stiffness and/or NO signalling could be implicated in APP processing in mediating cognitive effects.

9.6 Appendix

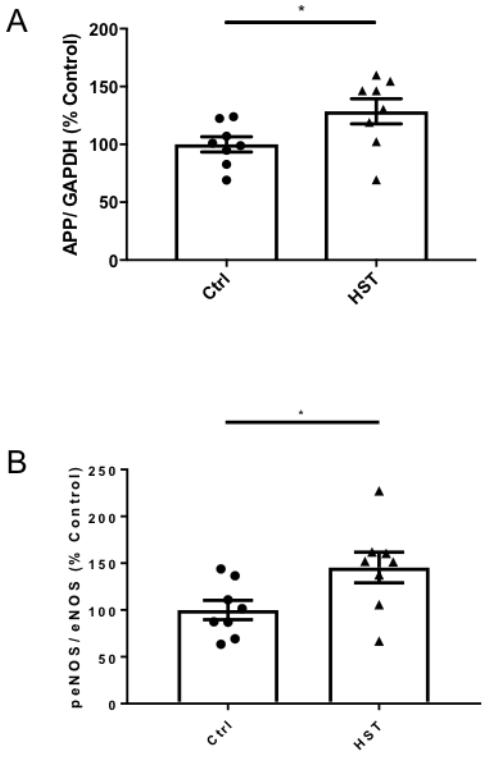

Figure 9.9 Unpaired t-test results showing differences between control and HST rat groups. APP processing between control and HST rats as analysed by the 60 KDa band (A), phosphorylation of eNOS at S1177 of control and HST rats (B). Abbreviations: HS, high salt, HST, high salt treated with an anti-hypertensive.

Chapter 10

Conclusions, limitations and future directions

10.1 Conclusions

Alzheimer's disease (AD), the most common cause of dementia is conventionally described as a neurodegenerative disease. However, it is now starting to become accepted as a multifactorial disease that encompasses many factors including vascular pathologies [1]. Amongst the vascular risk factors for AD, hypertension, elevated pulse pressure and arterial stiffness are receiving major attention since all these factors are cumulative with age, which is the foremost non-modifiable risk factor for AD [2–8]. One of the consequences of hypertension, elevated pulse pressure and arterial stiffness on the vasculature is elevated vascular pulsatility, which is not well studied in the context of AD, thus explored in this thesis. In particular, this thesis investigated the effect of cyclic stretch applied to brain vascular endothelial cells on amyloid precursor protein (APP) and associated proteins including endothelial nitric oxide synthase (eNOS), intercellular cell adhesion molecule (ICAM-1) and signalling molecules such as the serine/threonine-specific protein kinase, Akt and glycogen synthase kinase-3 (GSK-3) (Chapter 4-8).

Chapter 4 is based on the recently published seminal paper, which demonstrated for the first time that cyclic stretch of cerebral endothelial cells modulates APP expression and processing, and the expression and/or phosphorylation of eNOS and ICAM-1 [19]. This study further demonstrated that increasing stretch magnitude proportionally increased APP expression, the expression of APP processing enzyme, β-secretase 1 (BACE-1), Aβ42 secretion, eNOS expression, ICAM-1, concomitant with a decrease in phosphorylation of eNOS at S1177, a site of eNOS activation. Additionally, expression of pro-ADAM10 was increased significantly at the 10% stretch magnitude compared to the 0%, 5% and 15% stretch magnitudes (Chapter 5). Taken together results implicated the contribution of cerebral endothelial pulsatility in regulating APP processing towards amyloidogenic pathway, and inflammatory cell signalling since the inflammatory marker, ICAM-1, increased, with a decrease in peNOS at S1177, indicative of a dysfunctional endothelium.

Akt signalling is known to regulate phosphorylation of eNOS at S1177 [162,165]. Continuous stretching of human umbilical vein endothelial cells, and cyclic stretching (1 Hz) of bovine aortic endothelial cells at respective stretch magnitudes of 50% and 120% for 15-20 minutes led to an increase in eNOS phosphorylation at S1177 dependent upon Akt phosphorylation at S473 [162,165]. The work presented in this thesis demonstrated for the first time that, a prolonged stretch stimulus of 18 hours of cyclic stretching (1 Hz) at a stretch magnitude of 15% downregulates Akt phosphorylation at S473 and eNOS phosphorylation at S1177 (Chapter 4-8). Although these results pointed towards a possible downregulation of NO production, NO production did not correlate with these changes (Chapter 5-8). The results indicate that prolonged stretch stimulated NO through a different mechanism other than Akt/eNOS signalling pathway.

Age is the leading non-modifiable risk factor for AD [1]. Whilst age related cerebrovascular disease is considered to contribute for AD, endothelial cell senescence is associated with age-

related vascular diseases [22,23]. A recent study demonstrated that cell senescence altered APP expression, BACE-1 expression and Aβ40 secretion in primary human brain microvascular endothelial cells [21]. Endothelial senescence was also shown to decrease eNOS expression and induce inflammatory markers [303]. Thus, the effect of cyclic stretch (15% at 1 Hz for 18 hours), was investigated with an emphasis on endothelial cell senescence (Chapter 6). Stretched cells were compared between low (passage 7-9) and high (passage 17-19) passage numbers (Chapter 6). Expression of APP, BACE-1, eNOS and ICAM-1, and phosphorylation of GSK-3α and GSK-3β, and levels of Aβ42 and NO were significantly different between the two passage ranges (Chapter 6). In cells at higher passages, APP expression, BACE-1 and ICAM-1 expression, and Aβ42 secretion increased with decreases in eNOS, GSK-3α and GSK-3β phosphorylation and NO levels compared to cells at lower passages (Chapter 6). Collectively, results suggested amyloidogenic processing of APP and concurrent activation of inflammatory signalling in senescent cells (passage 17-19) compared to young cells (passage 7-9; Chapter 6). Parallel downregulation of GSK-3α and GSK-3β phosphorylation in the senescent cells indicated GSK-3 activation [114]. Since GSK-3 activation is known to be regulated by APP and Aβ, cyclic stretch of cells at senescence increase APP expression and BACE-1 expression, thereby increasing Aβ42, which may in turn activate GSK-3.

Sphingolipids such as ceramide are implicated in AD [14]. The recent Baltimore Longitudinal Study of Aging demonstrated that plasma ceramide and sphingomyelin levels were associated with risk of AD [15]. Chapter 7 demonstrated that hindering glycosphingolipid formation by using a synthetic ceramide analogue dl-threo-1-phenyl-2-decanoylamino-3-morpholino-1-propanol (D-PDMP) in the presence of cyclic stretch (15% at 1 Hz for 18 hours) increased APP expression and Aβ42 secretion in cerebral endothelial cells compared to the cells that had been stretched in the absence of D-PDMP. Concomitant with these results, the significant downregulation of eNOS phosphorylation at S1177 in response to 15% stretch was preserved

when cells were stretched in the presence of D-PDMP. Since D-PDMP acts by inhibiting glucosyl and lactosyl ceramide synthases, the results indicate a regulatory role of these enzymes in APP expression, Aβ42 secretion and eNOS phosphorylation. Additionally, as D-PDMP is synthetic ceramide analogue, the increase in Aβ42 secretion could be a consequence of stretch-mediated ceramide formation, thereby increasing the endogenous levels of overall ceramide reservoir, subsequently elevating Aβ42. This is because ceramide is known to modulate APP processing and lead to Aβ formation [138–141].

Hypertension, elevated pulse pressure and arterial stiffness are vascular risk factors for AD [2–8]. A diet rich in salt has been shown to induce hypertension, and to lead to cognitive deficits [24]. Chapter 9 included a preliminary study demonstrating that a high salt diet leads to altered APP processing and/or amyloid burden rat brain tissue concomitant with increased aortic stiffness. Altered APP processing in the brains of high salt fed rats was demonstrated both in soluble and insoluble fractions of Aβ, as shown through western blots and immunofluorescent staining. Aortic stiffness markers, pulse pressure amplification and pulse wave velocity were higher in the high salt fed groups compared to control rats. Furthermore, the increases in these aortic stiffness markers remained elevated regardless of anti-hypertensive therapy that normalised the slight increase in systolic blood pressure in the high salt fed rat groups. Taken together, these results implicate a possible role of large artery stiffness independent of blood pressure that in turn leads to changes in APP processing and eNOS signalling.

To summarise, the major findings of this thesis are listed below (Figure 10.1);

I. A well-detailed approach for cyclic stretching of human cerebral microvascular ECs (HCMECs) has been established since the work presented in this thesis is the first of its kind.

II. Cyclic stretch modulates APP expression and processing and inflammatory signalling in HCMECs.

III. Cyclic stretch modulates Akt and GSK-3 phosphorylation, which could underlie the stretch mediated-inflammatory signalling.

IV. There are passage dependent changes in the expression of APP, BACE-1, eNOS and ICAM-1, and phosphorylation of GSK-3α and GSK-3β, and levels of Aβ42 and NO in HCMECs subjected to 15% cyclic stretching at 1 Hz, thus showing a possible role of endothelial senescence in APP processing and inflammatory signalling.

V. Deregulation of glycosphingolipids by inhibiting glucosyl and lactosyl ceramide synthases combined with cyclic stretching favour APP expression and Aβ42 secretion

VI. A high salt diet induces large artery stiffness and altered APP processing in rat brain.

Overall, the findings presented in this thesis provided evidence in support of the associations of vascular pulsatility, hypertension, elevated pulse pressure and arterial stiffness, and AD. Since the concept presented in this thesis is quite novel, the findings open up further avenues for future research that will contribute towards elucidating molecular mechanisms into the involvement of vascular pulsatility in AD, which may ultimately assist in identifying potential therapeutic targets for this multifactorial disease.

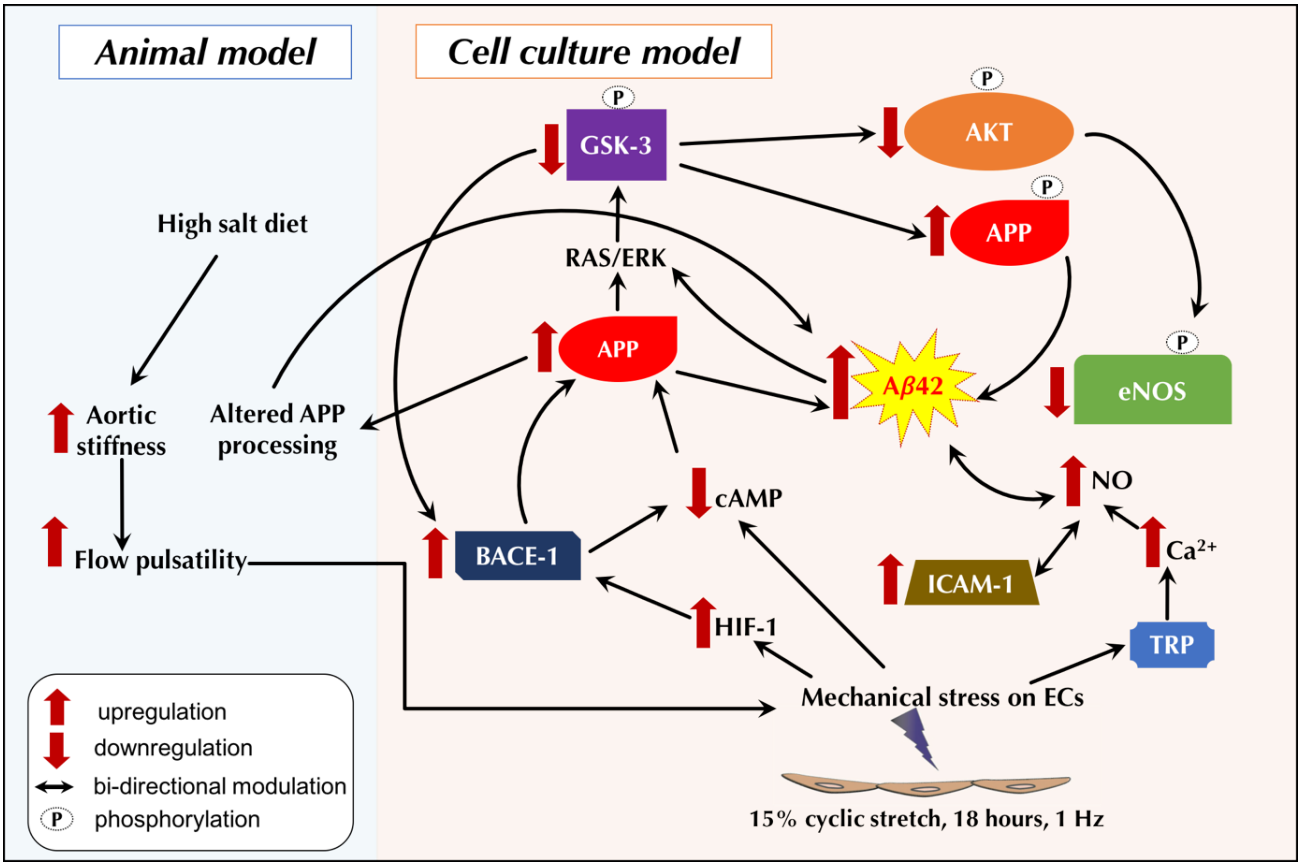

Figure 10.1 Representation of possible signalling pathways underlying overall thesis findings. Mechanical stretch is known to modulate TRP channels, HIF-1 and cAMP levels [173,212,304]. These changes in turn can regulate calcium levels, BACE-1, and APP, leading onto different signalling cascades as shown by the forward and bi-directional arrows. GSK-3 is central in mediating stretch-mediated responses in the thesis as GSK-3 activation is known to increase BACE-1 and pAPP at Thr668, decrease pAkt and peNOS leading to amyloidogenic processing, thus Aβ42 [251–253,273,305]. Additionally, increased BACE-1 expression leads to increased amyloidogenic processing of APP leading to Aβ42 generation [306,307]. This also justifies the differences between the early and late passage ECs in terms of APP processing, since GSK-3 activation in late passage ECs coincided with amyloidogenic processing of APP, thereby upregulating Aβ42, whilst in early passage cells opposite effects occurred in response to stretch. Increases in Aβ42 can be further exacerbated by elevated APP expression that in turn could intitiate RAS/ERK signalling that mediates GSK-3 activation and by BACE-1-mediated downregulation of cAMP, provide a positive feedback loop for accumulation of Aβ42 [114,308]. The results presented show that stretch downregulated pAkt and peNOS, without affecting NO levels, thus indicating a different mechanism of NO production, such as TRP-mediated calcium release, which could regulate ICAM-1 and Aβ42 [173,262,309]. The high salt animal model presented with elevated aortic stiffness, altered APP processing and increased Aβ levels compared to the control animals. It can be proposed that altered APP processing and aberrant APP signalling that leads to Aβ generation can be at least in part mediated by elevated vascular pulsatility as a result of aortic stiffness [8]. Abbreviations: Aβ, amyloid-beta; APP, amyloid precursor protein; BACE-1, β secretase-1; cAMP, cyclic adenosine monophosphate; EC, endothelial cell; eNOS, endothelial nitric oxide synthase; ERK, extracellular signal-regulated kinase; GSK, glycogen synthase kinase; HIF-1, hypoxia inducible factor-1; ICAM-1, intercellular cell adhesion molecule-1; TRP, transient receptor potential vanilloid

10.2 Limitations

As with any type of research would, the work presented in this thesis has some limitations that need to be addressed. This thesis project evaluated the pulsatile stretch component present within blood vessels by mimicking the pulsatility in an *in vitro* system that enabled artificial control of frequency and magnitude of stretch, simulating heart rate and pulse pressure. This allowed for a well-controlled platform to isolate the stretch component alone that is ideal for identifying stretch induced changes. However, the physiological milieu of the endothelium is much more complex than this simple system. The endothelium *per se* is exposed to other haemodynamic parameters such as shear stress and blood pressure, whilst the cerebral endothelium in particular, is an integral part of the blood brain barrier (BBB), which interacts with other cell types such as astrocytes, neurons and glia. Thus, it is a limitation that the dynamic nature of the physiological state of the cerebral endothelium is not completely incorporated in the study design.

Furthermore, the findings presented in this thesis are derived from an immortalised cerebral EC line of human origin. Whilst it is beneficial to use a cell line for cell culture processes due the versatility of cell lines compared to primary cells, and that the cell line used is of human origin that better characterises human ECs, primary cells may better represent the *in vivo* BBB endothelial characteristics.

Since the findings of this thesis demonstrate a novel role of endothelial pulsatility in support of the important associations between hypertension, elevated pulse pressure and arterial stiffness and AD, it has opened up a whole new array of future research, including the need for addressing these limitations in order to achieve closer simulation of the physiological scenario.

10.3 Future directions

10.3.1 Improvements to the stretch system

The findings of this thesis provided information on the effect of cyclic stretch on proteins associated with AD in a well-controlled system (Chapter 4-8). However, as stated in section 10.2, other haemodynamic stimuli such as shear stress are present *in vivo*. Thus, incorporation of shear stress component along with the pulsatile stretch component may give insights into how/if these two mechanical forces act in concert or independent of each other, in regulating the proteins that are studied in this thesis. This is because previous studies have shown independent and combinatory effects of shear stress and cyclic stretch [165,172,182,310].

The *in vitro* system utilised in this thesis included an immortalised cell line. Although this system was ideal in establishing whether there is a role of endothelial pulsatility, which was the main focus of this thesis, this system can be further improved by utilising primary cells in a co-culture system with astrocytic, neuronal or glial cells in future studies. These modifications will allow one to further investigate stretch mediated changes in ECs that may retain a phenotype closer to the BBB.

10.3.2 Elucidating molecular mechanisms

The findings presented in this thesis have demonstrated that stretch of HCMECs could modulate Akt and GSK-3 phosphorylation with concomitant changes in APP expression and processing. Genetic manipulation to knock down Akt or GSK-3 and then subjecting the cells to cyclic stretch could confirm whether the increase in APP or Aβ42 secretion in response to stretch were mediated by Akt or GSK-3 pathways. Knockdown of APP and subjecting the cells to cyclic stretch could confirm whether the downregulation of Akt and GSK-3 phosphorylation were dependent upon secreted Aβ42 in response to cyclic stretch. Additionally, since there is evidence that soluble APPα (sAPPα) can directly associate with

BACE-1 and GSK-3 to alter Aβ levels [260,261], future studies can verify whether the stretch mediated responses were mediated by a reduction in sAPPα.

Cyclic stretch is known to modulate micro-RNAs (miRNAs) expression that could in turn regulate GSK-3, whilst miRNAs such as miR-124-3p was shown to play a neuroprotective role to downregulate GSK-3 activity via a caveolin-1/Akt dependent mechanism [17,185]. Therefore, stretch mediated changes in miRNAs profile using an miRNA microarray approach in future studies will provide useful information in deciphering relevant miRNAs that are possibly involved.

Involvement of integrin signalling, including integrin β 1 (Itgβ1) and integrin β 3 (Itgβ3), in response to cyclic stretch was reported [176,178,212,311]. Soluble APPα (sAPPα) was shown to interact with Itgβ1 whilst Itgβ3 is shown to interact with low density lipoprotein receptor protein 1, which is known to facilitate Aβ clearance [248,312]. In a recent proteomic study that compared 0%, 5% and 20% stretch magnitudes in HCMECs stretched in the ShellPa (same approach as in the stretching experiments reported in this thesis), Itgβ3 in cells stretched at 20% was increased compared to 0% static control cells [212]. This proteomic study also revealed that cyclic adenosine monophosphate (cAMP)-dependent-protein-kinase-catalytic-subunit-β that regulates cAMP-dependent protein kinase activity, which is known to regulate non-amyloidogenic processing of APP, was significantly down-regulated at 20% stretch compared to 5% [212,249]. These studies together suggest the involvement of Itg signalling mediated by cyclic stretch, thus emphasing the need for investigating Itg and analysing sAPPα levels in response to stretch in future studies. This could be achieved by blocking the relevant Itg and investigating the effects on expression of proteins studied in this thesis, or measuring sAPPα as well in response to stretch.

The results presented in Chapter 6 demonstrated that the effect of stretch is altered between early and late passage cells, indicative of a possible role of cell senescence (Chapter 6). This study could be extended to characterise cell senescence markers in detail and confirm this association, and to investigate whether aberrant cell signalling is involved in mediating the stretch mediated responses between early and late passage cells that are reported in this thesis. Cell senescence could also alter miRNAs, thus an miRNA microassay could be useful in future studies to identify potential miRNAs involved [303].

Phosphorylation of eNOS at S1177 was downregulated with a concomitant decrease in pAkt, although the NO production did not correlate with this (Chapter 4-8). The results indicated that NO production is regulated via a different mechanism other than Akt signalling such as protein kinase A [162]. Previous studies have also established that eNOS can be regulated by stretch at different phosphorylation sites to regulate NO production such as eNOS-Serine 633 [162,165]. Stretch induced Ca^{2+} influx via transient receptor potential vanilloid 4 (TRPV4), TRP-classical 1 (TRPC1) and TRP-polycistin 2 (TRPP2), in urothelial cells and mouse brain microvessel endothelial cells (bEnd3) was also reported [173,313]. Furthermore, in bEnd3 cells, eNOS mediated-NO production was evident in response to stretch [173]. Thus, different phosphorylation sites of eNOS and/or stretch-induced Ca^{2+} influx could be potential mechanisms that are responsible for NO production in response to the stretch stimulus in the investigations presented in this thesis. Alterations in eNOS and NO could be further studied in future studies by analysing other phosphorylation sites of eNOS by western blotting, and blocking these TRP channels to confirm whether this response is mediated by TRP. Combinatory effects of cyclic stretch and NO inhibition is relevant in confirming whether the changes in APP processing between early and late passage HCMECs since NO concentration was implicated in bi-directional APP processing [262]. A pilot study performed with

pharmacological inhibition and cyclic stretching is detailed in an appendix at the end of the thesis.

Cyclic stretching of HCMECs in the presence of the d-threo-1-pheny-2-decanoylamino-3-morpholino-1-propanol (D-PDMP) treatment was demonstrated to increase APP expression and Aβ42 secretion (Chapter 8). This could be attributed to an increase in endogenous ceramide levels, thus this study could be extended to confirm in future studies by characterising the sphingolipid profiles of stretched cells in the presence or absence of D-PDMP using liquid chromatography–mass spectrometry based techniques.

10.3.3 Repetition

Some findings were shown to be close to statistical significance when analysed using an ANOVA with post-hoc multiple comparison tests, which were shown to be significant when the relevant groups were analysed using a t-test. These results were included in the appendices in corresponding chapters. These results showed that the studies were under-powered to show the effects shown in the t-tests through the ANOVA with post-hoc multiple comparison tests. Therefore, including more repeats will confirm these results.

The study including high salt treatment on APP processing (Chapter 9) requires to be extended to include more replicates for immunofluorescence staining (currently n=1) to confirm the qualitative data presented in Chapter 9, and to obtain some quantitative data. Since there were no preliminary studies in the existing literature, it was not possible to perform power calculations prior to commencing the study. However, power calculations performed using the data acquired from this pilot study indicate that n=9 is required to obtain a statistically significant result for Aβ fragment at 60 kDa, with an α level of 5% and a β level of 80%.

10.3.4 In vivo model

Since it is not plausible to incorporate all the *in vivo* parameters into an *in vitro* model, an animal model will ideally address this issue. The preliminary evidence from the high salt study (presented in this thesis, Chapter 9) and the SHR study (presented in MRes thesis)[299] are in line with the *in vitro* findings showing a possible role of arterial stiffness in AD. In support of this, a multitude of previous studies show an association of vascular stiffness parameters and AD [6,8,19,25,85,239]. Collectively, these findings point towards a role of arterial stiffness in APP processing, and thus, investigating APP processing in an *in vivo* model of arterial stiffness with complete characterisation of vascular parameters such as pulse pressure, pulse wave velocity and vessel characteristics such as collagen/elastin content along with amyloid pathologies will confirm this hypothesis.

Appendix 1

A pilot study investigating cyclic stretch and pharmacological inhibition of endothelial NO; L-Glutamine as a possible confounder

Summary—An inverse relationship between amyloidogenic processing of amyloid precursor protein (APP) and eNOS mediated nitric oxide (NO) has been reported. The serine/threonine-specific kinase, Akt, glycogen synthase kinase-3 (GSK-3) and ICAM-1 are associated with NO signalling in endothelial cells (ECs) and Alzheimer's disease pathology. This study aimed to investigate the combinatory effect of pharmacological inhibition of NO, by L-NAME treatment and mechanical stretch on APP, Aβ and APP processing enzymes, BACE-1, a disintegrin and metalloproteinase-10 (ADAM10), proteins associated with eNOS signalling, Akt, glycogen synthase kinase-3 (GSK-3), and ICAM-1, and NO in a cerebral EC line. APP, ADAM10, BACE-1, eNOS, phosphorylated eNOS, ICAM-1, Akt and GSK-3 were quantified using western blotting while Aβ42 and NO were measured by an ELISA or NO assay kit. L-NAME treatment did not appear to have any additional effects except for the significant increase in BACE-1. However, the effect of stretch on all proteins investigated was consistent with the main chapters. Inhibitory effect of L-NAME treatment could have been skewed due to the presence of L-glutamine in the culture media. Further studies are required to confirm this possibility, which will inform the significance of L-glutamine in maintaining NO production in ECs.

A1.1 Introduction

In the milieu of the endothelium, endothelial nitric oxide synthase (eNOS) serves as a major source of nitric oxide (NO), which is an important second messenger and a mediator of vasodilation [168,169,276]. Regulation of eNOS expression and phosphorylation by mechanical forces such as pulsatile stretch and shear stress resultant of haemodynamics within blood vessels [162,163,165–167,184,266,267].

NO signalling is known to modulate amyloid precursor protein (APP) processing and amyloid β (Aβ) peptide that aggregates to form Aβ plaques, characteristic of Alzheimer's disease (AD) [18,275]. In human brain microvascular endothelial cells (BMECs), treatment with the eNOS inhibitor, N(G)-Nitro-L-Arginine Methyl Ester (L-NAME) markedly increased APP, BACE-1 and Aβ levels [18]. Similarly, in late middle aged-eNOS knockout mice, APP, APP processing enzyme, β secretase 1 (BACE-1) and Aβ levels were elevated compared to control mice [18]. NO supplementation in eNOS null mice by treating the animals with nitroglycerine attenuated

these effects [104]. These studies elaborated a role of NO in modulating APP processing and Aβ levels.

Moreover, studies have shown that NO concentration dependently regulate APP processing [262]. NO bioavailability was demonstrated to regulate APP processing bi-directionally such that increased NO levels produced by the NO donor, sodium nitroprusside (SNP) in the range of 10 and 20 μM mediated amyloidogenic processing, whereas physiological SNP levels in the range of 0.01 and 0.1 μM leading to non-amyloidogenic processing in SH-SY5Y neuroblastoma cells stably transfected with wild-type APPwt695 treated with sodium nitroprusside, a potent NO donor [262].

eNOS mediated NO production is known to be modulated by the serine/threonine-specific kinase, Akt while glycogen synthase kinase-3 (GSK-3) is regulated by Akt [165,250–253]. NO could regulate inflammatory markers such intercellular cell adhesion molecule-1 (ICAM-1) [268]. All these factors are involved in AD pathophysiology and are known to be modulated by stretch [17,116,119,153,162,165,185,191,192,194,205,250,256–258] However, NO dependency on Akt, GSK-3 or ICAM-1 has not been studied in combination with pulsatile stretch in a cerebral endothelial cell line.

This study aimed to investigate the combinatory effect of L-NAME treatment and mechanical stretch on APP, Aβ and APP processing enzymes, BACE-1, a disintegrin and metalloproteinase-10 (ADAM10), proteins associated with eNOS signalling, Akt, glycogen synthase kinase-3 (GSK-3), and ICAM-1, and NO in a cerebral EC line since mechanical stretch effects on cerebral ECs and NO on these signalling molecules are not known in the context of AD.

A1.2 Methods

All methodological approaches including culture conditions are detailed in Chapters 3-5. HCMEC-SV40 used in this experiment were between 7-10 passages.

A1.2.1 L-NAME treatment

HCMECs were either treated with 0.5 mM L-NAME, added just prior to starting the 18 hour stretch regimen or pre-treated with 0.3 mM L-NAME for 3 days and stretched for 18 hours in the presence of 0.3 mM L-NAME treatment.

A1.2.2 Statistical analysis

Each data point represents an individual experiment and data are represented as mean±SEM analysed using one-way ANOVA with post-hoc Tukey-corrected multiple comparisons performed in GraphPad PRISM software version 7.02. Outliers were identified using the robust regression and outlier removal (ROUT) method (detailed in Motulsky *et al.* [228]) in GraphPad PRISM with a Q value set at 10% that defines the threshold for outliers.

Initially, two data sets for the proteins tested were generated from 0.5 mM and 0.3 mM L-NAME treated cells, which were later combined as one data set for each protein, after statistically confirming that there were no significant differences between the two data sets using t-tests or one-way ANOVA.

A1.3 Results

A1.3.1 Pulsatile stretch and NO inhibition in APP expression and processing

NO signalling is known to alter APP expression and processing and NO, and to be modulated by pulsatile stretch [18,103,165], thus the combinatory effect of NO inhibition and pulsatility was investigated in the cerebral EC line, HCMEC-SV40. Followed by 18 hours of stretching at 1 Hz, APP and BACE-1 expression were altered with no significant changes in ADAM10 expression (Figure A1.1). APP expression was significantly higher at the 15% stretch magnitude (159±19%) compared to L-NAME treated static control (89±9%, $P<0.001$) and static vehicle control (100%, $P<0.01$). BACE-1 expression significantly increased in L-NAME treated static cells (124±10%) compared to vehicle treated static control (100%, $P<0.05$) and cells stretched at 15% for 18 hours without L-NAME treatment (80±4%, $P<0.01$; Figure A10.1). In cells stretched with L-NAME (134±6%), BACE-1 levels significantly increased compared to those that had been stretched without L-NAME (80±4%, $P<0.01$; Figure A10.1). Nonetheless, Aβ42 secretion did not change significantly (Figure A1.1).

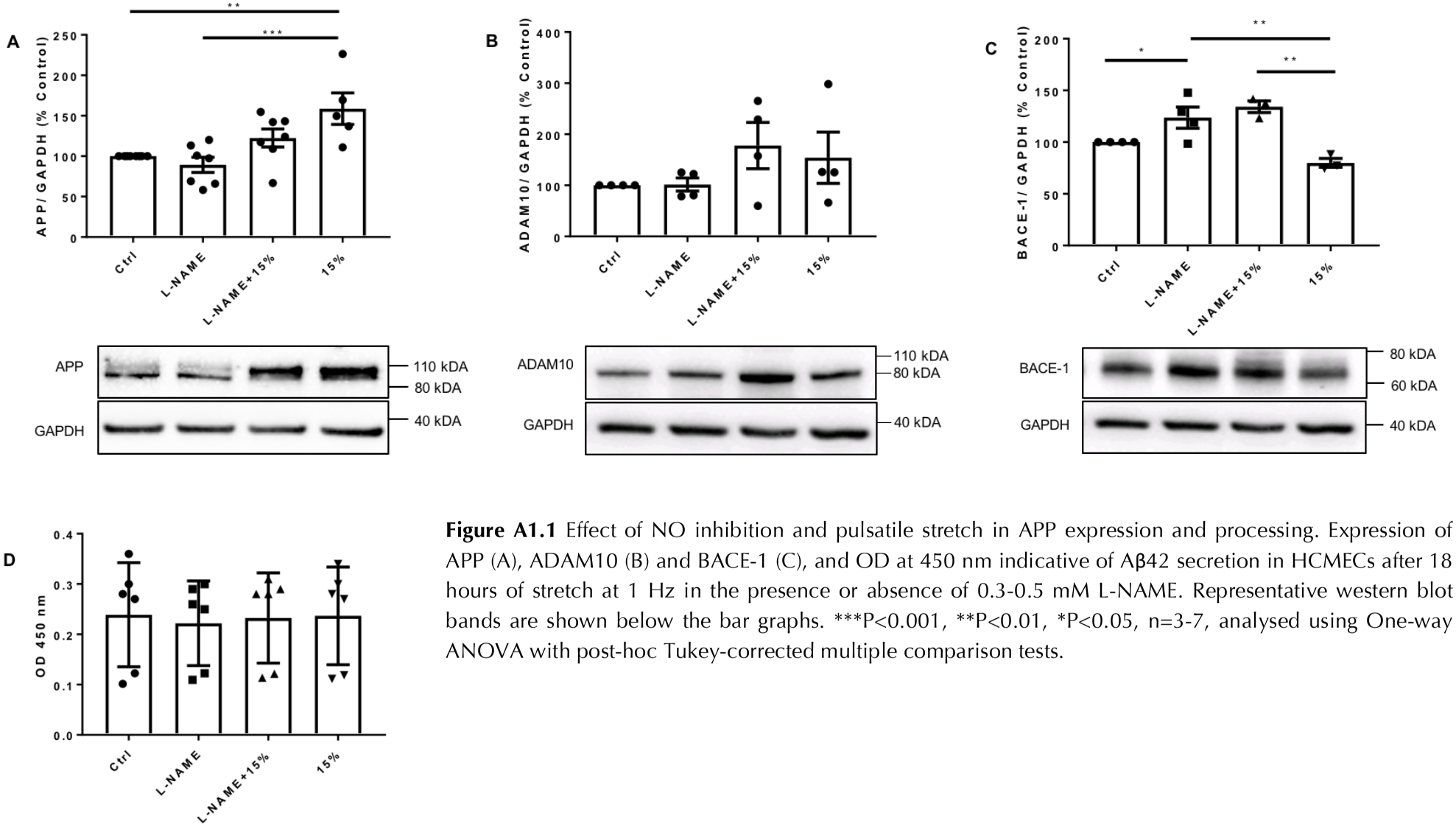

Figure A1.1 Effect of NO inhibition and pulsatile stretch in APP expression and processing. Expression of APP (A), ADAM10 (B) and BACE-1 (C), and OD at 450 nm indicative of Aβ42 secretion in HCMECs after 18 hours of stretch at 1 Hz in the presence or absence of 0.3-0.5 mM L-NAME. Representative western blot bands are shown below the bar graphs. ***P<0.001, **P<0.01, *P<0.05, n=3-7, analysed using One-way ANOVA with post-hoc Tukey-corrected multiple comparison tests.

A1.3.2 Pulsatile stretch and NO inhibition in eNOS signalling

To investigate whether increased APP expression correlated with eNOS expression or phosphorylation, eNOS expression, eNOS phosphorylation and NO production were next investigated. Followed by 18 hours of stretching in with or without NO inhibition using L-NAME, eNOS expression or eNOS phosphorylation at S1177 did not change significantly in response to stretch or L-NAME treatment (Figure A1.2). NO production however, was significantly higher at 15% stretch either in the presence (0.15±0.02 μM/μg, $P<0.05$) or absence (0.14±0.01 μM/μg, $P<0.05$) of the L-NAME treatment relative to the vehicle treated static control (0.06±0.01 μM/μg, $P<0.05$; Figure A1.2). The expression of the inflammatory marker, ICAM-1 did not change under any condition (Figure A1.2).

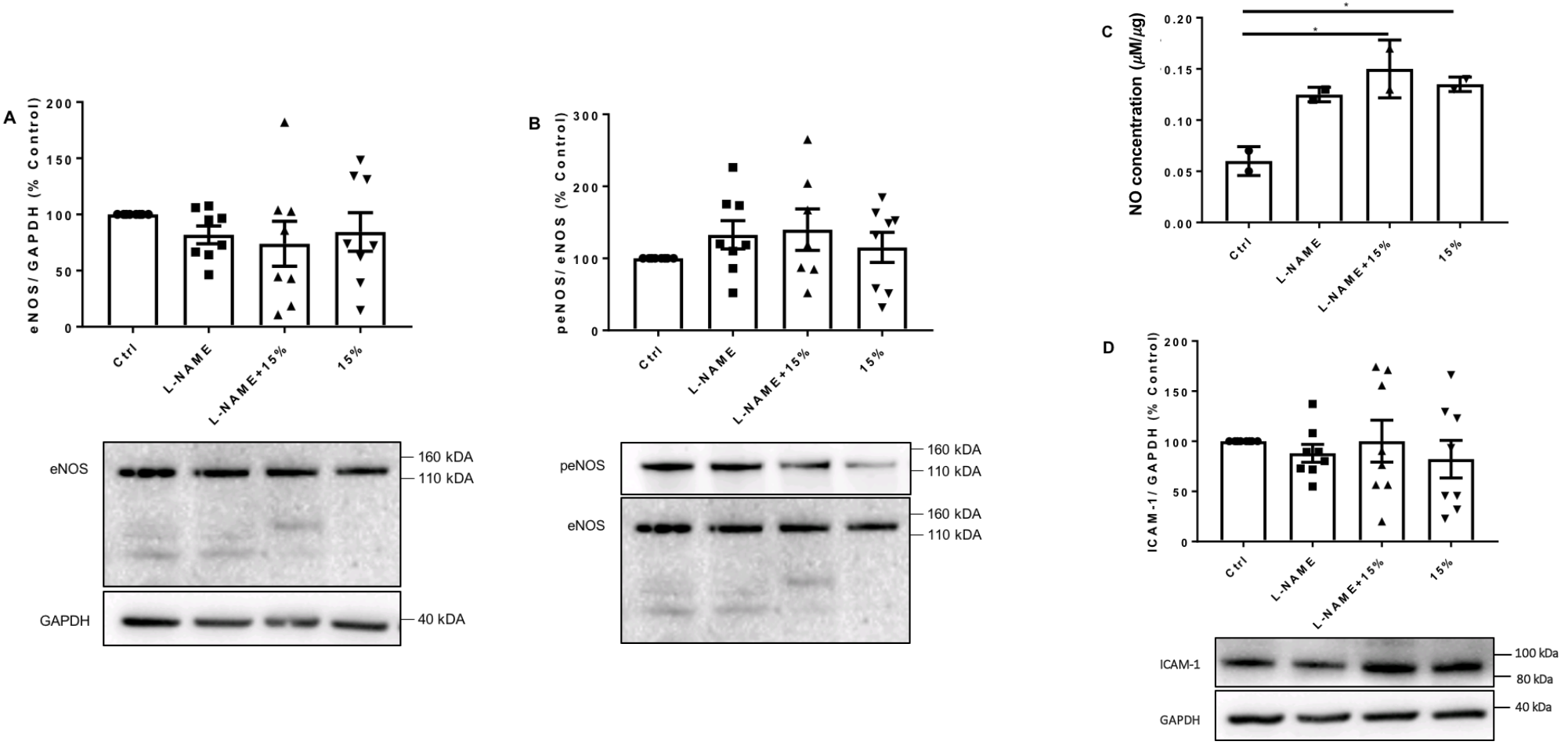

Figure A1.2 NO inhibition and pulsatile stretch in eNOS signalling. Expression of eNOS (A), phosphorylation of eNOS at S1177 (B), and NO production (C) in HCMECs after 18 hours of stretch at 1 Hz in the presence or absence of 0.3-0.5 mM L-NAME. Representative western blot bands are shown below the bar graphs. *P<0.05, n=2-8, analysed using One-way ANOVA with post-hoc Tukey-corrected multiple comparison tests.

A1.3.3 Pulsatile stretch and NO inhibition in Akt signalling

To explore regulatory mechanisms underlying eNOS mediated-NO production, Akt expression and phosphorylation of Akt S473, were investigated. Akt expression or phosphorylation of Akt at S473 did not change significantly in response to 18 hours of 15% stretch or NO inhibition along or combined with stretch (Figure A1.3).

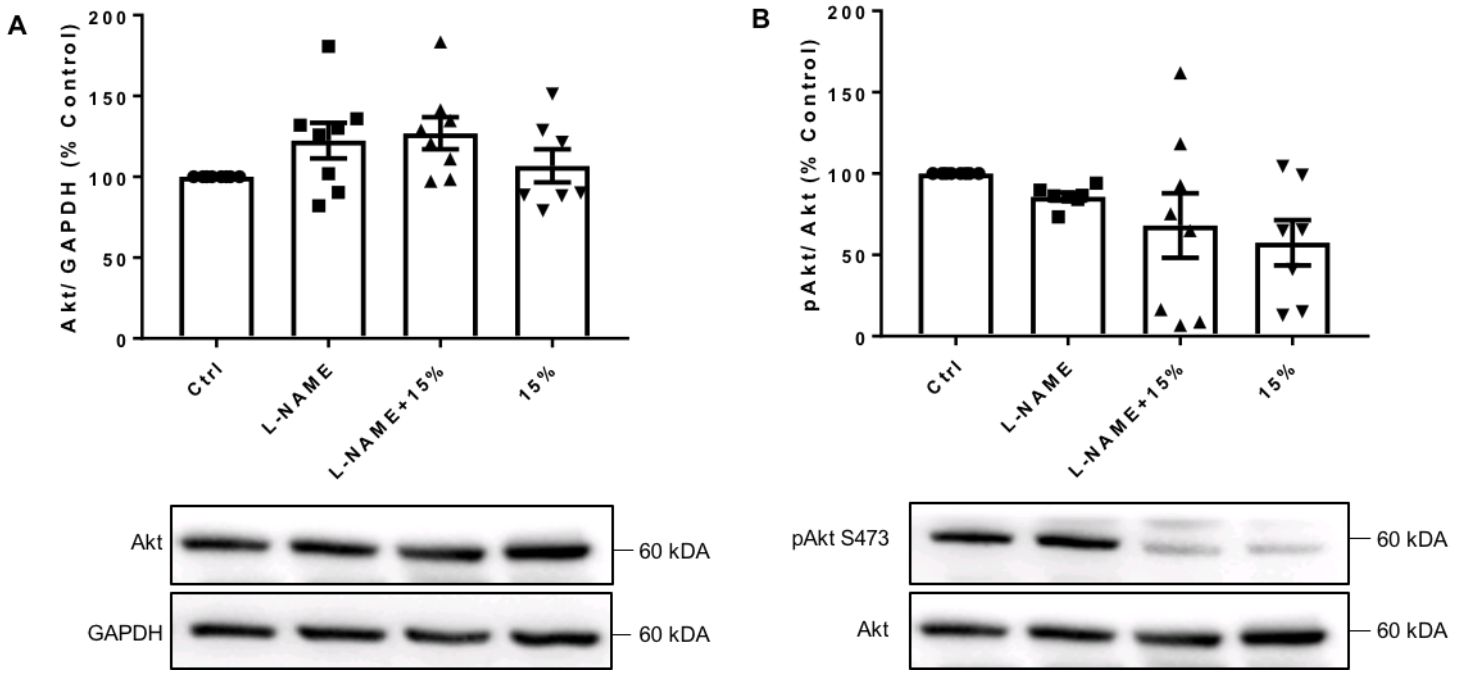

Figure A1.3 NO inhibition and pulsatile stretch in Akt signalling. Expression of Akt (A) and phosphorylation of Akt at S473 (B) in HCMECs after 18 hours of stretch at 1 Hz in the presence or absence of 0.3-0.5 mM L-NAME. Representative western blot bands are shown below the bar graphs. n=7-8, analysed using One-way ANOVA with post-hoc Tukey-corrected multiple comparison tests.

A1.3.4 NO inhibition and Pulsatile stretch in GSK-3 siganalling

Downstream target of Akt activation, GSK-3 was also investigated. 18 hours of stretching with or without L-NAME treatment did not change the expression of GSK-3α, GSK-3β or phosphorylation of GSK-3β at S9 in HCMECs. However, stretching resulted in a significant increase in GSK-3α phosphorylation at S21 compared to both L-NAME treated (93±5%, $P<0.05$), and vehicle treated (100%, $P<0.05$), static controls. (Figure A1.4).

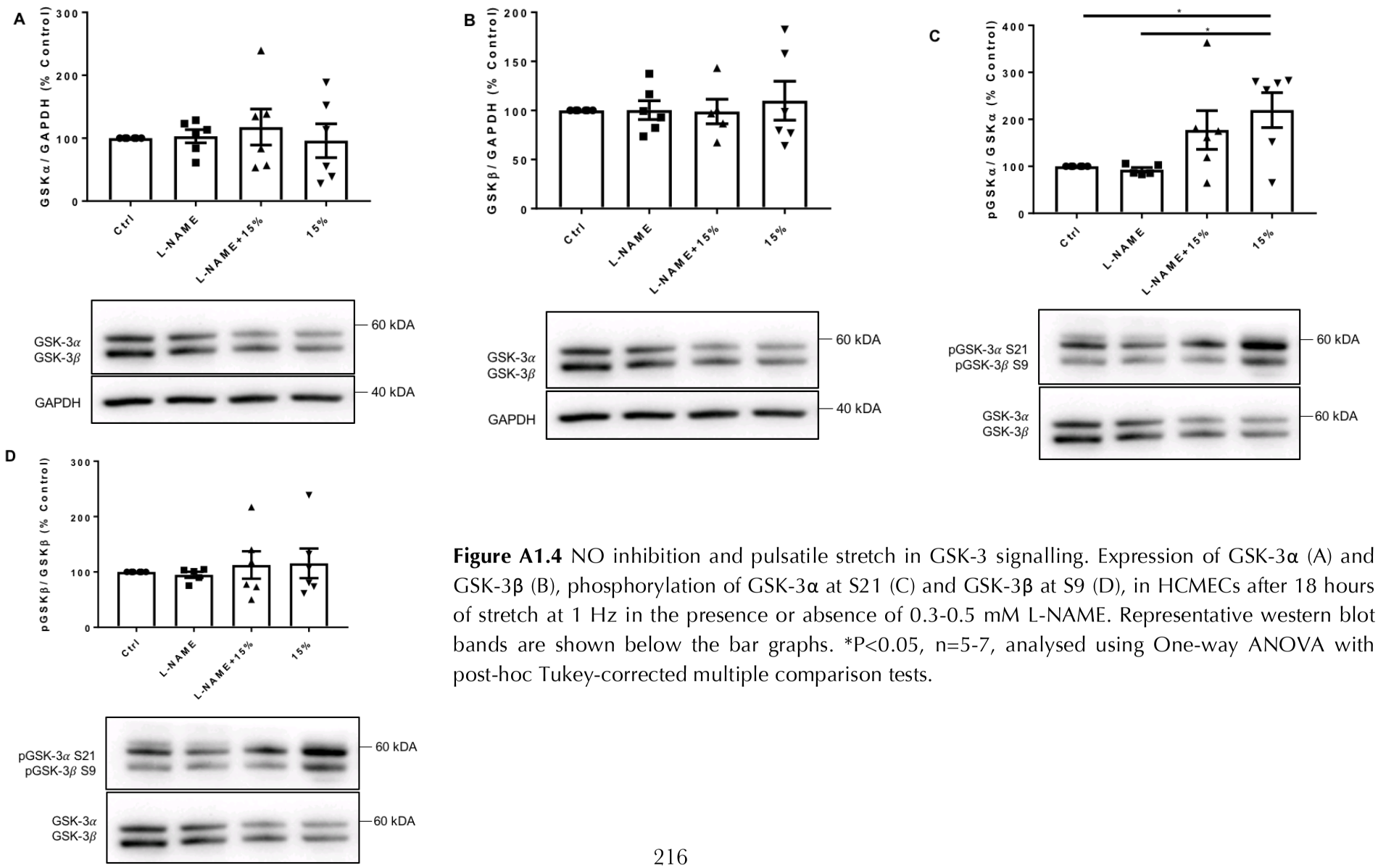

Figure A1.4 NO inhibition and pulsatile stretch in GSK-3 signalling. Expression of GSK-3α (A) and GSK-3β (B), phosphorylation of GSK-3α at S21 (C) and GSK-3β at S9 (D), in HCMECs after 18 hours of stretch at 1 Hz in the presence or absence of 0.3-0.5 mM L-NAME. Representative western blot bands are shown below the bar graphs. *P<0.05, n=5-7, analysed using One-way ANOVA with post-hoc Tukey-corrected multiple comparison tests.

A1.4 Discussion

Due to the relationship between NO and APP regulation, the current study combined the effect of pulsatility, which is known to modulate eNOS mediated NO production, and NO inhibition, in order to investigate NO dependency upon stretch-mediated changes in APP expression and processing that are reported in Chapter 4 [19]. The effect of stretch on APP expression as reported in Chapter 4, was still preserved in this study as stretching at 15% for 18 hours increased the expression of APP expression compared to the static controls (Figure A1.1) [19]. However, stretching at 15% in the presence of L-NAME treatment did not have any significant additional effects, except that the stretch effect on APP expression was not observed with NO inhibition (Figure A1.1). In contrast, the expression of the APP processing enzyme towards amyloidogenic APP processing, BACE-1, was increased with the L-NAME treatment, in the presence or absence of the stretch regimen, pointing out that NO inhibition could regulate BACE-1 expression (Figure A1.1). There were no changes in ADAM10 expression suggesting that NO does affect ADAM10 expression (Figure A1.1). The significant increase in Aβ42 secretion in response to 18 hours of stretching at 15% that was reported in Chapter 4 was absent, consistent with the passaging effect reported in Chapter 6, and the results of Aβ42 secretion reported in Chapters 7 and 8 (Figure A1.1).

Although upregulated BACE-1 expression in response to L-NAME was consistent with previous findings, not having any additional effects on APP expression and Aβ42 with the L-NAME treatment alone was an unexpected result, since a previous study has shown that NO inhibition could upregulate APP expression and Aβ42 in human BMECs (Figure A1.1) [18]. Additionally, 18 hour stretch regimen at a 15% stretch magnitude increased NO production regardless of the L-NAME treatment, another unexpected result (Figure A1.2). These unexpected results with L-NAME treatment suggested that the L-NAME treatment duration and/or the concentration was not sufficient to induce the anticipated inhibitory effect on NO

production. Since the data collected from the experiments where 0.3 mM L-NAME treatment for 3 days and 18 hours was utilised, were not statistically different from 0.5 mM L-NAME treatment for 18 hours, the time course or the concentration of the L-NAME treatment may not have been sufficient for these cells to induce a significant response. It was reported that in porcine aortic ECs 10 mM L-NAME treatment caused an apoptotic response [214]. Based on this study, the doses used in this study are likely to be well below the toxic levels, and using a higher dose of L-NAME is unlikely to cause any toxic effects, however the maximal tolerated dose of L-NAME in HCMECs needs to be tested in further experiments. Considering that L-NAME is a competitive inhibitor that inhibits eNOS mediated NO by competing with L-arginine and is analogous to L-arginine, the substrate of eNOS, the results suggest that the concentration in the present study was not sufficient to overwhelm any competitors that were present. L-NAME is reported to be a prodrug that is required to be turned into another active compound, N^G-nitro-L-arginine, to achieve its functionality, which was shown to be influenced by the buffer that the drug was dissolved in [314]. Thus, the APP, Aβ42 and NO results in response to L-NAME treatment could be explained by the differences in formulations of the culture media that had been used in the current study to the media that had been used by the previous study by Austin *et al.* [18]. The M199 media (M4530; Sigma) that had been used in the current study supplemented with 10% fetal bovine serum (FBS) and 1% penicillin/streptomycin contained L-glutamine, Earle's salts and $NaHCO_3$, in contrast to endothelial growth medium 2 (EGM2; Lonza) supplemented with 2% FBS, fibroblast growth factor, vascular endothelial growth factor, insulin-like growth factor, epidermal growth factor, ascorbic acid, hydrocortisone and heparin, which was used in the previous study by Austin *et al.* [18]. Further to this notion, while the presence of L-arginine is known to reverse the inhibitory effect of L-NAME, L-glutamine could act as a secondary substrate that contributes to *de novo* synthesis of L-arginine [315,316], which is a plausible explanation for the absence of inhibitory effect of L-NAME in the present study since the culture media contained L-

glutamine. Thus, the differences in culture media that the cells had been maintained in, could have affected the results of the present study. Additionally, the cell types are different between the two studies, such that used such that the present study utilised a cell line as opposed to primary cells in the previous study [18]

Consistently with all the results reported in the main chapters presented in this thesis, present study indicated that NO production in response to long term stretch is unlikely to be mediated by eNOS phosphorylation at S1177 as the eNOS phosphorylation and NO production did not correlate in this study, or in previous chapters (Figure A1.2). Increased NO levels mediated by the NO donor, SNP in the range of 10 and 20 μM resulted in amyloidogenic processing, whereas physiological SNP levels in the range of 0.01 and 0.1 μM leading to non-amyloidogenic processing in SH-SY5Y neuroblastoma cells stably transfected with wild-type APPwt695 [262]. The present study found NO concentrations in the range of 0.14-0.15 μM/μg after stretching for 18 hours at a stretch magnitude of 15%, which could be consistent with non-amyloidogenic processing of APP emphasising the importance of investigating NO and soluble APPα in future studies [262].

In addition to APP and ADAM10 expression, the present study showed the same stretch effect that was shown in previous chapters on BACE-1 expression, Aβ42 secretion, eNOS expression and phosphorylation, NO production, ICAM-1 expression, Akt phosphorylation and GSK-3 expression and/or phosphorylation except for pGSK-3α, consistently showing the passaging effect that was reported in Chapter 6 (Figure A1.1, A1.2, A1.3 & Figure A1.4). However, GSK-3α phosphorylation at S21 (Figure A1.4) was upregulated, which indicate that other studies that were conducted under the same conditions (reported in Chapters 7 and 8) were underpowered to show this effect.

Since the significant increase in BACE-1 concomitant with elevated Aβ42 secretion in response to stretch that was shown in Chapter 4 [19] was absent in the present study (Figure A1.1), this could mean that APP is processed differently at lower passages compared to higher passages of HCMECs, indicating a possible regulatory role of EC senescence in APP processing as reported in Chapter 6. These results also emphasise the relevance of investigating soluble APPα, which is known to exert neuroprotective effects in AD, which could explain the unaltered Aβ42 secretion in the present study as well as in the studies reported in Chapters 7 and 8 (Figure A1.1) [116]. Since GSK-3α is known to regulate Aβ plaque formation, the significant increase in GSK-3α phosphorylation at S21 [19], indicative of inactivation of the GSK-3α enzyme, further corroborates this hypothesis of altered APP processing at early passages towards non-amyloidogenic pathway, compared to ECs at late passages, since Chapters 4 and 5 (which used ECs at higher passages) showed an increase in BACE-1 concomitant with elevated Aβ42 and reduced GSK-3α phosphorylation at S21 in response to stretch. GSK-3α activation is reported to regulate APP processing [116]. Increased GSK-3α phosphorylation deactivates GSK-3α, thus this could be a possible mechanism by which Aβ42 secretion in early passage HCMECs is regulated, since increased GSK-3α activation was evident in late passage HCMECs concomitant with increased Aβ42 secretion and BACE-1 levels (Chapters 4 and 5) [19]. Alternatively, another proposed mechanism is that at early passages, NO regulation in response to stretch is altered leading to differential processing of APP. This is because NO bioavailability was demonstrated to regulate APP processing bi-directionally [262].

The cells that the previous studies reported in Chapters 4 and Chapter 5, were maintained within 17-19 passages, while the cells that had been used in the current study were between 7-10 passages. NO is involved in cell growth, proliferation and survival, and that Akt, GSK-3 and APP could all contribute towards cell survival-related signalling [17,317,318]. Since there is a

difference in the passage number, this could affect the signalling pathways that mediate cell survival signalling, such that at earlier passages cell survival signalling can differ from the cells at late passages [278]. In vascular smooth muscle cells (VSMC), Akt phosphorylation was demonstrated to be significantly higher in late passage cells (within passage 20-22) compared to cells that were in early passages (within passage 3-5), which was recapitulated in VSMC explants derived from old and young rats [278,279]. Furthermore, altered basal expression levels of Akt and eNOS were evident in primary porcine coronary ECs at passage 4 compared to that of passage 1 [280]. Both these studies along with many other studies support the idea of altered gene and protein expression with multiple passaging, and thus a possible role of cell senescence can be proposed, which is discussed in detail in Chapter 6 [278,280–282].

A1.5 Conclusions

Effect of cyclic stretch was consistent with results reported in all chapters, with no substantial changes in the presence of absence of L-NAME. The L-NAME treatment in the present study appeared to be insufficient to induce the anticipated inhibitory effect on NO, possibly due to the presence of L-glutamine in the culture media, which is known to compete with L-NAME in maintaining NO reservoirs. Future studies are warranted to confirm the results presented using increased concentration of L-NAME and/or prolonged exposure, or in the absence of L-glutamine.

References

1. Alzheimer's Association. 2017 Alzheimer's disease facts and figures. *Alzheimer's Dement.* **13,** 325–373 (2017).
2. Langbaum, J. B. S. *et al.* Blood pressure is associated with higher brain amyloid burden and lower glucose metabolism in healthy late middle-age persons. *Neurobiol. Aging* **33,** 827.e11-9 (2012).
3. Faraco, G. *et al.* Hypertension enhances Aβ-induced neurovascular dysfunction, promotes β-secretase activity, and leads to amyloidogenic processing of APP. *J. Cereb. Blood Flow Metab.* **36,** 241–252 (2016).
4. Cifuentes, D. *et al.* Hypertension Accelerates the Progression of Alzheimer-Like Pathology in a Mouse Model of the DiseaseNovelty and Significance. *Hypertension* **65,** 218–224 (2015).
5. Murphy, M. C. *et al.* Regional brain stiffness changes across the Alzheimer's disease spectrum. *NeuroImage Clin.* **10,** 283–290 (2016).
6. Qiu, C., Winblad, B., Viitanen, M. & Fratiglioni, L. Pulse Pressure and Risk of Alzheimer Disease in Persons Aged 75 Years and Older A Community-Based, Longitudinal Study. *Stroke* **594–599,** 1152–62 (2003).
7. Pase, M. P. *et al.* Aortic Stiffness and the Risk of Incident Mild Cognitive Impairment and Dementia. *Stroke* **47,** 2256–2261 (2016).
8. Mitchell, G. F. *et al.* Arterial stiffness, pressure and flow pulsatility and brain structure and function: the Age, Gene/Environment Susceptibility--Reykjavik study. *Brain* **134,** 3398–407 (2011).
9. Domanski, M. J., Davis, B. R., Pfeffer, M. A., Kastantin, M. & Mitchell, G. F. Isolated systolic hypertension: Prognostic information provided by pulse pressure. *Hypertension* **34,** 375–380 (1999).
10. Papaioannou, T. G. *et al.* Experimental and clinical study of the combined effect of arterial stiffness and heart rate on pulse pressure: Differences between central and peripheral arteries. *Clin. Exp. Pharmacol. Physiol.* **32,** 210–217 (2005).
11. Ferri, C. P. *et al.* Global prevalence of dementia: a Delphi consensus study. *Lancet* **366,** 2112–7 (2005).
12. Rajadas, J. *et al.* Enhanced Aβ1–40 production in endothelial cells stimulated with fibrillar Aβ1–42. *PLoS One* **8,** e58194 (2013).
13. Xia, W., Zhang, J., Perez, R., Koo, E. H. & Selkoe, D. J. Interaction between amyloid precursor protein and presenilins in mammalian cells: Implications for the pathogenesis of Alzheimer disease. *Proc. Natl. Acad. Sci.* **94,** 8208–8213 (1997).
14. Ogishima, S. *et al.* AlzPathway, an Updated Map of Curated Signaling Pathways: Towards Deciphering Alzheimer's Disease Pathogenesis. *Methods Mol. Biol.* **1303,** 423–32 (2016).

15. Mielke, M. M. *et al.* The Association Between Plasma Ceramides and Sphingomyelins and Risk of Alzheimer's Disease Differs by Sex and APOE in the Baltimore Longitudinal Study of Aging. *J. Alzheimer's Dis.* **60,** 819–828 (2017).
16. Apelt, J., Leßig, J. & Schliebs, R. β-amyloid-associated expression of intercellular adhesion molecule-1 in brain cortical tissue of transgenic Tg2576 mice. *Neurosci. Lett.* **329,** 111–115 (2002).
17. Kang, Q. *et al.* MiR-124-3p attenuates hyperphosphorylation of Tau protein-induced apoptosis via caveolin-1-PI3K/Akt/GSK3β pathway in N2a/APP695swe cells. *Oncotarget* **8,** 24314–24326 (2017).
18. Austin, S. A., Santhanam, A. V, Hinton, D. J., Choi, D.-S. & Katusic, Z. S. Endothelial nitric oxide deficiency promotes Alzheimer's disease pathology. *J. Neurochem.* **127,** 691–700 (2013).
19. Gangoda, S. V. S. *et al.* Pulsatile stretch as a novel modulator of amyloid precursor protein processing and associated inflammatory markers in human cerebral endothelial cells. *Sci. Rep.* **8,** 1689 (2018).
20. Gao, J. *et al.* Preconditioning effects of physiological cyclic stretch on pathologically mechanical stretch-induced alveolar epithelial cell apoptosis and barrier dysfunction. *Biochem. Biophys. Res. Commun.* **448,** 342–8 (2014).
21. Sun, R., He, T., Pan, Y. & Katusic, Z. S. Effects of senescence and angiotensin II on expression and processing of amyloid precursor protein in human cerebral microvascular endothelial cells. *Aging (Albany. NY).* (2018). doi:10.18532/aging.101362
22. Toledo, J. B. *et al.* Contribution of cerebrovascular disease in autopsy confirmed neurodegenerative disease cases in the National Alzheimer's Coordinating Centre. *Brain* **136,** 2697–2706 (2013).
23. Tian, X.-L. & Li, Y. Endothelial Cell Senescence and Age-Related Vascular Diseases. *J. Genet. Genomics* **41,** 485–495 (2014).
24. Guo, C.-P. *et al.* High salt induced hypertension leads to cognitive defect. *Oncotarget* **8,** 95780–95790 (2017).
25. Walton, S. L., Singh, R. R., Tan, T., Paravicini, T. M. & Moritz, K. M. Late gestational hypoxia and a postnatal high salt diet programs endothelial dysfunction and arterial stiffness in adult mouse offspring. *J. Physiol.* **594,** 1451–63 (2016).
26. WHO | Dementia. *WHO* (2017). Available at: http://www.who.int/mediacentre/factsheets/fs362/en/. (Accessed: 9th February 2018)
27. Dias, A. *et al. Neurological Disorders: public health challenges*. (World Health Organization, 2006).
28. Masters, C. L. & Selkoe, D. J. Biochemistry of amyloid β-protein and amyloid deposits in Alzheimer disease. *Cold Spring Harb. Perspect. Med.* **2,** a006262 (2012).
29. Grundke-Iqbal, I. *et al.* Amyloid protein and neurofibrillary tangles coexist in the same neuron in Alzheimer disease. *Proc. Natl. Acad. Sci.* **86,** 2853–2857 (1989).
30. LaFerla, F. M., Green, K. N. & Oddo, S. Intracellular amyloid-β in Alzheimer's disease. *Nat. Rev. Neurosci.* **8,** 499–509 (2007).
31. Barage, S. H. & Sonawane, K. D. Amyloid cascade hypothesis: Pathogenesis and therapeutic strategies in Alzheimer's disease. *Neuropeptides* **52,** 1–18 (2015).
32. Hardy, J. A. & Higgins, G. A. Alzheimer's disease: the amyloid cascade hypothesis. *Science* **256,** 184–5 (1992).
33. Nelson, P. T. *et al.* Correlation of Alzheimer disease neuropathologic changes with cognitive status: a review of the literature. *J. Neuropathol. Exp. Neurol.* **71,** 362–81 (2012).
34. Virchow, R. in *Cellular pathology as based upon physiological and pathological histology* 409–410 (RM De Witt, 1860).
35. Selkoe, D. J. Alzheimer's disease: genes, proteins, and therapy. *Physiol Rev* **81,** 741–766 (2001).

36. Goate, A. *et al.* Segregation of a missense mutation in the amyloid precursor protein gene with familial Alzheimer's disease. *Nature* **349,** 704–706 (1991).
37. Poorkaj, P. *et al.* Missense mutations in the chromosome 14 familial Alzheimer's disease presenilin 1 gene. *Hum. Mutat.* **11,** 216–221 (1998).
38. Maltese, W. A. *et al.* Retention of the Alzheimer's amyloid precursor fragment C99 in the endoplasmic reticulum prevents formation of amyloid β-peptide. *J. Biol. Chem.* **276,** 20267–79 (2001).
39. Chimon, S. *et al.* Evidence of fibril-like-β-sheet structures in a neurotoxic amyloid intermediate of Alzheimer's β-amyloid. *Nat Struct Mol Biol* **14,** 1157–1164 (2007).
40. Ahmed, M. *et al.* Structural conversion of neurotoxic amyloid-β(1–42) oligomers to fibrils. *Nat. Struct. Mol. Biol.* **17,** 561–7 (2010).
41. Dubnovitsky, A. *et al.* Amyloid-β protofibrils: size, morphology and synaptotoxicity of an engineered mimic. *PLoS One* **8,** e66101 (2013).
42. Cleary, J. P. *et al.* Natural oligomers of the amyloid-β protein specifically disrupt cognitive function. *Nat Neurosci* **8,** 79–84 (2005).
43. Scheidt, H. A., Morgado, I., Rothemund, S. & Huster, D. Dynamics of amyloid β fibrils revealed by solid-state NMR. *J. Biol. Chem.* **287,** 2017–21 (2012).
44. Shafer, T. J. & Atchison, W. D. Transmitter, ion channel and receptor properties of pheochromocytoma (PC12) cells: a model for neurotoxicological studies. *Neurotoxicology* **12,** 473–92 (1991).
45. Paravastu, A. K., Leapman, R. D., Yau, W.-M. & Tycko, R. Molecular structural basis for polymorphism in Alzheimer's β-amyloid fibrils. *Proc. Natl. Acad. Sci. U. S. A.* **105,** 18349–54 (2008).
46. Fandos, N. *et al.* Plasma amyloid β 42/40 ratios as biomarkers for amyloid β cerebral deposition in cognitively normal individuals. *Alzheimer's Dement. (Amsterdam, Netherlands)* **8,** 179–187 (2017).
47. Potter, R. *et al.* Increased *in vivo* amyloid-β42 production, exchange, and loss in presenilin mutation carriers. *Sci. Transl. Med.* **5,** 189ra77 (2013).
48. Blasko, I. *et al.* Conversion from cognitive health to mild cognitive impairment and Alzheimer's disease: Prediction by plasma amyloid beta 42, medial temporal lobe atrophy and homocysteine. *Neurobiol. Aging* **29,** 1–11 (2008).
49. Donohue, M. C. *et al.* Longitudinal plasma amyloid beta in Alzheimer's disease clinical trials. *Alzheimer's Dement. J. Alzheimer's Assoc.* **11,** 1069–1079 (2015).
50. Jensen, M. *et al.* Cerebrospinal fluid Aβ42 is increased early in sporadic Alzheimer's disease and declines with disease progression. *Ann. Neurol.* **45,** 504–511 (1999).
51. Hartz, A. M. S., Miller, D. S. & Bauer, B. Restoring Blood-Brain Barrier P-Glycoprotein Reduces Brain Amyloid- in a Mouse Model of Alzheimer's Disease. *Mol. Pharmacol.* **77,** 715–723 (2010).
52. Cirrito, J. R. *et al.* P-glycoprotein deficiency at the blood-brain barrier increases amyloid-β deposition in an Alzheimer disease mouse model. *J. Clin. Invest.* **115,** 3285–3290 (2005).
53. Deane, R. *et al.* LRP/amyloid-β peptide interaction mediates differential brain efflux of Aβ isoforms. *Neuron* **43,** 333–44 (2004).
54. Iliff, J. J. *et al.* A paravascular pathway facilitates CSF flow through the brain parenchyma and the clearance of interstitial solutes, including amyloid β. *Sci. Transl. Med.* **4,** 147ra111 (2012).
55. Lee, C. Y. D. & Landreth, G. E. The role of microglia in amyloid clearance from the AD brain. **117,** 949–960 (2013).
56. Wang, Y.-J., Zhou, H.-D. & Zhou, X.-F. Clearance of amyloid-β in Alzheimer's disease: progress, problems and perspectives. *Drug Discov. Today* **11,** 931–8 (2006).
57. Do, T. M. *et al.* Age-Dependent Regulation of the Blood-Brain Barrier Influx/Efflux Equilibrium of Amyloid-β Peptide in a Mouse Model of Alzheimer's Disease (3xTg-

AD). *J. Alzheimer's Dis.* **49,** 287–300 (2015).
58. Deane, R. *et al.* RAGE mediates amyloid-β peptide transport across the blood-brain barrier and accumulation in brain. *Nat. Med.* **9,** 907–913 (2003).
59. Roher, A. E. *et al.* Amyloid beta peptides in human plasma and tissues and their significance for Alzheimer's disease. *Alzheimer's Dement.* **5,** 18–29 (2009).
60. Nakamura, A. *et al.* High performance plasma amyloid-β biomarkers for Alzheimer's disease. *Nature* **554,** 249–254 (2018).
61. Mullane, K. & Williams, M. Alzheimer's therapeutics: continued clinical failures question the validity of the amyloid hypothesis-but what lies beyond? *Biochem. Pharmacol.* **85,** 289–305 (2013).
62. Glenner, G. G., Henry, J. H. & Fujihara, S. Congophilic angiopathy in the pathogenesis of Alzheimer's degeneration. *Ann. Pathol.* **1,** 120–9 (1981).
63. Ghiso, J., Fossati, S. & Rostagno, A. Amyloidosis associated with cerebral amyloid angiopathy: cell signaling pathways elicited in cerebral endothelial cells. *J Alzheimers Dis.* **42,** S167–76. (2014).
64. Brickman, A. M. *et al.* Cerebral autoregulation, beta amyloid, and white matter hyperintensities are interrelated. *Neurosci. Lett.* **592,** 54–58 (2015).
65. Park, L. *et al.* Age-dependent neurovascular dysfunction and damage in a mouse model of cerebral amyloid angiopathy. *Stroke.* **45,** 1815–1821 (2014).
66. Toda, N. & Okamura, T. Cerebral blood flow regulation by nitric oxide in Alzheimer's disease. *J. Alzheimer's Dis.* **32,** 569–578 (2012).
67. Thomas, T., McLendon, C., Sutton, E. T. & Thomas, G. Cerebrovascular endothelial dysfunction mediated by β-amyloid. *Neuroreport* **8,** 1387–1391 (1997).
68. Suo, Z. *et al.* Soluble Alzheimers β-amyloid constricts the cerebral vasculature *in vivo*. *Neurosci. Lett.* **257,** 77–80 (1998).
69. Park, L. *et al.* Aβ-Induced Vascular Oxidative Stress and Attenuation of Functional Hyperemia in Mouse Somatosensory Cortex. *J. Cereb. Blood Flow Metab.* **24,** 334–342 (2004).
70. Mosconi, L. *et al.* Oxidative Stress and Amyloid-Beta Pathology in Normal Individuals with A Maternal History of Alzheimer's. *Biol. Psychiatry* **68,** 913–921 (2010).
71. Son, S. J. & Kim, E. Effect of hypertension on the resting-state functional connectivity in patients with Alzheimer's disease. *Alzheimer's Dement.* **9,** P875–P876 (2013).
72. Wallace, S. M. L. *et al.* Isolated systolic hypertension is characterized by increased aortic stiffness and endothelial dysfunction. *Hypertension* **50,** 228–233 (2007).
73. McEniery, C. M. *et al.* Endothelial function is associated with pulse pressure, pulse wave velocity, and augmentation index in healthy humans. *Hypertension* **48,** 602–608 (2006).
74. Nation, D. A. *et al.* Pulse pressure is associated with Alzheimer biomarkers in cognitively normal older adults. *Neurology* **81,** 2024–7 (2013).
75. Arendash, G. W., Su, G. C., Crawford, F. C., Bjugstad, K. B. & Mullan, M. Intravascular β-amyloid infusion increases blood pressure: implications for a vasoactive role of β-amyloid in the pathogenesis of Alzheimer's disease. *Neurosci. Lett.* **268,** 17–20 (1999).
76. Meng, X.-F. *et al.* Midlife vascular risk factors and the risk of Alzheimer's Disease: a systematic review and meta-analysis. *J. Alzheimers. Dis.* In press (2014). doi:10.3233/JAD-140954
77. Kurata, T. *et al.* Telmisartan Reduces Progressive Accumulation of Cellular Amyloid Beta and Phosphorylated Tau with Inflammatory Responses in Aged Spontaneously Hypertensive Stroke Resistant Rat. *J. Stroke Cerebrovasc. Dis.* **23,** 2580–2590 (2014).
78. Kurata, T. *et al.* Telmisartan reduces progressive accumulation of cellular amyloid beta and phosphorylated tau with inflammatory responses in aged spontaneously hypertensive stroke resistant rat. *J. Stroke Cerebrovasc. Dis.* **23,** 2580–90 (2014).

79. Schreiber, S. *et al.* Interplay between age, cerebral small vessel disease, parenchymal amyloid-β, and Tau pathology: longitudinal studies in hypertensive stroke-prone rats. *J. Alzheimers. Dis.* **42,** S205-15 (2014).
80. Qia *et al.* Abnormal expression level of BACE1 and RAGE of hippocampus related to cognitive impairment in SHR. *Ann Clin Exp Hypertens.* **2,** 1010 (2014).
81. McKinnon, S. J. *et al.* Caspase activation and amyloid precursor protein cleavage in rat ocular hypertension. *Invest. Ophthalmol. Vis. Sci.* **43,** 1077–1087 (2002).
82. Stefani, A. *et al.* CSF biomarkers, impairment of cerebral hemodynamics and degree of cognitive decline in Alzheimer's and mixed dementia. *J. Neurol. Sci.* **283,** 109–15 (2009).
83. Tan, I., Butlin, M., Liu, Y. Y., Ng, K. & Avolio, A. P. Heart rate dependence of aortic pulse wave velocity at different arterial pressures in rats. *Hypertension* **60,** 528–33 (2012).
84. Petersen, K. S., Keogh, J. B., Meikle, P. J., Garg, M. L. & Clifton, P. M. Dietary predictors of arterial stiffness in a cohort with type 1 and type 2 diabetes. *Atherosclerosis* **238,** 175–181 (2015).
85. Hanon, O. *et al.* Relationship between arterial stiffness and cognitive function in elderly subjects with complaints of memory loss. *Stroke.* **36,** 2193–7 (2005).
86. Avolio, A., Butlin, M. & Protogerou, A. in *Blood Pressure and Arterial Wall Mechanics in Cardiovascular Diseases* (eds. Safar, M. E., O'Rourke, M. F. & Frohlich, E. D.) 281–295 (Springer London, 2014).
87. Tan, Y. *et al.* Stiffening-induced high pulsatility flow activates endothelial inflammation via a TLR2/NF-κB pathway. *PLoS One* **9,** e102195 (2014).
88. Wu, J. *et al.* Inflammation and mechanical stretch promote aortic stiffening in hypertension through activation of p38 mitogen-activated protein kinase. *Circ. Res.* **114,** 616–25 (2014).
89. Ng, K., Butlin, M. & Avolio, A. P. Persistent effect of early, brief angiotensin-converting enzyme inhibition on segmental pressure dependency of aortic stiffness in spontaneously hypertensive rats. *J. Hypertens.* **30,** 1782–90 (2012).
90. Laurent, S. *et al.* Aortic stiffness is an independent predictor of all-cause and cardiovascular mortality in hypertensive Patients. *Hypertension* **37,** 1236–1241 (2001).
91. Avolio, A., Jones, D. & Tafazzoli-Shadpour, M. Quantification of Alterations in Structure and Function of Elastin in the Arterial Media. *Hypertension* **32,** 170–175 (1998).
92. Toda, N., Hatano, Y. & Hayashi, S. Modifications by stretches of the mechanical response of isolated cerebral and extracerebral arteries to vasoactive agents. *Pflügers Arch. Eur. J. Physiol.* **374,** 73–77 (1978).
93. Wostyn, P., Audenaert, K. & De Deyn, P. P. Alzheimer's disease-related changes in diseases characterized by elevation of intracranial or intraocular pressure. *Clin. Neurol. Neurosurg.* **110,** 101–9 (2008).
94. Golomb, J. *et al.* Alzheimer's disease comorbidity in normal pressure hydrocephalus: prevalence and shunt response. *J. Neurol. Neurosurg. Psychiatry* **68,** 778–81 (2000).
95. Kizu, O., Yamada, K. & Nishimura, T. Proton chemical shift imaging in normal pressure hydrocephalus. *Am. J. Neuroradiol.* **22,** 1659–1664 (2001).
96. Fleminger, S. Head injury as a risk factor for Alzheimer's disease: the evidence 10 years on; a partial replication. *J. Neurol. Neurosurg. Psychiatry* **74,** 857–862 (2003).
97. Fulton, D. *et al.* Localization of endothelial nitric-oxide synthase phosphorylated on serine 1179 and nitric oxide in Golgi and plasma membrane defines the existence of two pools of active enzyme. *J. Biol. Chem.* **277,** 4277–84 (2002).
98. Tian, J. *et al.* A novel role for caveolin-1 in regulating endothelial nitric oxide synthase activation in response to H2O2 and shear stress. *Free Radic. Biol. Med.* **49,** 159–70 (2010).
99. Tran, J. *et al.* Activation of Endothelial Nitric Oxide (eNOS) Occurs through Different

Membrane Domains in Endothelial Cells. *PLoS One* **11,** e0151556 (2016).
100. Pollock, J. S. *et al.* The metabolism of L-arginine and its significance for the biosynthesis of endothelium-derived relaxing factor: cultured endothelial cells recycle L-citrulline to L-arginine. *Proc. Natl. Acad. Sci.* **87,** 8612–8616 (1990).
101. de Oliveira, F. F., Chen, E. S., Smith, M. C. & Bertolucci, P. H. F. Associations of Blood Pressure with Functional and Cognitive Changes in Patients with Alzheimer's Disease. *Dement. Geriatr. Cogn. Disord.* **41,** 314–23 (2016).
102. Facemire, C. S., Nixon, A. B., Griffiths, R., Hurwitz, H. & Coffman, T. M. Vascular endothelial growth factor receptor 2 controls blood pressure by regulating nitric oxide synthase expression. *Hypertension* **54,** 652–8 (2009).
103. Austin, S. A., Santhanam, A. V & Katusic, Z. S. Endothelial nitric oxide modulates expression and processing of amyloid precursor protein. *Circ. Res.* **107,** 1498–1502 (2010).
104. Austin, S. A., D'Uscio, L. V. & Katusic, Z. S. Supplementation of nitric oxide attenuates AβPP and BACE1 protein in cerebral microcirculation of eNOS-deficient mice. *J. Alzheimers Dis.* **33,** 29–33 (2013).
105. Thomas, T., Thomas, G., McLendon, C., Sutton, T. & Mullan, M. β-amyloid-mediated vasoactivity and vascular endothelial damage. *Nature* **380,** 168–171 (1996).
106. Selley, M. L. Increased concentrations of homocysteine and asymmetric dimethylarginine and decreased concentrations of nitric oxide in the plasma of patients with Alzheimer's disease. *Neurobiol. Aging* **24,** 903–7 (2003).
107. Carlsson, C. M. *et al.* Effects of atorvastatin on cerebral blood flow in middle-aged adults at risk for Alzheimer's disease: a pilot study. *Curr. Alzheimer Res.* **9,** 990–7 (2012).
108. Suhara, T. *et al.* Aβ42 generation is toxic to endothelial cells and inhibits eNOS function through an Akt/GSK-3β signaling-dependent mechanism. *Neurobiol. Aging* **24,** 437–451 (2003).
109. Bijur, G. N. & Jope, R. S. Proapoptotic Stimuli Induce Nuclear Accumulation of Glycogen Synthase Kinase-3β. *J. Biol. Chem.* **276,** 37436–42 (2001).
110. Pei, J.-J. *et al.* Distribution of Active Glycogen Synthase Kinase 3β (GSK-3β) in Brains Staged for Alzheimer Disease Neurofibrillary Changes. *J. Neuropathol. Exp. Neurol.* **58,** 1010–1019 (1999).
111. Hooper, C., Killick, R. & Lovestone, S. The GSK3 hypothesis of Alzheimer's disease. *J. Neurochem.* **104,** 1433–1439 (2008).
112. Leroy, K., Yilmaz, Z. & Brion, J.-P. Increased level of active GSK-3β in Alzheimer's disease and accumulation in argyrophilic grains and in neurones at different stages of neurofibrillary degeneration. *Neuropathol. Appl. Neurobiol.* **33,** (2007).
113. Hooper, C. *et al.* Glycogen synthase kinase-3 inhibition is integral to long-term potentiation. *Eur. J. Neurosci.* **25,** 81–86 (2007).
114. Kirouac, L., Rajic, A. J., Cribbs, D. H. & Padmanabhan, J. Activation of Ras-ERK Signaling and GSK-3 by Amyloid Precursor Protein and Amyloid Beta Facilitates Neurodegeneration in Alzheimer's Disease. *eNeuro* **4,** (2017).
115. Phiel, C. J., Wilson, C. A., Lee, V. M.-Y. & Klein, P. S. GSK-3α regulates production of Alzheimer's disease amyloid-β peptides. *Nature* **423,** 435–439 (2003).
116. Hurtado, D. E. *et al.* Selectively silencing GSK-3 isoforms reduces plaques and tangles in mouse models of Alzheimer's disease. *J. Neurosci.* **32,** 7392–402 (2012).
117. Sui, Z., Kovács, A. D. & Maggirwar, S. B. Recruitment of active glycogen synthase kinase-3 into neuronal lipid rafts. *Biochem. Biophys. Res. Commun.* **345,** 1643–1648 (2006).
118. Bai, Q., Song, D., Gu, L., Verkhratsky, A. & Peng, L. Bi-phasic regulation of glycogen content in astrocytes via Cav-1/PTEN/PI3K/AKT/GSK-3β pathway by fluoxetine. *Psychopharmacology (Berl).* **234,** 1069–1077 (2017).
119. Duran, J., Saez, I., Gruart, A., Guinovart, J. J. & Delgado-García, J. M. Impairment in Long-Term Memory Formation and Learning-Dependent Synaptic Plasticity in Mice

Lacking Glycogen Synthase in the Brain. *J. Cereb. Blood Flow Metab.* **33,** 550–556 (2013).
120. Ikezu, T. *et al.* Caveolae, plasma membrane microdomains for alpha-secretase-mediated processing of the amyloid precursor protein. *J. Biol. Chem.* **273,** 10485–95 (1998).
121. Kapoor, A. *et al.* Caveolin-1 regulates γ-secretase-mediated AβPP processing by modulating spatial distribution of γ-secretase in membrane. *J. Alzheimers. Dis.* **22,** 423–42 (2010).
122. Gaudreault, S. B., Dea, D. & Poirier, J. Increased caveolin-1 expression in Alzheimer's disease brain. *Neurobiol. Aging* **25,** 753–759 (2004).
123. van Helmond, Z. K. *et al.* Caveolin-1 and -2 and their relationship to cerebral amyloid angiopathy in Alzheimer's disease. *Neuropathol. Appl. Neurobiol.* **33,** 317–327 (2007).
124. Head, B. P. *et al.* Loss of Caveolin-1 Accelerates Neurodegeneration and Aging. *PLoS One* **5,** e15697 (2010).
125. Thomas, R. S. *et al.* Alterations in endocytic protein expression with increasing age in the transgenic APP695 V717I London mouse model of amyloid pathology. *Neuroreport* **28,** 963–968 (2017).
126. Gu, H., Wang, F. & Zhang, D. Caveolin-1 interacts with ATP binding cassette transporter G1 (ABCG1) and regulates ABCG1-mediated cholesterol efflux. *Biochim. Biophys. Acta - Mol. Cell Biol. Lipids* **1841,** 847–858 (2014).
127. Djelti, F. *et al.* CYP46A1 inhibition, brain cholesterol accumulation and neurodegeneration pave the way for Alzheimer's disease. *Brain* **138,** 2383–2398 (2015).
128. Igbavboa, U., Sun, G. Y., Weisman, G. A., He, Y. & Wood, W. G. Amyloid beta-protein stimulates trafficking of cholesterol and caveolin-1 from the plasma membrane to the Golgi complex in mouse primary astrocytes. *Neuroscience* **162,** 328–38 (2009).
129. Yu, C., Alterman, M. & Dobrowsky, R. T. Ceramide displaces cholesterol from lipid rafts and decreases the association of the cholesterol binding protein caveolin-1. *J. Lipid Res.* **46,** 1678–91 (2005).
130. Riboni, L., Viani, P., Bassi, R., Prinetti, A. & Tettamanti, G. The role of sphingolipids in the process of signal transduction. *Prog. Lipid Res.* **36,** 153–195 (1997).
131. Zeidan, Y. H., Jenkins, R. W. & Hannun, Y. A. Remodeling of cellular cytoskeleton by the acid sphingomyelinase/ceramide pathway. *J. Cell Biol.* **181,** 335–50 (2008).
132. Mizuno, S. *et al.* Network Analysis of a Comprehensive Knowledge Repository Reveals a Dual Role for Ceramide in Alzheimer's Disease. *PLoS One* **11,** e0148431 (2016).
133. Skinner, E. R., Watt, C., Besson, J. A. O. & Best, P. V. Lipid composition of different regions of the brain in patients with Alzheimer's disease. *Biochem. Soc. Trans.* **17,** 213–214 (1989).
134. Sooderberg, M., Edlund, C., Alafuzoff, I., Kristensson, K. & Dallner, G. Lipid Composition in Different Regions of the Brain in Alzheimer's Disease/Senile Dementia of Alzheimer's Type. *J. Neurochem.* **59,** 1646–1653 (1992).
135. He, X., Huang, Y., Li, B., Gong, C.-X. & Schuchman, E. H. Deregulation of sphingolipid metabolism in Alzheimer's disease. *Neurobiol. Aging* **31,** 398–408 (2010).
136. Molander-Melin, M. *et al.* Structural membrane alterations in Alzheimer brains found to be associated with regional disease development; increased density of gangliosides GM1 and GM2 and loss of cholesterol in detergent-resistant membrane domains. *J. Neurochem.* **92,** 171–182 (2005).
137. Noel, A., Ingrand, S. & Barrier, L. Ganglioside and related-sphingolipid profiles are altered in a cellular model of Alzheimer's disease. *Biochimie* **137,** 158–164 (2017).
138. Takasugi, N., Sasaki, T., Shinohara, M., Iwatsubo, T. & Tomita, T. *Synthetic ceramide analogues increase amyloid-β 42 production by modulating γ-secretase activity*. *Biochemical and Biophysical Research Communications* **457,** (2015).
139. Li, H. *et al.* Modulation of amyloid precursor protein processing by synthetic ceramide

analogues. *Biochim. Biophys. Acta - Mol. Cell Biol. Lipids* **1801,** 887–895 (2010).
140. Noel, A., Ingrand, S. & Barrier, L. Anti-amyloidogenic effects of glycosphingolipid synthesis inhibitors occur independently of ganglioside alterations. *Mol. Cell. Neurosci.* **75,** 63–70 (2016).
141. Tamboli, I. Y. *et al.* Inhibition of glycosphingolipid biosynthesis reduces secretion of the beta-amyloid precursor protein and amyloid beta-peptide. *J. Biol. Chem.* **280,** 28110–7 (2005).
142. Puglielli, L., Ellis, B. C., Saunders, A. J. & Kovacs, D. M. Ceramide stabilizes beta-site amyloid precursor protein-cleaving enzyme 1 and promotes amyloid beta-peptide biogenesis. *J. Biol. Chem.* **278,** 19777–83 (2003).
143. Lee, J.-T. *et al.* Amyloid-beta peptide induces oligodendrocyte death by activating the neutral sphingomyelinase-ceramide pathway. *J. Cell Biol.* **164,** 123–31 (2004).
144. Lopes Pinheiro, M. A. *et al.* Acid Sphingomyelinase-Derived Ceramide Regulates ICAM-1 Function during T Cell Transmigration across Brain Endothelial Cells. *J. Immunol.* **196,** 72–9 (2016).
145. Yeh, L. H., Kinsey, A. M., Chatterjee, S. & Alevriadou, B. R. Lactosylceramide mediates shear-induced endothelial superoxide production and intercellular adhesion molecule-1 expression. *J. Vasc. Res.* **38,** 551–9
146. Dustin, M. L., Rothlein, R., Bhan, A. K., Dinarello, C. A. & Springer, T. A. Induction by IL 1 and interferon-gamma: tissue distribution, biochemistry, and function of a natural adherence molecule (ICAM-1). *J. Immunol.* **137,** 245–54 (1986).
147. Rothlein, R., Mainolfi, E. A., Czajkowski, M. & Marlin, S. D. A form of circulating ICAM-1 in human serum. *J. Immunol.* **147,** 3788–93 (1991).
148. Snyder, H. M. *et al.* Developing novel blood-based biomarkers for Alzheimer's disease. *Alzheimer's Dement.* **10,** 109–114 (2014).
149. Nielsen, H. M., Londos, E., Minthon, L. & Janciauskiene, S. M. Soluble adhesion molecules and angiotensin-converting enzyme in dementia. *Neurobiol. Dis.* **26,** 27–35 (2007).
150. Rentzos, M. *et al.* Serum Levels of Soluble Intercellular Adhesion Molecule-1 and Soluble Endothelial Leukocyte Adhesion Molecule-1 in Alzheimer's Disease. *J. Geriatr. Psychiatry Neurol.* **17,** 225–231 (2004).
151. Janciauskiene, S. M., Erikson, C. & Warkentin, S. A link between sICAM-1, ACE and parietal blood flow in the aging brain. *Neurobiol. Aging* **30,** 1504–1511 (2009).
152. Frohman, E. M., Frohman, T. C., Gupta, S., de Fougerolles, A. & van den Noort, S. Expression of intercellular adhesion molecule 1 (ICAM-1) in Alzheimer's disease. *J. Neurol. Sci.* **106,** 105–111 (1991).
153. Verbeek, M. M. *et al.* Accumulation of intercellular adhesion molecule-1 in senile plaques in brain tissue of patients with Alzheimer's disease. *Am. J. Pathol.* **144,** 104–16 (1994).
154. Verbeek, M. M., Otte-Höller, I., Wesseling, P., Ruiter, D. J. & de Waal, R. M. W. Differential expression of intercellular adhesion molecule-1 (ICAM-1) in the Aβ containing lesions in brains of patients with dementia of the Alzheimer type. *Acta Neuropathol.* **91,** 608–615 (1996).
155. Lee, S. J. *et al.* ICAM-1-induced expression of proinflammatory cytokines in astrocytes: involvement of extracellular signal-regulated kinase and p38 mitogen-activated protein kinase pathways. *J. Immunol.* **165,** 4658–4666 (2000).
156. Rozemuller, J. M., Eikelenboom, P., Pals, S. T. & Stam, F. C. Microglial cells around amyloid plaques in Alzheimer's disease express leucocyte adhesion molecules of the LFA-1 family. *Neurosci. Lett.* **101,** 288–292 (1989).
157. Rieckmann, P. *et al.* Soluble intercellular adhesion molecule-1 in cerebrospinal fluid: An indicator for the inflammatory impairment of the blood-cerebrospinal fluid barrier. *J. Neuroimmunol.* **47,** 133–140 (1993).

158. Ciaramella, A. *et al.* Increased Pro-Inflammatory Response by Dendritic Cells from Patients with Alzheimer's Disease. *J. Alzheimer's Dis.* **19,** 559–572 (2010).
159. Akiyama, H. *et al.* Expression of intercellular adhesion molecule (ICAM)-1 by a subset of astrocytes in Alzheimer disease and some other degenerative neurological disorders. *Acta Neuropathol.* **85,** 628–34 (1993).
160. Xu, S., Zhou, X., Yuan, D., Xu, Y. & He, P. Caveolin-1 scaffolding domain promotes leukocyte adhesion by reduced basal endothelial nitric oxide-mediated ICAM-1 phosphorylation in rat mesenteric venules. *Am. J. Physiol. Heart Circ. Physiol.* **305,** H1484-93 (2013).
161. Di Paolo, G. & Kim, T.-W. Linking lipids to Alzheimer's disease: cholesterol and beyond. *Nat. Rev. Neurosci.* **12,** 284–296 (2011).
162. Hu, Z. *et al.* Acute mechanical stretch promotes eNOS activation in venous endothelial cells mainly via PKA and Akt pathways. *PLoS One* **8,** e71359 (2013).
163. Spescha, R. D. *et al.* Adaptor protein p66Shc mediates hypertension-associated, cyclic stretch-dependent, endothelial damage. *Hypertension* **64,** 347–53 (2014).
164. Thacher, T., Gambillara, V., da Silva, R. F., Silacci, P. & Stergiopulos, N. Reduced cyclic stretch, endothelial dysfunction, and oxidative stress: an *ex vivo* model. *Cardiovasc. Pathol.* **19,** e91–e98 (2010).
165. Takeda, H. *et al.* Bi-phasic activation of eNOS in response to uni-axial cyclic stretch is mediated by differential mechanisms in BAECs. *Life Sci.* **79,** 233–9 (2006).
166. Awolesi, M. A., Sessa, W. C. & Sumpio, B. E. Cyclic strain upregulates nitric oxide synthase in cultured bovine aortic endothelial cells. *J. Clin. Invest.* **96,** 1449–54 (1995).
167. Dancu, M. B., Berardi, D. E., Vanden Heuvel, J. P. & Tarbell, J. M. Asynchronous shear stress and circumferential strain reduces endothelial NO synthase and cyclooxygenase-2 but induces endothelin-1 gene expression in endothelial cells. *Arterioscler. Thromb. Vasc. Biol.* **24,** 2088–94 (2004).
168. Northcott, C. A. *et al.* Nitric oxide synthase, ADMA, SDMA, and nitric oxide activity in the paraventricular nucleus throughout the etiology of renal wrap hypertension. *Am. J. Physiol. Heart Circ. Physiol.* **302,** H2276-84 (2012).
169. Bauer, E. M. *et al.* Thrombospondin-1 supports blood pressure by limiting eNOS activation and endothelial-dependent vasorelaxation. *Cardiovasc. Res.* **88,** 471–81 (2010).
170. Wood, K. C. *et al.* Circulating blood endothelial nitric oxide synthase contributes to the regulation of systemic blood pressure and nitrite homeostasis. *Arterioscler. Thromb. Vasc. Biol.* **33,** 1861–71 (2013).
171. Cheng, W.-H. *et al.* Renin activates PI3K-Akt-eNOS signalling through the angiotensin AT_1 and Mas receptors to modulate central blood pressure control in the nucleus tractus solitarii. *Br. J. Pharmacol.* **166,** 2024–35 (2012).
172. Ziegler, T., Bouzourène, K., Harrison, V. J., Brunner, H. R. & Hayoz, D. Influence of oscillatory and unidirectional flow environments on the expression of endothelin and nitric oxide synthase in cultured endothelial cells. *Arterioscler. Thromb. Vasc. Biol.* **18,** 686–92 (1998).
173. Berrout, J., Jin, M. & O'Neil, R. G. Critical role of TRPP2 and TRPC1 channels in stretch-induced injury of blood–brain barrier endothelial cells. *Brain Res.* **1436,** 1–12 (2012).
174. Shikata, Y. *et al.* Differential effects of shear stress and cyclic stretch on focal adhesion remodeling, site-specific FAK phosphorylation, and small GTPases in human lung endothelial cells. *Exp. Cell Res.* **304,** 40–49 (2005).
175. Thodeti, C. K. *et al.* TRPV4 channels mediate cyclic strain–induced endothelial cell reorientation through integrin-to-integrin signaling. *Circ. Res.* **104,** 1123–1130 (2009).
176. Matthews, B. D. *et al.* Ultra-rapid activation of TRPV4 ion channels by mechanical forces applied to cell surface β1 integrins. *Integr. Biol.* **2,** 435–442 (2010).
177. Naruse, K., Sai, X., Yokoyama, N. & Sokabe, M. Uni-axial cyclic stretch induces c-src

activation and translocation in human endothelial cells via SA channel activation. *FEBS Lett.* **441,** 111–115 (1998).
178. Suzuki, M. *et al.* Up-regulation of integrin β3 expression by cyclic stretch in human umbilical endothelial cells. *Biochem. Biophys. Res. Commun.* **239,** 372–376 (1997).
179. Kuebler, W. M. *et al.* Stretch activates nitric oxide production in pulmonary vascular endothelial cells in situ. *Am. J. Respir. Crit. Care Med.* **168,** 1391–1398 (2003).
180. Gan, L. Temporal regulation of endothelial ET-1 and eNOS expression in intact human conduit vessels exposed to different intraluminal pressure levels at physiological shear stress. *Cardiovasc. Res.* **48,** 168–177 (2000).
181. Oemar, B. S. *et al.* Reduced endothelial nitric oxide synthase expression and production in human atherosclerosis. *Circulation* **97,** 2494–2498 (1998).
182. Ziegler, T., Silacci, P., Harrison, V. J. & Hayoz, D. Nitric oxide synthase expression in endothelial cells exposed to mechanical forces. *Hypertension* **32,** 351–355 (1998).
183. Silacci, P. *et al.* Unidirectional and oscillatory shear stress differentially modulate NOS III gene expression. *Nitric Oxide* **4,** 47–56 (2000).
184. Thacher, T. N., Silacci, P., Stergiopulos, N. & da Silva, R. F. Autonomous effects of shear stress and cyclic circumferential stretch regarding endothelial dysfunction and oxidative stress: an *ex vivo* arterial model. *J. Vasc. Res.* **47,** 336–45 (2010).
185. Mohamed, J. S., Lopez, M. A. & Boriek, A. M. Mechanical stretch up-regulates microRNA-26a and induces human airway smooth muscle hypertrophy by suppressing glycogen synthase kinase-3β. *J. Biol. Chem.* **285,** 29336–47 (2010).
186. Gayer, C. P. *et al.* Strain-induced proliferation requires the phosphatidylinositol 3-kinase/AKT/glycogen synthase kinase pathway. *J. Biol. Chem.* **284,** 2001–11 (2009).
187. Song, F. *et al.* Mechanical Stress Regulates Osteogenesis and Adipogenesis of Rat Mesenchymal Stem Cells through PI3K/Akt/GSK-3β/β-Catenin Signaling Pathway. *Biomed Res. Int.* **2017,** 6027402 (2017).
188. Yu, J. *et al.* Direct evidence for the role of caveolin-1 and caveolae in mechanotransduction and remodeling of blood vessels. *J. Clin. Invest.* **116,** 1284–91 (2006).
189. Lu, T. *et al.* Role of the endothelial caveolae microdomain in shear stress–mediated coronary vasorelaxation. *J. Biol. Chem.* **292,** 19013–19023 (2017).
190. Lei, L. *et al.* The role of mechanical tension on lipid raft dependent PDGF-induced TRPC6 activation. *Biomaterials* **35,** 2868–2877 (2014).
191. Albinsson, S., Nordström, I., Swärd, K. & Hellstrand, P. Differential dependence of stretch and shear stress signaling on caveolin-1 in the vascular wall. *Am. J. Physiol. Cell Physiol.* **294,** C271-9 (2008).
192. Zhang, B. *et al.* Caveolin-1 phosphorylation is required for stretch-induced EGFR and Akt activation in mesangial cells. *Cell. Signal.* **19,** 1690–1700 (2007).
193. Yeow, I. *et al.* EHD Proteins Cooperate to Generate Caveolar Clusters and to Maintain Caveolae during Repeated Mechanical Stress. *Curr. Biol.* **27,** 2951–2962.e5 (2017).
194. Sinha, B. *et al.* Cells Respond to Mechanical Stress by Rapid Disassembly of Caveolae. *Cell* **144,** 402–413 (2011).
195. Gilbert, G., Ducret, T., Savineau, J.-P., Marthan, R. & Quignard, J.-F. Caveolae are involved in mechanotransduction during pulmonary hypertension. *Am. J. Physiol. - Lung Cell. Mol. Physiol.* **310,** L1078–L1087 (2016).
196. Gervásio, O. L., Phillips, W. D., Cole, L. & Allen, D. G. Caveolae respond to cell stretch and contribute to stretch-induced signaling. *J. Cell Sci.* **124,** 3581–90 (2011).
197. Spijkers, L. J. A. *et al.* Hypertension Is Associated with Marked Alterations in Sphingolipid Biology: A Potential Role for Ceramide. *PLoS One* **6,** e21817 (2011).
198. Brittain, E. L. *et al.* Fatty Acid Metabolic Defects and Right Ventricular Lipotoxicity in Human Pulmonary Arterial HypertensionClinical Perspective. *Circulation* **133,** 1936–1944 (2016).

199. Bogaard, H. J. *et al.* Copper Chelation Mediated Resolution Of Angioproliferative Lesions In Experimental Pulmonary Hypertension Is Associated With An Altered Ceramide/sphingosine-1 Phosphate Balance. in *Pulmonary hypertension: Experimental models I* A3419–A3419 (American Thoracic Society, 2011). doi:10.1164/ajrccm-conference.2011.183.1_MeetingAbstracts.A3419
200. Zhang, Q.-J. *et al.* Ceramide Mediates Vascular Dysfunction in Diet-Induced Obesity by PP2A-Mediated Dephosphorylation of the eNOS-Akt Complex. *Diabetes* **61,** (2012).
201. Bharath, L. *et al.* Ceramide initiated protein phosphatase 2A activation contributes to arterial dysfunction *in vivo*. *Am Diabetes Assoc*
202. Fu, W. *et al.* Effects of cyclic stretch on expression of cytokines and intercelluar adhesion molecule-1 in human pulmonary artery endothelial cell. *Zhonghua Wei Zhong Bing Ji Jiu Yi Xue* **25,** 484–488 (2013).
203. Cheng, J., Wung, B.-S., Chao, Y.-J. & Wang, D. L. Cyclic strain enhances adhesion of monocytes to endothelial cells by increasing intercellular adhesion molecule-1 expression. *Hypertension* **28,** 386–391 (1996).
204. Breen, L. T., McHugh, P. E. & Murphy, B. P. HUVEC ICAM-1 and VCAM-1 Synthesis in Response to Potentially Athero-Prone and Athero-Protective Mechanical and Nicotine Chemical Stimuli. *Ann. Biomed. Eng.* **38,** 1880–1892 (2010).
205. Riser, B. L. *et al.* Cyclic stretching of mesangial cells up-regulates intercellular adhesion molecule-1 and leukocyte adherence: a possible new mechanism for glomerulosclerosis. *Am. J. Pathol.* **158,** 11–7 (2001).
206. Blair, L. A., Haven, A. K. & Bauer, N. N. Circulating microparticles in severe pulmonary arterial hypertension increase intercellular adhesion molecule-1 expression selectively in pulmonary artery endothelium. *Respir. Res.* **17,** 133 (2016).
207. Tong, S., Neboori, H. J., Tran, E. D. & Schmid-Schönbein, G. W. Constitutive expression and enzymatic cleavage of ICAM-1 in the spontaneously hypertensive rat. *J. Vasc. Res.* **48,** 386–96 (2011).
208. Wang, H. *et al.* The upregulation of ICAM-1 and P-selectin requires high blood pressure but not circulating renin-angiotensin system *in vivo*. *J. Hypertens.* **22,** 1323–32 (2004).
209. Pastore, L. *et al.* Angiotensin II stimulates intercellular adhesion molecule-1 (ICAM-1) expression by human vascular endothelial cells and increases soluble ICAM-1 release *in vivo*. *Circulation* **100,** 1646–52 (1999).
210. Hlubocká, Z. *et al.* Circulating intercellular cell adhesion molecule-1, endothelin-1 and von Willebrand factor-markers of endothelial dysfunction in uncomplicated essential hypertension: the effect of treatment with ACE inhibitors. *J. Hum. Hypertens.* **16,** 557–62 (2002).
211. Kamble, H., Barton, M. J., Jun, M., Park, S. & Nguyen, N.-T. Cell stretching devices as research tools: engineering and biological considerations. *Lab Chip* **16,** 3193–3203 (2016).
212. Farhana, N., Mohamedali, A., Ahn, B. S., Avolio, A. & Baker, M. S. Effects of acute and chronic biomechanical strain on human cerebral endothelial cells in altering their proteome profile. *Curr. Proteomics* **14,** 1–10 (2017).
213. Paolinelli, R. *et al.* Wnt activation of immortalized brain endothelial cells as a tool for generating a standardized model of the blood brain barrier *in vitro*. *PLoS One* **8,** e70233 (2013).
214. Bi, H. *et al.* Optimization of harvesting, extraction, and analytical protocols for UPLC-ESI-MS-based metabolomic analysis of adherent mammalian cancer cells. *Anal. Bioanal. Chem.* **405,** 5279–89 (2013).
215. Junqueira Santiago, M. Regulation of the μ-opioid receptor signalling in naturally occurring variants and phosphorylation site mutants. (2015).
216. Ranjan, A. & Webster, T. J. Increased endothelial cell adhesion and elongation on

micron-patterned nano-rough poly(dimethylsiloxane) films. *Nanotechnology* **20,** 305102 (2009).
217. Bhat, V. D., Truskey, G. A. & Reichert, W. M. Fibronectin and avidin–biotin as a heterogeneous ligand system for enhanced endothelial cell adhesion. *J. Biomed. Mater. Res. Part A* **41,** 377–385 (1998).
218. Burmeister, J. S., Vrany, J. D., Reichert, W. M. & Truskey, G. A. Effect of fibronectin amount and conformation on the strength of endothelial cell adhesion to HEMA/EMA copolymers. *J. Biomed. Mater. Res.* **30,** 13–22 (1996).
219. Burmeister, J. S., McKinney, V. Z., Reichert, W. M. & Truskey, G. A. Role of endothelial cell-substrate contact area and fibronectin-receptor affinity in cell adhesion to HEMA/EMA copolymers. *J. Biomed. Mater. Res.* **47,** 577–84 (1999).
220. Huang, C.-K. & Donald, A. Revealing the dependence of cell spreading kinetics on its spreading morphology using microcontact printed fibronectin patterns. *J. R. Soc. Interface* **12,** 20141064 (2015).
221. Ben Halima, S. *et al.* Specific Inhibition of β-Secretase Processing of the Alzheimer Disease Amyloid Precursor Protein. *Cell Rep.* **14,** 2127–2141 (2016).
222. d'Uscio, L. V *et al.* Activation of PPARδ prevents endothelial dysfunction induced by overexpression of amyloid-β precursor protein. *Cardiovasc. Res.* **96,** 504–12 (2012).
223. Lamoke, F. *et al.* Amyloid β peptide-induced inhibition of endothelial nitric oxide production involves oxidative stress-mediated constitutive eNOS/HSP90 interaction and disruption of agonist-mediated Akt activation. *J. Neuroinflammation* **12,** 84 (2015).
224. Kurata, T. *et al.* Long-term effect of telmisartan on Alzheimer's amyloid genesis in SHR-SR after tMCAO. *Transl. Stroke Res.* **6,** 107–15 (2015).
225. Naruse, K., Yamada, T. & Sokabe, M. Involvement of SA channels in orienting response of cultured endothelial cells to cyclic stretch. *Am. J. Physiol.* **274,** H1532-8 (1998).
226. Schmittgen, T. D. & Livak, K. J. Analyzing real-time PCR data by the comparative CT method. *Nat. Protoc.* **3,** 1101–1108 (2008).
227. Wan, X.-Z. *et al.* Activation of NMDA receptors upregulates a disintegrin and metalloproteinase 10 via a Wnt/MAPK signaling pathway. *J. Neurosci.* **32,** 3910–6 (2012).
228. Motulsky, H. J. & Brown, R. E. Detecting outliers when fitting data with nonlinear regression – a new method based on robust nonlinear regression and the false discovery rate. *BMC Bioinformatics* **7,** 123 (2006).
229. Nichols, W. W. *et al.* Effects of age on ventricular-vascular coupling. *Am J Cardiol* **55,** 1179–1184 (1985).
230. Pflanzner, T. *et al.* LRP1 mediates bidirectional transcytosis of amyloid-β across the blood-brain barrier. *Neurobiol. Aging* **32,** 2323.e1-11 (2011).
231. Gu, L., Tran, J., Jiang, L. & Guo, Z. A new structural model of Alzheimer's Aβ42 fibrils based on electron paramagnetic resonance data and Rosetta modeling. *J. Struct. Biol.* **194,** 61–67 (2016).
232. Kim, J. *et al.* Aβ40 inhibits amyloid deposition *in vivo*. *J. Neurosci.* **27,** (2007).
233. Kuperstein, I. *et al.* Neurotoxicity of Alzheimer's disease Aβ peptides is induced by small changes in the Aβ42 to Aβ40 ratio. *EMBO J.* **29,** 3408–20 (2010).
234. Takeshi, I. *et al.* Visualization of Aβ42(43) and Aβ40 in senile plaques with end-specific Aβ monoclonals: Evidence that an initially deposited species is Aβ42(43). *Neuron* **13,** 45–53 (1994).
235. Fagan, A. M. *et al.* Inverse relation between *in vivo* amyloid imaging load and cerebrospinal fluid Aβ42 in humans. *Ann. Neurol.* **59,** 512–519 (2006).
236. Gravina, S. A. *et al.* Amyloid β protein (Aβ) in Alzheimer's disease brain. Biochemical and immunocytochemical analysis with antibodies specific for forms ending at Aβ40 or Aβ42 42(43). *J. Biol. Chem.* **270,** 7013–6 (1995).

237. Iwatsubo, T., Mann, D. M. A., Odaka, A., Suzuki, N. & Ihara, Y. Amyloid β protein (Aβ) deposition: Aβ42(43) precedes Aβ40 in down Syndrome. *Ann. Neurol.* **37,** 294–299 (1995).
238. Loane, D. J. *et al.* Amyloid precursor protein secretases as therapeutic targets for traumatic brain injury. *Nat. Med.* **15,** 377–9 (2009).
239. Mojtaba Golzan, S. *et al.* Retinal vascular and structural changes are associated with amyloid burden in the elderly: ophthalmic biomarkers of preclinical Alzheimer's disease. doi:10.1186/s13195-017-0239-9
240. Cantara, S. *et al.* Physiological levels of amyloid peptides stimulate the angiogenic response through FGF-2. *FASEB J.* **18,** 1943–5 (2004).
241. Singh, U., Devaraj, S., Vasquez-Vivar, J. & Jialal, I. C-reactive protein decreases endothelial nitric oxide synthase activity via uncoupling. *J. Mol. Cell. Cardiol.* **43,** 780–791 (2007).
242. Ho, J. J. D. *et al.* Active Stabilization of Human Endothelial Nitric Oxide Synthase mRNA by hnRNP E1 Protects against Antisense RNA and MicroRNAs. *Mol. Cell. Biol.* **33,** 2029–2046 (2013).
243. Buras, J. A., Stahl, G. L., Svoboda, K. K. H. & Reenstra, W. R. Hyperbaric oxygen downregulates ICAM-1 expression induced by hypoxia and hypoglycemia: the role of NOS. *Am. J. Physiol. - Cell Physiol.* **278,** (2000).
244. Tian, Y., Gawlak, G., O'Donnell, J. J., Mambetsariev, I. & Birukova, A. A. Modulation of Endothelial Inflammation by Low and High Magnitude Cyclic Stretch. *PLoS One* **11,** e0153387 (2016).
245. Paris, D. *et al.* Soluble β-amyloid peptides mediate vasoactivity via activation of a pro-inflammatory pathway. *Neurobiol. Aging* **21,** 183–197 (2000).
246. Schmitt, M. M. N. *et al.* Endothelial Junctional Adhesion Molecule-A Guides Monocytes Into Flow-Dependent Predilection Sites of AtherosclerosisClinical Perspective. *Circulation* **129,** (2014).
247. Bjelik, A. *et al.* Human apoB overexpression and a high-cholesterol diet differently modify the brain APP metabolism in the transgenic mouse model of atherosclerosis. *Neurochem. Int.* **49,** 393–400 (2006).
248. Akkawi, S., Nassar, T., Tarshis, M., Cines, D. B. & Higazi, A. A.-R. LRP and vbeta3 mediate tPA activation of smooth muscle cells. *AJP Hear. Circ. Physiol.* **291,** H1351–H1359 (2006).
249. He, T., Santhanam, A. V. R., Lu, T., d'Uscio, L. V & Katusic, Z. S. Role of prostacyclin signaling in endothelial production of soluble amyloid precursor protein-α in cerebral microvessels. *J. Cereb. Blood Flow Metab.* **37,** 106–122 (2017).
250. Kuebler, W. M. *et al.* Stretch Activates Nitric Oxide Production in Pulmonary Vascular Endothelial Cells In Situ. *Am. J. Respir. Crit. Care Med.* **168,** 1391–1398 (2003).
251. Cross, D. A. *et al.* The inhibition of glycogen synthase kinase-3 by insulin or insulin-like growth factor 1 in the rat skeletal muscle cell line L6 is blocked by wortmannin, but not by rapamycin: evidence that wortmannin blocks activation of the mitogen-activated protein kinase pathway in L6 cells between Ras and Raf. *Biochem. J.* **303 (Pt 1),** 21–6 (1994).
252. Cross, D. A. E., Alessi, D. R., Cohen, P., Andjelkovich, M. & Hemmings, B. A. Inhibition of glycogen synthase kinase-3 by insulin mediated by protein kinase B. *Nature* **378,** 785–789 (1995).
253. Zhou, X., Wang, H., Burg, M. B. & Ferraris, J. D. Inhibitory phosphorylation of GSK-3β by AKT, PKA, and PI3K contributes to high NaCl-induced activation of the transcription factor NFAT5 (TonEBP/OREBP). *Am. J. Physiol. Renal Physiol.* **304,** F908-17 (2013).
254. Kim, C.-H., Hao, J., Ahn, H.-Y. & Kim, S. W. Activation of Akt/protein kinase B mediates the protective effects of mechanical stretching against myocardial ischemia-

reperfusion injury. *J. Vet. Sci.* **13,** 235 (2012).
255. Soltow, Q. A., Zeanah, E. H., Lira, V. A. & Criswell, D. S. Cessation of cyclic stretch induces atrophy of C2C12 myotubes. *Biochem. Biophys. Res. Commun.* **434,** 316–321 (2013).
256. Zheng, W., Christensen, L. P. & Tomanek, R. J. Differential effects of cyclic and static stretch on coronary microvascular endothelial cell receptors and vasculogenic/angiogenic responses. *Am. J. Physiol. Heart Circ. Physiol.* **295,** H794-800 (2008).
257. Liu, X., Ensenat, D., Wang, H., Schafer, A. I. & Durante, W. Physiologic cyclic stretch inhibits apoptosis in vascular endothelium. *FEBS Lett.* **541,** 52–56 (2003).
258. Wang, Q. *et al.* Myocardial Protection by MiR-126 Against Ischemia/Reperfusion Injury Through Suppression of GSK-3β. *J. Am. Coll. Cardiol.* **66,** C40 (2015).
259. Shrader, C., Prescott, M., Luo, J., Cilento, E. & Reilly, F. Acute stretch enhances expression of Akt and VEGF in healing mouse skin. *FASEB J.* **20,** A709–A709 (2006).
260. Deng, J. *et al.* Soluble amyloid precursor protein alpha inhibits tau phosphorylation through modulation of GSK3β signaling pathway. *J. Neurochem.* **135,** 630–637 (2015).
261. Obregon, D. *et al.* Soluble amyloid precursor protein-α modulates β-secretase activity and amyloid-β generation. *Nat. Commun.* **3,** 777 (2012).
262. Cai, Z.-X. *et al.* Double-Edged Roles of Nitric Oxide Signaling on APP Processing and Amyloid-β Production *In Vitro*: Preliminary Evidence from Sodium Nitroprusside. *Neurotox. Res.* **29,** 21–34 (2016).
263. Meng, X.-F. *et al.* Midlife Vascular Risk Factors and the Risk of Alzheimer's Disease: A Systematic Review and Meta-Analysis. *J. Alzheimer's Dis.* **42,** 1295–1310 (2014).
264. Fitch, R. M., Vergona, R., Sullivan, M. E. & Wang, Y.-X. X. Nitric oxide synthase inhibition increases aortic stiffness measured by pulse wave velocity in rats. *Cardiovasc. Res.* **51,** 351–358 (2001).
265. Wilkinson, I. B. *et al.* Nitric oxide regulates local arterial distensibility *in vivo*. *Circulation* **105,** 213–217 (2002).
266. Thacher, T., Gambillara, V., da Silva, R. F., Silacci, P. & Stergiopulos, N. Reduced cyclic stretch, endothelial dysfunction, and oxidative stress: an *ex vivo* model. *Cardiovasc. Pathol.* **19,** e91–e98 (2010).
267. Nakano, T., Tominaga, R., Nagano, I., Okabe, H. & Yasui, H. Pulsatile flow enhances endothelium-derived nitric oxide release in the peripheral vasculature. *Am. J. Physiol. - Hear. Circ. Physiol.* **278,** (2000).
268. Radisavljevic, Z., Avraham, H. & Avraham, S. Vascular endothelial growth factor up-regulates ICAM-1 expression via the phosphatidylinositol 3 OH-kinase/AKT/Nitric oxide pathway and modulates migration of brain microvascular endothelial cells. *J. Biol. Chem.* **275,** 20770–4 (2000).
269. Lee, H.-Y., Zeeshan, H. M. A., Kim, H.-R. & Chae, H.-J. Nox4 regulates the eNOS uncoupling process in aging endothelial cells. *Free Radic. Biol. Med.* **113,** 26–35 (2017).
270. Beckmann, T. F. *et al.* Effects of high passage cultivation on CHO cells: a global analysis. *Appl. Microbiol. Biotechnol.* **94,** 659–671 (2012).
271. Siissalo, S. *et al.* Effect of cell differentiation and passage number on the expression of efflux proteins in wild type and vinblastine-induced Caco-2 cell lines. *Eur. J. Pharm. Biopharm.* **67,** 548–554 (2007).
272. Cheng, J. P. X. *et al.* Caveolae protect endothelial cells from membrane rupture during increased cardiac output. *J. Cell Biol.* **211,** 53–61 (2015).
273. Chang, K.-A. *et al.* Phosphorylation of Amyloid Precursor Protein (APP) at Thr668 Regulates the Nuclear Translocation of the APP Intracellular Domain and Induces Neurodegeneration. *Mol. Cell. Biol.* **26,** 4327–4338 (2006).
274. Villemagne, V. L. *et al.* Amyloid β deposition, neurodegeneration, and cognitive decline in sporadic Alzheimer's disease: a prospective cohort study. *Lancet. Neurol.* **12,** 357–67

(2013).
275. Tong, X.-K., Nicolakakis, N., Kocharyan, A. & Hamel, E. Vascular Remodeling versus amyloid β-Induced Oxidative Stress in the Cerebrovascular Dysfunctions Associated with Alzheimer's Disease. *J. Neurosci.* **25,** 11165–74 (2005).
276. Cheng, J. *et al.* 20-hydroxyeicosatetraenoic acid causes endothelial dysfunction via eNOS uncoupling. *Am. J. Physiol. Circ. Physiol.* **294,** H1018–H1026 (2008).
277. Soriano, F. X., Galbete, J. L. & Forloni, G. Effect of β-amyloid on endothelial cells: lack of direct toxicity, enhancement of MTT-induced cell death and intracellular accumulation. *Neurochem. Int.* **43,** 251–261 (2003).
278. Stratton, M. S., Yang, X., Sreejayan, N. & Ren, J. Impact of insulin-like growth factor-I on migration, proliferation and Akt-ERK signaling in early and late-passages of vascular smooth muscle cells. *Cardiovasc. Toxicol.* **7,** 273–81 (2007).
279. Li, M., Chiu, J.-F., Gagne, J. & Fukagawa, N. K. Age-related differences in insulin-like growth factor-1 receptor signaling regulates Akt/FOXO3a and ERK/Fos pathways in vascular smooth muscle cells. *J. Cell. Physiol.* **217,** 377–387 (2008).
280. Lee, M. Y. K., Sørensen, G. L., Holmskov, U. & Vanhoutte, P. M. The presence and activity of SP-D in porcine coronary endothelial cells depend on Akt/PI3K, Erk and nitric oxide and decrease after multiple passaging. *Mol. Immunol.* **46,** 1050–1057 (2009).
281. Danesh Mesgaran, S. *et al.* Different inflammatory responses of bovine oviductal epithelial cells *in vitro* to bacterial species with distinct pathogenicity characteristics and passage number. *Theriogenology* **106,** 237–246 (2018).
282. Heinrich, F. *et al.* Passage-dependent morphological and phenotypical changes of a canine histiocytic sarcoma cell line (DH82 cells). *Vet. Immunol. Immunopathol.* **163,** 86–92 (2015).
283. Marco, S. & Skaper, S. D. Amyloid beta-peptide1-42 alters tight junction protein distribution and expression in brain microvessel endothelial cells. *Neurosci. Lett.* **401,** 219–24 (2006).
284. Berardi, D. E. & Tarbell, J. M. Stretch and Shear Interactions Affect Intercellular Junction Protein Expression and Turnover in Endothelial Cells. *Cell. Mol. Bioeng.* **2,** 320–331 (2009).
285. Dovey, H. F. *et al.* Functional gamma-secretase inhibitors reduce beta-amyloid peptide levels in brain. *J. Neurochem.* **76,** 173–181 (2009).
286. Dickinson, K. M., Clifton, P. M., Burrell, L. M., Barrett, P. H. R. & Keogh, J. B. Postprandial effects of a high salt meal on serum sodium, arterial stiffness, markers of nitric oxide production and markers of endothelial function. *Atherosclerosis* **232,** 211–216 (2014).
287. Butlin, M. *et al.* High Salt Diet Increases Aortic Stiffness and Pressure Pulse Amplification in Rat. *J. Hypertens.* **34,** e8 (2016).
288. Faraco, G. *et al.* Dietary salt promotes neurovascular and cognitive dysfunction through a gut-initiated TH17 response. *Nat. Neurosci.* 1 (2018). doi:10.1038/s41593-017-0059-z
289. Cheng, X.-J., Gao, Y., Zhao, Y.-W. & Cheng, X.-D. Sodium Chloride Increases Aβ Levels by Suppressing Aβ Clearance in Cultured Cells. *PLoS One* **10,** e0130432 (2015).
290. Taheri, S., Yu, J., Zhu, H. & Kindy, M. S. High-Sodium Diet Has Opposing Effects on Mean Arterial Blood Pressure and Cerebral Perfusion in a Transgenic Mouse Model of Alzheimer's Disease. *J. Alzheimer's Dis.* **54,** 1061–1072 (2016).
291. Butlin, M., Lindesay, G., Viegas, K. D. & Avolio, A. P. Pressure dependency of aortic pulse wave velocity *in vivo* is not affected by vasoactive substances that alter aortic wall tension *ex vivo*. *Am. J. Physiol. Circ. Physiol.* **308,** H1221–H1228 (2015).
292. You, Y., Gupta, V. K., Graham, S. L. & Klistorner, A. Anterograde Degeneration along the Visual Pathway after Optic Nerve Injury. *PLoS One* **7,** e52061 (2012).
293. Paxinos, G. & Watson, C. *The Rat Brain in Stereotaxic Coordinates*. (Elsevier Inc. Academic Press, 2007).

294. Henwood, A. F. Hematoxylin and eosin staining of mucins of the gastrointestinal tract. *J. Histotechnol.* **40,** 21–24 (2017).
295. Dickson, T. . & Vickers, J. . The morphological phenotype of β-amyloid plaques and associated neuritic changes in Alzheimer's disease. *Neuroscience* **105,** 99–107 (2001).
296. Mitew, S., Kirkcaldie, M. T. K., Dickson, T. C. & Vickers, J. C. Neurites containing the neurofilament-triplet proteins are selectively vulnerable to cytoskeletal pathology in Alzheimer's disease and transgenic mouse models. *Front. Neuroanat.* **7,** 30 (2013).
297. Martino Adami, P. V. *et al.* Worsening of memory deficit induced by energy-dense diet in a rat model of early-Alzheimer's disease is associated to neurotoxic Aβ species and independent of neuroinflammation. *Biochim. Biophys. Acta - Mol. Basis Dis.* **1863,** 731–743 (2017).
298. Pryor, N. E., Moss, M. A. & Hestekin, C. N. Unraveling the early events of amyloid-β protein (Aβ) aggregation: techniques for the determination of Aβ aggregate size. *Int. J. Mol. Sci.* **13,** 3038–72 (2012).
299. Gangoda, S. V. S. High blood pressure and cyclic stretch after cerebral amyloid deposition and endothelial function. (Macquarie University, Sydney, Australia, 2014).
300. Oberleithner, H. *et al.* Salt overload damages the glycocalyx sodium barrier of vascular endothelium. *Pflugers Arch.* **462,** 519–28 (2011).
301. Galmiche, G. *et al.* Smooth muscle cell mineralocorticoid receptors are mandatory for aldosterone-salt to induce vascular stiffness. *Hypertens. (Dallas, Tex. 1979)* **63,** 520–526 (2014).
302. Benetos, A. *et al.* Influence of age, risk factors, and cardiovascular and renal disease on arterial stiffness: clinical applications. *Am. J. Hypertens.* **15,** 1101–1108 (2002).
303. Rippe, C. *et al.* MicroRNA changes in human arterial endothelial cells with senescence: Relation to apoptosis, eNOS and inflammation. *Exp. Gerontol.* **47,** 45–51 (2012).
304. Wang, Y., Dang, Z., Cui, W. & Yang, L. Mechanical stretch and hypoxia inducible factor-1 alpha affect the vascular endothelial growth factor and the connective tissue growth factor in cultured ACL fibroblasts. *Connect. Tissue Res.* **58,** 407–413 (2017).
305. Ly, P. T. T. *et al.* Inhibition of GSK3β-mediated BACE1 expression reduces Alzheimer-associated phenotypes. *J. Clin. Invest.* **123,** 224–235 (2013).
306. Zhu, L. *et al.* Dynamin 1 Regulates Amyloid Generation through Modulation of BACE-1. *PLoS One* **7,** e45033 (2012).
307. Luo, G. *et al.* Deposition of BACE-1 Protein in the Brains of APP/PS1 Double Transgenic Mice. *Biomed Res. Int.* **2016,** 1–9 (2016).
308. Chen, Y. *et al.* Alzheimer's β-secretase (BACE1) regulates the cAMP/PKA/CREB pathway independently of β-amyloid. *J. Neurosci.* **32,** 11390–5 (2012).
309. Biffl, W. L., Moore, E. E., Moore, F. A. & Barnett, C. Nitric oxide reduces endothelial expression of intercellular adhesion molecule (ICAM)-1. *J. Surg. Res.* **63,** 328–32 (1996).
310. Toda, M. *et al.* Differential gene responses in endothelial cells exposed to a combination of shear stress and cyclic stretch. *J. Biotechnol.* **133,** 239–44 (2008).
311. Browe, D. Stretch of Beta-1 Integrin Activates a Chloride Current Via FAK And/or Src, Angiotensin (AT1) Receptors, and NADPH Oxidase in Ventricular Myocytes. (Virginia Commonwealth University, 2003).
312. Young-Pearse, T. L., Chen, A. C., Chang, R., Marquez, C. & Selkoe, D. J. Secreted APP regulates the function of full-length APP in neurite outgrowth through interaction with integrin beta1. *Neural Dev.* **3,** 15 (2008).
313. Mochizuki, T. *et al.* The TRPV4 cation channel mediates stretch-evoked Ca2+ influx and ATP release in primary urothelial cell cultures. *J. Biol. Chem.* **284,** 21257–64 (2009).
314. Pfeiffer, S., Leopold, E., Schmidt, K., Brunner, F. & Mayer, B. Inhibition of nitric oxide synthesis by NG-nitro-L-arginine methyl ester (L-NAME): requirement for bioactivation to the free acid, NG-nitro-L-arginine. *Br. J. Pharmacol.* **118,** 1433–40

(1996).
315. Dhanakoti, S. N., Brosnan, J. T., Herzberg, G. R. & Brosnan, M. E. Renal arginine synthesis: studies *in vitro* and *in vivo*. *Am. J. Physiol. Metab.* **259,** E437 (1990).
316. Boelens, P. G., Melis, G. C., van Leeuwen, P. A., ten Have, G. A. & Deutz, N. E. Route of administration (enteral or parenteral) affects the contribution of l -glutamine to de novo l -arginine synthesis in mice: a stable-isotope study. *Am. J. Physiol. Metab.* **291,** E683–E690 (2006).
317. Wang, S. *et al.* Amyloid β precursor protein regulates neuron survival and maturation in the adult mouse brain. *Mol. Cell. Neurosci.* **77,** 21–33 (2016).
318. Fuchs, C. *et al.* Loss of CDKL5 impairs survival and dendritic growth of newborn neurons by altering AKT/GSK-3β signaling. *Neurobiol. Dis.* **70,** 53–68 (2014).